PHYSICS AND CONTROL ASSESSMENT

OF

AN 850 MW(e)-LEU-CANDU-PHW REACTOR

BY

MICHELANGELO BARBONE

DEPARTMENT OF PHYSICS

A thesis submitted in conformity with the requirements
for the Degree of Doctor of Philosophy at

Concordia University.
Montréal, Canada

September 1982

"A tutti i bambini; ragazzi e ragazze, genitori e nonni del Sud Italia che nell'indimenticabile giorno del 20 novembre 1980 persero la vita sotto il crollo delle mura causato dal terremoto e a tutti i giovani e adulti che all'unanimità giurarono voler ridare ai bambini del Sud i loro villaggi perduti".

"To all the children, boys and girls, men and women, parents and grand parents of my native country who on the unforgettable day of November 20, 1980 lost their lives under the heavy weight of the falling walls caused by the earthquake and to all the young people and adults who unanimously were determined to give back to their children their lost towns and villages".

ABSTRACT

Michelangelo Barbone

PHYSICS AND CONTROL ASSESSMENT OF AN 850 MW(e)-LEU-CANDU-PHW REACTOR

The physics and control assessment of an 850 MW(e) Low Enriched Uranium CANDU Pressurized Heavy Water (LEU-CANDU-PHW) reactor constitute the major objective of this thesis.

The use of Low Enriched Uranium fuel in the present CANDU nuclear power generating stations is recognized as economically beneficial due to reduced fuelling costs. The LEU fuel cycle is also recognized as a stepping stone to transit from the present CANDU-PHW once-through natural Uranium cycle to advanced cycles such as those based on Plutonium recycle, once-through Th + U-235 cycle, Thorium with Uranium recycle and net U-235 feed, Thorium with Uranium recycle and Plutonium feed.

However, although the use of Low Enriched Uranium in the present CANDU-PHW reactor has economic advantages, and it would act as a technical bridge between the present cycle and advanced cycles, technical problems in different areas of reactor physics and fuel management were anticipated.

The present thesis research work adresses the areas of reactor physics, fuel management, and control (in particular, the spatial control of large CANDU-PHW reactors).

The main conclusions that have been drawn following these studies are as follows:

1. The Low Enriched Uranium Cycle is feasible in a CANDU-PHW reactor of present design and provided that:

   a) The enrichment is kept relatively low (that is, about 1% instead of 0.711%);

   b) The number of bundles to be replaced at every refuelling operation is about one-half that of the natural Uranium fuel case;

   c) The channels are refuelled in the same direction as the coolant.

2. The response of an LEU-CANDU-PHW reactor to reactivity perturbation such as single- and two-channel refuelling operation, shim transient, shutdown-start-up transient with enrichment levels of 0.9% and 1.2% is essentially very similar [provided that certain conditions in (1) are respected] to that of the natural uranium reactor core case without any reactor reoptimization. The general behaviour of the reactor regulating systems to refuelling and shim reactivity perturbation studies with LEU core cases offered results that were in almost perfect agreement with those obtained when the natural reactor core was considered. In the case of shutdown-start-up

reactivity perturbation, however, a slight shortening in the Decision and Action (DA) time is encountered. This is due to the lower reactivity worth that is associated with the reactivity devices in the case of the Low Enriched Uranium core. The power profile for the natural, 0.9% and 1.2% reactor core cases was essentially similar with only the exception of the slight difference in the DA time.

The author's main contributions to the physics and control assessment of the LEU introduction in the present CANDU-PHW-850 MW(e) reactor were especially prominent in the following areas:

PHYSICS

i) Optimize the burnup split between the inner core (higher burnup) and outer core (lower burnup) in order to minimize power peaking problems.

ii) Calculation of reactivity devices (liquid zone controllers, adjusters, mechanical control absorbers) worth for the natural, 0.9% and 1.2% reactor core cases.

iii) Matching LATREP and POWDERPUFFS reactivity devices incremental cross-sections and diffusion theory parameters.

iv) Reactor physics parametric calculation to support the operational transient and control assessment.

CONTROL ASSESSMENT

Extensive modifications and improvements to the "modal analysis" computer code required by this study.

OPERATIONAL TRANSIENTS

Planning, execution, documentation and assessment of results.

TABLE OF CONTENTS

TABLE OF CONTENTS (cont'd)

TABLE OF CONTENTS (cont'd)

TABLE OF CONTENTS (cont'd)

TABLE OF CONTENTS (cont'd)

TABLE OF CONTENTS (cont'd)

TABLE OF CONTENTS (cont'd)

LIST OF FIGURES

LIST OF FIGURES (cont'd)

LIST OF FIGURES (cont'd)

LIST OF FIGURES (cont'd)

LIST OF FIGURES (cont'd)

LIST OF TABLES

LIST OF TABLES (cont'd)

LIST OF TABLES (cont'd)

* Different reference source

ACKNOWLEDGEMENTS

> "..... replied I with bashful front to him: O honor and light of other poets! May the long study avail me and the great love which have made me search thy volume! Thou art my master and my author; thou alone art he from whom I took the fair style that has done me honor. Behold the beast because of which I turned; help me against her, famous sage, for she makes my veins and pulses tremble."
>
> Dante, "Divine Comedy"

I would like to take this opportunity to acknowledge the help of Dr. R.A. Bonalumi of Ontario Hydro and Dr. N. Eddy of Concordia University for their combined technical, scientific and academic support.

I would also like to thank the Physics Department of Concordia University for giving me permission to perform this Ph.D. research work at Ontario Hydro under the close supervision of Dr. R.A. Bonalumi of Nuclear Studies and Safety Department, headed by Dr. D.A. Menely. My acknowledgements are also addressed to the help of Dr. J.C. Luxat of Ontario Hydro who, despite his very busy work schedule, always found the time to provide the technical guidance for the control assessment aspect of this thesis.

A particular appreciation goes to Mr. F.J. Giaccio, Director of Special Projects of Canatom Inc., for his encouragment and recognition of the importance of this work and its social, technical and economic impact with regard to energy programs, both national and international.

I would like to extend my gratitude to Ontario Hydro, Atomic Energy of Canada Limited (AECL) and Canatom Inc. for their support of this work, for their hospitality, and for providing a rich intellectual environment. A number of persons have contributed suggestions: Mr. L. Amyot, Dr. P.E. Tremblay, of Atomic Energy of Canada Limited; Mr. G. Polisois of Energy, Mines and Resources (Gouvernement du Québec); Professor D.J. Andrews of University of Toronto.

Finally, I thank Daria Finnie for her dedication, perseverance and excellent typing.

PREFACE

It is almost ten years since a new dimension was added to our lives: "The Energy Crisis". The amounts of oil, gas, coal and uranium ore in the Earth are finite. We know our reserves and we can guess on the resources. We know how much we can recover with present technology and we are able to predict some improvements in the near future. However, we can estimate only on the basis of weak assumptions the increase in demand for energy and the awareness of environmental costs over the next twenty years. Much depends on the future expansion of economies of both developed and developing nations, the economic and political disturbances of those economies, and how well political leaders are able to cope with the hard choices that they and the people they govern must make.

A conclusion is certain: "However we calculate future demand and supply, it is unavoidable that by the year 2000 we will have to substitute other energy sources conservation for a good part of the oil and gas we have been burning without concern for the past decades."

Several oil-importing nations are promoting measures to become less dependent on oil - particularly the imported oil - while there is still time. Energy literature indicates that a historical time for some developed nations to become energy self-sufficient is around 1990-1995. A vital important decision to be taken without delay and the important contribution which nuclear energy can make toward the solution of world energy problems should not be overlooked.

It is now recognized that the solution for the production of electric power until at least the end of this century is coal and nuclear energy and, for some nations or provinces, hydro power is also a contender. Of course, we have to use all alternative energy sources available and capable of development, but one should realize that, by the end of this century, those sources can only make a marginal contribution.

The less nuclear power that the industrial nations generate, the more oil they will consume, the higher the price will go, and less oil will be available to the developing world. The same is true for coal. A healthy nuclear industry in the industrial nations is an indispensable basis for the expansion of nuclear power in the developing countries themselves.

How many nuclear power reactors will the world need to meet the electrical energy demand without being heavily dependent on oil? How much nuclear fuel will be required to feed the nuclear power reactors for producing a given electrical energy projection? Is there more than one fuel cycle that can be selected within a given nuclear technology? Will the introduction of a new fuel cycle have a considerable economic impact on a national nuclear program? Will the introduction of a new fuel cycle impose major nuclear technology changes? These questions will be discussed throughout this thesis.

CHAPTER ONE

1. FUTURE CANDU FUEL CYCLES

1.1 INTRODUCTION

The first CANDU (Canadian Natural Deuterium Uranium) reactor to be commissioned in CANADA was NPD (for Nuclear Power Demonstration), which came into operation in 1962. Since that time, commitments and firm plans for nuclear power installations have grown to slightly over 15,000 MW(e) (Ref. 4, 9, 44). Of this potential electrical power output, approximately half is already being injected into the Canadian electrical systems, accounting for as much as 10% of the country's electrical energy. This percentage ranks Canada sixth amongst the nations of the world in nuclear energy production.

There is little doubt that nuclear capacity will continue to be installed at a lively pace. Some energy projections (Appendix EN) indicate that a planned nuclear capacity of 50,000 MW(e) by the turn of this century may become a reality (projected capacities of the order of 100,000 MW(e) were quoted in earlier times).

CANDU PHWR's with the once-through natural uranium fuel cycle have been commercially successful in Ontario since the early 1970's. One of the main reasons for their economic advantage

TABLE 1.1: Canadian Nuclear Power Stations

STATION	UNIT	UNIT RATING MW(e)-net	POWER SYSTEM
NPD	1	22	O-H
DOUGLAS POINT	1	208	O-H
PICKERING A	4 UNITS	514	O-H
PICKERING B	4 UNITS	514	O-H
GENTILLY 1	1	250	H-Q
GENTILLY 2	1	600	H-Q
LEPREAU	1	600	NBEPC
BRUCE A	4 UNITS	750	O-H
BRUCE B	4 UNITS	750	O-H
DARLINGTON	4 UNITS	850	O-H

O-H = Ontario Hydro
H-Q = Hydro-Québec
NBEPC = New Brunswick Electric Power Commission

over fossil-fuelled generating stations is the current abundance of low-cost uranium in Canada and especially in Ontario. Since uranium is indigenous to Ontario and fossil fuels are not, long range forecasts have suggested that nuclear power should constitute up to two-thirds of the installed generating capacity in the Province of Ontario following the turn of this century.

Ontario Hydro has secured uranium supplies for much of the life of its presently committed nuclear stations. However, it is not possible to confidently estimate the availability or price of uranium after the turn of the century.

Currently, the annual uranium requirements of Canada's nuclear power program are relatively small compared to the estimated potential production capability from low-cost resources. However, as the installed capacity grows, there is concern that annual demand could exceed supply if the natural uranium once-through cycle is retained indefinitely. There are several reasons why annual production capability, rather than quantity of uranium resources in the ground, could limit a rapidly expanding nuclear program. Apart from concerns of acquiring equipment, manpower and investment of capital, there are problems associated with developing sites in remote and hostile terrain. Changing regulating requirements to meet necessary safety standards at specific sites could delay the establishment of new production centers. It is, therefore, both in our

national interest and that of the world energy supply situation that the CANDU reactor system be developed for as high uranium utilization as possible.

The development of fuel conserving options which can be invoked without a change in reactor concept and supporting infrastructure would remove a major source of indecision on the part of utilities which face long lead times and major capital investments.

1.2 LIMITATIONS OF URANIUM AND THE LEU CYCLE

It is well accepted that nuclear power is expected to make a significant contribution to the total energy needs of mankind.

Although presently-known resources of uranium appear adequate to sustain the anticipated growth of nuclear power into the 1990's, two conditions must be fulfilled if uranium supplies are not to be limiting, either in the short or long term:

- There must be sufficient incentive to provide the basis for the necessary increase in production capacity; and

- There must be a continuing increase in the tempo of exploration activity to bring greater quantities of known resources and new discoveries into the "reserve" category, from which production is normally drawn.

Also, although there is a favourable prognosis for further uranium discovery, the need for nuclear power to serve as a major long-term source of energy implies a need for a reactor strategy that is viable by virtue of its efficient utilization of nuclear fuels. This signifies the earliest possible phasing out of today's converters in favour of advanced reactor systems. Advanced converters (including those using thorium) can do much to conserve uranium as compared to present light and heavy water reactors, but they, too, lead to depletion of

foreseeable resources. Only the fast breeder can essentially place an upper limit upon the amounts of uranium that may eventually be required. This makes the breeder of particular importance to countries that are neither endowed with uranium or conventional fuels, and of broad significance in the event that "inexhaustible" sources of energy do not become available by the turn of this century.

The transition from the present generation of nuclear reactors to advanced reactor systems poses, however, severe technological problems. Adequacy of fuel cycles, fuel processing, reactor technology, are but a few examples of technological areas that will require considerable work before society can base itself on a practically unlimited source of energy.

In the Canadian nuclear context, the use of the Low Enriched Uranium (LEU) fuel cycle as a stepping stone to an advanced fuel cycle is shown to have numerous advantages over proceeding directly from the natural uranium cycle to an advanced cycle. Technical expertise necessary for the introduction of any of the advanced cycles (to be discussed later) would be gained by first introducing the LEU cycle. Furthermore, utilizing the LEU cycles as an intermediate cycle would reduce the impact of fluctuating throughput rates on the secondary industries, as well as reduce annual and cumulative uranium requirements. Thus, the LEU cycle would facilitate the better commercialization of an advanced cycle. The physics of the LEU fuel cycle

will show in the following sections of this chapter that reduced fuel costs will be another most important advantage of this cycle.

1.3 SELECTION OF CANDU FUEL CYCLE

The CANDU PHW reactor is capable of operating with a wide range of fuel cycles, including the Low Enrichment Uranium, Mixed Oxide and a variety of thorium fuels, without radical design changes. It has also been estimated that the time to develop these options to commercial application will range from 15 to 20 years.

Clearly, there is a good deal of incentive to develop the fuel conserving options and demonstrate that advanced technologies will open the door to vast and untapped energy resources.

Considerable effort is being devoted to the study of advanced fuel cycles in various CANDU reactor types. The question of present study on alternate fuel cycles may be split into two categories:

a) the short-term prospects (next 20 years);

b) the long-term prospects.

The short-term prospects - During the next twenty years, Canada may install a large number of nuclear-electric generating units with a total capacity approaching 50,000 MW(e).

The prospect is that these will use extrapolation of current designs of natural heavy water reactors. This will not be

because of any doctrinaire adherence to natural uranium. Depending on the future course of enrichment and heavy water production costs, it could conceivably prove to be more economical to use some enrichment in heavy water reactors.

It is shown in this study that enrichment can be economically attractive, even in the assumption of purchasing enrichment sources abroad, so that for a long time there would be insufficient incentive to develop a domestic enrichment plant. In any event, it would take quite a few years before such plants and their economics are sufficiently proven to justify construction of one for the Canadian market. Overall, adherence to natural uranium will likely be predominant, and thus enrichment for the domestic market alone is likely to have little influence on the course of commercial installations over the next twenty years; since, however, a low enrichment is proven to have major savings on long-term prospects (Ref. 1, 2, 3, 4, 5), conversion of natural fuel design stations to low enriched fuel is a very attractive option whose feasibility is justified in this work.

In the long term, several factors combine to make evolution of the heavy water reactor to use other than natural uranium fuel desirable. The natural uranium heavy water reactor operating on a once-through fuel cycle requires almost as much uranium to be mined as the LWR (Light Water Reactor) operating on fuel recycle. If low enrichment uranium (1.2% enriched vs 0.71%

natural) is used, the energy extracted per kilogram of natural uranium mixed jumps from 7.5 MWd to 11.2 MWd, so that the requirement for raw uranium is halved. More significant for the long term, the heavy water reactor operating on the U233-thorium cycle could conceivably be developed to reduce uranium requirements by an order of magnitude.

With the passing of time and the growth of energy requirements, larger generating units will be required. Furthermore, nuclear units will supply an increasing fraction of the total energy and will, therefore, have to operate at lower capacity factors than today's units.

Both of these factors favour higher core power density which, in turn, favours fuels with higher than natural fissile content.

The incentives for more efficient use of resources and the requirements for more power-intensive designs therefore both invite development of systems employing fuels with higher than natural fissile content.

It is, however, important to consider that the introduction of new fuel cycles is not a simple matter. It should also be clear that, if new cycles are required to be introduced twenty years from now, a considerable amount of work must be done in advance to accommodate new nuclear fuel cycles.

CHAPTER TWO

2. NUCLEAR FUEL CYCLES: THEIR PHYSICS AND ECONOMICS

2.1 PHYSICS CONSIDERATIONS OF FERTILE AND FISSILE MATERIALS

Nuclear reactors produce power by "burning" fissile material. U-235 is the only naturally occurring fissile material. Large scale, commercial, electricity-generating nuclear power reactors extend the supply of fissile material by converting fertile material to fissile material. All types of commercial power reactors, both existing and potential, have this conversion feature.

There are two naturally occurring fertile materials: uranium U-238 and thorium Th-232. By far, the majority of current nuclear power stations use U-238 as the fertile material. In particular, this is the fertile material used in our CANDU power reactors, both PHW and BLW (Boiling Water Reactor).

The question naturally arises as to whether we should develop the option of using other types of fuel to feed the members of our CANDU family of power reactors.

The fissile and fertile isotopes U-235 and U-238 occur together in natural uranium in the ratio of 1:137.8. It so happens that with this ratio one can use natural uranium directly in a D_2O-moderated power reactor. (This option is not open if H_2O

is used as moderator, and is more difficult, although possible, with graphite. No fast reactor systems have this option.) Canada chose the option of using natural uranium in her CANDU systems initially, since this route does not involve expensive isotopic separation to increase the ratio of fissile to fertile material in the fuel or to separate the U-235 so that it can be combined with Th-232.

Fissile materials different from U-235 are produced in reactors. Fissile Pu-239 and Pu-241 are produced from U-238, and fissile U-233 comes from Th-232. Only chemical separation, not isotopic separation, is required to separate plutonium from uranium or uranium from thorium. Thus, once one has a reactor system to produce fissile material, it becomes possible to separate that fissile product from the fertile material by chemical separation means.

In particular, the plutonium produced in our CANDU power reactors can be separated from the spent fuel chemically. Once this is done, we obviously have the flexibility to choose with which fertile material to combine it.

It should also be pointed out that isotopic separation of uranium is now a routine process in the United States and elsewhere. A shortage of such separation will occur within a decade unless there is considerable expansion, and it seems clear that this will become a commercially competitive activity

involving several alternative sources of supply in the 1990's. Therefore, there is no a priori reason why systems using separated U-235 as the fissile feed with Th-232 as the fertile material and systems using enriched uranium (i.e., U-235 as the fissile feed with U-238 as the fertile material, but with a higher ratio of U-235 to U-238 than in natural uranium) should not also be considered for the future.

In this chapter, we outline the reason why the first fertile feed to be developed and exploited was U-238 (basically, because it is found in nature with the only naturally occurring fissile U-235), the basic difference between various fuel cycles, and a qualitative rationale for launching a program to develop the option of using low enriched uranium fuel cycle. Some quantitative aspects of this rationale will also be given in later sections.

The physics difference between U-238 and Th-238 in thermal reactors, as well as additional control and safety requirements introduced by thorium cycles and higher U-235 content in thorium and uranium fuel, are discussed in Appendix F.

2.2 INFLEXIBILITY OF NATURAL URANIUM

The energy derived per gram of U-235 fed to a CANDU-PHW reactor operating on a once-through cycle is shown in Figure 2.1 as a function of U-235 concentration in the feed uranium. Note that the energy derived per unit of fissile feed reaches a peak in the region of 1.7-1.8% U-235 in uranium. If natural uranium happened to have this isotopic composition, we would derive approximately 80% more energy from a given amount of U-235 using a once-through cycle in CANDU-PHW than we do now.

Therefore, even in heavy water moderated reactors operating on a once-through cycle, there is a basic incentive to enrich the uranium feed. The decision as to whether or not to do so is largely an economic factor. Figure 2.2 illustrates the effect of one economic factor. The enrichment process has an inefficiency associated with it since some U-235 is left in the tailings from the plant. For reasonable enrichment costs, the composition of the tails is in the range of 0.2-0.3% U-235 in uranium.

The curves of Figure 2.2 illustrate the effect of this inefficiency by displaying the energy derived from a once-through CANDU-PHW reactor fuel cycle per gram of U-235 mined as a function of enrichment of the feed for several values of the tails essay. Even here, the optimum overall basic efficiency

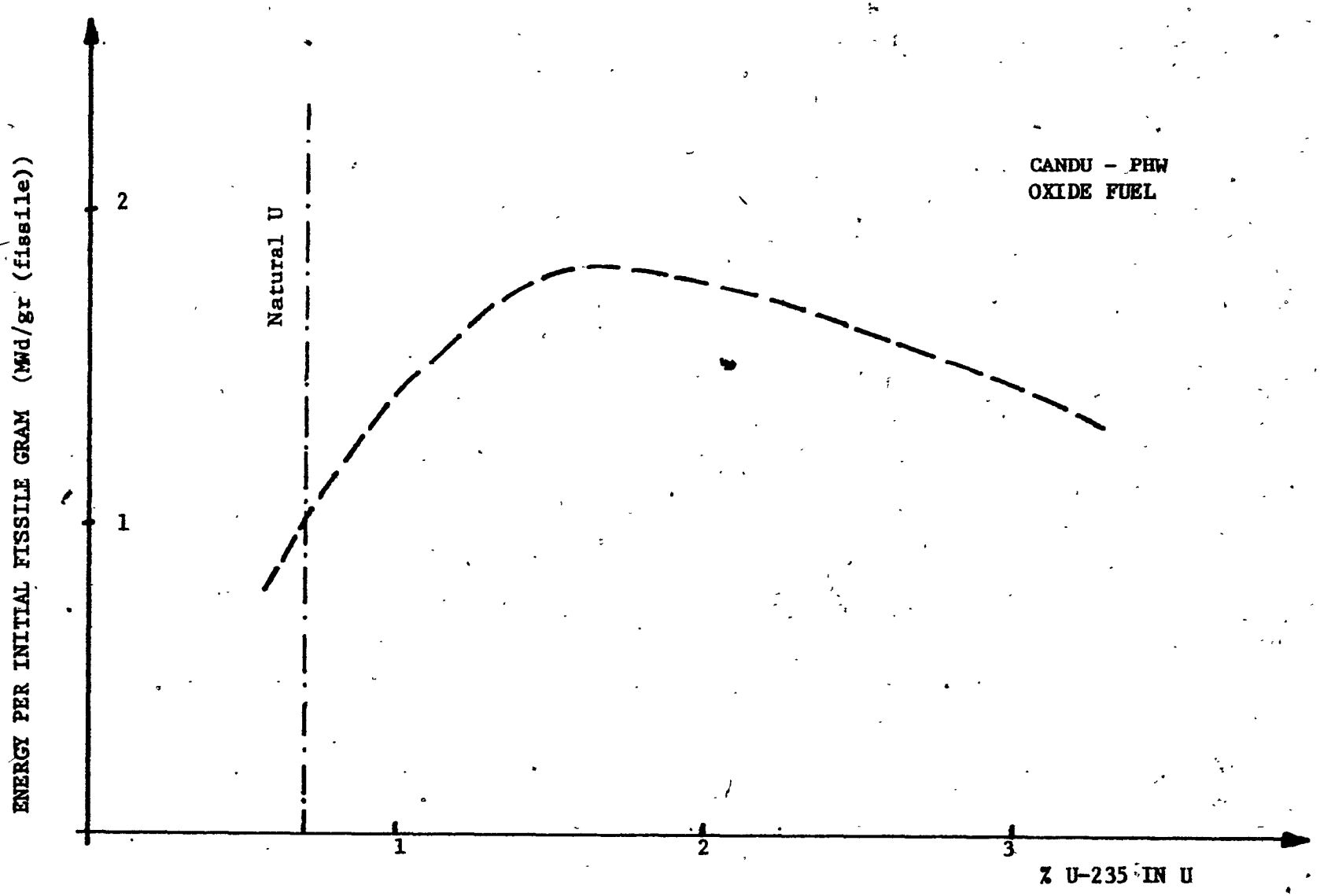

Figure 2.1: EFFICIENCY OF ONCE-THROUGH U-CYCLE VS U-235 IN U

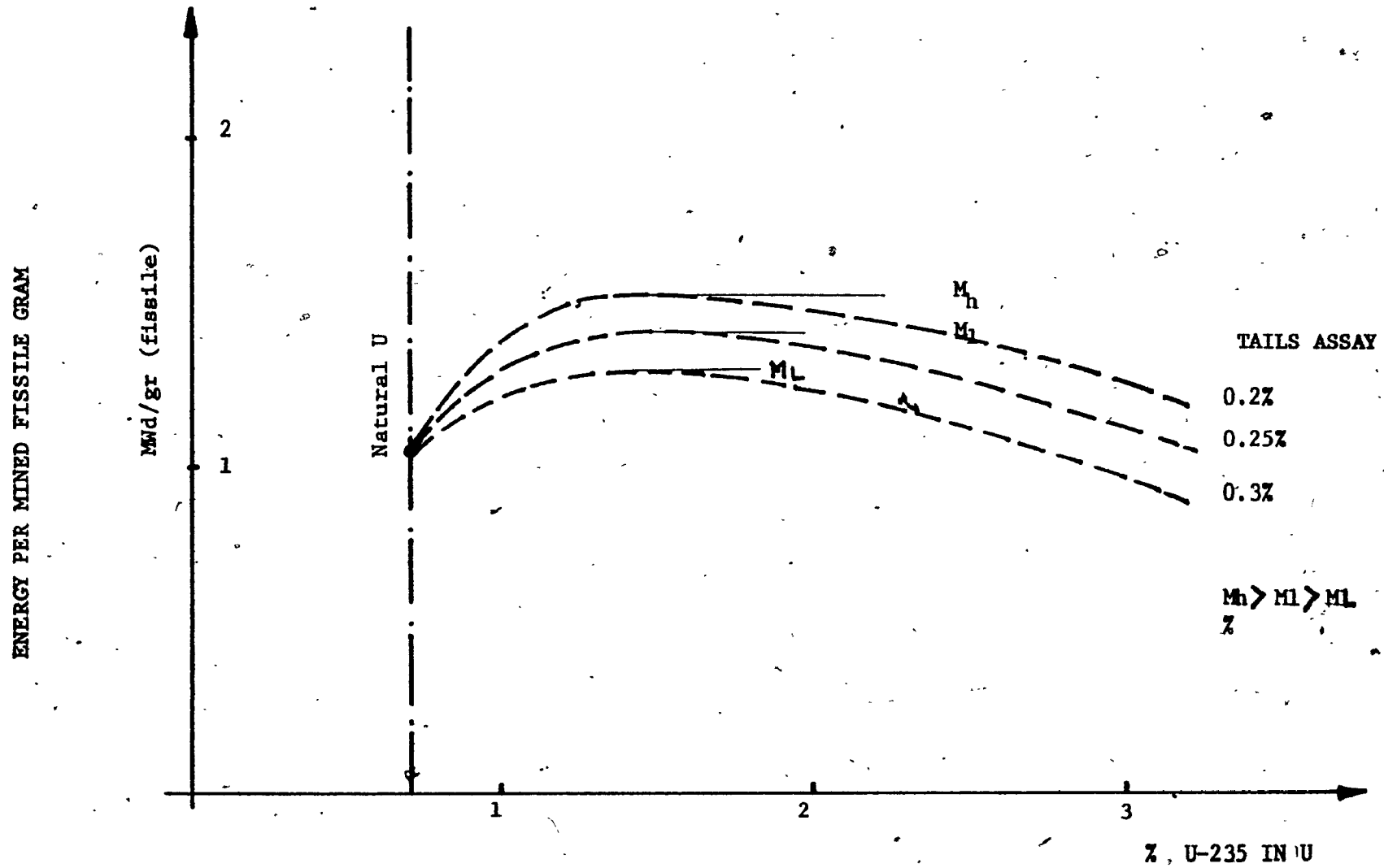

Figure 2.2: EFFICIENCY OF ONCE-THROUGH U-CYCLE CORRECTED FOR ENRICHMENT TAILS AS FUNCTION OF U-235 IN U

is obtained with low enrichment uranium in the region of 1.5% U-235 in uranium.

The maximum level of enrichment that was investigated for CANDU-PHW reactors was, however, only 1.2%. Overall basic efficiencies are not the only factors to be considered. Technical constraints associated with a given design of CANDU-PHW reactor limit the enrichment level. CANDU-PHW reactors are known to be natural uranium fuelled. It is, however, shown that technically enrichment of up to 1.2% is can be handled with present CANDU-PHW reactor designs.

2.3 ECONOMICS OF FUEL CYCLES

U-235 in the form of natural uranium is a relatively cheap fissile material. This is an extremely important factor in the comparison of U and other fuel cycles. Uranium cycles, in general, derive some advantages from the ability to use this cheap form of U-235.

Fissile plutonium may be cheaper than highly enriched uranium (say 90%), provided the cost of separating it from spent fuel is changed. Under these conditions, it tends to compete favourably in cost with U-235 in the low enrichment form. [Note that in the thorium cycle (see Appendix F) Pu would tend to be competing with highly enriched uranium whereas in the uranium cycle it can be thought of as competing with low enrichment uranium.]

In the last few years and, most likely, for the years to come, the price of yellowcake (U_3O_8) has experienced cost jumps of factors not less than 2 ($16/kg to $36/kg).

Figure 2.3 shows the price patterns of natural uranium, plutonium reprocessing costs and enriched uranium separation costs.

Fissile material costs have a direct bearing on fuel inventory costs. For CANDU reactors based on natural uranium fuel cycles the fuel inventory change is an almost negligible part of the

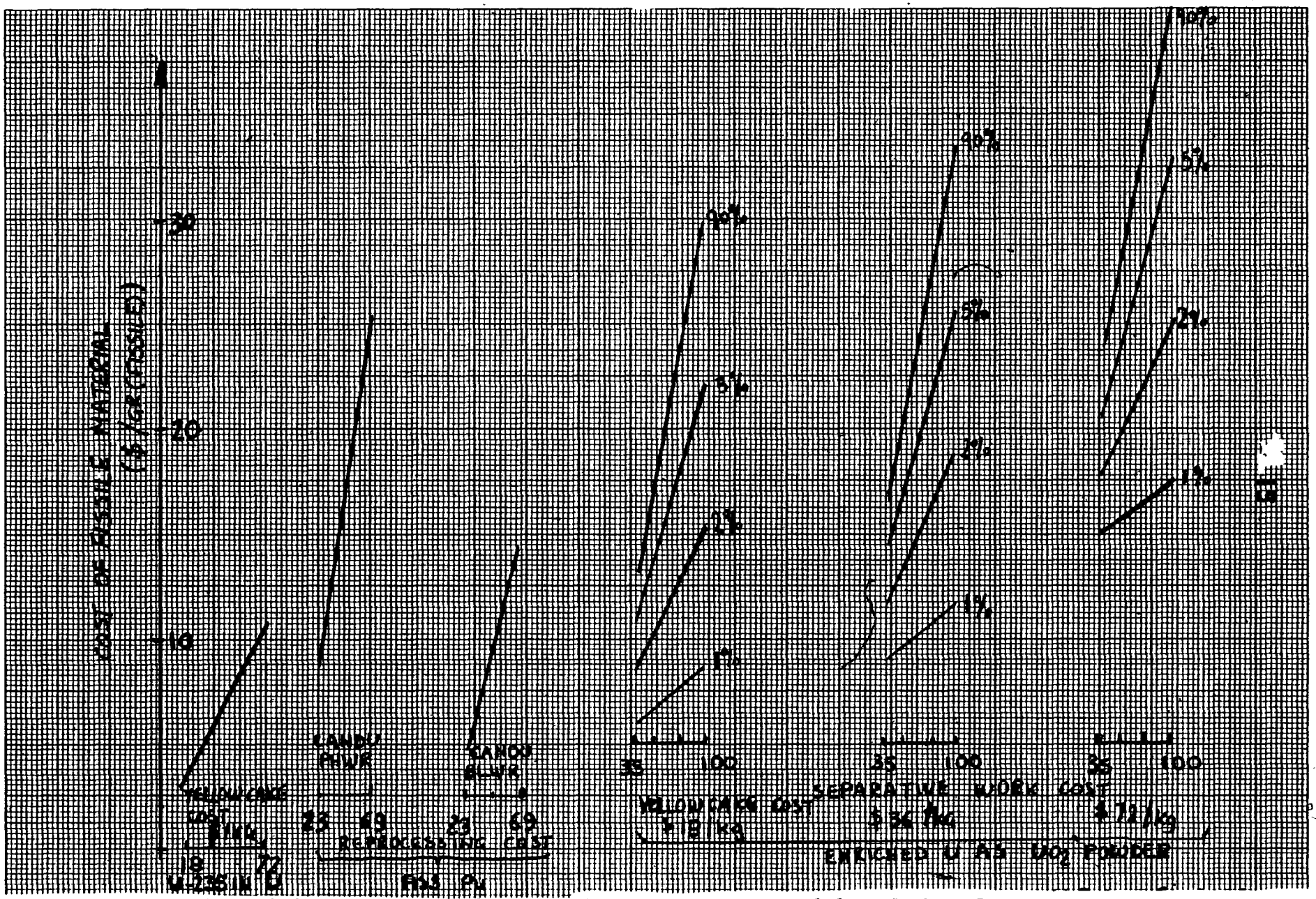

FIGURE 2.3: Cost of Fissile Material in Various Forms and from Various Sources

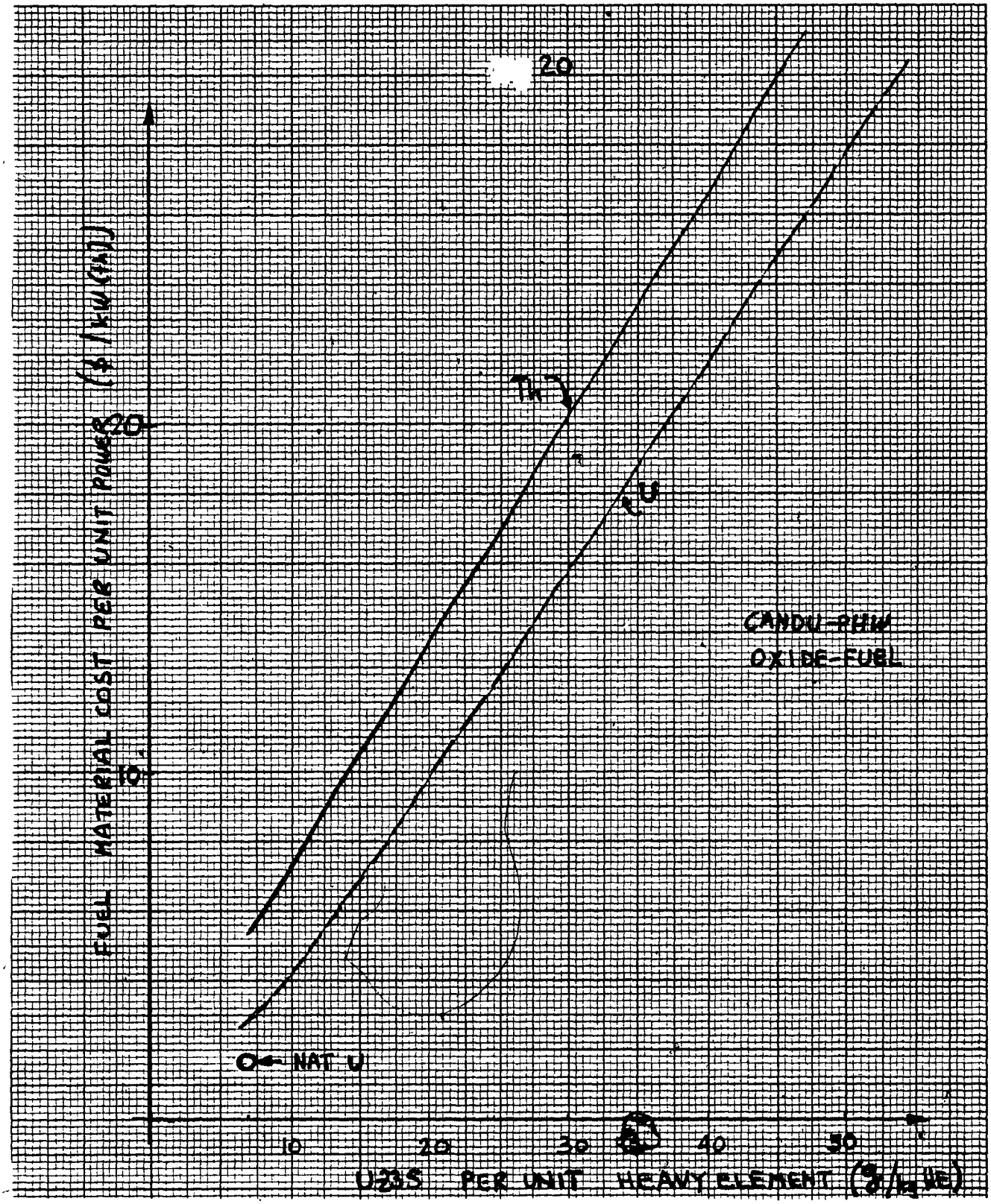

FIGURE 2.4: Cost of Fuel Material per Unit Power Capability

unit energy costs. Figure 2.4 shows how the value of fuel material inventory can change for full density fuel having high U-235 content. The fuel material cost per unit power capability climbs very rapidly with U-235 content. For cycles involving fuels with relatively high fissile contents, fuel inventory charges increase steeply and become a significant factor in the comparison of different concepts. Figure 2.8 illustrates qualitatively the fuel material cost per unit power versus U-235 per unit heavy element (g/kg HE). The figure shows that the thorium curve lies well above the uranium one. This is because highly enriched uranium is added to thorium whereas uranium, at relatively low enrichment, derives benefit from the relatively cheap U-235 in natural uranium.

2.4 FUTURE URANIUM REQUIREMENTS

2.4.1 Reactor Strategies

Adequacy in uranium supply should be given proper international attention if power supply stability, less economic impact and common peaceful nuclear energy objectivess are desired.

Although presently known resources of uranium appear adequate to sustain the anticipated growth of nuclear power into the 1990's, two conditions must be fulfilled if uranium supplies are not to be limiting, either in the short or long term. First, there must be sufficient incentive to provide the basis for the necessary increase in production capacity and, second, there must be a continuing increase in the tempo of exploration activity to bring greater quantities of known resources and new discoveries into the "reserve" category, from which production is normally drawn.

Nuclear fuel is not, however, the only deciding factor for a long-term source of energy. Early phasing out of present generation thermal reactors in favour of advanced reactor systems will be an even more important factor to contribute in limiting uranium requirements. Fast breeder reactors can essentially place an upper limit upon the amounts of uranium that may eventually be required. These reactors convert fertile material such as U-238 into fissile fuel such as Pu-239. This makes the breeder reactors of particular importance to countries that are

endowed with neither uranium nor conventional fuels, and of broad significance in the event that "inexhaustible" sources of energy do not become available by the turn of the century (Ref. 9).

2.4.2 CANDU-PHW Reactor Alternative Fuel Cycles

Many different fuel cycles could be used in fuelling each of the members of the CANDU family. Five fuel cycles are listed below. In the next section, considerable detail is given on what is considered the fuel cycle having the greatest potential, that is, the LEU cycle.

a) Once-Through Uranium Cycles (including both natural uranium and enriched uranium). Uranium is fabricated in either a natural or enriched form, used in a reactor, and the spent fuel stored.

b) Uranium Cycle with Plutonium Recycle. In the self-sufficient version, natural uranium is mixed with recycled Pu, fabricated into fuel, and irradiated in a reactor. The spent fuel is reprocessed and the separated Pu is added to more natural uranium, fabricated into fuel and the cycle repeated. Variations include a Pu-burning version in which additional Pu from an external source is added to the fuel in each cycle, and a Pu-producing version in which some of the recycled Pu is available for sale.

c) Once-Through (Th + U^{235}) Cycle. Highly enriched uranium (93%) is added to thorium. The mixture is fabricated into fuel and fed into a reactor. The spent fuel is stored.

d) The Thorium Cycle with U Recycle and Net U^{235} Feed. Highly enriched uranium (93%) is added to thorium along with recycled uranium. After fabrication, the fuel is used in a reactor. The spent fuel is reprocessed and the separated uranium is added to more thorium, plus highly enriched uranium, and the cycle is repeated.

e) The Thorium Cycle with U Recycle and Net Pu Feed. An external source of Pu takes the place of the U^{235} in the previous cycle. (Graphical representation of fuel cycles are provided in Appendix FC, Figures FC.1 through FC.5.)

2.4.3 Economic Considerations

The natural uranium supply may meet the growth rate of nuclear power demand from now until the turn of this century. However, it is not possible to confidently estimate the availability or price of uranium after the turn of the century. The uncertainty of an assumed long-term supply of low-cost uranium has led to consideration of uranium-conserving alternate fuel cycles for use in CANDU-PHWR's. Ontario Hydro has examined six fuel-cycle strategies discussed in the previous section. The Ontario government-owned utility has also examined the cycles

in terms of their uranium-conserving properties and their ease of commercialization for given growth rate of installed nuclear capacity in Ontario. The increasing worldwide demand for natural uranium will stimulate increased exploration, resulting in a continued uranium supply. It is likely that increasing mining costs and the need to exploit lower grade deposits will result in increasing uranium prices. The depletion of presently known low-cost resources, and the subsequent need to develop higher-cost resources, will result in uranium prices increasing with time. Advanced fuel cycles possess the potential to sharply reduce uranium consumption, thereby reducing the depletion of low-cost reserves. A suitable strategy of making a fuel cycle efficient for fuel consumption reduction would be the following:

1. Assume the continued use of the natural uranium fuel cycle up to the mid-1990's.

2. At that time, the low enriched uranium (LEU) cycle is gradually introduced into the existing power generation grid.

3. In the mid-2020's, one of the four advanced fuel cycles is introduced.

The use of the LEU fuel cycle as a stepping stone to an advanced fuel cycle is shown to have numerous advantages over

proceeding directly from a natural uranium cycle to an advanced cycle. Technical expertise necessary for the introduction of any of the advanced cycles would be gained by first introducing the LEU cycle. Furthermore, omitting the LEU cycle as an intermediate cycle would require more rapidly fluctuating throughout rates for the secondary industries, as well as higher annual and cumulative uranium requirements. Thus, in addition to reducing fuelling costs, the introduction of the LEU cycle would facilitate the later commercialization of an advanced fuel cycle (Ref. 10, 11, 12).

2.5 FUEL CYCLES - ECONOMIC ANALYSIS

Figure 2.5 illustrates the variation of equilibrium system economic efficiencies for "close-to-optimum" cases as a function of yellowcake cost for two values of reprocessing cost.

The once-through natural uranium cycle (average burnup of 7500 MWd/te) has been plotted with a solid line, and is useful as a reference for the other curves. The other curves correspond to:

a) A 1.2% enriched uranium once-through cycle with an average burnup of 20,800 MWd/te;

b) A uranium cycle with self-sustaining Pu recycle and average burnup of 18,000 MWd/te;

c) A thorium cycle with fissile Pu topping and uranium recycle (average burnup in Pu burner = 30,000 MWd/te) with fissile Pu supplied from a natural uranium PHW (average burnup: 7500 MWd/te);

d) A (Th + U-235) cycle with U recycle and an average burnup of 30,000 MWd/te;

e) A (Th + U-235) once-through cycle with an average burnup of 52,000 MWd/te.

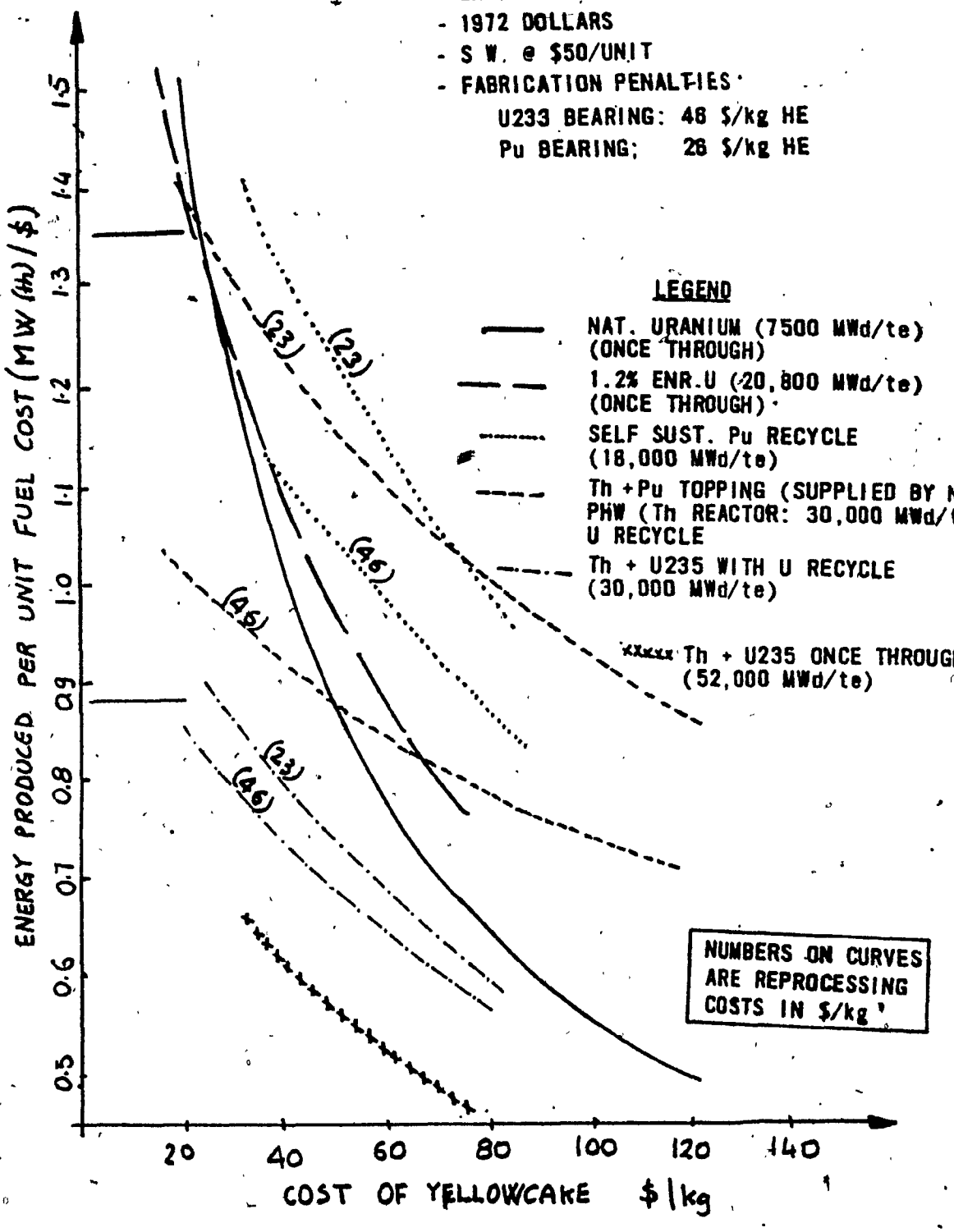

FIGURE 2.5: Comparison of Equilibrium Economic Efficiencies for Various Systems

The main points that can be drawn from Figure 2.9 are the following:

a) While the natural uranium cycle does seem to reign supreme at very low yellowcake price, other cycles start to become attractive at current yellowcake costs.

b) If reprocessing costs are low (i.e., $23/kg), the first cycle to compete favourably with natural uranium is the uranium cycle with Pu recycle, followed closely by the thorium system using Pu topping made in a natural PHW reactor. It can be seen qualitatively why the Pu recycle competes first. The advantages are lower fabrication penality, lower inventory charges, fewer natural PHW reactors to supply plutonium and, at this yellowcake cost, lower fissile material supply cost (i.e., the U-235 in natural uranium is cheaper than Pu). The only advantage which the thorium cycle has is the better physics.

c) At high reprocessing costs (i.e., $46/kg), the first cycle to compete with natural uranium cycle as yellowcake costs increase is the <u>enriched uranium</u> once-through cycle.

d) The once-through (Th + U-235) cycle does not seem attractive under any foreseeable circumstances.

e) The rate of decrease of economic efficiency with increasing yellowcake cost goes in the following order (highest to lowest):

- natural uranium once-through;
- enriched uranium once-through;
- U cycle with Pu recycle;
- Th cycles with U recycle.

f) If yellowcake prices continue to increase indefinitely, the thorium cycles with U recycle would eventually become the most attractive.

g) One further point is worth commenting on. If fissile Pu were available in unlimited amounts at the price assumed here (i.e., reprocessing cost), the curves for the thorium + Pu topping case would be horizontal lines at the positions shown by the bars at the left of the curves. This case, if reprocessing costs were low, would be an obvious choice at all yellowcake costs above about $35/kg U.

CHAPTER THREE

3. REACTOR CORE PHYSICS: SPATIAL KINETICS

3.1 INTRODUCTION

The critical condition (criticality) in a large thermal power reactor represents a delicate balance between the rates of two dynamic processes - the creation rate and destruction rate of the neutron population. In a reactor operating at about 3000 MW(th), for example, there are about 2.2×10^{20} neutrons created per second and 2.2×10^{20} neutrons destroyed. The average lifetime of these neutrons lies in the range of 10^{-7} to 10^{-4} seconds, depending on the type of reactor. It follows that, if the production rate were to exceed the destruction rate by one part in a thousand for one second with the average neutron lifetime of, say, 5×10^{-5} seconds, the power level at the end of that second would increase by a factor of approximately $(1.001)\exp(1/5 \times 10^{-5}) = 4.8 \times 10^{8}$. At that instant the reactor, if it were still in one piece - which it would not be - would be producing around a quarter of a ton of neutrons per second (and absorbing all but one part in a thousand of them).

All the above, fortunately, does not normally happen; in particular, a 0.1% excess production of neutrons is "felt" by the reactor with an effective delay of about 0.08 seconds, because about 0.5% of neutrons (i.e., more than the excess) are

produced with roughly that delay. This implies that the 1-second runaway would increase the power by a factor of

$$1.001 \exp (1/0.08) = 1.01257$$

On top of that, of course, the control and safety systems have response times easily below one second, so their intervention is very effective. Also, the intrinsic physics is such that a negative feedback on neutron production is normally caused by increased power.

Nevertheless, predicting the spatial distribution of neutron flux and balancing the neutron creation and destruction rates in a core of a CANDU-PHW reactor is still a delicate matter and the study of how such a balance is re-established when it is disturbed is quite important. Reactor kinetics is the area of reactor physics concerned with predicting what happens to the neutron flux density (r,E,t) when the balance condition associated with the critical state is disturbed. More generally, it concerns the space-time-energy behaviour of the neutron population density in a material array.

A number of computer codes are presently used within Ontario-Hydro and other related organizations for this purpose. Common to these codes is a two-energy group diffusion theory representation of the neutron flux, coupled with a finite-difference

iterative numerical scheme for solving the diffusion equation in three dimensions (3-D).

Despite representing the most rigorous calculational tool, a finite-difference is relatively expensive to run for realistic three-dimensional reactor models [e.g. the simulation of the first 2.5 seconds after a major LOCA (Loss of Coolant Accident) in a Bruce-A reactor costs a few thousand dollars].

The costs may limit the usefulness of these codes if many space-time-dependent transient simulations are required. An alternate approach which has proven to be very satisfactory in treating space-time kinetics and at the same time offers major computer cost savings is the Spatial-MOdal KINetics (SMOKIN) formulation which will be described in detail in Chapter Four. However, before the formulation of SMOKIN is presented, an outline of the necessity of this technique with respect to reactor kinetics is presented (Ref. 13).

3.2 CANDU-PHW REACTOR UNIT CELL

In a power reactor, fuel is contained in "fuel channels" or "fuel assemblies" which are cooled by a coolant and embedded in a neutron-slowing-down material called moderator. In some reactors (LWR) coolant and moderator may coincide. At any rate, the resulting core configuration is, over at least large portions of the core, a repetitive "lattice" array of such fuel channels. Every core fraction composed of a fuel channel and its share of the surrounding moderator is called a "lattice cell", and is normally highly heterogeneous. The heterogeneity of a CANDU-PHW reactor is better appreciated when we consider that in a unit cell (Figure 3.1) we can identify:

- moderator;
- fuel;
- structural material;
- coolant.

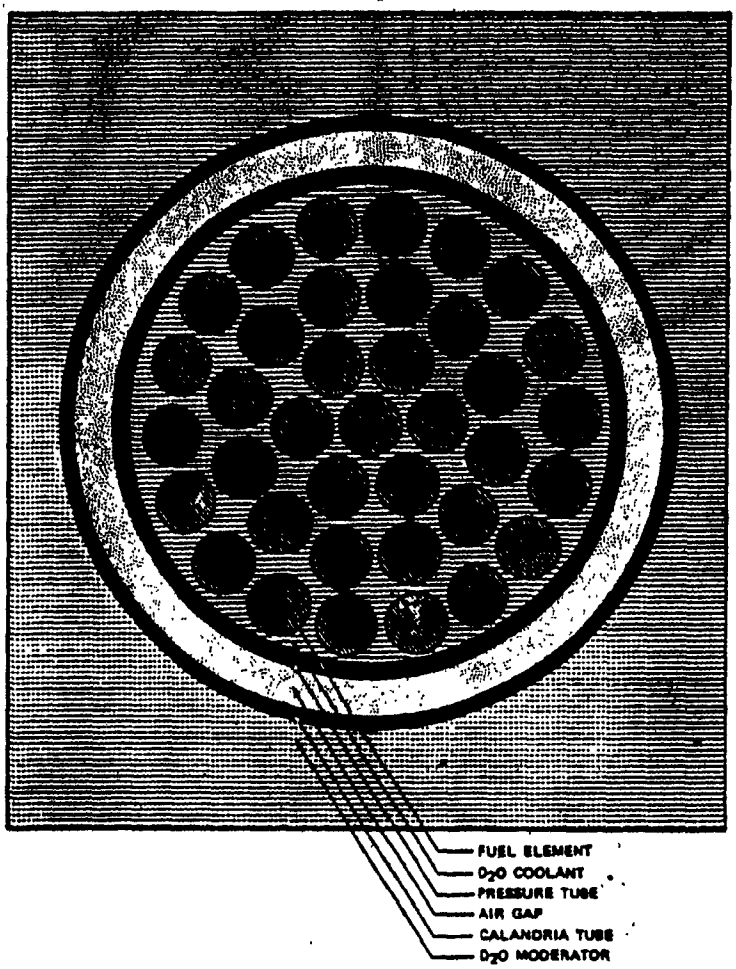

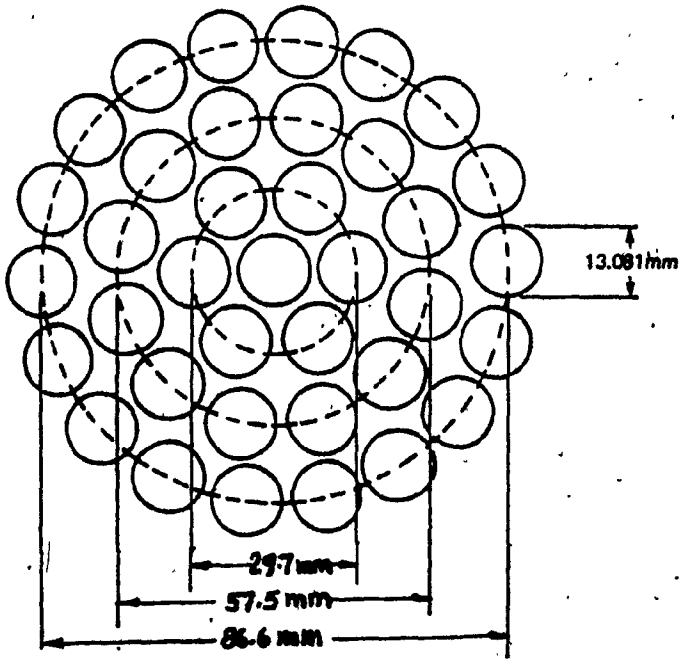

FIGURE 3.1: 37-Element Fuel Unit Cell

3.3 THE NEUTRON CYCLE IN A THERMAL REACTOR

Nuclear reactors are usually designed to balance the neutron absorption and leakage with the rate of fission neutron production. When the net rate of neutron production in the reactor equals the rate of neutron loss (absorption plus capture) in the reactor, we usually say that the reactor is critical.

The criticality conditions are usually expressed in terms of a factor labelled "k" and, depending on the value of k, we have:

supercritical - critical - subcritical

conditions for $k > 1$, $k = 1$, $k < 1$, respectively. In order to calculate k, we must determine the fate of neutrons in a given fission generation. Fortunately, this is rather easy to do since there are only two possible alternative destinies available to the neutron. Production, capture and leakages are shown graphically in Figure 3.2.

From Figure 3.2 we are able to describe and summarize the following parameters:

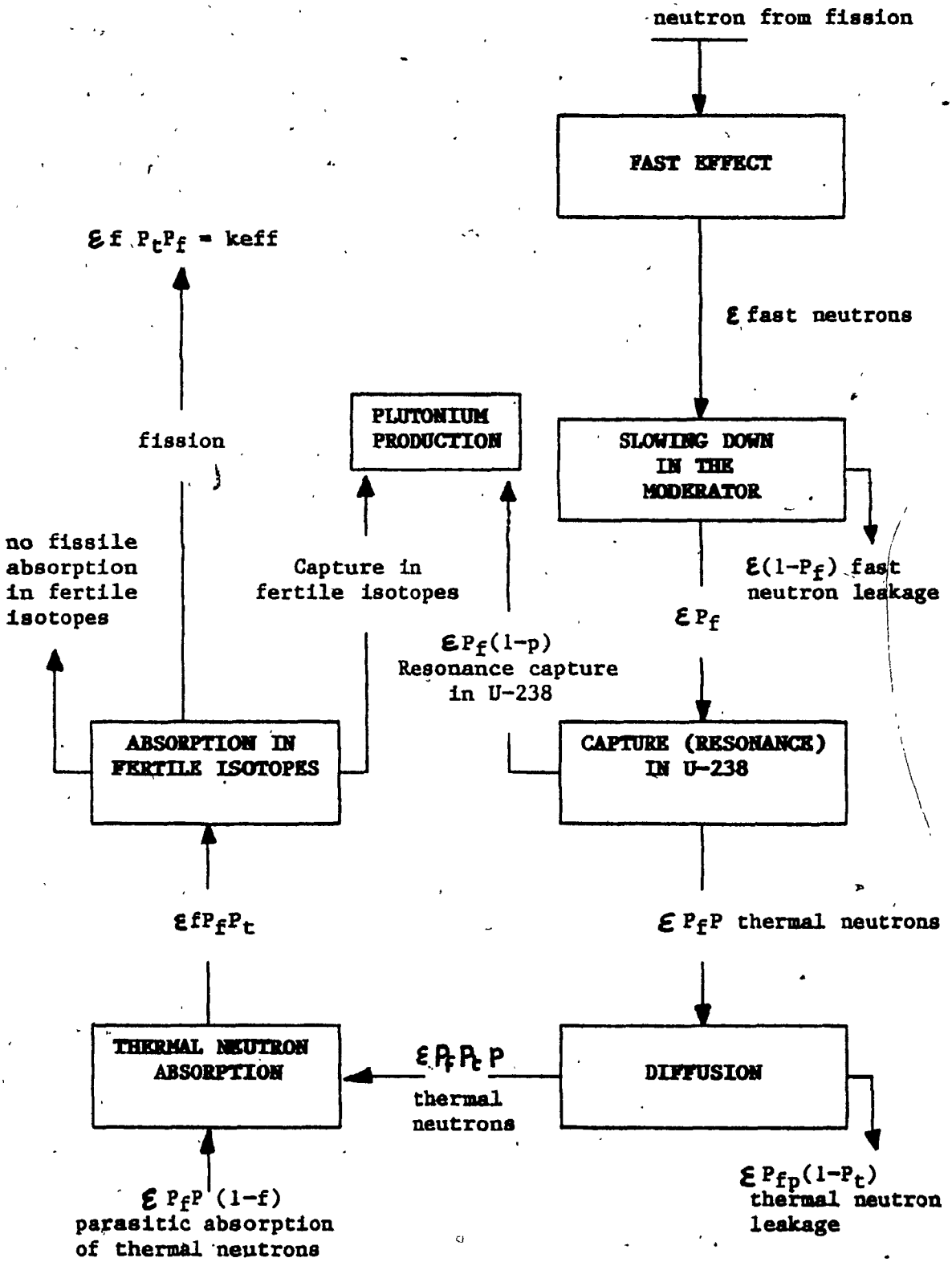

FIGURE 3.2: Neutron Cycle in Fission Process

In the neutron cycles, we define the parameters as follows:

P : Fraction of fission neutrons that manage to slow down from fission to thermal energies without being absorbed.

ε : $\dfrac{\text{Total number of fission neutrons (both from fast and thermal fission)}}{\text{Number of fission neutrons from thermal fission}}$

f : Thermal utilization factor

$$= \frac{\text{Absorption rate in fuel material (e.g. } UO_2)}{\text{Absorption rate in core materials (defined for the lattice cell)}}$$

η : Number of fission neutrons produced per absorption in the fuel.

$$= \nu \frac{\sigma_f^F}{\sigma_a^F}$$

ν : Number of neutrons per fission (as usual).

Suppose now that we deal with a reactor of infinite extent. Then, since no neutrons can leak out, we can write a non-leakage probability $P_{NL} = 1$. Therefore, for a non-leaking system, the multiplication factor is readily written (for one initial neutron):

$$k = \eta f \varepsilon p \qquad \text{Eq. 3.1}$$

Now, of course, no reactor is of infinite size. Nevertheless, koo is a useful parameter in reactor analysis since it essentially characterizes the multiplication properties of the material in the reactor, as distinct from the geometry of the reactor core. Of course, since $P_{NL} < 1$, more generally for a finite reactor from which some neutron leakage can occur, we must have $k_{oo} > 0$ in order to have any chance of achieving a critical chain reaction. In thermal reactors with neutrons born at high energies and slowed down to thermal regions, two distinct non-leakage probabilities are considered to account for fast neutron leakages and thermal neutron leakages.

We can then readily write (Ref. 6) the four-factor and the six-factor expression for koo and keff respectively:

$$k_\infty = \eta f p \varepsilon \qquad \text{Eq. 3.2}$$

$$k = \eta f p \varepsilon P_f P_t \qquad \text{Eq. 3.3}$$

The expression provided by Equation 6.3 is also often written as:

$$keff = k_\infty P_f P_t \qquad \text{Eq. 3.4}$$

3.4 TWO-GROUP CONSTANTS

Every lattice cell is characterized by two group diffusion parameters which actually represent the heterogeneous cell by its equivalent homogenized cell, i.e. a homogeneous cell with some average reaction rates, group fluxes, leakage rates.

The two-group diffusion theory model can be used to demonstrate a number of the various applications of the multigroup formalism (Appendix MG). For example, one frequently wishes to generate group constants for a few-group calculation using the neutron spectrum generated by a many-group calculation. Such a procedure is known as group collapsing, since it expresses few-group constants in terms of many-group constants.

For example, we can derive the expressions for the two-group multiplication constants k_1 and k_2 in terms of two-group constants.

We start by identifying E_2, E_1 and E_o representing the energy boundaries for a two-group model as depicted below:

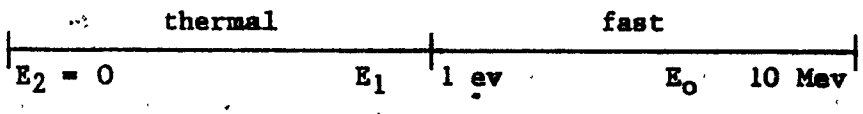

The fluxes in the two groups are defined as follows:

$$\phi_1(\vec{r},t) = \int_{E_1}^{E_0} dE\, \phi(\vec{r},E,t) \equiv \text{fast flux} \qquad \text{Eq. 3.5}$$

$$\phi_2(\vec{r},t) = \int_{E_2}^{E_1} dE\, \phi(\vec{r},E,t) \equiv \text{thermal flux} \qquad \text{Eq. 3.5a}$$

Now we rewrite here for convenience the two-group generalized equation from Appendix MG (superscript k is removed):

$$-D_1\nabla^2\phi_1(\vec{r}) + \Sigma_1\phi_1(\vec{r}) = \frac{1}{k}\chi_1\left[\nu\Sigma_{f1}\phi_1 + \nu\Sigma_{f2}\phi_2\right] \qquad \text{Eq. 3.6}$$

$$-D_2\nabla^2\phi_2(\vec{r}) + \Sigma_2\phi_2(\vec{r}) = \frac{1}{k}\chi_2\left[\nu\Sigma_{f1}\phi_1 + \nu\Sigma_{f2}\phi_2\right] + \Sigma_{12}\phi_1(\vec{r}) \qquad \text{Eq. 3.7}$$

and making the assumptions that:

$$\chi_1 = \int_{E_1}^{E_2} dE\, \chi(E) = 1 \qquad \text{Eq. 3.8}$$

$$\chi_2 = \int_{E_2}^{E_1} dE\, \chi(E) = 0 \qquad \text{Eq. 3.9}$$

i.e., fission source will only appear in the fast group equation:

$$S_{f1} = \nu\Sigma_{f1}\phi_1(\vec{r}) + \nu\Sigma_{f2}\phi_2(\vec{r}) \qquad \text{Eq. 3.10}$$

$$S_{f2} = 0 \qquad \text{Eq. 3.11}$$

Hence, we can write the simplified two-group diffusion equation as:

$$-D_1\nabla^2\phi_1(\vec{r}) + \Sigma_1\phi_1(\vec{r}) = \chi_1\frac{1}{k}\left[\nu\Sigma_{f1}\phi_1 + \nu\Sigma_{f2}\phi_2\right] \quad \text{Eq. 3.12}$$

$$-D_2\nabla^2\phi_2(\vec{r}) + \Sigma_2\phi_2(\vec{r}) = \Sigma_{12}\phi_{12}(\vec{r}) \quad \text{Eq. 3.12a}$$

Assuming that both fast and thermal fluxes can be characterized by the same spatial shape $\Psi(r)$:

$$\nabla^2\Psi(\vec{r}) + B^2\Psi(\vec{r}) = 0\,; \quad \Psi(\vec{r}_s) = 0 \quad \text{Eq. 3.13}$$

where B^2 is designated as geometric buckling and represents a curvature of the flux shape and is defined as:

$$B^2 = -\frac{1}{\Psi}\frac{d^2\Psi(\vec{r})}{dx^2} \quad \text{Eq. 3.14}$$

Substitution of B^2 and

$$\phi_1(\vec{r}) = \phi_1\Psi(\vec{r}) \quad \text{Eq. 3.15}$$

$$\phi_2(\vec{r}) = \phi_2\Psi(\vec{r}) \quad \text{Eq. 3.16}$$

into Equations 3.12 and 3.12a will give us:

$$\left[D_1B^2 + \Sigma_1 - k^{-1}\nu\Sigma_{f1}\right]\phi_1 - k^{-1}\nu\Sigma_{f2}\phi_2 = 0 \quad \text{Eq. 3.17}$$

$$-\Sigma_{12}\phi_1 + (D_2B^2 + \Sigma_{12})\phi_2 = 0 \quad \text{Eq. 3.18}$$

The set of Equations 3.17 and 3.18 has solution if and only if:

$$(D_1B^2+\Sigma_1 - k^{-1}\nu\Sigma_{f1})(D_2B^2+\Sigma_{a2}) - \frac{\nu_2\Sigma_{f2}\Sigma_{12}}{k} = 0 \qquad \text{Eq. 3.19}$$

We can now solve for the value of the multiplication factor k, which will yield a non-trivial solution of the two-group equations:

$$k = \frac{\nu_1\Sigma_{f1}}{\Sigma_1 + D_1B^2} + \frac{\Sigma_{12}}{\Sigma_1 + D_1B^2}\cdot\frac{\nu_2\Sigma_{f2}}{\Sigma_{a2} + D_2B^2} \qquad \text{Eq. 3.20}$$

The first term of Equation 3.20 represents neutron multiplication due to fission occurring in the fast group, whereas the second term represents multiplication due to thermal fission. Since we expect the thermal fission contribution to be dominant in those situations in which such a two-group makes sense, let us first examine:

$$k_2 = \frac{\Sigma_{12}}{\Sigma_1 + D_1B^2}\,\frac{\nu_2\Sigma_{f2}}{\Sigma_{a2} + D_2B^2}$$

$$= \frac{\Sigma_{12}/\Sigma_1}{1 + L_1^2B^2}\,\frac{\nu\Sigma_{f2}/\Sigma_{a2}}{1 + L_2^2B^2}$$

$$= \frac{\Sigma_{12}}{\Sigma_1}\cdot\frac{\nu_2\Sigma_{f2}}{\Sigma_{a2}}\cdot P_{NL1}\cdot P_{NL2} \qquad \text{Eq. 3.21}$$

where:

$$P_{NL1} = \frac{1}{1 + L_1^2 B^2} \equiv \text{fast non-leakage probability} \qquad \text{Eq. 3.22}$$

$$P_{NL2} = \frac{1}{1 + L_2^2 B^2} \equiv \text{thermal non-leakage probability} \qquad \text{Eq. 3.23}$$

With the support of the previous section, we write an expression for k_2 as:

$$k_2 = \eta_2 f_2 p P_{NL1} P_{NL2} \qquad \text{Eq. 3.24}$$

In a very similar manner we can identify the fast multiplication factor as:

$$k_1 = \frac{\nu_1 \Sigma_{f1}}{1 + L_1^2 B^2} \eta_1 f_1 P_{NL1} \qquad \text{Eq. 3.25}$$

where:

$$\eta_1 = \frac{\nu_1 \Sigma_{f1}}{\Sigma_1^F} \qquad \text{Eq. 3.26}$$

and it is added the "fast utilization factor":

$$f_1 = \frac{\Sigma_1^F}{\Sigma_1} \qquad \text{Eq. 3.27}$$

In order to express k in the conventional six-factor formula, we evidently must identify the fast fission factor ε as just:

$$\varepsilon = \left(1 + \frac{k_1}{k_2}\right) = \left[1 + \left(\frac{\nu_1 \Sigma_{f1}}{\nu_2 \Sigma_{f2}}\right)\left(\frac{\Sigma_{a2} + D_2 B^2}{\Sigma_{12}}\right)\right] \qquad \text{Eq. 3.28}$$

Then we find:

$$k = k_1 + k_2 = \varepsilon k_2 = \eta_2 f_2 P \varepsilon P_{NL1} P_{NL2} \qquad \text{Eq. 3.29}$$

which is the usual six-factor formula. Normally, however, ε is calculated in ∞ lattice, with $B^2 = 0$, in Eq. 3.28.

In a similar fashion, we can derive expressions for the one-group constants in terms of two-group constants. For example:

$$\Sigma_a = \frac{\int_{E_2}^{E_0} dE \Sigma_a(E)\phi(E)}{\int_{E_2}^{E_0} dE\, \phi(E)} = \frac{\int_{E_1}^{E_0} dE \Sigma_a(E)\phi(E) + \int_{E_2}^{E_1} dE \Sigma_a(E)\phi(E)}{\int_{E_1}^{E_0} dE \phi(E) + \int_{E_2}^{E_1} dE \phi(E)}$$

$$= \frac{\Sigma_1 \phi_1 + \Sigma_{a2}\phi_2 + \Sigma_{12}\phi_1}{\phi_1 + \phi_2} \qquad \text{Eq. 3.30}$$

or using Equations 3.17 and 3.18 to eliminate ϕ_2 in terms of ϕ_1:

$$\Sigma_a = \frac{(\Sigma_1 + \Sigma_{12})(D_2 B^2 + \Sigma_{a2}) + \Sigma_{a2}\Sigma_{12}}{D_2 B^2 + \Sigma_{a2} + \Sigma_{12}} \qquad \text{Eq. 3.31}$$

The remaining one-group constants can be written as:

$$D = \frac{D_1 \phi_1 + D_2 \phi_2}{\phi_1 + \phi_2} = \frac{(D_2 B^2 + \Sigma_{a2}) D_1 + \Sigma_{12} D_2}{D_2 B^2 + \Sigma_{a2} + \Sigma_{12}} \qquad \text{Eq. 3.32}$$

$$\nu\Sigma_f = \frac{\nu_1 \Sigma_{f1} \phi_1 + \nu_2 \Sigma_{f2} \phi_2}{\phi_1 + \phi_2} = \frac{(D_2 B^2 + \Sigma_{a2}) \nu\Sigma_{f1} + \nu_2 \Sigma_{12} \Sigma_{f2}}{D_2 B^2 + \Sigma_{a2} + \Sigma_{12}} \qquad \text{Eq. 3.33}$$

In order to complete this review of diffusion constants, we define the so-called migration area M^2 as:

$$M^2 = \frac{D_2}{\Sigma_{a2}} + \frac{D_1}{\Sigma_{a1} + \Sigma_{12}} \qquad \text{Eq. 3.34}$$

3.5 PRINCIPLE OF CELL AVERAGE TECHNIQUES

In order to perform core analysis, we need to calculate effective group constants that are spatially averaged over flux distribution in a lattice cell and, therefore, can be used to characterize the cell in subsequent multigroup diffusion calculations in which the cell structure is ignored. To discuss this subject of cell averaging in more detail, let us consider the calculation of the cell-averaged group constant characterizing a two-region cell (partial cell of Figure 3.2) in which material composition is uniform in each region. Consider these two regions to be the moderator and the fuel denoted by M and F respectively.

The cell-averaged group constants characterizing a general cross-section would then be defined as:

$$\langle \Sigma_g \rangle_{CELL} = \frac{\int_{E_g}^{E_{g-1}} dE \int_{CELL} dV \, \Sigma(\bar{r},E)\,\phi(\bar{r},E)}{\int_{E_g}^{E_{g-1}} dE \int_{CELL} dV \, \phi(\bar{r},E)} \qquad \text{Eq. 3.35}$$

If we assume that the cross-section $\Sigma(r,E)$ is constant within each region and we define the cell-averaged intrafluxes as:

$$\bar{\phi}_M(E) = \frac{1}{V_M} \int_{V_M} dV \, \phi(\bar{r},E) \qquad \text{Eq. 3.36}$$

$$\bar{\phi}_F(E) = \frac{1}{V_F} \int_{V_F} dV \, \phi(\bar{r},E) \qquad \text{Eq. 3.37}$$

we can rewrite $\langle \Sigma_g \rangle_{cell}$ as:

$$\langle \Sigma_g \rangle_{CELL} = \frac{V_M \int_{E_g}^{E_{g-1}} dE\, \Sigma^M(E) \bar{\Phi}_M(E) + V_F \int_{E_g}^{E_{g-1}} dE\, \Sigma^F(E) \bar{\Phi}_F(E)}{V_M \int_{E_g}^{E_{g-1}} dE\, \bar{\Phi}_M(E) + V_F \int_{E_g}^{E_{g-1}} dE\, \bar{\Phi}_F(E)} \qquad \text{Eq. 3.38}$$

Now, if in fact the neutron flux in the cell were separable in space and energy such that:

$$\phi(\bar{r}, E) = \phi(\bar{r})\, \psi(E) \qquad \text{Eq. 3.39}$$

that is, if both regions of the cell were characterized by the same intragroup spectrum, then one could collapse Equation 3.38 to:

$$\langle \Sigma_g \rangle_{CELL} = \frac{V_M \Sigma_g^M \bar{\Phi}_M + V_F \Sigma_g^F \bar{\Phi}_F}{V_M \bar{\Phi}_M + V_F \bar{\Phi}_F}$$

$$\pm \frac{\Sigma_g^F + \Sigma_g^M (V_M / V_F)\}}{1 + (V_M / V_F)\}} \qquad \text{Eq. 3.40}$$

where the regionwise group constants are defined as:

$$\Sigma_g^F = \int_{E_g}^{E_{g-1}} dE\, \Sigma^F(E)\, \psi(E) \Big/ \int_{E_g}^{E_{g-1}} dE\, \psi(E) \qquad \text{Eq. 3.41}$$

$$\Sigma_g^M = \int_{E_g}^{E_g} dE\, \Sigma^M(E) \psi(E) \Big/ \int_{E_g}^{E_{g-1}} dE\, \psi(E) \qquad \text{Eq. 3.42}$$

while the spatial flux averages are defined as:

$$\bar{\phi}_M = \frac{1}{V_M} \int_{V_M} dV\, \phi(\bar{r}) \qquad \text{Eq. 3.43}$$

$$\bar{\phi}_F = \frac{1}{V_F} \int_{V_F} dV\, \phi(\bar{r}) \qquad \text{Eq. 3.44}$$

and the cell disadvantage factor is defined as:

$$\xi = \frac{\bar{\phi}_M}{\bar{\phi}_F} \qquad \text{Eq. 3.45}$$

For thermal neutrons, the thermal utilization factor can be written as follows:

$$f = \frac{\Sigma_a^F \bar{\phi}_F V_F}{\Sigma_a^F \bar{\phi}_F V_F + \Sigma_a^M \bar{\phi}_M V_M}$$

$$= \frac{1}{1 + \frac{\Sigma_a^M}{\Sigma_a^F} \frac{V_M}{V_F} \xi}$$

3.6 THE SPATIAL KINETICS PROBLEM IN NUCLEAR REACTORS

Prediction of the space-time kinetics of a nuclear reactor requires the solution of a set of partial differential equations which describe the variation of the neutron flux, delayed neutron precursors, iodine I-135 and xenon Xe-135 concentration in both space and time. Ideally, the neutron flux is also a function of neutron energy. However, the approximation is made that the neutron flux is well described by a one-group diffusion equation for thermal energy neutrons, plus one group of fast neutrons. Approximate solution methods for space-time nuclear reactor dynamics are discussed in References 14, 15, 16.

There is more than one method of attacking the space-time problem in nuclear reactors.

There are the finite-difference, the nodal and the modal or synthesis techniques. The finite differences and the nodal techniques are mathematically similar but differ as to the spatial scale to which they are applied. A sub-region of the reactor is recognized and identified with a mesh point. The partial differential equations are replaced by ordinary differential equations (with respect to the time variable) at each mesh point. The coupling between adjacent sub-regions is achieved by requiring continuity of neutron current at the

interfacial boundaries of the sub-regions. The synthesis technique (Ref. 13) involves expressing the space-time dependent variables of the reactor dynamics equations set in terms of a finite sum of products of shape functions and corresponding amplitude functions. The shape function can be space-time dependent or space dependent only, while the amplitude functions are functions of time only. For CANDU-PHW reactors, space-time problems are most often investigated by using the modal technique approximation which has the potential for accurate and low-cost solution to nuclear reactor transients. Reference calculations, however, are done using a special "synthesis" technique in which one time-dependent shape function is generated along with one amplitude function (Improved Quasi Static Method).

3.7 REACTOR PHYSICS ASPECTS OF SPATIAL POWER CONTROL

A useful parameter for assessing the effective size of a reactor core is the neutron migration length M, a measure of the average distance travelled by a neutron from its appearance as a fission neutron to its absorption as a thermal neutron. For a given design, such as a CANDU-PHW with natural uranium fuel, M is determined by the material composition of the reactor core, primarily the fuel-to-moderator ratio, and is essentially independent of core size.

As the reactor core size increases, the migration length becomes a smaller fraction of the core dimensions. Thus, each neutron's zone of influence becomes a smaller fraction of the core volume, and the various reactor core regions become less tightly coupled. The size of CANDU core radii R have increased by more than a factor of two from NPD (R 170 cm) to Bruce or Darlington (R 400 cm). The migration length M for neutrons in most CANDU reactors is approximately 19 cm, therefore reactor core radii have increased from the order of 9 M to approximately 21-22 M.

The need for spatial flux control in a reactor may also be assessed by employing what is called "modal analysis", whereby the neutron flux distribution in an idealized cylindrical reactor is described in terms of cosine functions azimuthally and axially, and Bessel functions radially. Spatial perturbations,

transients and oscillations of the neutron flux can be described by a superposition of the fundamental modes and higher harmonics of these functions. The most important of these higher order modes in a typical CANDU-PHW reactor (Darlington, for example) are shown schematically in Figure 3.2a.

A subcritical reactivity is associated with each of these higher order modes as is used to assess its importance from a spatial control point of view. This modal reactivity can be thought of as a measure of the susceptibility of the reactor to flux shape disturbances which include the particular mode shape.

Large CANDU-PHW reactors have been found to be most susceptible to first azimuthal or side-to-side flux disturbances (flux tilts). It is also well recognized that the newer generation of CANDU-PHW reactors (large-scale) has a narrower stability margin as the result of the increased size and greater flattening of the core power distribution. Flattening the power distribution reduces the stability margins since the neutron behaviour in a "flattened" reactor is equivalent to that in a larger, unflattened reactor. These effects are illustrated in Table 3.1, where the first azimuthal mode subcriticality is given as a function of the reactor size and flux flattening. For example, a reactor with a core radius of 350 cm and flattening region of 0.8 R has the same modal subcriticality as an unflattened reactor with a radius of 500 cm.

		Uniform Reactor Case
Fundamental Mode	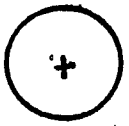	$J_o(B_o r)\sin\alpha_o z$
1st Azimuthal (T/B)	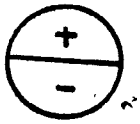	$J_1(B_1 r)\cos\delta$
1st Azimuthal (S/S)	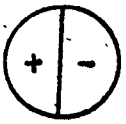	$J_1(B_1 r)\sin\delta$
2nd Azimuthal (oblique)		$J_2(B_2 r)\cos 2\delta$
2nd Azimuthal (V/H)	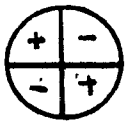	$J_2(B_2 r)\sin 2\delta$
1st Axial	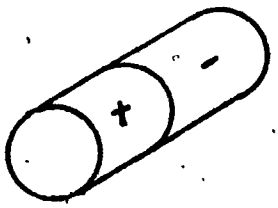	$\sin 2\alpha_o z$

B_o, B_1, B_2, α_o are related to the core extrapolated dimensions ($z = 0$ at one end)

FIGURE 3.2a. Darlington Modes Representation

		Uniform Reactor Case
2nd Axial	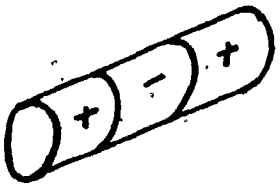	$\sin 3\alpha_o z$
1st Radial	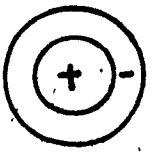	$J_o(B'r)$
2nd Radial	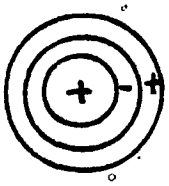	$J_o(B''r)$
3rd Azimuthal	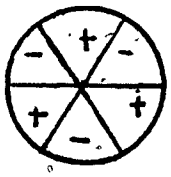	
Higher		

FIGURE 3.12(cont'd): Darlington Modes Representation

TABLE 3.1: Subcriticality of Important Higher Order Flux Modes in CANDU-PHW Reactors (Ref. 17)

REACTOR	RADIAL FORM FACTOR*	MODE SUBCRITICALITY (mk)			
		First Azimuthal	Second Azimuthal	First Axial	First Radial
NPD	0.6	100	230	50	280
DOUGLAS POINT	0.7	45	116	42	170
PHW-600	0.8	16**	44	24**	60
PICKERING	0.8	16**	44	24**	60
BRUCE	0.8	14**	33	30	50
PHW-1250	0.85	7**	22**	20**	34

* Form factor = average channel power/maximum channel power.

** Since the xenon load is ~30 mk for all reactors, these modes are unstable against xenon-induced oscillations.

As a concluding remark to large reactor stability, it is added that increase in reactor size and degree of flux flattening results in reactors which become increasingly more susceptible to xenon-induced flux transients (Ref. to M.Sc. thesis).

Most thermal power reactors have a xenon load of the order of 30 mk. Because the new larger generation of thermal power reactors has a large number of modes with subcriticality rarely exceeding 25 mk, these modes are unstable against xenon-induced oscillations.

3.8 SPATIAL CONTROL REQUIREMENTS

In the previous section, a brief background of some reactor physics aspects has been provided. We now turn to the spatial control requirements for large scale CANDU-PHW reactors [i.e., 850 MW(e)] and hope that with little change the same principles can be applied to large scale LEU-CANDU-PHW (Low Enriched Uranium CANDU-PHW) reactors.

In the case of large reactors that need to be controlled spatially and over different time frames, the discussion is more easily understood if reactor transient events are time classified first. The time span over which events may occur is defined as follows:

- very slow (hours _____ days)
- slow (minutes _____ hours)
- fast (1-100 seconds)

Most important in the slow category is the reactivity change associated with burnup of the fuel. The variation of the reactivity with burnup has the same shape of the keff shown graphically and qualitatively in Chapter Six for a typical CANDU-PHW natural fuel reactor.

The qualitative behaviour of the reactivity is illustrated by Figure 3.2.

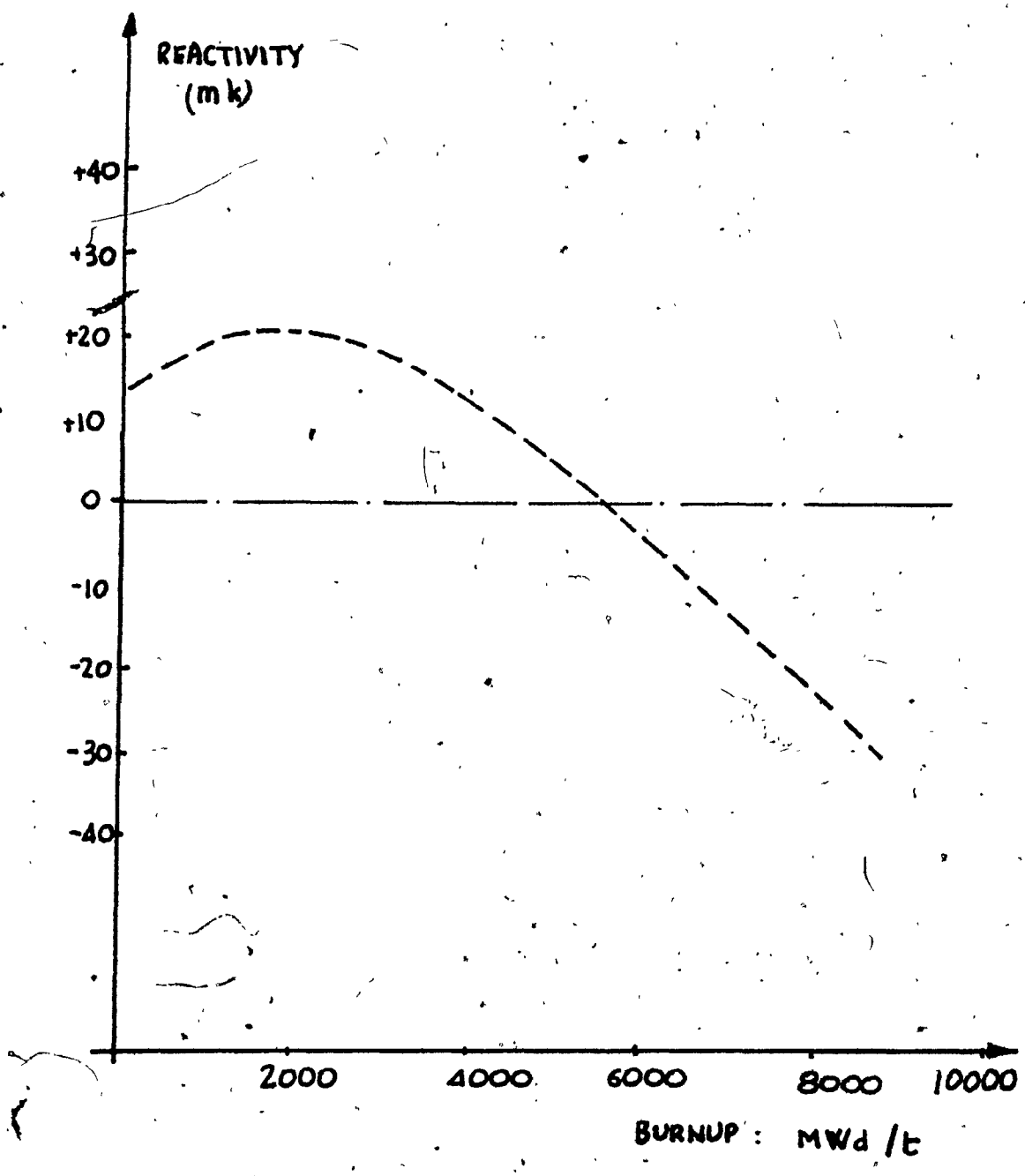

FIGURE 3.2: Reactivity Behaviour versus Reactor Core Burnup

There is a small initial rise in reactivity due to the buildup of Pu(239), followed by a decrease due to the burnup of U(235) and Pu(239) and the accumulation of fission products. Eventually, the reactivity decreases to the point where the spatial reactivity regulation systems become inefficient and the fuel must be replaced. Thus, the long-term control of CANDU-PHW reactors is achieved by refuelling (that is, by introducing a number of fresh fuel bundles in one end of the reactor core and discharging the same number of irradiated bundles from the other end. Depending on if we introduce two, four or eight bundles at a time, we call this two-, four- or eight-bundle shift scheme). The extra reactivity present during the time period the reactor approaches equilibrium (first 8-9 months) fuelling is controlled by using depleted uranium fuel and/or moderator poison.

In the second category we have "slow" effects, which occur when the reactor is operated at a reasonably high power level (1014 neutrons/cm^2/sec), and a buildup of fission products will occur. Fission fragments are produced in every fission event and, because some of these products have substantial absorption cross-sections, their presence in the reactor reduces the reactivity (Ref. 6). The fission products can be categorized as saturating or non-saturating. The saturating fission products reach an equilibrium concentration in a relatively short time, with their production rate balanced by their burnout rate. The most important of these saturating

fission products is the Xe-135, whose thermal absorption cross-section is $\sim 3 \times 106$ barns, compared to 1-100 barns for most other elements.

Neutron absorption in Xe-135 is an important effect in CANDU-PHW reactors for two reasons:

a) During steady-state operation of the reactor, neutron absorption in the Xe-135 is about 40% of the neutron absorption in fission products and $\sim$ 3% of the total neutron absorption in the reactor.

In this mode of operation, the rate of increase of the Xe-135 concentration is given by the decay of I-135 plus the xenon fractional yield directly from fission, minus the xenon decay and neutron absorption.

The equilibrium concentration of xenon during reactor operation is given by Reference 6:

$$\underset{t\to\infty}{X_e(t)} = X_e^{\infty} = \frac{(\gamma_I + \gamma_{Xe})\,\Sigma_{f1}\,\phi_{01}}{\lambda^{Xe} + \sigma_{a1}^{Xe}\,\phi_{01}} \qquad \text{Eq. 3.46}$$

(Because σ_a^{Xe} is large, $\lambda^{Xe} + \sigma_{a1}^{Xe}\phi_{01} > \lambda^{Xe}$).

The poison reactivity is usually defined as:

$$\Delta\rho \equiv - \frac{\Sigma_a^P}{\Sigma_a} \qquad \text{Eq. 3.47}$$

where Σ_a^P is the poison thermal absorption cross-section and Σ_a is the thermal absorption cross-section for all reactor constituents. The reactivity equivalent $\Delta\rho_o$ of the equilibrium xenon poisoning effect is consequently:

$$\Delta\rho_o \simeq - \frac{\sigma_a^{Xe} X_o}{\Sigma_a} = \frac{\sigma_a^{Xe}(\gamma^I + \gamma^{Xe})\Sigma_f \phi_{01}}{(\lambda^{Xe} + \sigma_a^{Xe}\phi_{01})\Sigma_a} \qquad \text{Eq. 3.48}$$

The terms in Equation 3.48 are all constants for a given reactor except for the variable ϕ_{01} which is the flux level at which the reactor is operated. Typical values of $\Delta\rho$ as a function of ϕ_{01} are reported in Table 3.2.

TABLE 3.2: Reactivity Equivalents of Equilibrium Xenon Poisoning During Reactor Operation

THERMAL FLUX (ϕ_{01})	EQUILIBRIUM POISONING ($\Delta\rho_o$) in k
10^{12} n/cm^2.sec	-0.005
10^{13} n/cm^2.sec	-0.023
10^{14} n/cm^2.sec	-0.036
10^{15} n/cm^2.sec	-0.038

For flux levels of 10^{11} n/cm^2.sec, the value of $\Delta\rho$ is of the order of 10^{-4} to reach the order of only 0.5% at $\phi_{01} \simeq 10^{12}$ n/cm^2.sec. We confirm with this what we just said previously, that at current power reactor flux levels (10^{13}–10^{14} n/cm^2.sec) only the order of 3% of neutrons is absorbed by the equilibrium amount of xenon and, for above 10^{15} n/cm^2.sec, $\Delta\rho_0$ reaches a limiting value expressed by:

$$\Delta\rho^{\infty} \simeq -(\gamma^{I} + \gamma^{Xe}) \frac{\Sigma_f}{\Sigma_a} \qquad \text{Eq. 3.49}$$

Equation 3.49 indicates that $\Delta\rho^{\infty}$ does not depend on ϕ_{01} any more and it is found that, in practice, $\Delta\rho$ has the behaviour depicted in Figure 3.3.

b) Following a reactor shutdown, the xenon concentration will build up to several times its steady-state value.

Because iodine-135 has a shorter half-life (time at which the concentration of a decaying element becomes half the initial concentration) than xenon-135, i.e., $\lambda^{I} > \lambda^{Xe}$, the conditions are suitable for xenon concentration to increase to a maximum after the reactor is shut down completely. This occurs because the iodine-135 present at shutdown forms xenon-135 by radioactive decay at a rate that is initially greater than the rate of decay of

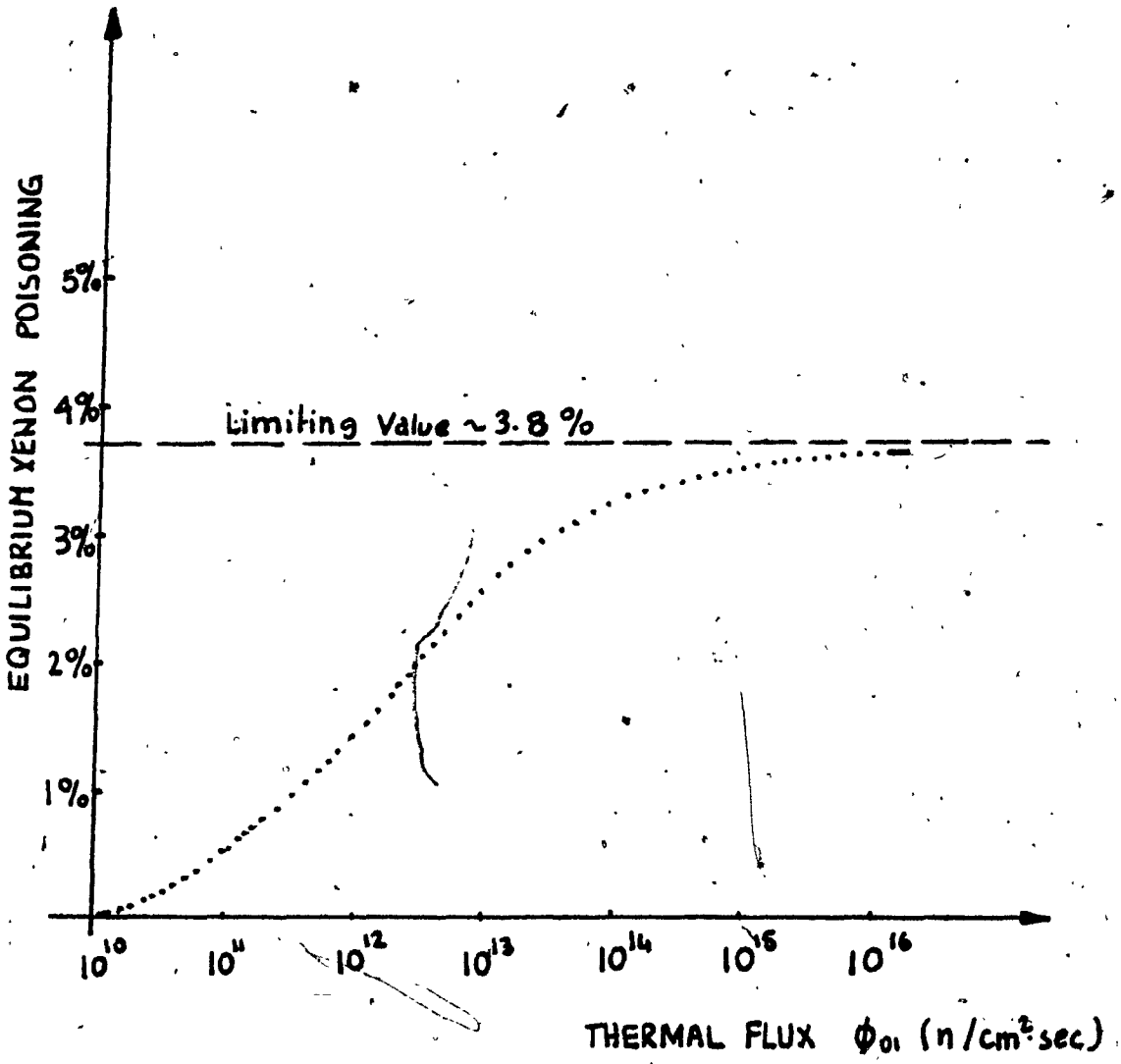

FIGURE 3.3: Equlibrium Reactivity During Reactor Operation

Xe-135, almost none of the latter now being lost by neutron capture.

The one-point behaviour of xenon and iodine concentration and xenon reactivity feedback following reactor shutdown situations were analyzed in detail in my Master Thesis (Ref. 6) and the graphical results of the analysis are reported here for convenience: Figures 3.4, 3.5, 3.6, 3.7, 3.8, 3.9, 3.10, 3.11, 3.12 and 3.13. Each figure is self-explanatory. The data suporting the figures is provided hereinafter.

ϕ_{L1} = 5×10^{11} neutrons/cm^2 sec

ϕ_{L2} = 10^{12} neutrons/cm^2 sec

ϕ_{L3} = 10^{13} neutrons/cm^2 sec

ϕ_{L4} = 9.7694×10^{13} neutrons/cm^2 sec

ϕ_{L5} = 5×10^{14} neutrons/cm^2 sec

ϕ_{L6} = 10^{15} neutrons/cm^2 sec

σ_a^{Xe} = 3.5×10^{-18} cm^2

Σ_{f1} = .1112 cm^{-1}

λ_{Xe} = 2.09×10^{-5} sec^{-1}

λ_I = 2.87×10^{-5} sec^{-1}

where ϕ, σ_a^i, Σ_{fi}, λ^i are the flux levels, thermal absorbing cross-sections, macroscopic fission cross-sections and fission product decay constants.

Inspection of Figures 3.3, 3.4 and 3.5 indicates that excess reactivity must be available to permit start-up of the reactor shortly after shutdown, or to maintain operation after a reactor power reduction, e.g., during power cycling. The spatial behaviour of xenon reactivity feedback shown on Figures 3.3, 3.4 and 3.5 will be analyzed in detail in Chapter Seven for an 850 MW(e) natural and LEU CANDU-PHW reacor core.

c) Figures 3.3, 3.4, 3.7 and 3.8 indicate that the time to attain the maximum concentration of xenon after shutdown is of the order of 11 hours. This time is calculated by differentiating the reactivity equation (Ref. 6).

$$\Delta\rho(t)\Big|_{\text{SHUTDOWN}} \simeq -\frac{(\gamma^I+\gamma^{Xe})\phi_{01}\exp\{-\lambda^{Xe}t\}\,\sigma_a^{Xe}}{\lambda^{Xe}+\sigma_{a1}^{Xe}\phi_{01}} +$$

$$+\frac{\gamma^I\phi_{01}\sigma_{a1}^{Xe}}{\lambda^I-\lambda^{Xe}}\left[\exp\{-\lambda^{Xe}t\}-\exp\{-\lambda^I t\}\right]\frac{\Sigma_{f1}}{\Sigma_a}$$

$$\approx -\frac{1}{\nu\varepsilon p}\left\{\frac{(\gamma^I+\gamma^{Xe})\phi_{01}}{\lambda^{Xe}/\sigma_{a1}^{Xe}+\phi_{01}}\exp\{-\lambda^{Xe}t\}\right. \qquad \text{Eq. 3.50}$$

$$\left.+\frac{\gamma^I\phi_{01}\sigma_{a1}^{Xe}}{\lambda^I-\lambda^{Xe}}\left[\exp\{-\lambda^{Xe}t\}-\exp\{-\lambda^I t\}\right]\right\}$$

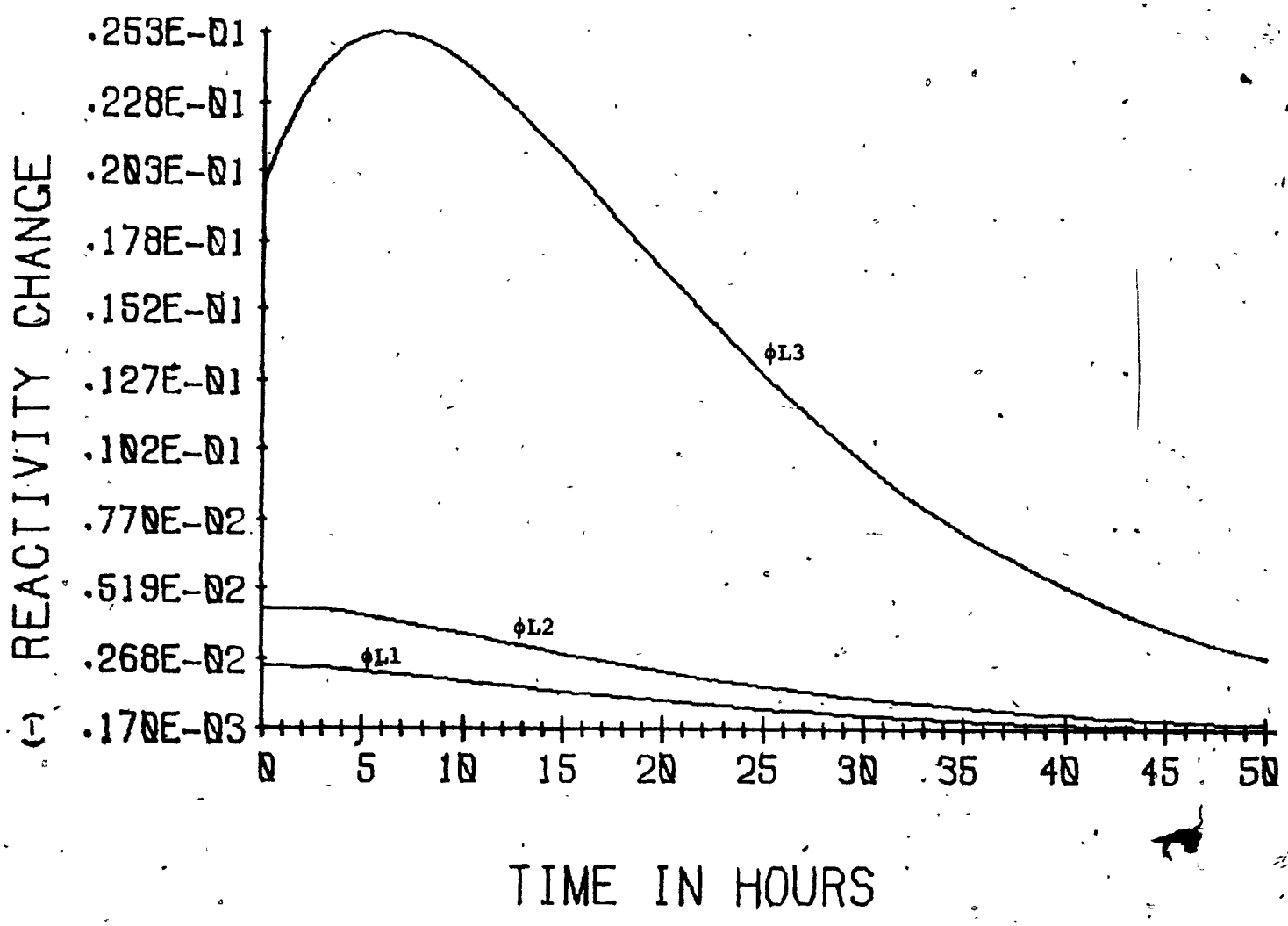

FIGURE 3.4: Reactivity Time Behaviour Following Reactor Shutdown

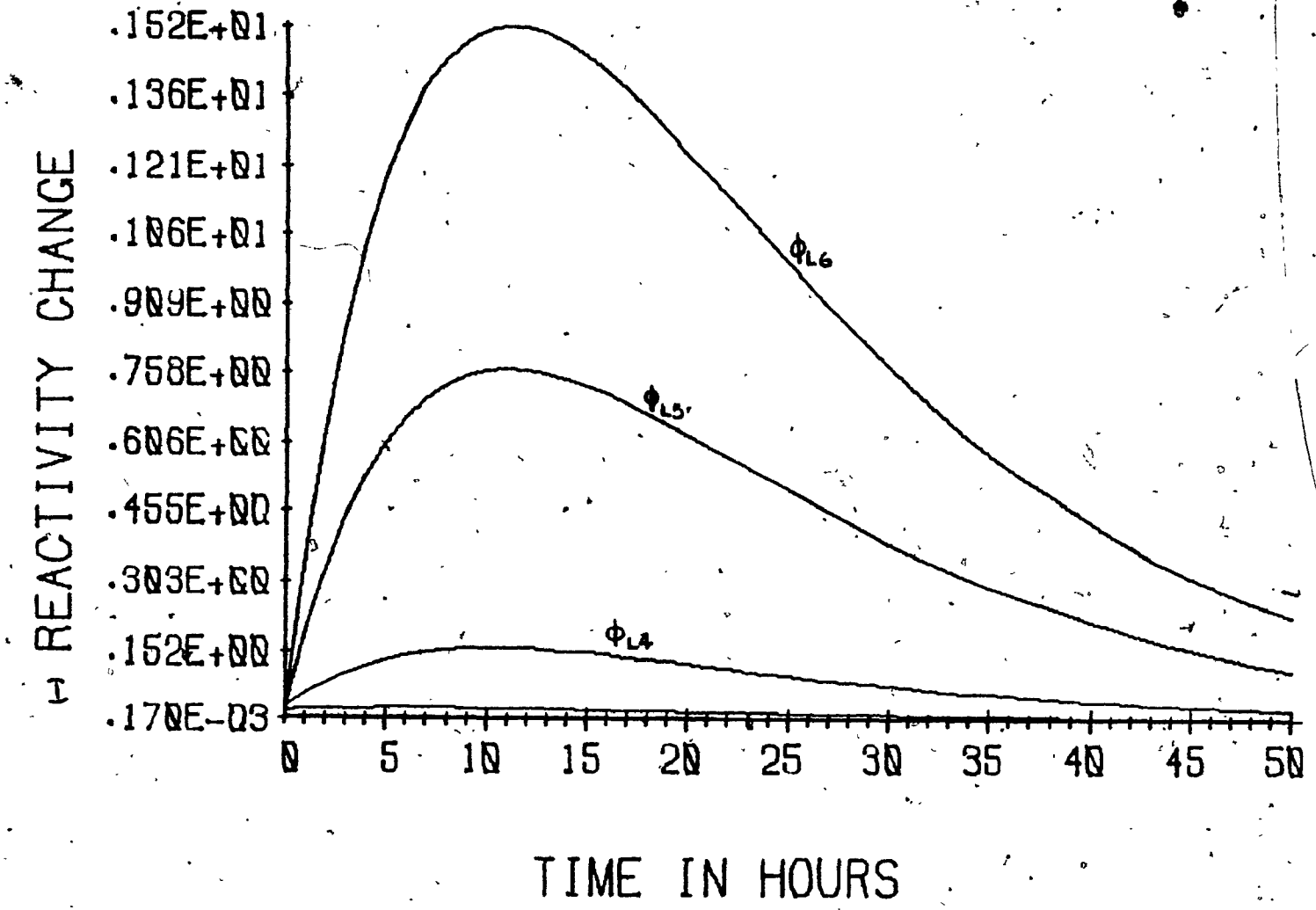

FIGURE 3.5: Reactivity Time Behaviour Following Reactor Shutdown

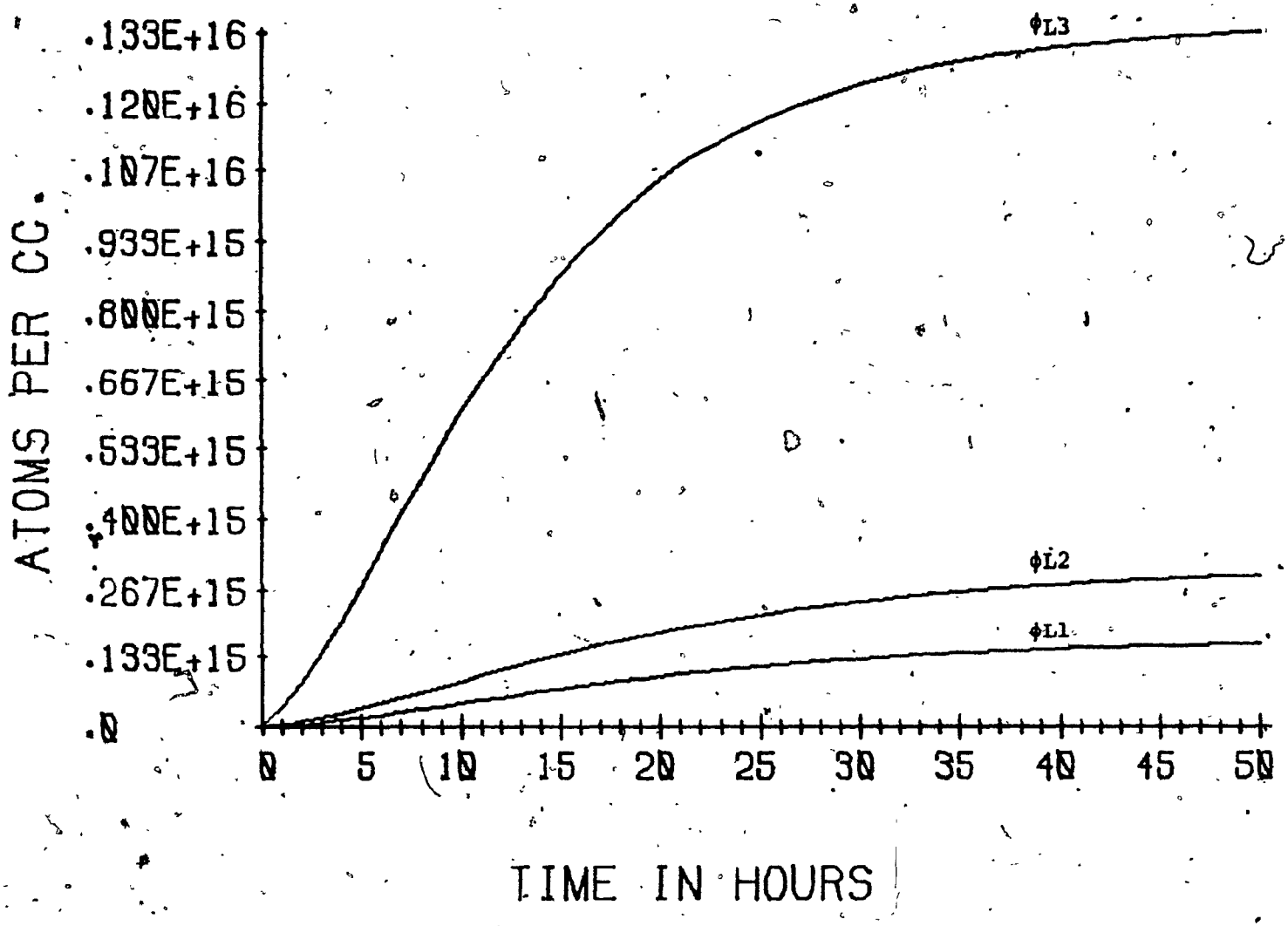

FIGURE 3.6: Xenon Concentration Following Reactor Start-Up

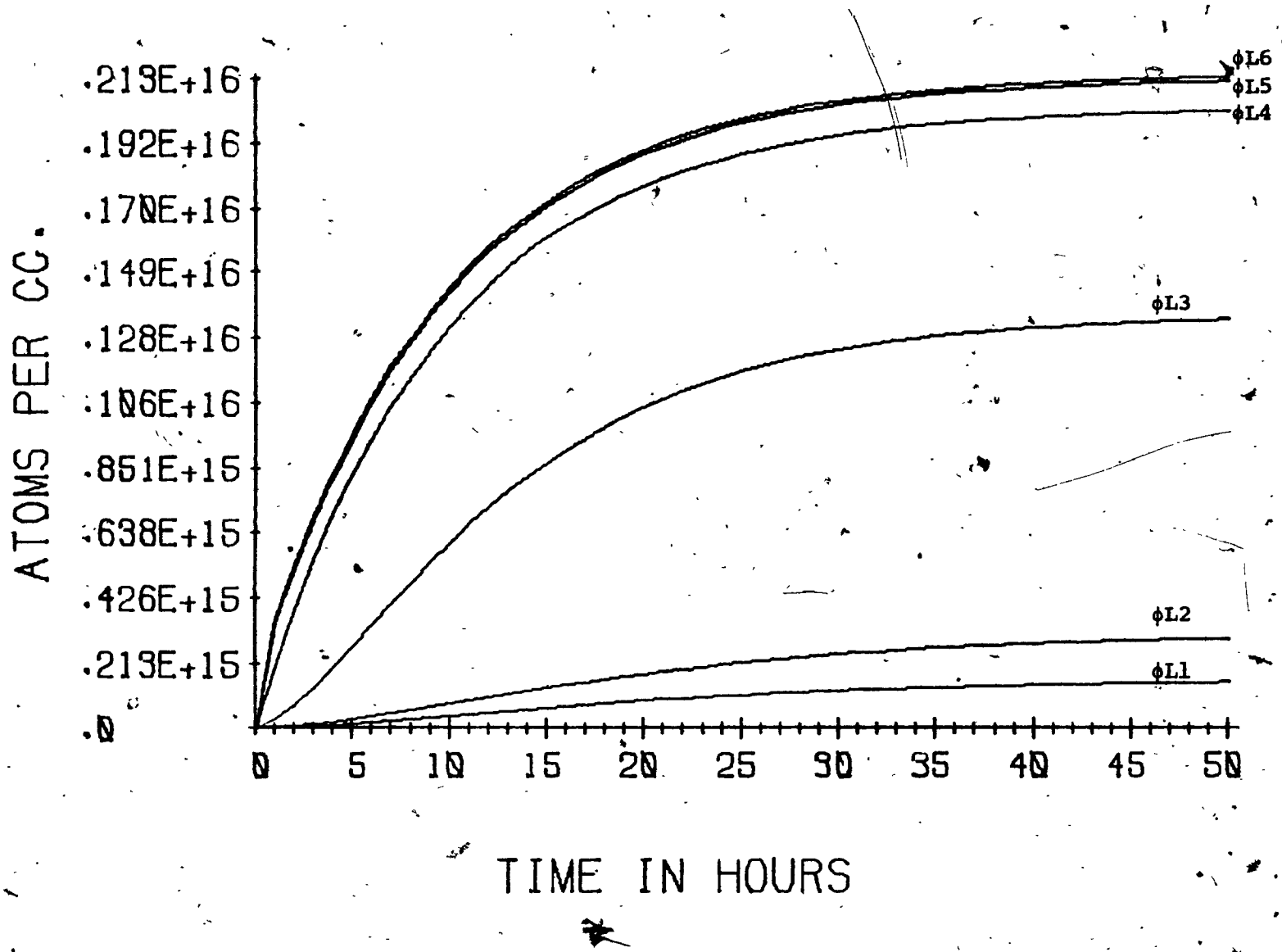

FIGURE 3.7: Xenon Concentration Following Reactor Start-Up

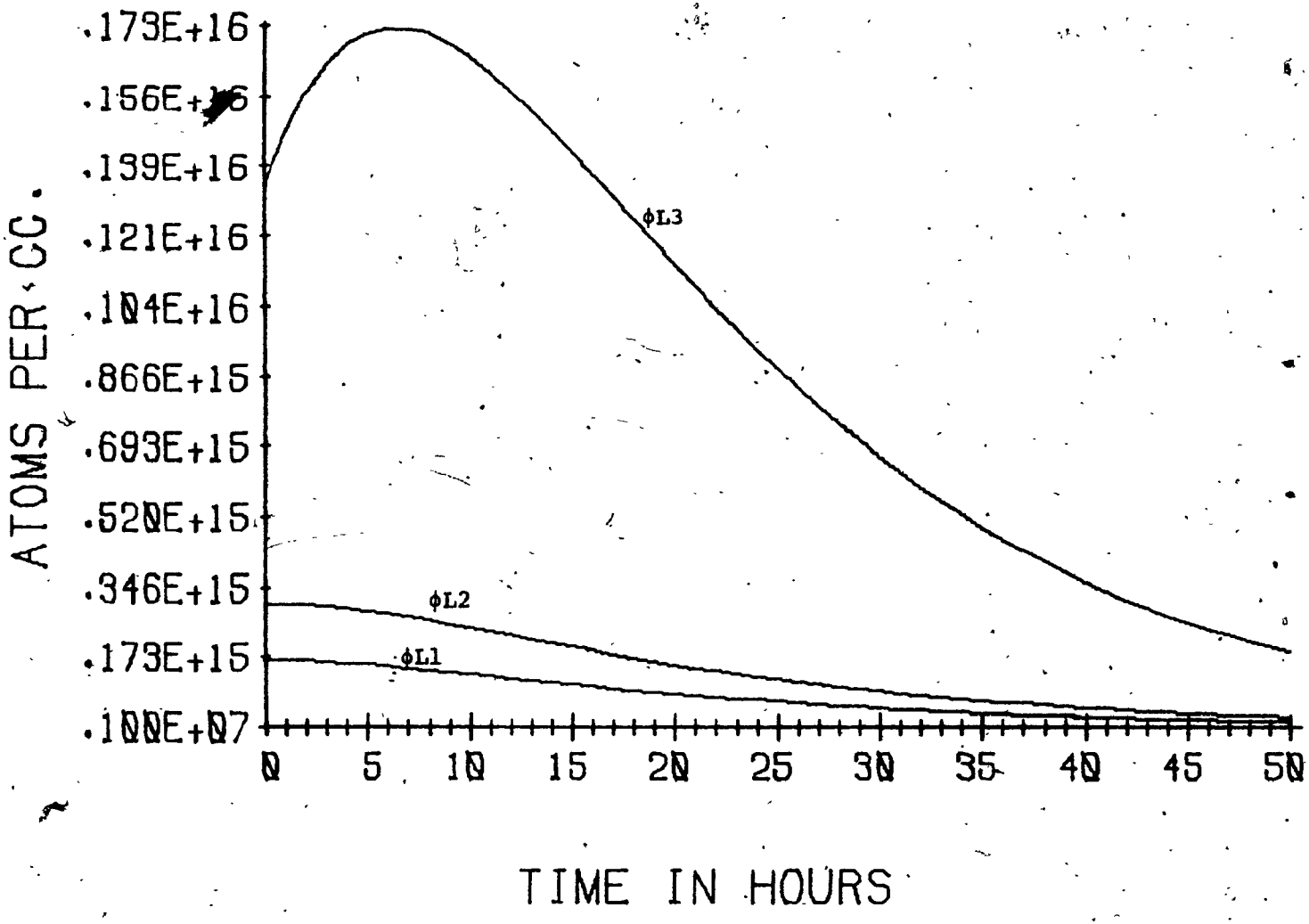

FIGURE 3.8: Xenon Concentration Following Reactor Shutdown

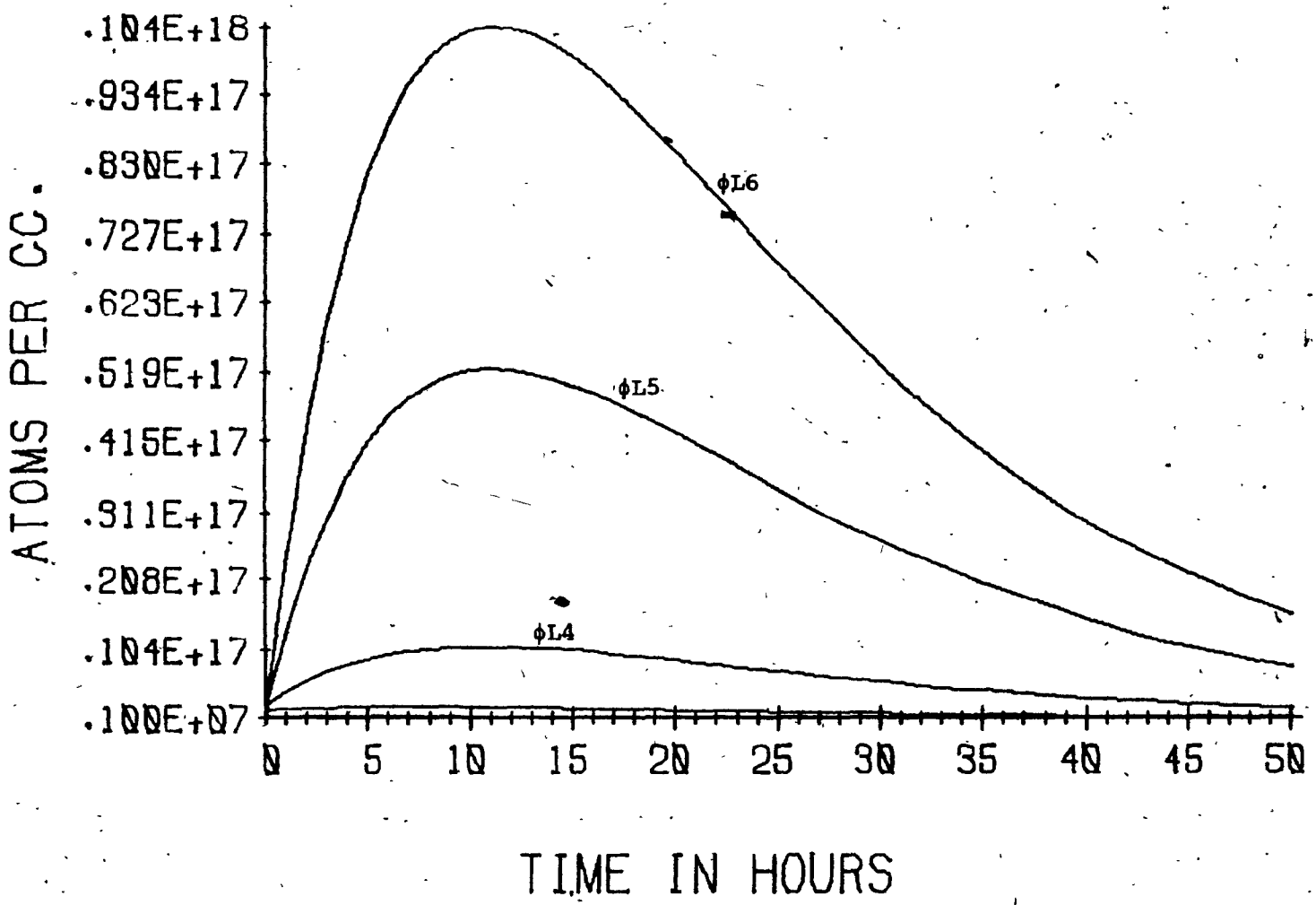

FIGURE 3.9: Xenon Concentration Following Reactor Shutdown

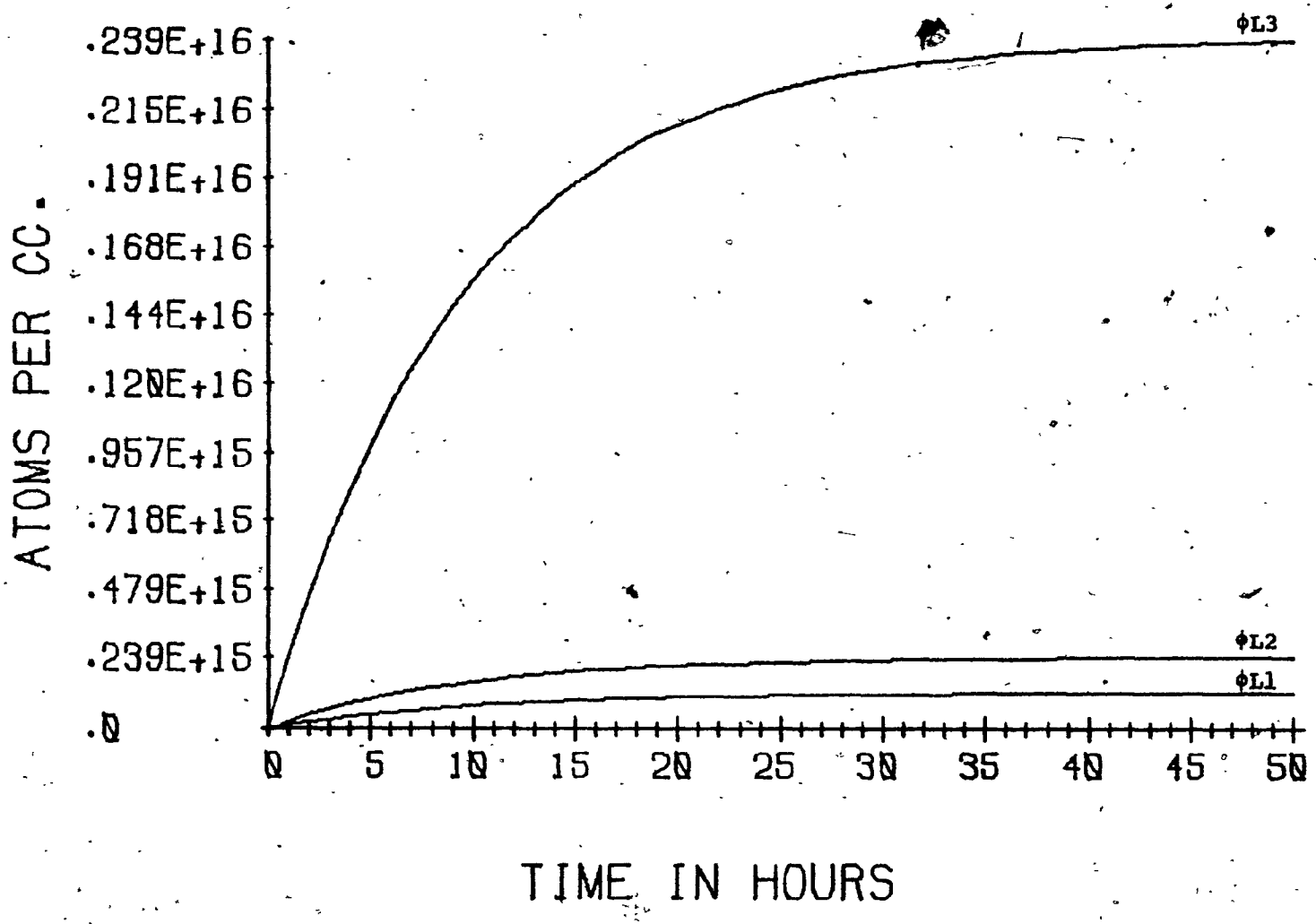

FIGURE 3.10: I^{135} Concentration Following Reactor Shutdown

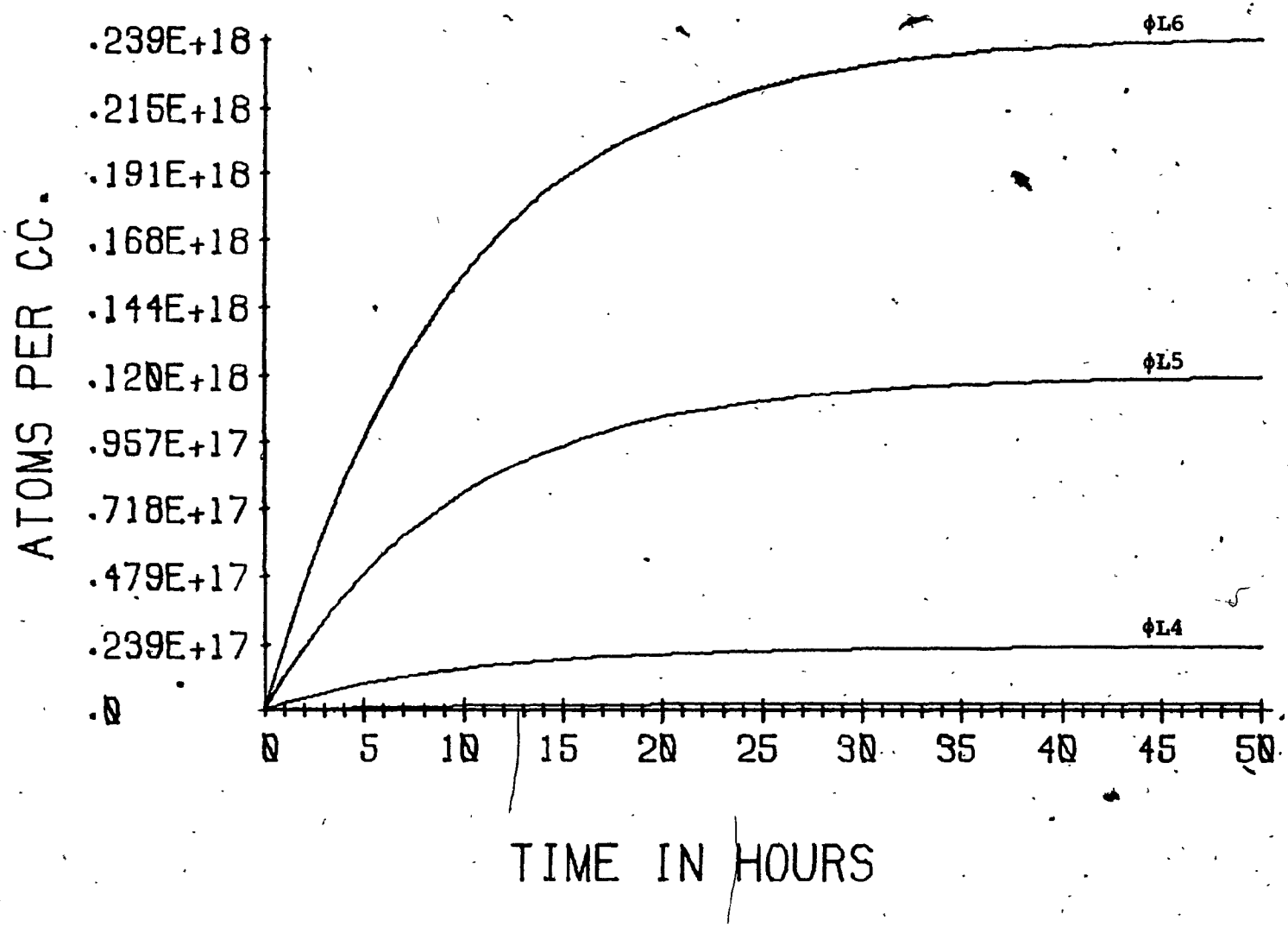

FIGURE 3.11: I^{135} Concentration Following Reactor Start-Up

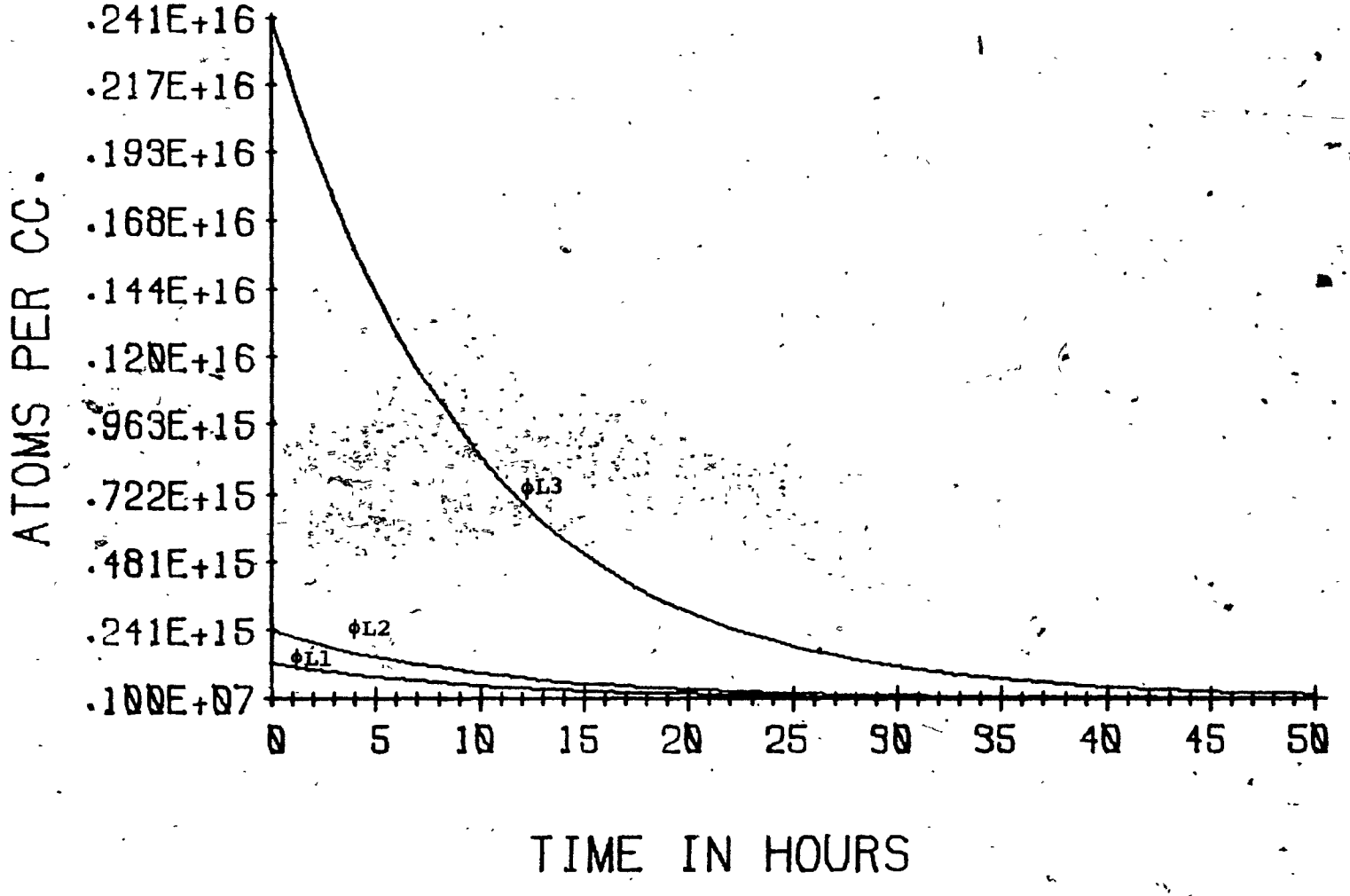

FIGURE 3.12: I^{135} Concentration Following Reactor Shutdown

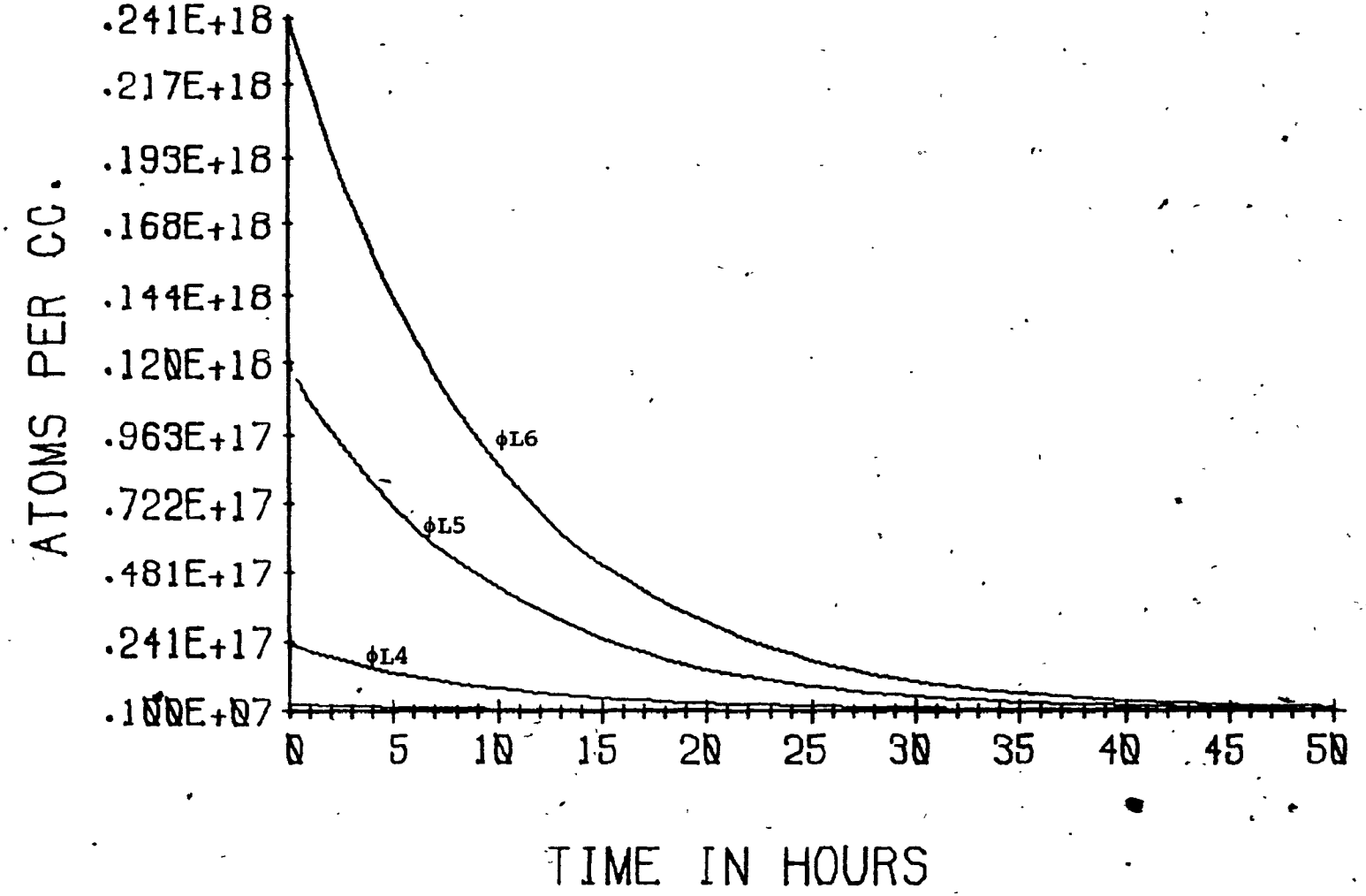

FIGURE 3.13: I^{135} **Concentration Following Reactor Shutdown**

and equating it to zero to get:

$$t_{max} = \frac{1}{\lambda^I - \lambda^{Xe}} \ln \left[\frac{\lambda^I / \lambda^{Xe}}{1 + \frac{\lambda^{Xe}}{\lambda^I}\left[\frac{\lambda^I}{\lambda^{Xe}} - 1\right]\frac{X_e^\infty}{I^\infty}} \right]$$

$$= \frac{1}{\lambda^I - \lambda^{Xe}} \ln \left[\frac{\lambda^I / \lambda^{Xe}}{1 + \frac{\lambda^{Xe}}{\lambda^I}\left[\frac{\lambda^I}{\lambda^{Xe}} - 1\right]\frac{\gamma^I + \gamma^{Xe}}{\lambda^{Xe} + \sigma_a^{Xe}\phi_{01}} \Big/ \frac{\gamma_I \phi_{01}}{\lambda^I}} \right] \quad \text{Eq. 3.51}$$

and for $\phi_{01} \gg \frac{\lambda^{Xe}}{\sigma_a^{Xe}}$

$$t_{max} = \frac{1}{\lambda^I - \lambda^{Xe}} \ln \frac{\lambda^I}{\lambda^{Xe}} \approx 11.6 \text{ hr} \quad \text{Eq. 3.52}$$

d) It is evident that if a high flux reactor is to be capable of being restarted at any time after shutdown, it must have an appreciable amount of excess multiplication (or reactivity) in the form of control. In order that a thermal reactor, normally operating at a flux of the order of 10^{14} n/cm^2.sec, be able to "override" the maximum xenon concentration after shutdown, it must have in excess of 30 mk of reactivity.

Fast events, which occur on a time scale of seconds, e.g. perturbation in the heat transport system, and their associated fuel temperature and coolant-density/temperature feedback effects require a fast response from the bulk/spatial control system. The control requirements are also influenced by reactor power feedback effects. As the reactor power changes, the fuel temperature and coolant temperature and density change, which in turn alter the net production rate of neutrons. In CANDU-PHW reactors, where the coolant is a pressurized liquid (heavy water), the power coefficient associated with these effects is near zero, and is thus readily controlled.

3.9 XENON-INDUCED POWER OSCILLATIONS IN LARGE POWER REACTORS: CANDU

Thus far we have ignored the effect of the reactivity introduced by the fission product poisons on the neutronic behaviour of the core. The interaction between xenon fission product buildup and the changes in the neutron flux distribution that accompanies local changes in reactivity can lead to spatial oscillations in the power distribution in a large thermal core.

To explain this phenomenon, let us first consider a point-reactor model in which the reactor has been operating at a steady-state flux level for a period of time. Then, our earlier study of xenon fission product poisoning has indicated that there will be a saturation in the Xe^{135} concentration resulting from the balance of Xe^{135} production (via direct fission and I^{135} decay) and loss due to decay to Cs^{135} and transmutation (via neutron absorption) to Xe^{136}. Now suppose a small perturbation increase in the flux occurs. Then Xe^{135} will transmute more rapidly to Xe^{136} (instantaneously), depleting the Xe^{135} concentration, hence decreasing the absorption and increasing the reactivity and the flux. However, the increased flux transmutes even more Xe^{135} and, hence, the initial flux perturbation grows with time (unstable). Such an instability can only exist for power levels higher than a certain threshold value. For U-235-fuelled reactors, this threshold ix 3×10^{11} neutrons/cm^2.sec. Below this threshold,

the stabilizing effect of the direct xenon yield from fission is more important than the destabilizing effect of the xenon decaying from I^{135}.

Actually, this type of instability is relatively unimportant in practical reactor operations since it is easily controlled by normal control rod movement. A much more serious spatial xenon instability can arise, however, which requires a more complex control rod program. To understand this, consider the very simple model illustrated in Figure 3.14, consisting of two coupled xenon-unstable point reactors, separated by a region of non-multiplying material. Suppose further that there is a control system keeping the total power of all three core regions constant (although the flux or power in an individual region is not constant).

A slight increase in the power level on one side of the core will give rise to the unstable xenon process described for a point reactor. Since the control system keeps the total power constant, the flux on the other side decreases. This process continues with an increasingly steeper tilt resulting in the flux. Two effects will limit this tilt: (a) burnup of most of the xenon on the high flux side; and (b) the steep flux tilt which creates a flux gradient and, hence, a current that carries all the excess neutrons being produced to the other side. The flux will remain tilted for several hours. Eventually, the high flux side will have created an I^{135} concentration much

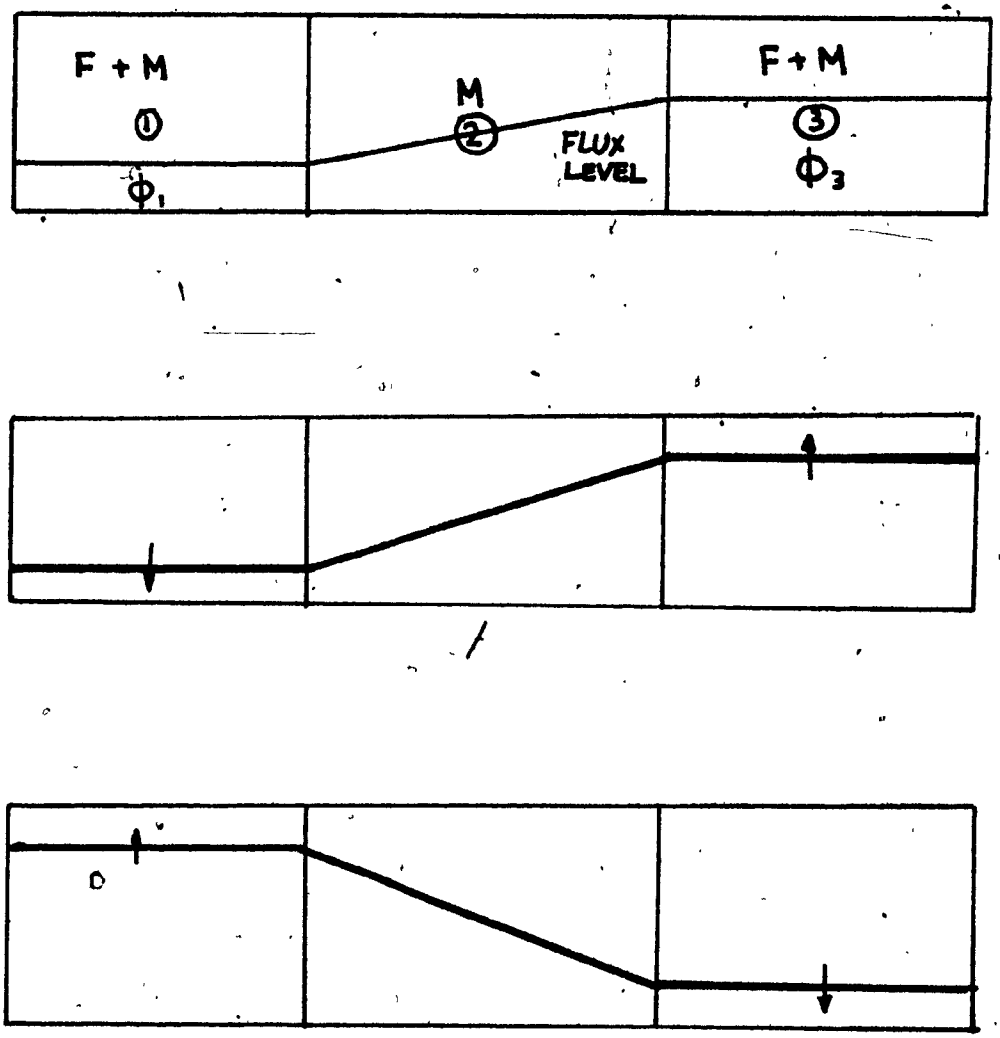

FIGURE 3.14: A Simple Model of Xenon-Induced Power Oscillations

greater than that originally present. Since the decay half-life of I^{135} is 6.7 hours, more xenon will be created after this delay period. Similarly, on the low side less xenon will be created. This reverses the flux tilt eventually and produces a side-to-side oscillation with a period of 15-30 hours. Thus, the xenon process tends to be self-limiting and produces the effect of a moving "hot spot" to the reactor operator.

Although xenon oscillations can be controlled by control rod motion, there is strong motivation to design the reactor core in such a way that xenon oscillations are minimized, since the load-following requirements of a power reactor operating on a utility power grid imply that such control adjustments may incur considerable economic penalty. In general, negative feedback mechanisms such as moderator void formation or development of spatial control devices (Section 3.10) are the key control aspects of modern and large thermal power reactors.

The stability of the spatial power distribution with respect to xenon-induced oscillations will decrease with increasing core size or decreasing neutron migration length. As a rule of thumb, xenon oscillations will be a problem if the reactor core is over 30 migration lengths in size (Chapter Five).

3.10 DEVELOPMENT OF SPACE-TIME CONTROL DEVICES

A description of Darlington control devices is provided in Chapter Five. This section is merely dedicated to describing the time development of reactor spatial control. The first commercial CANDU type power reactor (NDP) had no in-core reactivity control devices. Its reactivity control means was the moderator level control. It has been indicated in previous sections that the reactor core sizes have been increasing and this process has been accompanied by an increase in control complexity. The simple moderator level control scheme used in NPD has been superseded by spatial control and xenon-override systems that utilize an increasing number of in-core reactivity devices as illustrated by Table 3.3.

Following is provided a summary description of reactivity control philosophy and reactivity devices for CANDU-PHW reactors.

TABLE 3.3: In-Core Reactivity Control Devices in CANDU-PHW Reactors (Excluding Darlington)

REACTOR	CONTROL RODS		ADJUSTER RODS		BOOSTER RODS	
	#	Worth (mk)	#	Worth (mk)	#	Worth (mk)
NPD	Moderator Level		-	-	1	2.5
Douglas Point	4*	-3	-	-	8	10
Pickering	14**	-4.6	18	-18		
Bruce A	14**	-6			16	18
	4*	-7				
Darlington	14*	-6.2	24	17.7		
	4*	-7				
600 MW	14**	-5.6	18	-16		
	4*	-6.5				

* Mechanical Control Absorbers

** Liquid Zone Controllers

3.11 DESCRIPTION OF REACTIVITY CONTROL DEVICES

In CANDU-PHW reactors, the long-term reactivity control is achieved by on-power refuelling, replacing the burned-out fuel bundles with fresh ones. Short- and medium-term control under normal operating conditions is usually achieved by the use of booster elements and combination of zone control units and mechanical control absorbers as in Bruce GS "A" or by the use of adjusters and combination of zone control units and mechanical control absorbers as in Bruce GS "B", Pickering GS "B" and Darlington GS "A". Our discussion will be limited to the second group only.

Reactivity control devices consist of zone control absorbers, mechanical control absorbers, adjusters and shut-off units.

The liquid zone control system performs two basic functions:

a) Spatial flux distribution control - by suppressing regional power transients associated with reactivity perturbations, such as during channel refuelling;

b) Short-term bulk reactivity control - to maintain the core power at the demanded level during normal operation.

The system consists of 14 in-core, thermal neutron flux platinum detectors and 14 independently-controlled, light water

compartments. Accordingly, the reactor core is divided into 14 zones, each zone corresponding to one compartment. Locations of the flux detectors associated with the corresponding water compartments were selected to ensure that for each zone the ratio of thermal flux values before and after local perturbation was approximately equal to the ratio of zonal powers. Local control of neutron absorption in the zones is accomplished by varying the amount of water in the compartments. Details on liquid zone control layout are provided in Chapter Five.

Differential adjustment of the water level in individual zone compartments is designed to control the spatial power distribution by suppressing regional flux tilts associated with local reactivity perturbations. Unison adjustment of the water level in all 14 zone compartments provides bulk reactivity control, associated via the Reactor Regulating Program (RRP) with the Overall Unit Control (OUC) System.

The mechanical absorbers are used mainly to initiate rapid power reductions and to provide reactivity override for negative fuel temperature effects. For a given setback in power, in particular at low fuel burnups, the increase in reactivity could be higher than the negative reactivity depth provided by the zone control system, and the mechanical absorbers are used to augment the zonal absorbers' worth. They also provide a

much faster reduction of reactivity than can be achieved by using the zone control system.

Adjuster unit absorbers are of the form of thin-walled stainless steel vertical tubes with central stainless steel shim rods. The absorbers have different lengths and various effective thicknesses along their lengths to provide the best neutron absorption characteristics.

The adjuster rods are normally fully inserted into the core but are capable of being driven in and out at variable speeds to provide reactivity shim as required by the control system, usually for Xe-135 poison override following the reactor trip. They are normally driven in pre-designed groups (banks) but can also be driven individually if required.

The adjusters satisfy the following main objectives:

a) With all adjusters fully inserted, the thermal flux is flattened radially and axially to ensure best power distribution and optimum fuel burnup, while minimizing variation in the discharge burnup across the core.

b) The positive reactivity (18 mk) obtained upon adjusters' withdrawal from the core provides the desired xenon override capability for the reactor start-up after a short shutdown.

c) In the case of fuelling machine unavailability, the selected withdrawal of one or two adjuster banks can be utilized for reactivity shim (with minor derating of the reactor power).

Upon adjusters' withdrawal, after the reactor trip from 100% FP, the resulting excess positive reactivity provides a nominal xenon override time of about 37 minutes or so, depending on the degree of Low Enriched Uranium content. Corresponding decision and reaction time is of the range of 25 minutes (as discussed in Chapter Seven).

Total reactivity worths of control devices for a 2800 MW (thermal) CANDU core for equilibrium fuel, steady state xenon distribution and 100% FP are as follows:

- Zone control system, all 14 absorbers (from empty to full): 5.6 mk;

- Mechanical control absorbers, all four absorbers fully inserted: 9.5 mk;

- Adjusters, all 24 adjusters fully inserted: 17.6 mk.

Coupled with the use of more in-core reactivity devices is the requirement, for control purposes, for a more detailed knowledge of the spatial flux (power) distribution throughout the

reactor core. This has led to an increased dependence on channel power measurements and in-core flux measurements using self-powered detectors. In the modern generation of CANDU-PHW reactors, vanadium and platinum self-powered detectors are used almost exclusively for in-core flux (power) information and control purposes. Douglas Point had a total of only 24 in-core flux-detectors against just over three hundred that may populate the reactor core volume of future CANDU-PHW 1250 M(e) reactors. The 600 MW(e) CANDU-PHW reactors are also equipped with an even higher number of in-core flux detectors than the total number used in all four Bruce reactors.

CHAPTER FOUR

4. SPACE-TIME MODAL ANALYSIS OF CANDU-PHW REACTORS

4.1 INTRODUCTION

Predicting the space-time kinetics of any large thermal nuclear power reactor (a CANDU-PHW reactor for example) requires the solution of partial differential equations which describe the rate of change of neutron flux, delayed neutron precursors, xenon and iodine concentrations, in both space and time, and taking into account the thermal and fast energy spectrum of the neutron flux.

The set of generalized partial differential equations that would fully describe the space-time kinetics of CANDU-PHW reactors were derived in the Master Thesis and with the support of Appendix MG are reported here for convenience.

$$\frac{d}{dt}\left[\frac{1}{v}\phi(\bar{r},E,t)\right] = \sum_j \chi_p^j(E)(1-\beta^j)\int_0^\infty dE\,\nu^j\Sigma_f(\bar{r},E,t)\phi(\bar{r},E,t)$$

$$+ \sum_i \chi_i \lambda_i C_i(\bar{r},t) + q(\bar{r},E,t)$$

$$+ \nabla\cdot D\nabla\phi(\bar{r},E,t) - \Sigma_t(\bar{r},E,t)\phi(\bar{r},E,t)$$

$$+ \int_0^\infty \Sigma_s(\bar{r},E'\to E)\,\phi(\bar{r},E',t)\,dE' \qquad \text{Eq. 4.1}$$

The mathematical foundation of the spatial kinetics of large thermal power reactors, that including the delayed neutron precursors, the six delayed neutron families in CANDU-PHW reactors, the energy-dependent diffusion equation and a full treatment of the fission process, together with the mathematical derivation of the fission products space-time equation, was fully examined in the Master Thesis (Ref. 6). The space-time dependent poisoning effects in CANDU-PHW reactors and the space-time equations of the iodine and xenon fission products equations were also derived in detail.

Equation 4.1 expresses the difference between the net rate of appearance and the rate of disappearance.

The rates of change of delayed neutron precursors, iodine and xenon concentrations are provided by Equations 4.2, 4.3 and 4.4 respectively,

$$\frac{\partial C_i(\vec{r},t)}{\partial t} = \sum_j \beta^j \int_0^\infty dE\, \nu^j \Sigma_f^j \phi(\vec{r},E,t) - \lambda_i C_i(\vec{r},t) \qquad \text{Eq. 4.2}$$

$$\frac{\partial I(\vec{r},t)}{\partial t} = \gamma^I \int_0^\infty dE\, \Sigma_f(\vec{r},E,t)\, \phi(\vec{r},E,t) - \lambda^I I(\vec{r},t) \qquad \text{Eq. 4.3}$$

$$\frac{\partial X_e(\vec{r},t)}{\partial t} = \gamma^{Xe} \int_0^\infty dE\, \Sigma_f(\vec{r},E,t)\,\phi(\vec{r},E,t) + \lambda^I I(\vec{r},t)$$

$$-\lambda^{Xe} X_e(\vec{r},t) - \int_0^\infty dE\, \sigma_a^{Xe}(t)\,\phi(\vec{r},E,t)\,X_e(\vec{r},t) \quad \text{Eq. 4.4}$$

where symbols appearing in these equations have the usual meaning established in Reference 6. The above set of equations is applicable to neutron continuous energy representation. Direct solutions of the above set of equations is a very complex task. They can be obtained by using a finite-difference (FD) iterative numerical scheme.

This approach is very time consuming and, therefore, is very costly. These factors limit the usability of FD schemes for realistic 3-D reactor core studies. Neutronic flux transients have been handled by several approximation methods. An example of approximation that is often used to handle transients in time scale of the order of iodine and xenon dynamics is called the adiabatic approximation and consists of ignoring time derivatives. For neutronic transients of a relatively short time basis where the delayed neutronic effect on the flux cannot be ignored, an Improved Quasi-Static (IQS) method has been developed (Ref. 14, 15). The IQS method is a rigirous factorization of the space-time neutron flux into two parts: a strongly time-dependent amplitude factor and a less strongly time-dependent spatial shape factor (Refs. 18, 19, 20). This method introduces some approximations in the numerics only. In the

early seventies, a technique was developed which was an economical, less expensive and very manageable technique to handle a large number of neutronic transients. It is called SPACE-TIME MODAL KINETICS (SMOKIN) (Refs. 21, 22, 23).

4.2 POINT-KINETICS PARAMETERS

Let us consider the case of "small size" reactors, typical of the early generation of power reactors. We shall call a reactor "small" whenever the effects of local perturbations of $\phi(r,E,t)$ quickly spread throughout a reactor. This will happen when the reactor linear dimensions are just a few migration lengths; in a matter of milliseconds a neutron can travel across the core, thus making every event felt throughout the core quite quickly.

The immediate consequence of perturbing a reactor locally (for example, by changing the position of a control rod) is thus a readjustment in the shape of the flux which, in many cases, is completed in a few milliseconds. After that, the readjusted shape rises or falls as a whole, depending on whether the initial perturbation increased or decreased k_{eff}. For reactors in which transients proceed in this manner, merely being able to predict the change in the level (i.e., average value) of the flux is sufficient to permit a very accurate prediction of the consequences of the perturbation. Thus, instead of having to face the very difficult problem of solving Equations 4.1 and 4.2, we shall find a simple set of equations that specify how the overall magnitude of the flux changes with time.

When this reveals itself to be an acceptable treatment of the flux in nuclear reactors, the so-called "Point-Kinetics

Equations" are derived (Ref. Master Thesis). The equations are reported here for convenience.

$$\frac{dT(t)}{dt} = \frac{\rho - \beta}{\Lambda} T(t) + \sum_{i=1}^{I} \lambda_i C_i(t) + Q(t) \qquad \text{Eq. 4.5}$$

$$\frac{dC_i(t)}{dt} = \frac{\beta_i}{\Lambda} T(t) - \lambda_i C_i(t) \qquad \text{Eq. 4.6}$$

where:

$$T(t) = \int_{REACTOR} dV \int_0^\infty dE\, W(\bar{r},E) \frac{\Phi(\bar{r},E,t)}{v(E)} \qquad \text{Eq. 4.7}$$

W(r,E) : weighting function [T(t) is a weighted integral of the total number of neutrons present in the reactor at any time. If W(r,E) = 1, T(t) is exactly the total number of neutrons present].

The above equations are rigorous and can be used always, provided that the definitions for the various parameters (ρ, β, Λ, etc.) are consistent. Of course, the point-kinetics equations are all that is needed if the spatial behaviour of W is known (which will define ρ, β, Λ, etc); in general, however, such equations are not sufficient to describe transients. The consistent definition of the point-kinetics is given below.

$$\rho(t) \equiv \frac{\int dV \int dE\, W(\bar{r},E) \left\{ \nabla \cdot D(r,E,t) \nabla S(\bar{r},E,t) - \Sigma_t(r,E,t) S(r,E,t) + \int dE' \Sigma_s(r,E' \to E,t) S(\bar{r},E',t) + \sum_j \left[\chi_p^j(E)(1-\beta^j) + \sum_i \chi_i \beta_i^j \right] \int dE' \nu^j \Sigma_f(\bar{r},E,t) S(\bar{r},E,t) \right\}}{\int dV\, dE\, W(\bar{r},E) \sum_j \left[\chi_p^j(E)(1-\beta^j + \sum_i \chi^i \beta_i^j \right] \int dE' \nu^j \Sigma_f^j(\bar{r},E',t) S(\bar{r},E',t)}$$

Eq. 4.8

$$\int dV \int dE \; W(\bar{r},E) \sum_j \chi_i \beta_i^j \int \nu^j \Sigma_f(\bar{r},E',t) \, S(\bar{r},E',t) \, dE'$$

$$\beta_i(t) \equiv \frac{\int dV \int dE \; W(\bar{r},E) \sum_j \left[\chi_p^j (1-\beta^j) + \sum_i \chi_i \beta_i^j \right] \int dE' \, \nu^j \Sigma_f^j(\bar{r},E',t) \, S(\bar{r},E',t)}{}$$

Eq. 4.9

$$\int dV \int dE \; W(\bar{r},E) \; \frac{1}{v(E)} \; S(\bar{r},E,t)$$

$$\Lambda(t) \equiv$$

$$\int dV \int dE \; W(\bar{r},E) \sum_j \left[\chi_p^j (1-\beta^j) + \sum_i \chi_i \beta_i^j \right] \int dE' \nu^j \Sigma_f(\bar{r},E',t) \; S(\bar{r},E',t)$$

Eq. 4.10

$$\beta(t) \equiv \sum_{i=1}^{I} \beta_i(t) \qquad \text{Eq. 4.11}$$

$$Q(t) \equiv \frac{\int dV \int dE\, W(\bar{r},E)\, q(\bar{r},E,t)}{\int dV \int dE\, W(\bar{r},E,t)\, \frac{1}{v(E)}\, S(\bar{r},E,t)} \qquad \text{Eq. 4.12}$$

$$C_i(t) \equiv \frac{\int dV \int dE\, W(\bar{r},E)\, \chi_i\, C_i(r,t)}{\int dV \int dE\, W(\bar{r},E)\, \frac{1}{v(E)}\, S(\bar{r},E,t)} \qquad \text{Eq. 4.13}$$

4.3 INTERPRETATION OF POINT KINETICS PARAMETERS

Q(t) : is a weighted integral number of the total number of neutrons being introduced into the reactor per second from extraneous sources at time t.

Ci(t): is a weighted integral of the total number of delayed-neutron precursors present in the reactor at time t.

If W(r,E) is taken as unity, and we use the fact that the $\chi i(E)$ are normalized so that $\int_0^\infty \chi_i(E)dE = 1$, then for W(r,E) = 1

$$Q(t) = \int dV \int dE\, q(\bar{r},E,t) \qquad \text{Eq. 4.14}$$

$$C_i(t) = \int dV\, C_i(\bar{r},t) \qquad \text{Eq. 4.15}$$

Q(t) : is the total number of source neutrons introduced per second of time t and

Ci(t): is the total number of precursors present in the reactor at that time.

ρ (t) : The parameter $\rho(t)$ defined by Equation 4.8 is called the reactivity of the reactor.

To provide a physical interpretation of $\rho(t)$ we replace the term $S(r,E,t)$ in the expression for $\rho(t)$ by $S(r,E,t)T(t)$ [i.e., $\phi(r,E,t)$]. We also recognize that the expression

$$\chi_p^j (1 - \beta^j) + \sum_i \chi_i \beta_i^j$$

is the total fission spectrum χ_i for isotope j.

Thus, Equation 4.8 may be written as:

$$\int dV \int dE\ W(\bar{r},E)\ \left\{\nabla\cdot D(\bar{r},E,t)\nabla\phi(r,E,t) - \Sigma_t(\bar{r},E,t)\,\phi(\bar{r},E,t)\right\}$$

$$+ \int dE' \Sigma_s(\bar{r},E'\rightarrow E,t)\,\phi(\bar{r},E',t)$$

$$+ \sum_j \chi^j(E) \int dE' \Sigma_f^j(\bar{r},E',t)\,\phi(\bar{r},E',t)$$

$$\rho(t) \equiv \frac{}{\int dV \int dE\ W(\bar{r},E) \sum_j \chi^j(E) \int dE' \nu^j \Sigma_f^j(\bar{r},E',t)\,\phi(\bar{r},E',t)}$$

Eq 4.16

The term

$$\sum_j \chi^j(E) \int dE' \nu^j(E) \Sigma_f^j(\bar{r},E',t) \phi(\bar{r},E',t)$$

is the rate at which events that are occurring at time t will ultimately (.i.e, after delayed neutron precursors decay) produce neutrons in dVdE.

We shall call it the instantaneous production rate due to fission. It follows that the denominator of Equation 4.16 is a weighted integral over the whole reactor of this instantaneous production rate. If W(r.E) were unity, it would be exactly the instantaneous production rate throughout the reactor of neutrons due to fission. Even then, the term is a bit artificial in that only $1-\beta^j$ of the neutrons "instantaneously produced" at time t from fission isotope J appear physically at that time.

The term

$$\nabla \cdot D(\bar{r},E,t) \nabla \phi(\bar{r},E,t) + \Sigma_t(\bar{r},E,t) \phi(\bar{r},E,t) - \int dE' \Sigma_s(\bar{r}, E' \to E) \phi(\bar{r},E',t)$$

in the numerator of Equation 4.16 is the destruction rate of neutrons in dVdE at time t. (This destruction rate is truly "instantaneous".) Thus the numerator of $\rho(t)$ is a weighted integral of the net "instantaneous" production rate of neutrons in the reactor.

Reactivity is then the ratio of this net weighted rate due to the weighted fission source. It can be thought of loosely as the fractional increase per generation in the number of neutrons present in the core when one imagines all fission neutrons born instantaneously (i.e., when DN are included).

The reactivity of a reactor is, in general, time-dependent, primarily because D, Σ_t, Σ_s and $\nu\Sigma_f$ depend on time, but also because of the time dependence of the shape part of $\phi(r.E.t)$. Since in a critical reactor D, Σ_t, Σ_s, $\nu\Sigma_f$ are independent of time and the flux shape is the critical flux shape, we see that the numerator of $\rho(t)$ and hence $\rho(t)$ itself is zero for a critical reactor. If the production rate exceeds the destruction rate, $\rho(t) > 0$ and the reactor is said to be supercritical; if the production rate is less than the destruction rate, $\rho(t) < 0$ and the reactor is subcritical. Also, if $\rho = \beta$, the reactor is said to be prompt-critical and if $\rho > \beta$, it is super-prompt-critical.

Reactivity, being a ratio of rates, is dimensionless. It is thus often expressed as a pure number (0.001 in reactivity) or in percent (0.1 percent in reactivity). It is also expressed in multiples of β, and when this is done the units of "dollars" and "cents" are used. Thus, $\rho = \beta$ implies a reactivity of one dollar or 100 cents. In other words, ρ/β is the "dollar reactivity".

$\beta_i(t)$: The parameter β_i is called the effective delayed neutron fraction for the i-th precursor family. The sum β is then the "total effective delayed neutron fraction". As with $\rho(t)$, we can rewrite Equation 4.9 as:

$$\beta_i(t) = \frac{\int dV \int dE\, W(\bar{r},E) \sum_j \chi_i \beta_i^j \int_0^\infty dE'\, \nu^j \Sigma_f^j(\bar{r},E',t)\, \phi(\bar{r},E',t)}{\int dV \int dE\, W(\bar{r},E) \sum_j \chi^j(E) \int_0^\infty dE'\, \nu^j \Sigma_f^j(\bar{r},E',t)\, \phi(\bar{r},E',t)} \qquad \text{Eq. 4.17}$$

In view of the earlier discussion, we can interpret $\beta_i(t)$ as the "instantaneous" weighted rate of production of delayed neutrons belonging to group i throughout the reactor, divided by the "instantaneous" weighted rate of all neutron production due to fission. If W(r.E) is taken as unity, and there is only one fissionable isotope in the reactor (i.e., only one term in the sum over j), $\beta_i(t)$ becomes the β_i of that isotope. If several fissioning isotopes (U-235, Pu-239, Pu-241, etc.) are present and, again, if $W(r,E) = 1$, the $\beta_i(t)$ become averages of the different β_i^j weighted by the amount of fissioning due to each isotope.

$\Lambda(t)$ The final kinetics parameter is called the prompt-neutron lifetime. This is interpreted as the time an average neutron survives after it appears as either a prompt neutron or one emitted from a delayed-neutron precursor. This interpretation is quite accurate for the studies performed in this thesis, since we will deal with reasonably slow transients.

4.4 MATHEMATICAL FOUNDATION OF SPATIAL REACTOR KINETICS

In Sections 4.1 and 4.2, it has been pointed out that point-reactor kinetics is an analytical tool to handle reactor kinetics problems provided certain conditions are satisfied. However, discussions carried out throughout Chapter Three and in Section 4 of this chapter indicate that the space-time kinetics of the modern generation of nuclear power reactors cannot be handled accurately with the point-reactor kinetics techniques. Predicting the space-time kinetics of a CANDU-PHW reactor requires the solution of a set of partial differential equations which describe the variation of the neutron flux, delayed neutron precursors, iodine and xenon concentrations in both space and time.

The set of equations used to define the CANDU-PHW reactor kinetics is:

$$\frac{1}{v}\frac{d\phi(\bar{r},t)}{dt} = \nabla\cdot D(\bar{r},t)\nabla\phi(\bar{r},t) - \Sigma_a(\bar{r},t)\phi(\bar{r},t) - \sigma_{Xe}X_e(\bar{r},t)\phi(\bar{r},t) + \sum_i \lambda_i C_i(\bar{r},t)$$

$$\frac{\partial C_i(\bar{r},t)}{\partial t} = -\lambda_i C_i(\bar{r},t) + \beta_i \nu\Sigma_f(\bar{r},t)\phi(\bar{r},t)$$

$$\frac{\partial I(\bar{r},t)}{\partial t} = \gamma^I\Sigma_f(\bar{r},t)\phi(\bar{r},t) - \lambda^I I(\bar{r},t)$$

$$\frac{\partial X_e(\bar{r},t)}{\partial t} = \gamma^{Xe}\Sigma_f(\bar{r},t)\phi(\bar{r},t) + \lambda^I I(\bar{r},t) - \lambda^{Xe}X_e(\bar{r},t) - \sigma_{Xe}\phi(\bar{r},t)X_e(\bar{r},t)$$

Eq. 4.17 to 4.20

where the terms have the same meaning as in the detailed analysis of previous sections and in Chapter Three.

The above set of equations is applicable to the one group neutron energy representation. Although the one group approximation is utilized in the modal formulation of SMOKIN equations, there is, in principle, no requirement that such a restriction be applied. The purpose of this thesis was not to develop a modal analysis approximation but is merely its application to assess the controllability of an 850 MW(e) CANDU-PHW reactor fuelled with natural and Low Enriched Uranium (LEU-CANDU-PHW). From now on throughout this thesis, we will call this: 850 MW(e) LEU-CANDU-PHW reactor (Ref. 24).

4.5 FOUNDATION OF MODAL ANALYSIS

4.5.1 General Considerations

Equations 4.17 through 4.20 are coupled non-linear partial differential equations. Practically speaking, partial differential equations cannot be used as such for control system development. The partial differential equations must be converted to or approximated by finite-difference equations, or, with some special techniques, to integratable ordinary differential equations in the time variable.

The Spatial MOdal KINetics method will be outlined in this section. This approach has some similarity to the quasi-static method due to D.A. Meneley (Ref. 14), and the improved quasi-static method (Ref. 15).

However, it does differ significantly from these two approaches in that time-independent spatial mode functions are used to obtain time-varying equations for modal amplitude weightings. The mode shapes are not solved in a dynamic sense but are obtained in an off-line, static manner from a flux harmonic code such as MONIC (Ref. 25).

4.5.2 Approximate Solution Methods for Nuclear Reactor Spatial Dynamics

When considering a numerical method, one must keep in mind the intended use of the model. The model being developed is intended to form the basis of a multivariable problem. In the past, a solution of the nuclear reactor dynamics equation set was primarily for safety requirements. Today, with the increasing demand for nuclear energy, additional requirements are extended to control studies. The requirements of safety and control studies differ. Control requires accuracy (w.r.t. to some target); safety requires conservatism (which may well be grossly inaccurate). Control studies' accuracy requirements imply an extensive set of transient simulations.

Several numerical solution methods for space-time nuclear reactor dynamics have been developed (Ref. 24). Three main categories can be found: finite difference, nodal and modal or synthesis techniques. The finite-difference and nodal techniques are mathematically similar but differ as to the spatial scale to which they are applied. In principle, provided mesh spacing and time steps are small enough and an implicit (i.e. unconditionally stable) solution strategy is used, a finite difference is exact; spatial approximations required by large nodes make nodal methods approximate. Discussions of these two techniques were provided earlier in this thesis. The modal synthesis technique provides the potential for accurate and low cost solutions to nuclear reactor transients.

4.5.3 Factorization of Space-Time Distribution

The space-time kinetics Equations 4.17 through 4.20 are factored into a weighted sum of a finite set of fixed spatial shape functions $\psi_m(r)$ which have no time dependence and a set of time-dependent weighting amplitudes (Refs. 21, 22, 26).

$$\phi(\bar{r},t) = \sum_{m=1}^{M} L_m(\bar{r},r_0)\,\psi_m(\bar{r})\,a_m(t) \qquad \text{Eq. 4.21}$$

$$C_i(\bar{r},t) = \frac{1}{U}\sum_{m=1}^{M} \psi_m(\bar{r})\,C_{im}(t) \qquad \text{Eq. 4.22}$$

$$I(\bar{r},t) = \frac{1}{U}\sum_{m=1}^{M} \psi_m(\bar{r})\,I_m(t) \qquad \text{Eq. 4.23}$$

$$X_e(\bar{r},t) = \frac{1}{U}\sum_{m=1}^{M} \psi_m(\bar{r})\,X_m(t) \qquad \text{Eq. 4.24}$$

where:

$\phi(r,t)$ = space-time-dependent neutron flux;

$C_i(r,t)$ = space-time-dependent distribution of i-th delayed-neutron precursor family;

$I(r,t)$ = space-time concentration of I-135;

$X(r,t)$ = space-time concentration of Xe-135;

$\psi_m(r)$ = spatial shape function for the m-th flux harmonic (nodes);

$a_m(t)$, $C_{mi}(t)$, $I_m(t)$, $X_m(t)$ = time-dependent weighting amplitude for the m-th spatial shape function m(r);

υ = mean neutron velocity;

$L_m(r,r_o)$ = is a space-dependent shape multiplier function which is introduced to account for localized neutron flux effects associated with a change in core material properties of a location r_o relative to a reference distribution of core material properties.

The above weighting expansion will allow us to transform the space-time dependent kinetics Equations 4.17 through 4.20 into a set of time-dependent, coupled, ordinary differential equations describing the dynamics of the amplitudes $a_m(t)$, $C_{mi}(t)$, $I_m(t)$, $X_m(t)$.

4.5.4 The Space-Dependent Part of Modal Kinetics Analysis

The mathematical formulation of two group diffusion theory is summarized as follows:

- the scalar flux function for r in region k as

$$\phi_1(\bar{r}) = \int_{E_c}^{E_\infty} dE\, \phi(\bar{r},E) \equiv \text{fast flux} \qquad \text{Eq. 4.25}$$

$$\phi_2(\bar{r}) = \int_{0}^{E_c} dE\, \phi(\bar{r},E) \equiv \text{thermal flux} \qquad \text{Eq. 4.26}$$

From Appendix MG, the two group diffusion equations that are the basis for handling most physics calculations in thermal reactor design are rewritten here for convenience (superscript k is dropped).

$$-D(E)\,\Psi_1(E)\,\nabla^2\phi_1(\bar{r}) + \Sigma_t(E)\Psi_1(E)\phi_1(\bar{r}) =$$
$$\int_{E_c}^{\infty}\left[\frac{1}{\lambda}\chi(E)\,\nu\Sigma_f(E') + \Sigma_s(E'\to E)\,\Psi_1(E)\right]dE'\,\phi_1(\bar{r})$$
$$+\int_{0}^{E_c}\left[\frac{1}{\lambda}\chi(E)\,\nu\Sigma_f(E')\,\Psi_2(E')\right]dE'\,\phi_2(\bar{r})$$

Eq. 4.27

$$-D(E)\,\Psi_2(E)\,\nabla^2\phi_2(\bar{r}) + \Sigma_t(\bar{r})\,\Psi_2(E)\,\phi_2(\bar{r}) =$$

$$\int_{E_c}^{E_\infty}\left[\frac{1}{\lambda}\chi(E)\,\nu\Sigma_f(\bar{r})\,\Psi_1(E') + \Sigma_s(E'\to E)\,\Psi_1(E)\right]dE'\phi_1(\bar{r})$$

$$+\int_{0}^{E_c}\left[\frac{1}{\lambda}\chi(E)\,\nu\Sigma_f(\bar{r})\,\Psi_2(E') + \Sigma_s(E'\to E)\,\Psi_2(E')\right]dE'\phi_2(\bar{r})$$

Eq. 4.28

Making the same substitution made in Appendix MG, it is possible to rewrite the typically used two-group diffusion equations in thermal power reactors:

$$D_1\nabla^2\phi_1(\bar{r}) - \Sigma_1\phi_1(\bar{r}) + \frac{1}{\lambda}\chi_1\left[\nu\Sigma_{f1}(\bar{r})\phi_1(\bar{r}) + \nu\Sigma_{f2}(\bar{r})\phi_2(\bar{r})\right] = 0$$

$$D_2\nabla^2\phi_2(\bar{r}) - \Sigma_2\phi_2(\bar{r}) + \frac{1}{\lambda}\chi_2\left[\nu\Sigma_{f1}(\bar{r})\phi_1(\bar{r}) + \nu\Sigma_{f2}(\bar{r})\phi_2(\bar{r})\right]$$

$$+ \Sigma_{12}\phi_1(\bar{r}) = 0$$

Eq. 4.29, 4.30

However, in most thermal reactors, the energy boundary between fast and thermal neutron groups is low enough (of the order 1 eV) that $\chi_2 = 0$. The term is included in Equation 4.30 for those cases we wish to deal with such as fast reactors for which E_c is much higher.

In CANDU reactors, the further simplification $\Sigma_{f1} = 0$ is used, which can be justified with a proper redefinition of Σ_{f2}. The

global shape functions that we use in CANDU-PHW reactor core studies are the neutron eigenfunctions associated with the two group static diffusion equations for a reference core configuration. The eigenfunctions are the solutions of the following set of equations:

$$D_1^0 \nabla^2 \phi_{1m}(\bar{r}) - \Sigma_1^0(\bar{r})\,\phi_{1m}(\bar{r}) + \frac{\nu\Sigma_{f2}^0}{k_m}\,\phi_{2m}(\bar{r}) = 0$$

$$D_2^0 \nabla^2 \phi_{2m}(\bar{r}) - \Sigma_{a2}^0(\bar{r})\,\phi_{2m}(\bar{r}) + \Sigma_{12}^0(\bar{r})\,\phi_{1m}(r) = 0 \qquad \text{Eq. } \begin{matrix}4.31\\4.32\end{matrix}$$

where:

D_1, D_2 : fast and thermal neutron diffusion coefficients;

$\nu\Sigma_{f2}$: thermal fission yield (as said above, $\Sigma_{f1} = 0$);

Σ_{a2} : thermal neutron absorption cross-section;

Σ_1^0 : total fast neutron removal cross-section

Σ_{12}^0 : fast-to-thermal group down-scattering cross-section;

Σ_{a1} : fast-neutron group absorption cross-section;

k_m : k effective eigenvalue associated with the m-th eigenfunctions.

The superscript "o" denotes that the core properties are for a fixed reference core configuration.

A typical reference core configuration is the equilibrium burn-up fuelled core with all normally inserted rods (adjusters) in the core, all normally withdrawn rods (mechanical control absorbers, shut-off rods) out of the core, and liquid zone control compartments of some nominal fill (for example, 40%, 50% full). For the given reference core configuration, the global shape functions are selected to be the thermal group mode distribution, that is

$$\Psi_m(\bar{r}) = \Psi_{m2}(\bar{r}) \qquad \text{Eq. 4.33}$$

These mode functions are obtained from a finite-difference, two-group diffusion theory code "MONIC" (Ref. 25). The modal functions generated by MONIC are essentially biorthogonal with respect to the state neutron production operator $\nu\Sigma_{f2}$, that is

$$\int_{REACTOR} \Psi_m(\bar{r})\, \nu\Sigma_{f2}(\bar{r})\, \Psi_n(\bar{r}) = B_m \delta_{mn} \qquad \text{Eq. 4.34}$$

with

$$\delta_{mn} = 1 \qquad m = n$$
$$\delta_{mn} = 0 \qquad m \neq n \qquad \text{Eq. 4.34a}$$

Provided localized perturbations are not strong, the modes determine the global changes in neutron flux distribution throughout the core resulting from changes in neutron balance anywhere in the core, irrespective of whether changes are localized or widely distributed. For the case of relatively strong perturbations in core properties with respect to reference properties, the modal functions are no longer sufficient to describe the changes in the flux distribution. For example, the mode shapes are not capable of representing the localized flux depression resulting from the insertion of a strong absorbing control rod (shut-off rod). To account for this localized effect, the SPACE-TIME MODAL KINETICS analysis is completed with the addition of local effect multiplier functions.

4.5.5 The Local Effects Function

4.5.5.1 Plane Source

The local effect function is derived starting with the introduction of diffusion equations applied to the determination of spatial distribution of neutrons by considering infinite media which contains a plane of isotropic neutron sources of strength S_o neutrons per unit area per unit time. The problem is to determine the neutron flux distribution throughout the infinite medium in the steady state, that is, long after the source has begun emitting neutrons. The concept of a plane distribution of isotopic sources reduces to the problem of finding the

spatial dependence of the flux in terms of a single coordinate, in the time-independent case. If x denotes the coordinate normal to the infinite-source plane (which is placed at x = o), then clearly the flux must be independent of y and z.

Thus, $\phi(x,y,z) \Rightarrow \phi(x)$, and for $x \neq o$ the diffusion equation governing this problem is readily written:

$$\nabla^2\phi(x) - \frac{1}{M^2}\phi(x) = 0 \; ; (x \neq 0) \qquad \text{Eq. 4.35}$$

where we define the diffusion length M by

$$M^2 = \frac{D}{\Sigma_a} \qquad \text{Eq. 4.36}$$

The general solution of Equation 4.35 may be written in the exponential form as:

$$\phi(x) = A \exp\left\{+\frac{x}{M}\right\} + B \exp\left\{-\frac{x}{M}\right\}$$

and applies only to regions away from the origin. We note, however, that the system is symmetric about x = o; thus we may consider the solution for x > o alone. Boundary conditions applied to the flux (finite and non-negative in all regions in which the diffusion equation applies) implies A = o. We have then:

$$\phi(x) = B \exp\left\{-\frac{x}{M}\right\} \qquad \text{Eq. 4.38}$$

B is determined from the boundary condition

$$J_2(0) - J_1(0) = S_0 \qquad \text{Eq. 4.39}$$

In the present situation, the source is isotropic, therefore, exactly one-half the neutrons must be released in each side. Thus,

$$\lim_{|x|=0} J(x) = \frac{1}{2} S_0 \qquad \text{Eq. 4.40}$$

and with the help of Fick's Law (one-dimension)

$$J(x) = -D \nabla \phi(x) = -D \frac{d\phi(x)}{dx} \qquad \text{Eq. 4.41}$$

leads to

$$B = \frac{M}{2D} S_0 \qquad \text{Eq. 4.42}$$

The solution of Equation 4.35 is, therefore,

$$\phi(x) = \frac{M S_0}{2D} \exp\left\{ - \frac{x}{M} \right\} \qquad \text{Eq. 4.43}$$

Equation 4.43 gives the spatial distribution of neutrons in an infinite medium with a plane isotopic source. Figure 4.1.

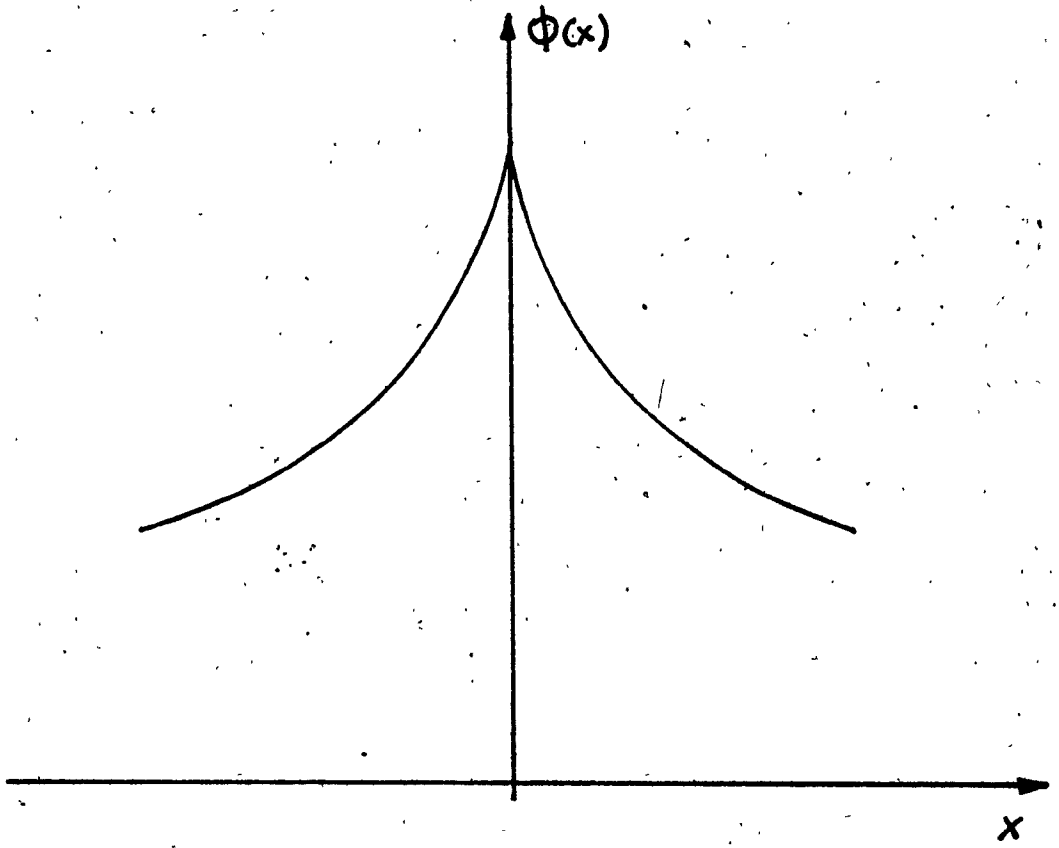

FIGURE 4.1: Flux Distribution Due to Plane Source

To complete this section, we look for a solution kernel for the plane source that is closer to the case for a power reactor. In the previous section, we found a solution for the flux resulting from a plane source at the origin:

$$\phi(x) = \frac{M S_0}{2D} \exp\left\{-\frac{x}{M}\right\} \qquad \text{Eq. 4.44}$$

If this source had been located at x', then the flux at a position x would be

$$\phi(x) = \frac{M S_0}{2D} \exp\left\{|x-x'|/M\right\} \qquad \text{Eq. 4.45}$$

Thus, in general, for $S(x')dx'$ we find

$$\phi(x) = \int_{-\infty}^{\infty} dx' \left[\frac{L}{2D} \exp\left\{\frac{-|x-x'|}{M}\right\}\right] S(x')$$

$$= \int_{-\infty}^{\infty} dx' \, G_{pl}(x,x') \, S(x') \qquad \text{Eq. 4.46}$$

where Gpl(x,x') is known as the plane diffusion kernel for an infinite medium and is identified as:

$$G_{pl}(x,x') = \frac{L}{2D} \exp\left\{-\frac{|x-x'|}{M}\right\} \qquad \text{Eq. 4.47}$$

4.5.6 The Localised Flux Perturbation

The local flux effect at the site of the perturbation is related to the unperturbed flux at the site and the changes in cross-sections introduced by the perturbation. The neutron balance equation for the cells in which a perturbation occurs may be expressed as:

$$D\nabla^2\phi(\bar{r}) - [\Sigma_a + \Delta\Sigma_a][\phi(\bar{r}) + \Delta\phi(\bar{r})]$$

$$+[\nu\Sigma_f(\bar{r}) + \Delta\nu\Sigma_f(\bar{r})][\phi(\bar{r}) + \Delta\phi(\bar{r})] = \Delta S(\bar{r}) \quad \text{Eq. 4.48}$$

where:

$\phi(\bar{r})$ = flux prior to perturbation;

$\Delta\phi(\bar{r})$ = change in the flux due to the perturbation;

$\Sigma_a, \nu\Sigma_f$ = cell cross-sections prior to the perturbation;

$\Delta\nu\Sigma_f, \Delta\Sigma_a$ = are incremental cell cross-sections associated with the perturbation;

$\Delta S(\bar{r})$ = incremental neutron sink/source term.

We now define the incremental neutron source/sink as the change in the fission source associated with the perturbation and write it as:

$$\Delta S(\bar{r}) = \left[\nu \Sigma_f(\bar{r}) + \Delta\nu \Sigma_f(\bar{r})\right] \Delta\phi(\bar{r}) \qquad \text{Eq. 4.49}$$

Substituting Equation 4.49 into Equation 4.48, and utilizing the steady-state relationship for the unperturbed cell flux given by:

$$D\nabla^2\phi(\bar{r}_0) - \Sigma_a(r_0)\phi(\bar{r}_0) + \nu\Sigma_f(\bar{r}_0)\phi(\bar{r}_0) = 0 \qquad \text{Eq. 4.50}$$

yields a convenient flux correction factor given by:

$$\alpha(\bar{r}_0) = \frac{\Delta\phi(\bar{r}_0)}{\phi(\bar{r}_0)} = \frac{\Delta\nu\Sigma_f(\bar{r}_0) - \Delta\Sigma_a(\bar{r}_0)}{\Sigma_a(r_0) + \Delta\Sigma_a(\bar{r}_0)} \qquad \text{Eq. 4.51}$$

The flux of any location r due to a perturbation at r_0 characterized by the incremental local effect factor $\alpha(r_0)$ is given by (Refs. 15, 16, 17).

$$\phi_{PERT}(\bar{r}_0) = \phi(r) + \Delta\phi(\bar{r}_0) = b(\bar{r})\phi(r) \qquad \text{Eq. 4.52}$$

with the local effect flux multiplier given by:

$$b(\bar{r}) = 1 + \alpha(\bar{r}_0)\frac{\phi(\bar{r}_0)}{\phi(\bar{r})}\exp\left\{-\frac{|\bar{r}-\bar{r}_0|}{M}\right\} \qquad \text{Eq. 4.53}$$

At the perturbed cell itself, the flux multiplier is simply

$$b(r_o) = 1 + \alpha(r_o) \qquad \text{Eq. 4.54}$$

which is consistent with the definition of $\alpha(r_o)$ in Equation 4.51.

4.5.7 Neutron Source/Sink Perturbation

Depending on whether the numerator of Equation 4.51 is greater or less than zero, the incremental local flux is an effective source or sink respectively.

The Equation 4.51 is rewritten here:

$$\alpha(r_o) = \frac{\Delta\phi(r_o)}{\phi(r_o)} = \frac{\Delta\nu\Sigma_f(r_o) - \Delta\Sigma_a(r_o)}{\Sigma_a(r_o) + \Delta\Sigma_a(r_o)}$$

If

$$\Delta\Sigma(r_o) \equiv \Delta\nu\Sigma_f(r_o) - \Delta\Sigma_a(r_o) > 0$$

then

$$\Delta\phi(r_o) = \alpha(r_o)\,\phi(r_o) > 0 \qquad \text{Eq. 4.55}$$

This incremental neutron source appears as an incremental fast flux which will be thermalized by the moderator. Therefore, in the surrounding cells, the constant M appears to be exactly the neutron migration length given by (Ref. 27).

$$M^2 = L_1^2 + L_2^2 = \frac{D_1}{\Sigma_{R1}} + \frac{D_2}{\Sigma_{R2}}$$

$$= \frac{D_1^\circ}{\Sigma_{a1}^\circ} + \frac{D_2^\circ}{\Sigma_{a2}^\circ} \qquad \text{Eq. 4.56}$$

where D_2, D_1, Σ_{a1}, Σ_{a2}, have the same meaning in Equation 4.32.

If the incremental cross-sections associated with the perturbation are such that

$$\Delta\Sigma(\bar{r}_0) = \Delta\nu\Sigma_f(\bar{r}_0) - \Delta\Sigma_a(r_0) < 0 \qquad \text{Eq. 4.57}$$

and the flux is depressed. The perturbation site is therefore a sink for thermal neutrons with the surrounding cells acting as a source of thermal neutrons.

4.6 DERIVATION OF SMOKIN EQUATIONS

The set of coupled partial differential equations describing the dynamics of neutron thermal flux, delayed neutron precursors, and fission products iodine and xenon concentration are reduced to a set of coupled ordinary differential equations as follows. The space-time factorization for $\phi(r,t)$, $C_i(r,t)$, $I(r,t)$ and $Xe(r,t)$ is rewritten here for convenience.

This is essentially a weighted residual procedure with the weighting functions taken as the harmonic modes (Galerkin weighting). Utilizing the inner product notation for weighted integrals, the space-time reactor dynamical equations may be expressed as:

$$\phi(\bar{r},t) = \sum_{m=1}^{M} L_m(\bar{r},r_0)\,\psi_m(\bar{r})\,a_m(t) \qquad \text{Eq. 4.58}$$

$$C_i(\bar{r},t) = \frac{1}{V}\sum_{m=1}^{M} \psi_m(\bar{r})\,c_{im}(t) \qquad \text{Eq. 4.59}$$

$$I(\bar{r},t) = \frac{1}{V}\sum_{m=1}^{M} \psi_m(\bar{r})\,I_m(t) \qquad \text{Eq. 4.60}$$

$$Xe(\bar{r},t) = \frac{1}{V}\sum_{m=1}^{M} \psi_m(\bar{r})\,Xe_m(t) \qquad \text{Eq. 4.61}$$

The space-time factorization for $\phi(r,t)$, $C_i(r,t)$, $I(r,t)$ and $X(r,t)$ given by the above equations are substituted into Equations 4.17 through 4.20. Premultiplication of the new equations by the harmonic mode ψ_k and integration over the

volume of the reactor and using the inner product notation, the following set of equations is derived:

$$\sum_{m=1}^{M} \langle \psi_k | \frac{1}{v} | \psi_m \rangle \frac{da_m(t)}{dt} =$$

$$\sum_{m=1}^{M} \left\{ \langle \psi_k | D\nabla^2 - \Sigma_{a2} + (1-\beta)\nu\Sigma_f | \psi_m \rangle a_m(t) \right\}$$

$$- \sum_{m=1}^{M} \sum_{n=1}^{M} \langle \psi_k | \frac{\sigma_x}{v} \psi_n | \psi_m \rangle \chi_n(t) a_m(t)$$

$$+ \sum_{i} \sum_{m=1}^{M} \langle \psi_k | \frac{\lambda_i}{v} | \psi_m \rangle c_{mi}(t)$$

Eq. 4.62.

$$\sum_{m=1}^{M} \langle \psi_k | \frac{1}{v} | \psi_m \rangle \frac{dc_{mi}(t)}{dt} =$$

$$-\lambda_i \sum_{m=1}^{M} \langle \psi_k | \frac{1}{v} | \psi_m \rangle c_{mi}(t)$$

$$+ \beta_i \sum_{m=1}^{M} \langle \psi_k | \nu\Sigma_f | \psi_m \rangle a_m(t)$$

Eq. 4.63

$$\sum_{m=1}^{M} \langle \psi_k | \frac{1}{v} | \psi_m \rangle \frac{dI_m(t)}{dt} =$$

$$-\lambda_I \sum_{m=1}^{M} \langle \psi_k | \frac{1}{v} | \psi_m \rangle I_m(t)$$

$$+ \gamma^I \sum_{m=1}^{M} \langle \psi_k | \Sigma_f | \psi_m \rangle a_m(t)$$

Eq. 4.64

$$\sum_{m=1}^{M} \langle \psi_k | \frac{1}{v} | \psi_m \rangle \frac{d x_m(t)}{dt} =$$

$$- \lambda_x \sum_{m=1}^{M} \langle \psi_k | \frac{1}{v} | \psi_m \rangle x_m(t)$$

$$+ \lambda_I \sum_{m=1}^{M} \langle \psi_k | \frac{1}{v} | \psi_m \rangle a_m(t)$$

$$+ \gamma^x \sum_{m=1}^{M} \langle \psi_k | \Sigma_f | \psi_m \rangle a_m(t)$$

$$- \hat{\sigma}^x \sum_{m} \sum_{n} \langle \psi_k | \frac{1}{v} \psi_n | \psi_m \rangle x_n(t) a_m(t) \qquad \text{Eq. 4.65}$$

The above equation may be substantially simplified utilizing the biorthogonalization property of the modes: (Ref. 21)

$$\langle \psi_k | \nu \Sigma_f | \psi_m \rangle = 0 ; \quad k \neq m \qquad \text{Eq. 4.66}$$

$$\langle \psi_k | \nu \Sigma_f | \psi_m \rangle \neq 0 ; \quad k = m \qquad \text{Eq. 4.67}$$

$$\langle \psi_k | \psi_m \rangle \approx 0 ; \quad k \neq m \qquad \text{Eq. 4.68}$$

$$\langle \psi_k | \psi_m \rangle \neq 0 ; \quad k = m \qquad \text{Eq. 4.69}$$

in addition to the properties

$$\langle \psi_k | \psi_n | \psi_m \rangle \ll \psi_i | \psi_m | \psi_m \rangle \qquad \text{Eq. 4.70}$$

$$\langle \psi_i | \psi_m | \psi_m \rangle = \langle \psi_m | \psi_m | \psi_i \rangle = \langle \psi_m | \psi_i | \psi_m \rangle \qquad \text{Eq. 4.71}$$

Furthermore, defining the cross-sections and diffusion coefficients at any time as the reference values plus incremental perturbations, according to:

$$\nu\Sigma_f = \nu\Sigma_f^{\circ} + \Delta\nu\Sigma_f \qquad \text{Eq. 4.72}$$

$$\Sigma_a = \Sigma_a^{\circ} + \Delta\Sigma_a \qquad \text{Eq. 4.73}$$

$$D = D^{\circ} + \Delta D \qquad \text{Eq. 4.74}$$

and utilizing the solutions for the modes $\psi_m(r)$ obtained with the reference configuration parameters ($D^{\circ}, \nu\Sigma_f^{\circ}, \Sigma_a^{\circ}$), the equations for the mode amplitudes are obtained in the following form (Ref. 21)

$$\frac{da_m(t)}{dt} = \frac{\rho_{scm} + \rho_{mn} - \beta}{\Lambda_m} a_m(t) + \sum_{\substack{m \\ n \neq m}}^{M} \sum_{n}^{M} \frac{\rho_{mn}}{\Lambda_m} a_m(t) + \sum_{i=1}^{I} \lambda_i C_{mi}(t) + \sum_{n}^{M} \frac{\rho_{mn}^{Xe}}{\Lambda_m} a_n(t) \qquad \text{Eq. 4.75}$$

$$\frac{dc_{mi}(t)}{dt} = -\lambda_i C_{mi}(t) + \frac{\beta_i}{\Lambda_m} a_m(t) \qquad \text{Eq. 4.76}$$

$$\frac{dI_m(t)}{dt} = -\lambda_I I_m(t) + \frac{\gamma'_I}{\Lambda_m} a_m(t) \qquad \text{Eq. 4.77}$$

$$\frac{dX_{cm}(t)}{dt} = -\lambda_x X_m(t) + \lambda_I I_m(t) + \frac{\gamma'_x}{\Lambda_m} a_m(t) - \sigma_x \sum_k \sum_n A_{mnk} X_{ka_n} \qquad \text{Eq. 4.78}$$

where the parameters are defined as follows:

ρ_{scm} : subcritical reactivity of mode in relation to fundamental mode (mode 1);

$$= \rho^{o}_{scm} + \rho_{mn} - \rho_{11} \qquad \text{Eq. 4.79}$$

ρ^{o}_{scm} : subcritical reactivity of mode m in the reference configuration;

$$= \frac{1}{k_1} - \frac{1}{k_m} \qquad \text{Eq. 4.80}$$

Λ_m : prompt neutron generation time for mode m;

ρ_{mn} : modal reactivity coupling modes m and n due to a perturbation in a region $\delta(r)$ of the core;

$$= \frac{\langle \psi_m | (\Delta \nu\Sigma_f - \Delta\Sigma_a) R\delta(r) | \psi_n \rangle + \langle \psi_m | \Delta D \Omega | \psi_n \rangle}{\langle \psi_m | \nu\Sigma_f^{\circ} | \psi_n \rangle} \qquad \text{Eq. 4.81}$$

R : local effect perturbation factor;

$$= \frac{\nu\Sigma_f(r_0)\phi(r_0) + \Delta S(r_0)}{\Sigma_a^c(r_0)\phi(r_0)}$$

$$= k_{\infty}^{th}\,(1 + \alpha(r_0)) \qquad \text{Eq. 4.82}$$

$\delta(r)$ = Dirac delta function defined over perturbation region;

= 1.0 in region of perturbation;

= 0.0 outside region of perturbation;

Ω = operator defining product of flux gradients on surface of region of perturbation, i.e.;

$$\langle \psi_m | \Omega | \psi_n \rangle = \langle \nabla\psi_m | \nabla\psi_n \rangle \delta(r) \qquad \text{Eq. 4.83}$$

ρ_{mn}^{Xe} = xenon reactivity coupling modes m and n;

$\dot{X}_k$ = equilibrium value of mode k xenon amplitude;

$$A_{mnk} = \frac{\langle \psi_m | \frac{\psi_n}{v} | \psi_k \rangle_{CORE}}{\langle \psi_m | \frac{1}{v} | \psi_k \rangle_{CORE}}$$

$$\gamma'_I = \gamma_I / \nu$$

$$\gamma'_{Xe} = \gamma_{Xe} / \nu$$

ν = average neutrons/fission;

$$\hat{\sigma}_x = \sigma_x \phi_o$$

ϕ_o = maximum flux in the fuel at 100% F.P. ($n/cm^2/sec$).

4.7 SMOKIN CODE DESCRIPTION

SMOKIN (Spatial MOdal KINetics) is a simulation program for CANDU Pressurized Heavy Water (CANDU-PHW) reactor space-time kinetics and reactor control system dynamics. The SMOKIN modelling basically replaces the conventional FD system of diffusion equations at thousands of spatial meshpoints with just a few (8 to 12) coupled point-kinetics-like equations based on as many predetermined modes.

SMOKIN is designed and implemented with a high degree of modularity. The basic structure consists of main control programme which calls a series of major functional subroutines. These subroutines perform basic functions such as solution of the modal amplitudes (flux, delayed-neutron precursors, xenon, iodine), synthesizing detector signals, moving reactivity devices, computing device reactivities, etc.

Discrete time solution of the various ordinary differential equations is utilized. Reactor flux and delayed-neutron precursor equations are solved using an exponential approximation with a small "minor" time step equal to the specified reactor control bulk sampling period. Xenon and iodine equations are solved using "major" time step and Euler approximations.

The SMOKIN code is designed to provide a means of simulation for a diversity of reactor operating and postulated accident

transients. Transients of the order of milliseconds to hours or days may be simulated. Reactivity perturbation studies such as channel refuelling operation, shim, start-up and shutdown were performed with the SMOKIN code.

The SMOKIN code has the capability of automatically introducing fresh fuel bundles, moving in and out adjuster banks and shut-off rods, as well as filling and draining liquid zone control compartments at a rate that depends on the operational transient being investigated. The code also has all the capabilities of partial selection of reactivity devices, and printing the study results partially or totally with the flexibility of printing at time steps different from the execution steps.

4.8 SMOKIN MODAL KINETICS EQUATIONS

The modal kinetics Equations 4.82 through 4.85 constitute the analytical basis for the SMOKIN code. The modal equations, together with their parametric equations, are summarized below:

- Neutronic Flux Time-Dependent Modal Amplitude

$$\frac{da_m(t)}{dt} = \left[\frac{\rho_{scm} + \rho_{mn} - \beta}{\Lambda_m}\right] a_m(t) + \frac{\rho_{mi}\, a_i(t)}{\Lambda_m}$$

$$+ \sum_i \lambda_i C_{mi}(t) + \sum_{m=1}^{M} \frac{\rho_{mn}^{xe}}{\Lambda_m} a_m(t)$$

- Delayed Neutron Precursor Time-Dependent Amplitude

$$\frac{d C_{mi}(t)}{dt} = -\lambda_i C_{mi}(t) + \frac{\beta_i}{\Lambda_m} a_m(t)$$

- Iodine-135 Time-Dependent Amplitude

$$d I_m(t) = -\lambda_I I_m(t) + \frac{\gamma_I'}{\Lambda_m} a_m(t)$$

- Xenon-135 Time-Dependent Amplitude

$$\frac{d X_{em}(t)}{dt} = \lambda^I I_m(t) + \frac{\gamma_{xe}'}{\Lambda_m} a_m(t)$$

$$- \lambda_x X_m(t) - \sum_{\substack{m,n \\ m \neq n}}^{M} \hat{\sigma}_{xe} A_{mnk} \left\{X_n a_m(t) + X_m a_n(t)\right\}$$

- Local Flux Effect Multiplier

$$b(r) = \left(1 + \alpha(r_0)\ \frac{\psi_1(r_0)}{\psi_1(r)}\ \exp\{-k|r-r_0|\}\right.$$

$$\alpha(r_0) = \frac{\Delta\nu\Sigma_f - \Delta\Sigma_d}{\Sigma_a(r_0) + \Delta\Sigma_a(r_0)}$$

- Effective Incremental Cross-Sections

$$\Delta\Sigma_{eff} = R\left\{\Delta\nu\Sigma_f - \Delta\Sigma_a\right\}$$

$$R = \left[\frac{\nu\Sigma_f(\bar{r}_0)}{\Sigma_a(r_0)}\right]_{\text{FUEL LATTICE}}$$

- Perturbed Flux

$$\Phi(r,t) = b(r)\,\psi_1(r)\,a_1(t) + \sum_{m\neq 1}^{M} \psi_m(r)\,a_m(t)$$

with reactivity devices included in the reference model, and

$$\phi(\bar{r},t) = b(r) \sum_{m=1}^{M} \psi_m(\bar{r})\,a_m(t)$$

with reactivity devices not included in the reference model.

CHAPTER FIVE

5. DARLINGTON NUCLEAR REACTOR CORE ANALYSIS

5.1 INTRODUCTION

Darlington nuclear power generating station consists of four CANDU-PHW (850 MWe) reactors.

The Darlington reactors have many design features common to all CANDU-PHW reactors. The reactor is essentially a horizontal cylinder with short (50 cm) fuel bundles lying in horizontal channels 6 m long. Fuel bundles consist of 37 cylindrical elements of uranium dioxide sheathed in zircolloy tubes. Fuel channels consist of concentric cylindrical pressure and calandria tubes made of zirconium alloy and are positioned on a square lattice with a 28.575 cm pitch. The pressure and calandria tubes provide physical separation of the pressurized coolant from the very low pressure moderator system. Both coolant and moderator consist of heavy water. The 37-element fuel bundle, the CANDU-PHW flow diagram, reactor assembly and a CANDU-PHW isometric view are shown on Figures 5.1, 5.2, 5.3 and 5.4 respectively.

CANDU-PHW reactors are equipped with physically independent reactor regulating and safety systems. All regulating and safety devices are inserted in interstitial locations in the low pressure moderator environment. The regulating system

makes use of three distinctly different reactivity devices. Fourteen liquid zone controllers consisting of compartments of variable amounts of light water are used to provide continuous bulk and spatial flux control. Top, east and west face views of Darlington reactors showing the reactor zone designation and the locations of the reactivity devices are given in Figures 5.5, 5.6 and 5.7 respectively. More details about liquid zone controllers, mechanical control absorbers, shut-off rods, adjusters and measurement systems are provided in the following sections.

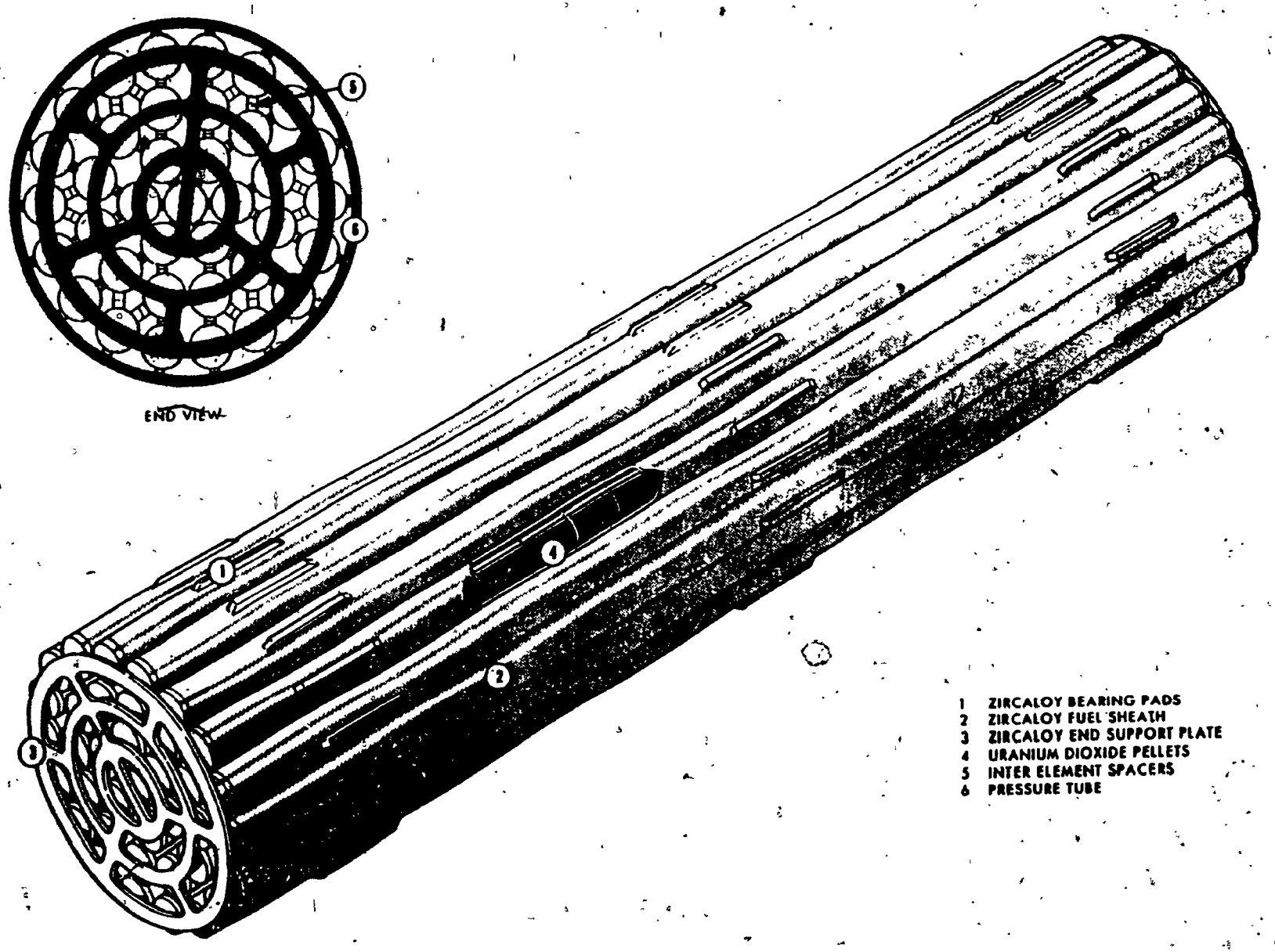

FIGURE 5.1: 37-Element Fuel Bundle

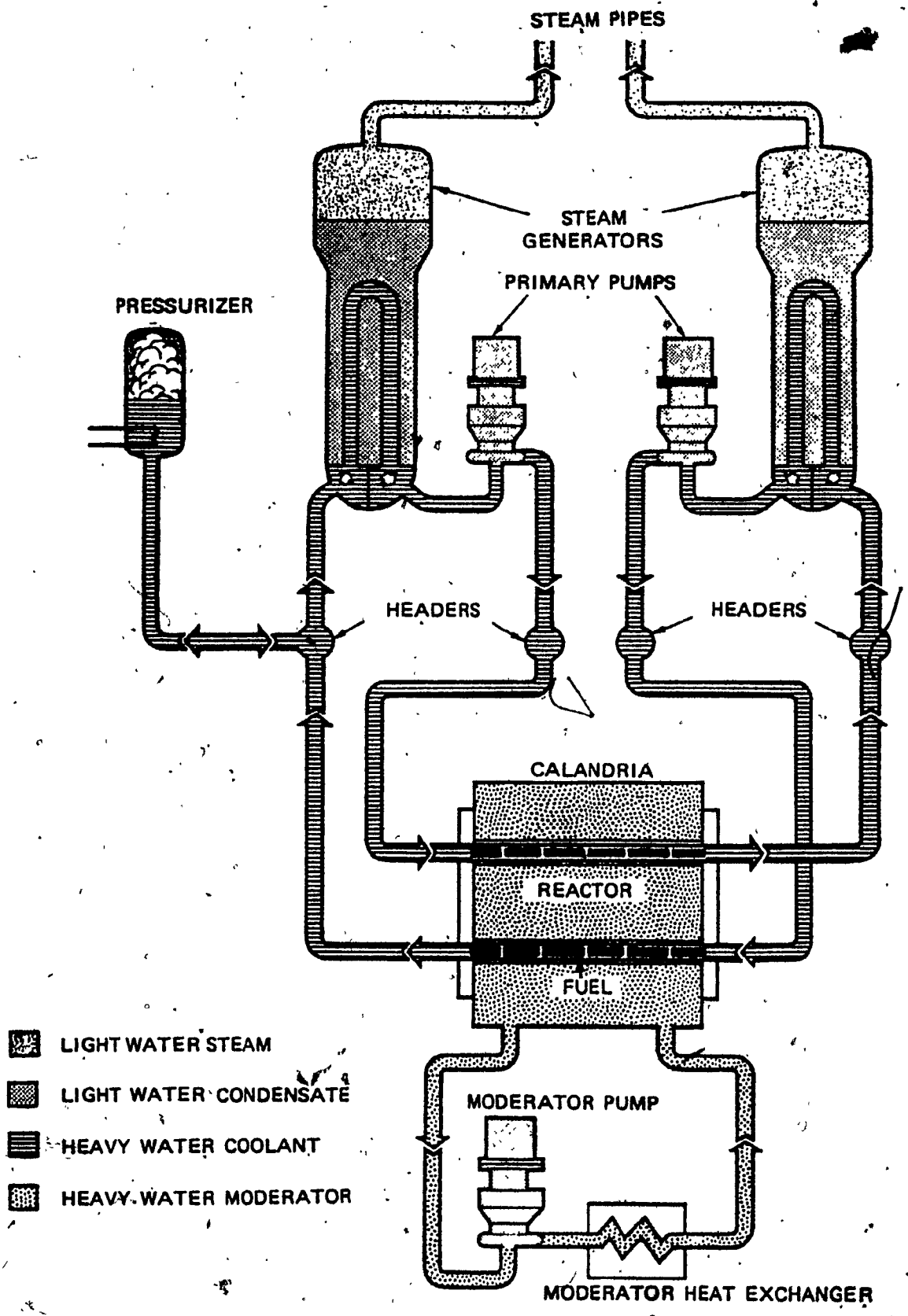

FIGURE 5.2: CANDU Reactor Simplified Flow Diagram

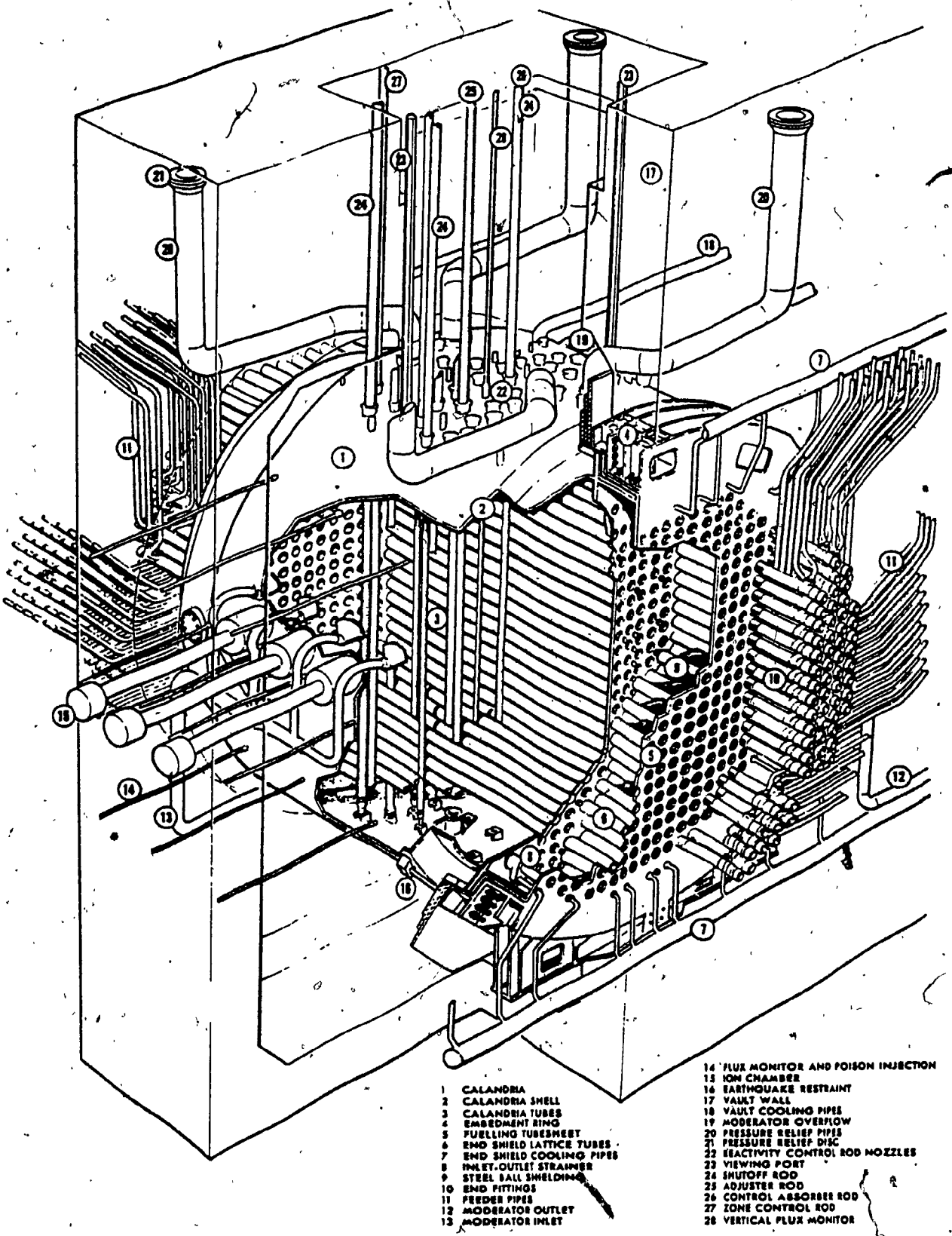

FIGURE 5.3: Reactor Assembly

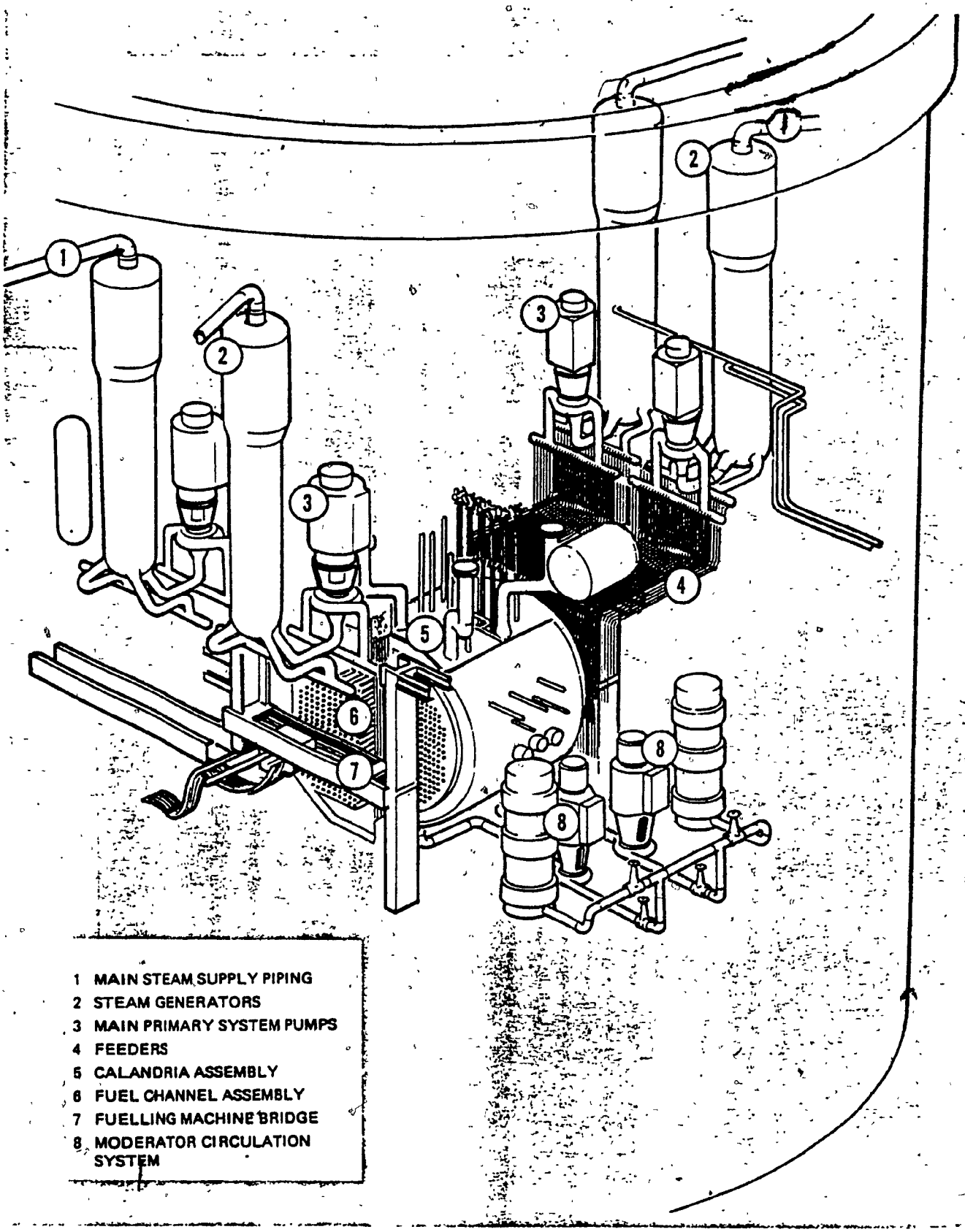

FIGURE 5.4: CANDU-PHW Reactor

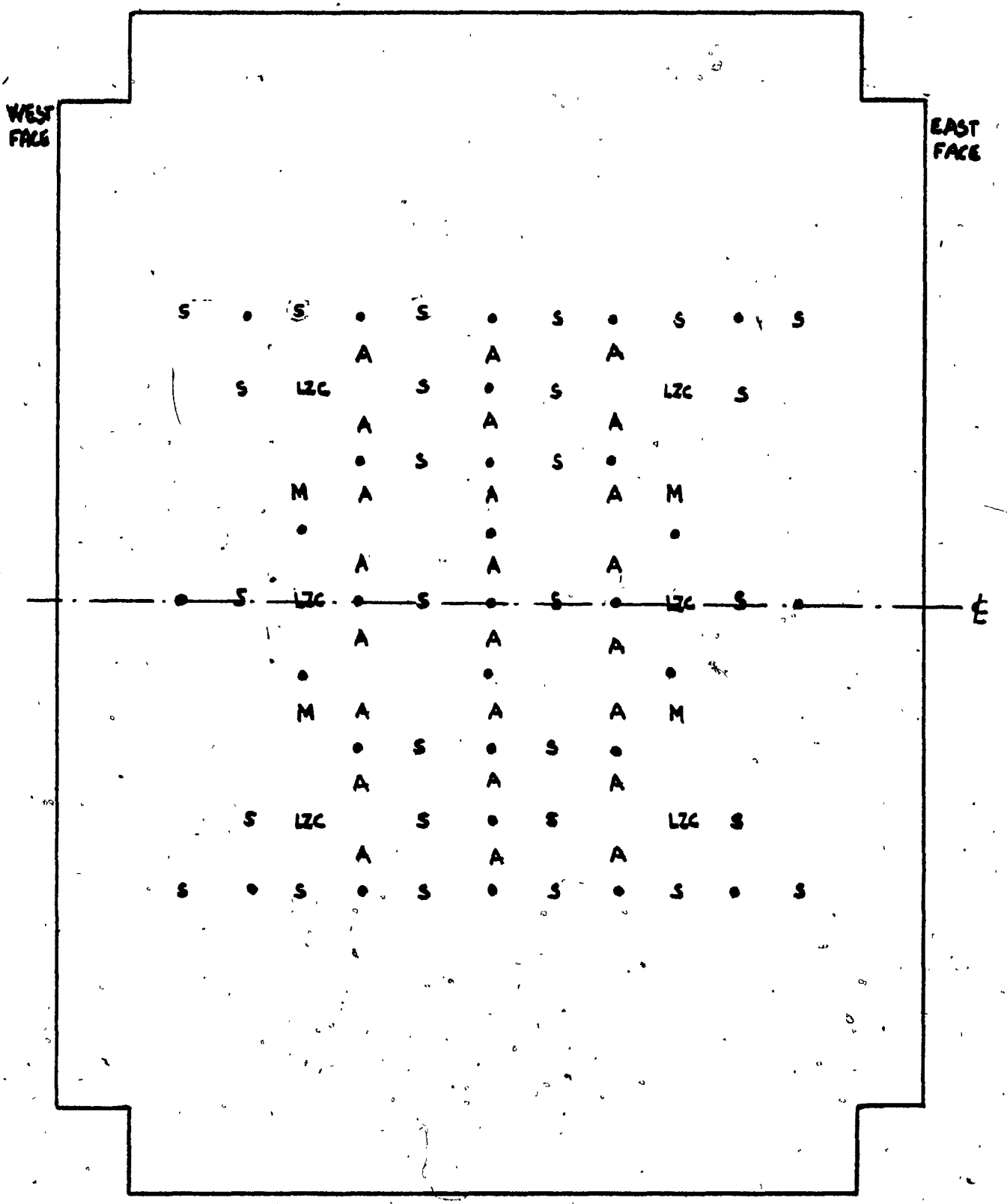

●: VERTICAL FLUX DETECTORS A: ADJUSTERS S: SHUTOFF RODS
LZC: LIQUID ZONE CONTROLLER M: MECHANICAL CONTROL ABSORBER

FIGURE 5.5: Darlington NGS - Reactivity Mechanisms (Top View)

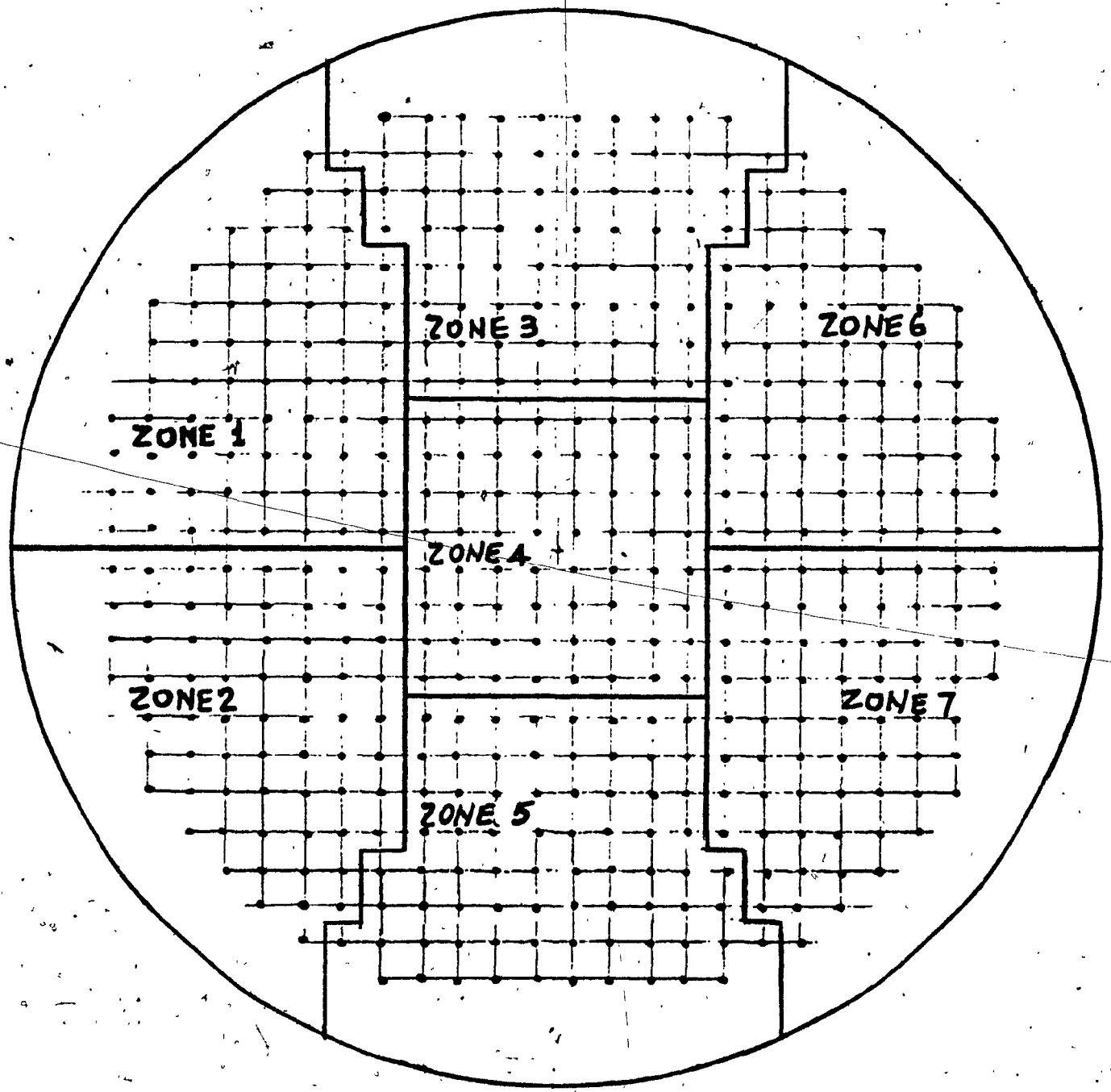

FIGURE 5.6: Darlington NGSA (Face: East)

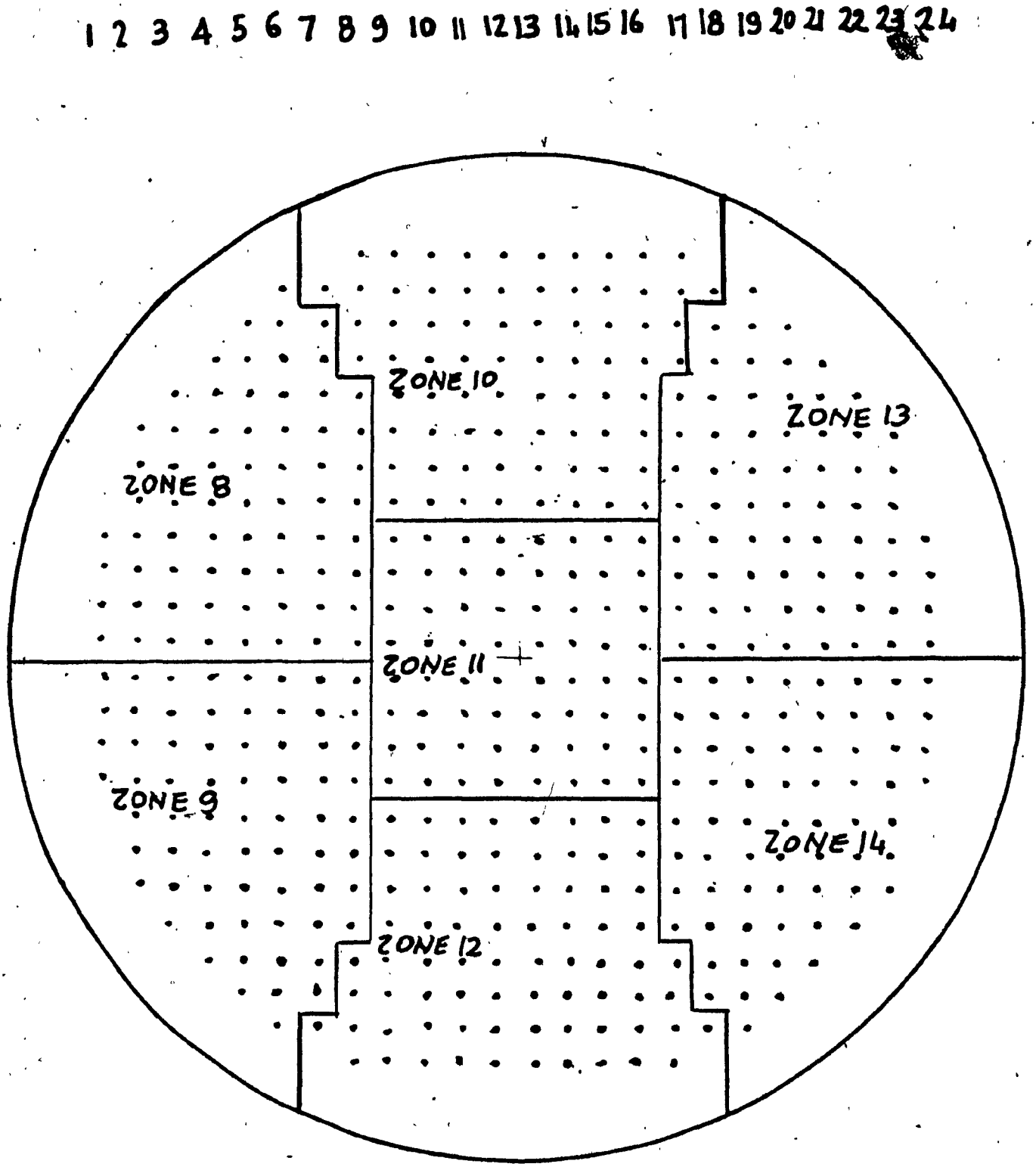

FIGURE 5.7: Darlington NGSA (Face: West)

5.2 DARLINGTON NGS BASE DATA

Considering that this thesis is exclusively concentrated on the behaviour of the Darlington nuclear power reactor when fuelled with natural or low enriched uranium fuel, it was felt appropriate to provide in this section some core properties, channel ratings, and fuel bundle and channel physical characteristics. Figures 5.1, through 5.7 illustrate what we may define as the physical arrangement of the Darlington reactor core.

More precise data are provided here:

- Core radius: 3.5 m;
- Number of fuel channels: 480;
- Number of bundles per channel: 13;
- Number of bundles in core portion of fuel channel: 12;
- Reactor length: 5.944 m;
- Average reflector thickness at midpoint: 0.699 m;
- Coolant temperature: 276°C;
- Moderator temperature: 80°C;
- Fuel temperature, core average: 882°C;
- Radial power form factor: 0.863;
- Axial power form factor: 0.679;
- Overall form factor: 0.586;
- Total fission power: 2798 MW;
- Heat removal by coolant: 2651 MW;
- Unit electrical output: 850 MW;

- Time averaged maximum channel power: 6.4 MW;
- Time averaged maximum bundle power: 787 kW;
- Linear bundle rating corresponding to maximum bundle power: 1590 kW/m of bundle length;
- Fuel: natural uranium dioxide;
- Number of elements per bundle: 37;
- Element outside diameter: 13 mm;
- Pellet outside diameter: 12 mm;
- Bundle length: 495.3 mm;
- Average uranium dioxide density: 10.6 mg/m^3;
- Uranium dioxide weight per bundle: 21.23 kg;
- Zircolloy weight per bundle: 2.27 kg;
- Pressure tube material: Zr-Nb;
- Inner radius: 51.7 mm;
- Calandria tube material: Zr-2;
- Inner radius: 64.5 mm.

5.3 DARLINGTON REACTOR PHYSICS DESIGN

The objective in the design of large nuclear power reactors is to obtain a nuclear core that offers as close to uniform a power distribution as practicable, when all constraints are taken into account so as to provide sufficient reactivity to yield adequate fuel burnups, while maintaining adequate reactor control. Core power distributions are usually dependent on core enrichment, moderator to fuel ratio, core geometry, the location and type of reactivity control devices, fuel element design and, of course, on time because of fuel burnup and isotope production over core life.

Power peaking factors which will allow the determination of thermal limitations on core performance, as well as core temperature feedback that influences core reactivity, are also of great interest in thermal reactor core analysis.

Various types, both hardware and software, of control systems are designed and used in CANDU-PHW reactors to satisfy these goals.

General information regarding reactivity mechanism used for CANDU-PHW reactors is offered by Figures 5.5, 5.8, 5.9, 5.10 and 5.11. A qualitative description of each reactivity control system, shutdown system and neutron flux measurement device was provided in Chapter Three. Interaction (static and dynamic) of

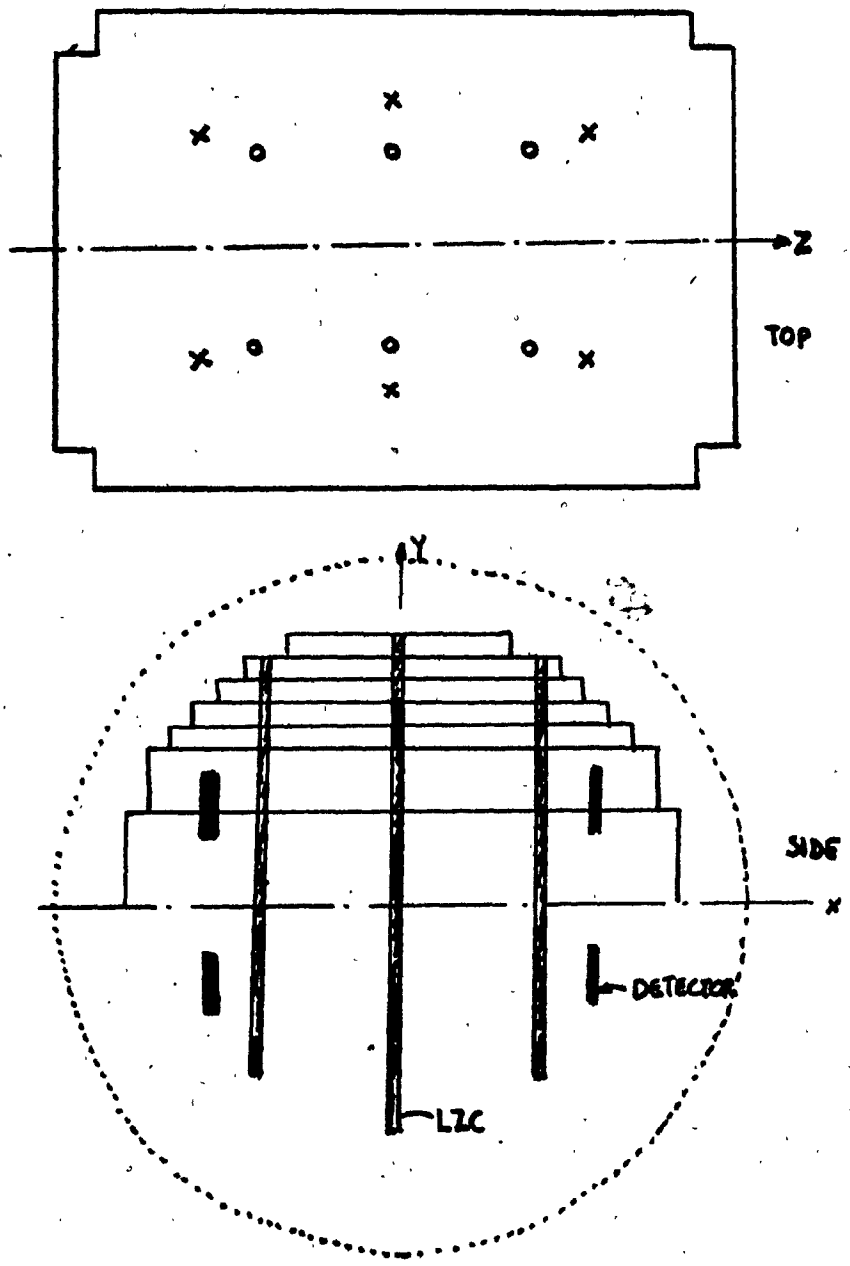

FIGURE 5.8: Liquid Zone Controller and Associated Flux Detector Locations

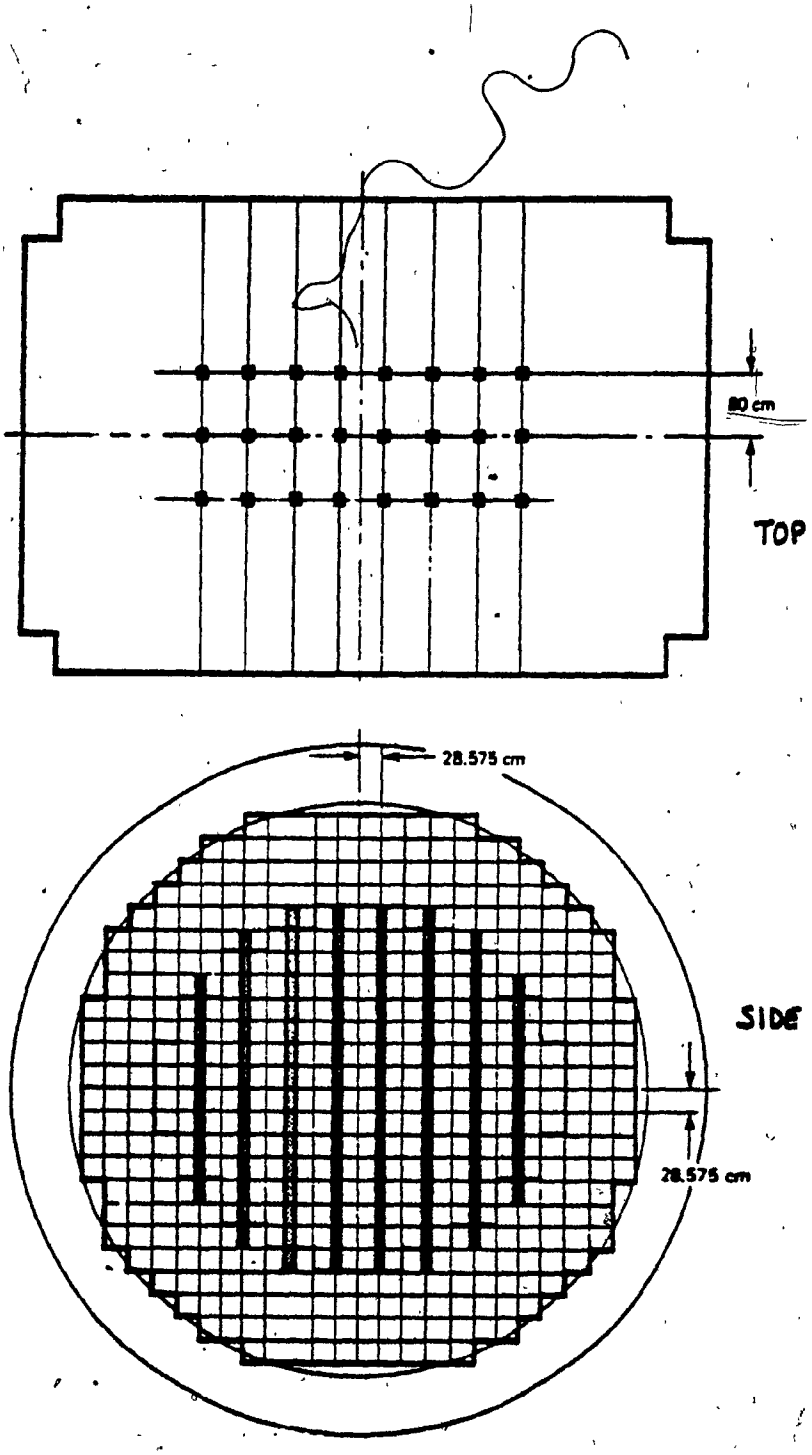

FIGURE 5.9: Darlington NGS - Locations of Adjuster Rods

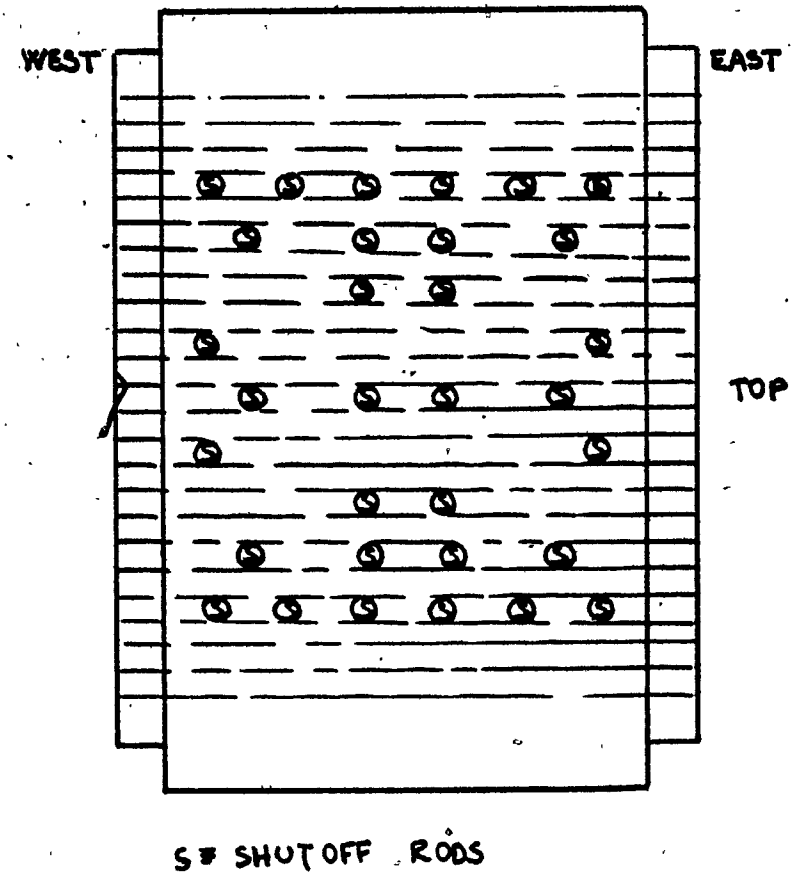

FIGURE 5.10: Darlington NGS - Locations of Shut-Off Rods

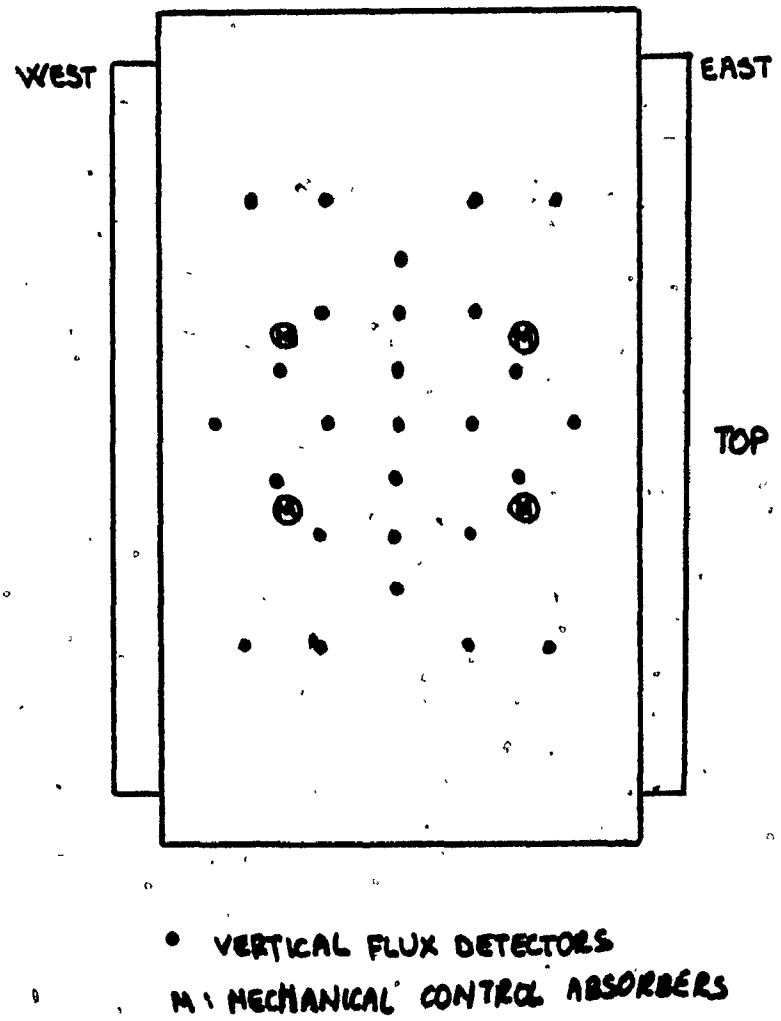

FIGURE 5.11: Darlington NGS - Location of Vertical Flux Detectors and Mechanical Control Absorbers

reactivity control rods, power distribution calculations, long-term and short-term reactivity studies, core thermal analysis, etc., are all investigated by means of computer programs or "codes" that have been developed over the years and are still objects of continuous development due to infinitely many reasons.

Generally, these codes could be grouped into four different types, such as:

- Cross-section library processing codes;
- Multi-group constant generation codes;
- Static design and analysis codes;
- Time-dependent design and analysis codes.

Since the primary concern of this thesis is with the controllability assessment of Low Enriched Uranium (LEU)-CANDU-PHW reactors, the attention is confined to a general discussion of those code packages which usually perform calculations describing the nuclear behaviour of a 850 MW(e) LEU-CANDU-PHW reactor.

Although such nuclear code packages or computer models will vary even with a given nuclear reactor type, the general features are very similar.

Numerous approximations are usually required in order to develop the mathematical models that serve as the basis of

reactor design and analysis codes. Typically, these codes suppress certain independent variables in order to allow a detailed analysis of the process of interest. For example, in time-dependent codes, one frequently ignores both spatial and energy dependence.

The basic interacting structure of these codes consists of a module to generate macroscopic group constants, followed by a module to utilize these group constants to determine core multiplication, flux and power distribution. The power distribution can then be used as an input to a thermohydraulic module which solves the equation of heat transfer and fluid flow to determine the temperature and coolant density distribution in the core. Of course, this latter is required for the generation of macroscopic group constants, hence, feedback to the earlier multi-group constant generation module (and possible iteration) will be necessary.

At this point, one has presumably calculated the core multiplication k_{eff} and power distribution but, in general, the core will not be critical ($k_{eff} \neq 1$). Hence, a control adjustment module is necessary to calculate the degree of control element withdrawal or insertion to return the core to a critical state (again via an iterative process). When a critical core configuration has been achieved, one passes to a fuel depletion module that uses the resulting flux distribution as input for a

solution of the rate equations describing fuel isotope depletion, fertile isotope transmutation, and fission buildup for a given period of reactor operation. After this depletion step, the new isotopic composition of the fuel is returned to the group-constant module, and the entire calculation is repeated (since the core is now no longer critical unless a new control adjustment is performed).

After a series of depletion steps, the fissile inventory drops sufficiently low that the control system can no longer return the core to criticality.

At this point, the useful operating life is deemed to have ended, and a transfer to an economic module is initiated to compute the fuel costs of the operating cycle.

Various different types of input data are needed for this sequence of calculations, including the geometry of the reactor core, lattice, control systems, initial core loading (composition, etc.), inlet coolant conditions, as well as fundamental cross-section data.

5.4 REACTIVITY CONTROL

CANDU nuclear power reactors are initially loaded with fresh fuel that contains an excess of reactivity to compensate for fuel burnup and fission product production. Sufficient excess of reactivity is also provided to compensate for negative reactivity feedback effects such as those represented by the temperature and power defects on reactivity. In contrast to the core geometry and volume which are primarily determined by thermal considerations (i.e., achieving the required core thermal power output utilizing a power density consistent with thermal design limitations), the fuel loading or enrichment is usually determined on the basis of a target discharge burnup. In off-power, batch-refuelled reactors (e.g., light water reactors), one must build into the core a sufficient excess reactivity to allow full power operation for a predetermined period of time. In the CANDU's, the on-power refuelling frequency and enrichment are determined to ensure a <u>minimum</u> oscillation in reactivity between refuellings.

To compensate for this excess of reactivity, it is necessary to introduce an amount of negative reactivity into the core which one can adjust or control at will. This control reactivity can be used both to compensate for the excess reactivity necessary for long-term core operation and also to adjust the power level of the reactor in order to bring the core to power, follow load

demands and shut the core down. The control reactivity is most often present in the form of strong neutron absorbers that can be inserted into or withdrawn from the core. Liquid poison is also a very frequent means of reactivity control used in the CANDU-PHW reactor technology. The determination of the control reactivity requirements and the apportionment of control reactivity among various types of control elements is a very important aspect of nuclear reactor core physics analysis. Following are provided several definitions characterizing reactivity control:

- Excess reactivity ρ_{ex}: The core reactivity present with all reactivity control elements out from the core. ρ_{ex} is a function of both time (due to fuel burnup and isotope production) and temperature (due to reactivity feedback). Larger values of will generally imply longer core lifetimes, but at the expense of larger control requirements and power neutron economy (since with more control reactivity in the core there will be more neutron absorption).

- Shutdown: ρ_{sd}. The negative reactivity of the core when all control absorbers have been fully introduced in the core. In the case of CANDU, two shutdown reactivity control elements are available: the shutdown rods and liquid poison injection.

Again, ρ_{sdm} is a function of time and temperature. For example, the shutdown margin for a "cold", "clean" core, that is, a core at ambient temperatures and with a fresh fuel composition in which no depletion or fission product buildup has occurred, will be quite different from the shutdown margin characterizing a core that has been operating at power for some time. Typically, shutdown margins are chosen such that core multiplication is below critical (e.g. k = .99) even with some shutdown rods stuck in the full "out" position.

- Total worth of reactivity control systems $\Delta\rho$. $\Delta\rho$ is the difference between the excess reactivity and the minimum reactivity when all reactivity control elements are in core full influencing action.

$$\Delta\rho = \rho_{ex} - \rho_{sdm}$$

Reactivity control requirements can be distinguished in several types.

- Reactor shutdown: The reactor control systems must be capable of shutting the reactor down under any credible operating conditions. Elements used for such shutdown purposes must be capable of inserting negative reactivity very rapidly and must operate with an extremely high degree of reliability.

- Reactor regulation: A considerable number of reactivity mechanisms is provided to compensate for small reactivity transients caused by changes in load demand, core temperature, and for general power level manoeuvring.

- Shim control: Shim control elements are designed to cover the excess reactivity necessary to compensate for long-term fuel depletion and fission products buildup, as well as to shape power distribution in the core in order to obtain a better thermal performance and more uniform fuel burnup. Although the reactivity worth of such elements must of necessity be quite large, shim control adjustments are made very gradually over long periods of time.

There are several schemes used for introducing control absorption into a nuclear reactor core. The most common method is to insert movable rods of absorbing material into the core. Such movable control elements not only can be used to adjust the core power, but, because of their rapid response, can also be used for scramming the reactor as well as for shim and power shaping. Movable control rods in CANDU are arranged such that certain of them are always out of reactor core and others are always inserted into the core for reactor normal operation.

Two more methods used for reactivity control in CANDU-PHW reactors are:

a) Dissolved boron in moderator to compensate for excess reactivity (especially at start-up or during transition to equilibrium);

b) Injection of liquid poison for reactor shutdown, as a back-up system to shutoff rods.

Power regulation in CANDU-PHW reactors is usually performed by the so-called liquid zone controllers that were fully described in Chapter Three.

A large thermal power reactor contains many of these reactivity control elements distributed in a pattern about the core in an effort to achieve efficient reactivity control within flux-peaking limitations, as well as to facilitate power shaping. The grouping of such control rods, the liquid poison and the liquid zone controllers, the determination of the control reactivity element operation (withdrawal and insertion sequence), coordination of solid movable control elements with liquid zone controllers and liquid poison injection all fall within the realm of what is known as advanced reactor physics kinetics. In the case of the Darlington nuclear power reactor, it is worth mentioning that there is a great deal of symmetry in

reactivity control devices, vertical shutdown systems, and neutron flux measurements. It is the strategic location of these devices that allows nuclear designers to provide a reactor with an optimized power output.

5.5 REACTOR OPERATING STAGES

From an operating point of view, a CANDU-PHW power reactor's operating life may be divided into three major periods.

The first period is from first criticality until the onset of fuelling. This period usually lasts from 100 to 150 full power days (a "full power day" is the energy generated by a reactor when operating at rated power for 24 hours). The reactor is initially loaded with fresh fuel. Consequently, there is considerable excess of reactivity which is compensated by adding boron poison to the moderator. When the excess reactivity in the core falls to a small value, fuelling begins to keep the reactor critical. During this transitional or pre-equilibrium period, the reactor gradually approaches the final or equilibrium state.

The equilibrium condition in a CANDU-PHW reactor is reached after approximately 400 to 500 full power days. It is characterized by an unchanging core configuration in which the macroscopic or global power and burnup distributions do not vary significantly with time. Although the macroscopic power distribution does not change considerably, the microscopic or local power distribution is constantly changing as fuel burns up and is replaced. This important effect is taken care of by the reactor regulating system. The equilibrium period covers about 95% of the reactor life.

5.6 CANDU ON-POWER BIDIRECTIONAL FUELLING

One of the major characteristics of CANDU-PHW reactors is their refuelling activity while the reactor is operating at full power. After the excess reactivity of the initial fuel load has decreased to a small value, several fuelling operations are carried out every day on various channels in the core. Only a very small fraction of the core is changed at one refuelling operation, so that refuelling is essentially continuous. This avoids the need for a fuelling shutdown, making it unnecessary to tailor the fuelling schedule to the utility power grid's system requirements.

Fuelling is the primary method of controlling the long-term core reactivity and maintaining the desired power distribution. By adjusting the overall fuelling rate, we can control the core reactivity. By fuelling one region more frequently than another, we can control the power distribution. A lower fuelling rate leads to an increased irradiation and reduces the region's relative power.

An important consequence of this feature is that the reactor regulating system has only to compensate for changes in reactivity due to power manoeuvring, fuelling of one channel at a time, and short-term xenon transients. Therefore, the reactivity control margin can be maintained at a small value

resulting in good neutron economy and contributing to low fuelling costs.

Another important aspect of the CANDU refuelling is its bidirectionality. Alternate fuel channels are fuelled in opposite directions by inserting new fuels in one end and removing irradiated fuel at the other end. This results in a symmetric axial flux and power distribution and approximately constant burnup for all discharged fuel bundles in a radial burnup region.

Normally, only a portion of the fuel in a channel is replaced in a single fuelling operation. The remaining fuel is shifted along the channel. During its life in the reactor, each fuel bundle moves along the channel in a series of steps.

5.7 DARLINGTON REACTOR OPERATING TRANSIENTS

5.7.1 Introduction

During the operating life of a CANDU-PHW reactor, several situations arise which will induce reactor core reactivity changes that have to be compensated with reactor reactivity systems. While reactors approach equilibrium and equilibrium operation, fuel scheduling or fuel replacement patterns must be determined. For CANDU reactors, fuel scheduling requires determination of:

- bundle shift scheme;
- sequence of channels to be fuelled.

A large programme of detailed simulations of reactor operation is performed to provide the operator with broad guidance of fuelling rules.

Rules for channel selections and how they are used in computer programs are discussed in this chapter.

In general, fuelling priority is given to channels with the highest burnup. The power distribution must be controlled to approximate the reference power distribution in order to limit overpowers and minimize the channel power peaking factor (CPPF). Underpower zones are fuelled preferentially and overpower zones are avoided. Distortions in the power distribution

would increase the load on the reactor regulating system and increase the probability of reactor trips by reducing the margin available in the Regional Over Power (ROP) detectors. In order to maintain a symmetrical power distribution, two factors have to be considered:

- Axial distortion can be minimized by fuelling an equal number of channels having opposite fuelling directions at about the same time. It is desirable to have an equal amount of fresh fuel on each end in order to avoid end-to-end tilts.

- Radial and azimuthal distortion can be avoided by fuelling an equal number of channels in each control zone. As we have seen, CANDU reactors are divided for control purposes into seven radial azimuthal zones, each containing two axial light water controllers and a set of measuring devices. Fuelling an equal number of channels in each zone controller helps to keep the level of light water in each controller compartment close to the average for the reactor and to minimize radial and azimuthal distortions in the power distribution. If distortions are already present, low zones are preferentially fuelled to raise the power.

Maximum separation is maintained between channels fuelled at about the same time. Concentration of freshly fuelled channels

would create "hot-spots" in the power distribution, increasing the probability of fuel defects and increasing the CPPF, thereby reducing the margin in ROP-trip.

5.7.2 Approach-to-Equilibrium Fuelling

CANDU reactors, before they approach the equilibrium state, pass through some initial transient refuelling periods. It was pointed out previously that CANDU reactors are characterized by two burnup regions when at equilibrium. This different burnup is used in combination with adjuster rods to flatten the flux distribution. Initially, the cores are fuelled entirely with fresh fuel. In order to be able to operate the reactor at full power without exceeding the target values and maximum channel and bundle power, additional flux flattening is required.

The inner burnup region is fuelled with bundles having a slightly lower concentration of U-235 than natural uranium. These bundles have a lower reactivity than natural UO_2 bundle, and hence tend to reduce the flux and power in the inner regions. While time elapses, differential burnup will be created and depleted bundles are no longer required.

It was noted in Chapter Three that reactor cores experience an increase in reactivity during startup. During this period, the excess reactivity is compensated for by dissolving boron in the moderator. As the fuel burns up, plutonium is produced so that

the core excess reactivity increases to a maximum that occurs at approximately 50 full power days. From this time, the concentration of fissionable isotopes in the fuel decreases, as does the reactivity. By approximately 110 full power days, the core excess reactivity falls to zero and some fuelling must be done to keep the reactor operating.

The maximum channel power versus time has a trend similar to that of core reactivity. Typical channel power, excess reactivity and channel power along a channel row are illustrated in Figures 5.12, 5.13 and 5.14 respectively.

At the onset of fuelling, the inner burnup zone channels have the highest burnup and the lowest power relative to the equilibrium power distribution. Fuelling of the inner channels will then be preferential and gradually the fuelling scheme moves from inner to outer burnup region until an approximately uniform distribution is reached.

The fuelling operation to bring the reactor from onset of fuelling to equilibrium state presents considerable power variations around the average, and more care is required to keep the power distribution near desired limits.

In the approach to equilibrium, we are not always near optimum burnup for each bundle. Many fuel bundles from the outer region or end positions have low burnup and they can be

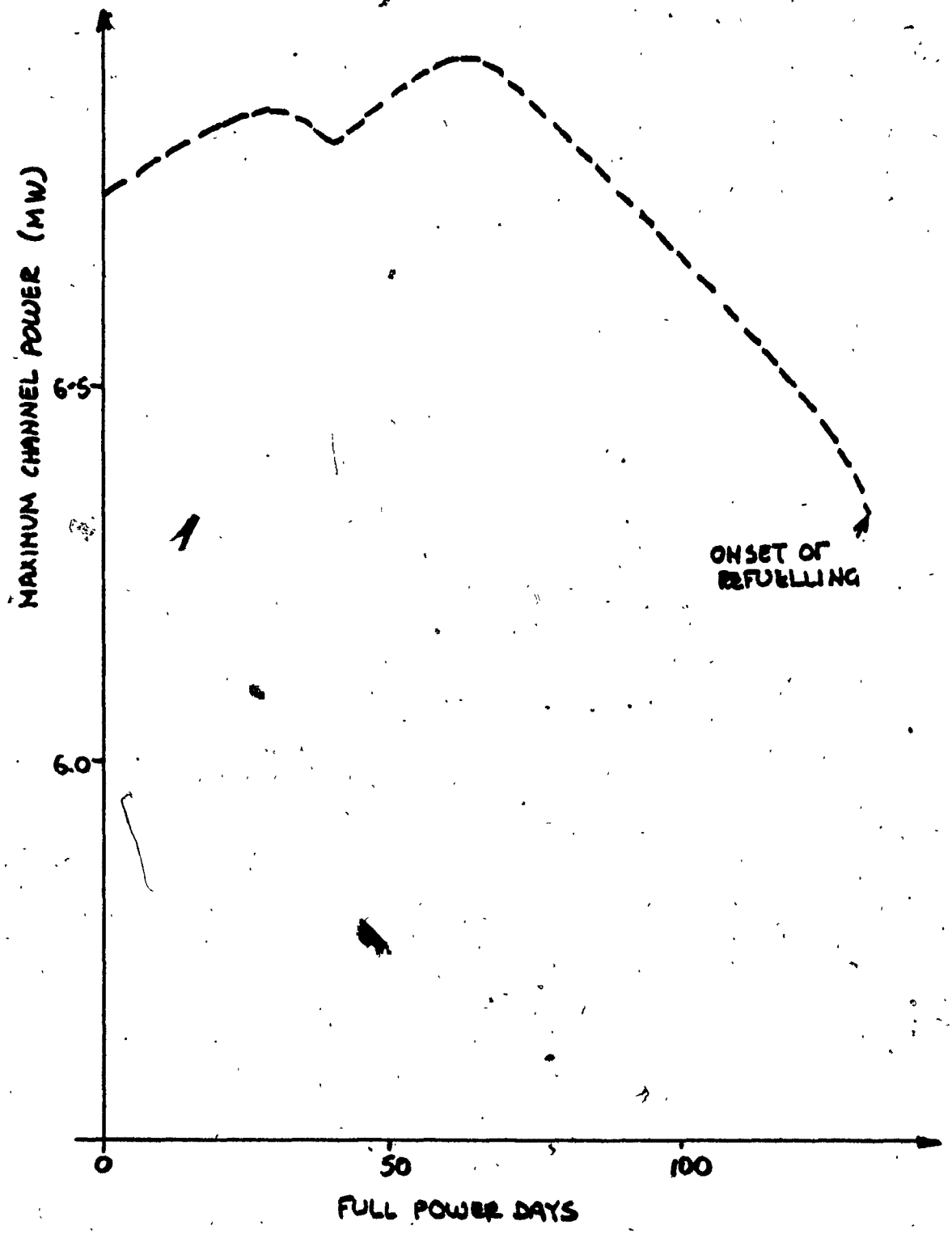

FIGURE 5.12: CANDU-PHW Reactor Maximum Channel Power vs Time

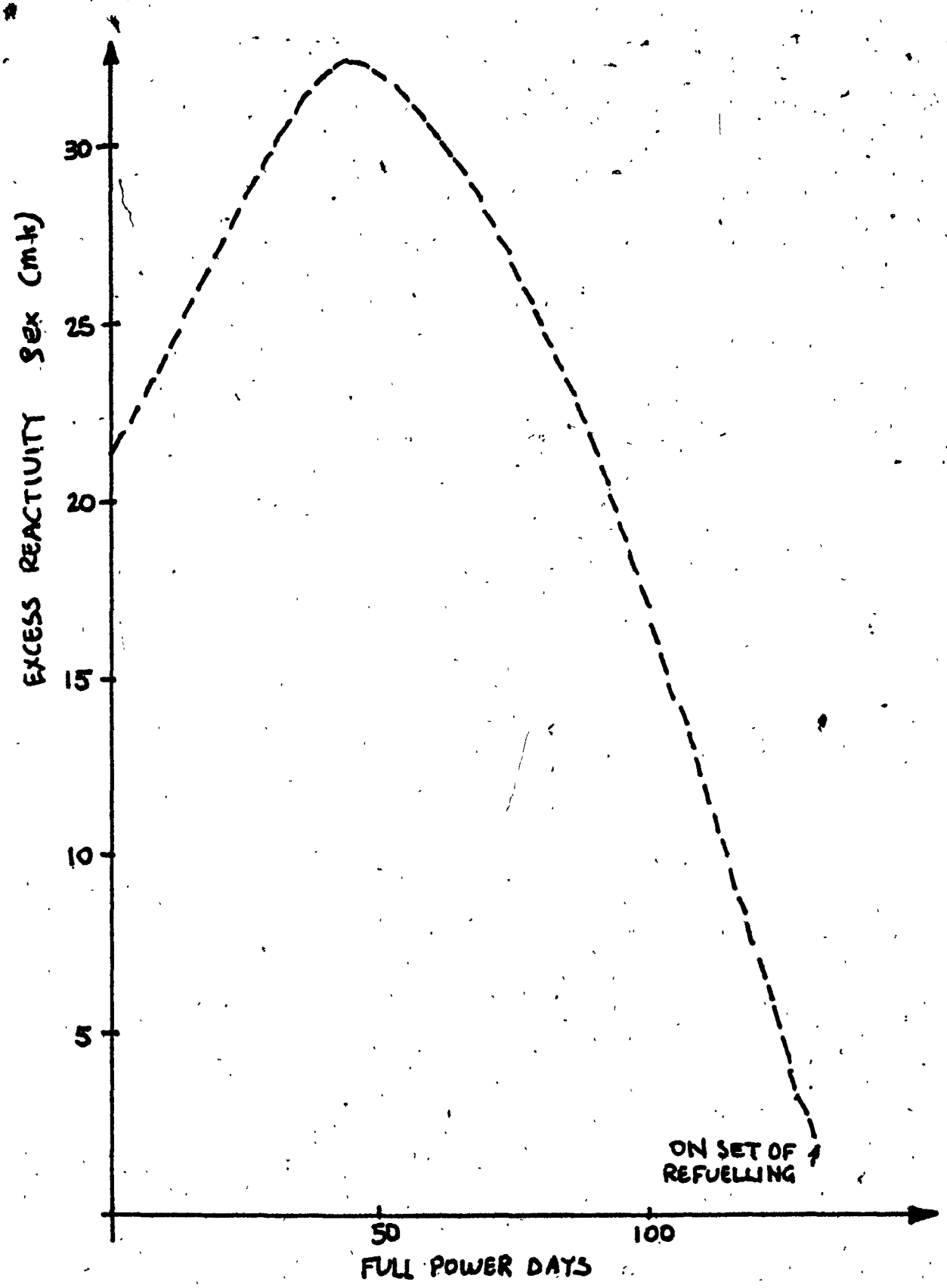

FIGURE 5.13: Excess Reactivity Versus Time for Typical CANDU-PHW Reactors

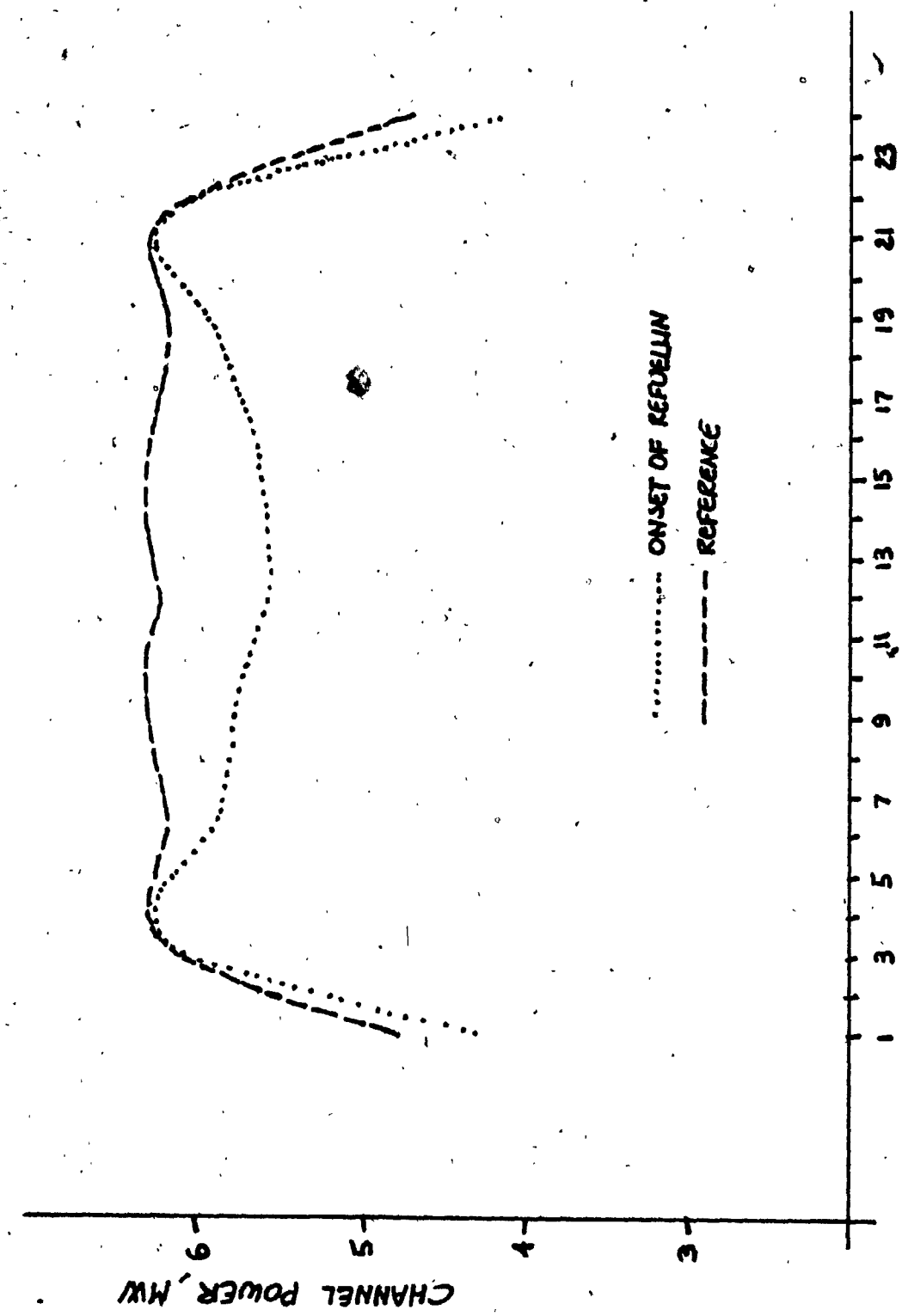

FIGURE 5.14: Typical Channel Power at Onset of Refuelling

re-inserted in other reactor channels to acquire additional burnup. This operation has, however, a drawback in the sense that the fuelling machine will be overused.

5.7.3 Shim Transients

Since the reactivity control worth of the liquid zone controllers is of the order of 6 mk, whenever the fuel handling equipment becomes unavailable, additional positive reactivity must be provided to keep the reactor operating. For most CANDU reactors, reactivity shim is accomplished by withdrawing adjuster rods from the core in a pre-specified sequence. Removal of adjuster rods leads to a distortion in the normal flux distribution. In most cases, some derating is required to keep the maximum bundle and channel power within target limits. The derating depends on the number of adjuster rods withdrawn from the core and, hence, on the duration of the fuel handling system outage.

Typically, the reactivity worth of a single adjuster rod is approximately 1 mk on average, while the reactivity loss due to fuel burnup is in the order of 0.3 - 0.4 mk per full power day so that, in the great majority of cases, only the first few adjuster rods need to be withdrawn from the reactor core. If, however, the inability to fuel persists for a significant time, a special fuel management strategy must be followed and this strategy (no part of this thesis) varies from case to case.

5.8 REACTOR REGIONAL OVERPOWER

Reactor core reactivity changes from equilibrium values are always accompanied by fuel bundle and channel overpowers.

An "overpower" is a fuel bundle or channel power in excess of specific safety-related limits and must be kept below given setpoints beyond which the reactor trips. These limits are distinct and above the normal operating limits on bundles and channel powers.

Associated with CANDU reactors is a Regional Over Power (ROP) system whose function is to protect fuel bundles and other hardware should certain power limits be exceeded. The ROP system consists of a grid of in-core detectors, usually 40 to 60, distributed throughout the core perpendicular to fuel channels. The detectors are approximately 1 m long and are characterized by a fast response in neutron flux. If, in response to a flux change, the signal from ROP detectors (properly grouped) exceeds a predetermined setpoint, a reactor trip is initiated. Current CANDU reactors have two independent and diverse shutdown systems, each with its own set of ROP detectors.

CHAPTER SIX

6. LEU-CANDU-PHW-850 MW(e) REACTOR CORE PHYSICS ASSESSMENT

6.1 GENERAL PHYSICS CONSIDERATIONS

It was shown in Chapter Two that the introduction of advanced fuel cycles in the CANDU-PHW nuclear power reactor generating stations is recognized as economically beneficial due to reduced refuelling costs. Atomic Energy of Canada Limited and Ontario Hydro have analyzed several different advanced nuclear fuel cycles for the CANDU family of reactors to investigate the economic advantages offered by each cycle and also the inherent technical problems associated with each of them.

The introduction of low enriched uranium (LEU) fuel into CANDU-PHW reactors was illustrated as conducive to economic gains, due to the reduced fuelling costs.

The LEU fuel cycle offers also the advantage of being a stepping stone for CANDU-PHW reactor technology to allow the usage of advanced fuel cycles (Chapter Two).

As for any other fuel cycle discussed in Chapter Two, it is well recognized that nuclear fuels with higher U-235 content present higher reactivity in the fresh fuel. One of the possible strategies for use of LEU fuel cycle in CANDU-PHW reactors is to refuel the reactor with Low Enriched Uranium at

approximately 450 days after first criticality (equilibrium core, Chapter Five) with low enriched uranium fuel.

Several bundle shift schemes (Appendix G) are possible in CANDU-PHW reactors, depending on the core region being refuelled, as well as on the fuel enrichment content level. Four- and eight-bundle shift schemes are presently being utilized to refuel natural uranium core CANDU-PHW reactors.

Two-, four- and eight-bundle shifts will be considered for the core physics analysis of LEU-CANDU-PHWR reactor cases.

For a given bundle shift order, a higher enrichment will introduce more local reactivity than a lower enrichment, thereby creating a higher Channel Power Peaking Factor (CPPF).

In a CANDU-PHW reactor, for a fixed header-to-header pressure drop (ΔPHH), and depending on the axial power distribution, one can calculate a particular channel power value such that (with the coolant flow rate consistent with the given ΔPHH) thermal crisis of the coolant occurs at some point in the channel; this is the Critical Channel Power (CCP; Appendix G). The maximum channel power allowed is CCP/1.15 with 15% uncertainty allowance (regardless of the enrichment); this limit is therefore more stringent for a higher CPPF.

The higher peaking associated with enriched rather than natural fuel must be counteracted and can be offset in a number of ways; e.g., by reducing the bundle shift order or by derating the reactor with respect to the natural fuel case.

A lower bundle shift order increases the fuelling machine usage. Derating is a severe economic penalty if the reactor power is limited to lower-than-target values.

This chapter and the following document the detailed LEU-CANDU-PHW reactor core physics as a basis for the technical feasibility assessment. The analysis has been performed by considering an 850 MW(e) CANDU-PHW reactor (e.g., Darlington, as described in Chapter Five). The technical feasibility assessment and the qualitative description of economic considerations are summarized in the following main objectives:

- Determine under what condition the use of LEU is technically feasible, with respect to power peaking and reactor controllability.

- Determine the optimum fuel management (enrichment/fuel bundle shift).

- Determine how the use of LEU would affect the fuelling machine demand.

6.2 MAIN ASSUMPTIONS AND GROUND RULES

The LEU technical feasibility assessment and the description of economic considerations were based on the following assumptions:

- The 850 MW(e) CANDU-PHW reactor core layout (Chapter Five) was considered without any modification other than the fuel enrichment.

- The reference target power was 92% of full power [850 MW(e) gross).

- The reference reactor core consists of two fuelling (bundle-shifting) zones with the inner zone on a 4-bundle shift and comprising 256 of the 480 fuel channels, whereas the outer zone uses an 8-bundle shift. Burnupwise, the reference core is divided also into two zones (inner and outer) but, for the burnup case, the inner zone consists of 208 instead of 256 channels. The 4-bundle shift zone is larger than the inner-burnup zone (practically power-flattened) in order to allow the channel power to drop to low enough values that the 8-bundle shifting (with a CPPF higher than 4-bundle shifting) does not lead to excessive channel powers. The reference zone remained unchanged with respect to natural core configuration because of the natural-LEU fuel character differential investigation.

- Three fuel enrichment levels [namely natural (0.711%), 0.9%, 1.2%] have been chosen for a full technical assessment.

- Natural fuel and low enriched uranium (with enrichment of 0.9%, 1.0%, 1.1% and 1.2%) were considered to investigate the differences between diffusion theory parameters versus irradiation. The diffusion theory parameters analyzed in detail were chosen to be:

  - Burnup;
  - keff;
  - k_∞;
  - D_1, D_2;
  - $\nu\Sigma_f$, Σ_{a2}, Σ_{a1}.

  Detailed graphical representations of these parameters for natural and LEU fuel will be shown in a later section.

- Single- and two-channel refuelling with 2-4-8-bundle shift scheme was chosen to investigate the reactor regulating system behaviour during refuelling.

- Shim transient simulations involving one, two, three and five adjuster bank withdrawal were performed to investigate the reactor regulating system and the respective reactor power derating requirements.

The following calculational ground rules were adopted:

- In the thermal-hydraulic area, the critical channel power (CCP) was calculated as the basis of a "local conditions" correlation between critical heat-flux and quality, coupled with the channel heat balance and a given flow rate power characteristic. The CCP values were normalized to 8.3 MW for the reference design case (natural fuel 4/8-bundle shift, fuelling against flow).

- Standard reactor physics and fuel management codes were used to provide burnup, power peaking and bundle power history.

- Only the equilibrium cycle was considered at assessment time; transitions between start-up core and equilibrium core may be investigated in further research.

6.3 METHODS

6.3.1 Choice of Lattice Physics Codes

The computer programs or "codes" that provide mathematical simulations of the reactor core are generally very complex and are frequently the result of many years of extensive development and testing at the various nuclear laboratories around the world. These codes are generally grouped into six different types:

- Cross-section library processing codes;
- Multi-group constant generation codes;
- Lattice codes (transport theory);
- Core codes (3-D diffusion theory);
- Time-dependent design and analysis codes;
- Fuel management codes.

In general, the first and second types of codes generate the few group constants that will then be used in static and kinetic design analysis.

Static design analysis codes are used to obtain the global spatial dependence of the neutron flux throughout the reactor core. This information is required for accurate prediction of the fuel loading (refuelling), power distributions, temperature dependence of reactivity, shutdown margins, shielding requirements and other quantities. One customarily uses such codes to

determine the multiplication factor (eigenvalue) and the flux distribution in the system of interest.

The local diffusion theory constants needed in the calculation of the core power distribution are obtained from special computer programs ("lattice codes") that, in principle, solve the transport equation over an individual "cell" in an infinite uniform lattice. In the CANDU case, a cell is composed of a fuel channel and the share of surrounding moderator delimited by planes midway between adjacent fuel channels. For the LEU technical feasibility assessment, three lattice codes are available:

- WIMS (Ref. 28);
- LATREP (Ref. 29);
- POWDERPUFS-V (Ref. 30).

WIMS is a very precise but expensive lattice physics cell code whose use has until recently been somewhat restricted in survey calculations involving many different enrichments.

LATREP and POWDERPUFS-V (PPV) are especially developed for CANDU-PHW reactors, fairly inexpensive to run and, therefore, ideal for survey calculations.

All core calculations for natural UO_2 use PPV-generated lattice cross-sections plus specially smeared "incremental cross-sections" to describe the effect of reactivity devices: adjusters, liquid zone controllers, shut-off rods, mechanical control absorbers, etc.

Although there is a lot in common between LATREP and PPV-lattice codes, their difference in thermal neutron cut-off and in the definition of some related quantities leads to considerable differences in the lattice cross-sections and correspondingly in the reactivity device incremental cross-sections.

6.3.2 Core Calculations and Reactivity Perturbations

In the operating reactors, the quantity of interest is the change in the core reactivity produced by some perturbation in operating conditions, and, to assess this quantity accurately, two complete reactor calculations are necessary using the appropriate lattice data for conditions prevailing before and after the perturbation.

Nuclear reactors are generally too heterogeneous to be calculated with explicit heterogeneity (computer limitations); therefore, the reactor physicist normally bases core simulations on describing possible large and very heterogeneous core regions "supercell" as if they are:

- homogeneous;
- obeying the few-group diffusion theory.

Changes in coolant and moderator densities have reactivity feedbacks that must be determined accurately for safety and control concerns.

The coolant void coefficient of reactivity, the main contribution to the reactor power coefficient, is slightly positive in a CANDU reactor; in a large Loss-of-Coolant Accident (LOCA) in which there is rupture of the reactor primary coolant system, voiding of coolant channels would lead to a reactivity increase of about 10 mk (1%) over several seconds in the extreme case of a total loss of high density coolant. The shutdown systems, however, are designed to shut off the reactor within approximately 3 seconds of a large LOCA, with a peak reactivity during the shutdown transient of about 3 mk at 1 second (this reactivity is always well below prompt-criticality, when $\$=\beta\cong 7$ mk). These reactivity effects can be reversed if an appreciable amount of neutron moderation takes place in the coolant (as happens in light water reactors).

To minimize the economic penalties associated with control and safety of natural or Low Enriched Uranium fuelled thermal power reactors, theoretical methods have been developed for accurate prediction of the large reactivity effects caused by operational perturbations.

Theoretical results are compared with experimental results whenever possible and different calculations are inter-compared always, when different lattice codes are used for the analysis.

Many lattice codes are currently being used to assess reactivity coefficients of power reactors. Depending on the neutron temperature and cut-off point, it is expected that between lattice codes we may observe slight result differences.

6.3.3 Lattice Physics Codes and Nuclear Core Analysis

As indicated in the previous section, it is customary in reactor physics to repeat theoretical lattice calculations more than once in the process of power reactor cell reactivity coefficient evaluations. This process is part of the iterative core design and analysis process.

Axial and radial flattening of the power distribution through core life and provision of adequate reactivity to yield adequate fuel burnups while maintaining adequate reactor control are basic objectives of reactor core physicists.

Analysis must be performed to determine the amount of negative reactivity or control required to compensate for the excess of reactivity contained in the initial fuel loading, as well as to allow flexible and safe operation. One must also study the inherent reactivity changes that will occur in the core with

power and temperature changes by calculating the various reactivity feedback coefficients that determine the short-time kinetics behaviour of the core.

During reactor operation, the fuel composition will change as fissile isotopes are consumed and fission products are produced.

The reactor core physics codes occupy a key area in the design of nuclear power reactors.

Figure 6.1 shows that lattice physics codes are an integral part of most reactor core calculations. The neutron cycle model as it is implemented in the LATREP code is slightly different from the one implemented in PPV lattice code (Ref. 29), as it can be observed by comparing Figure 6.2 with Figure 3.2.

6.3.4 Nuclear Cross-Sections: Homogeneous Model(*)

The isotopic composition of the fuel varies with the irradiation of the fuel bundle and depends on the flux history to which the bundle has been exposed. The cross-sections for the lattice cell containing the fuel bundle depend, in turn, on

(*) The word "homogeneous" is used here in a different sense than in cell homogenization. "Homogeneous" refers here to an ideal, core-averaged fuel irradiation to which there corresponds a unique set of (homogenized) two-group cross-sections.

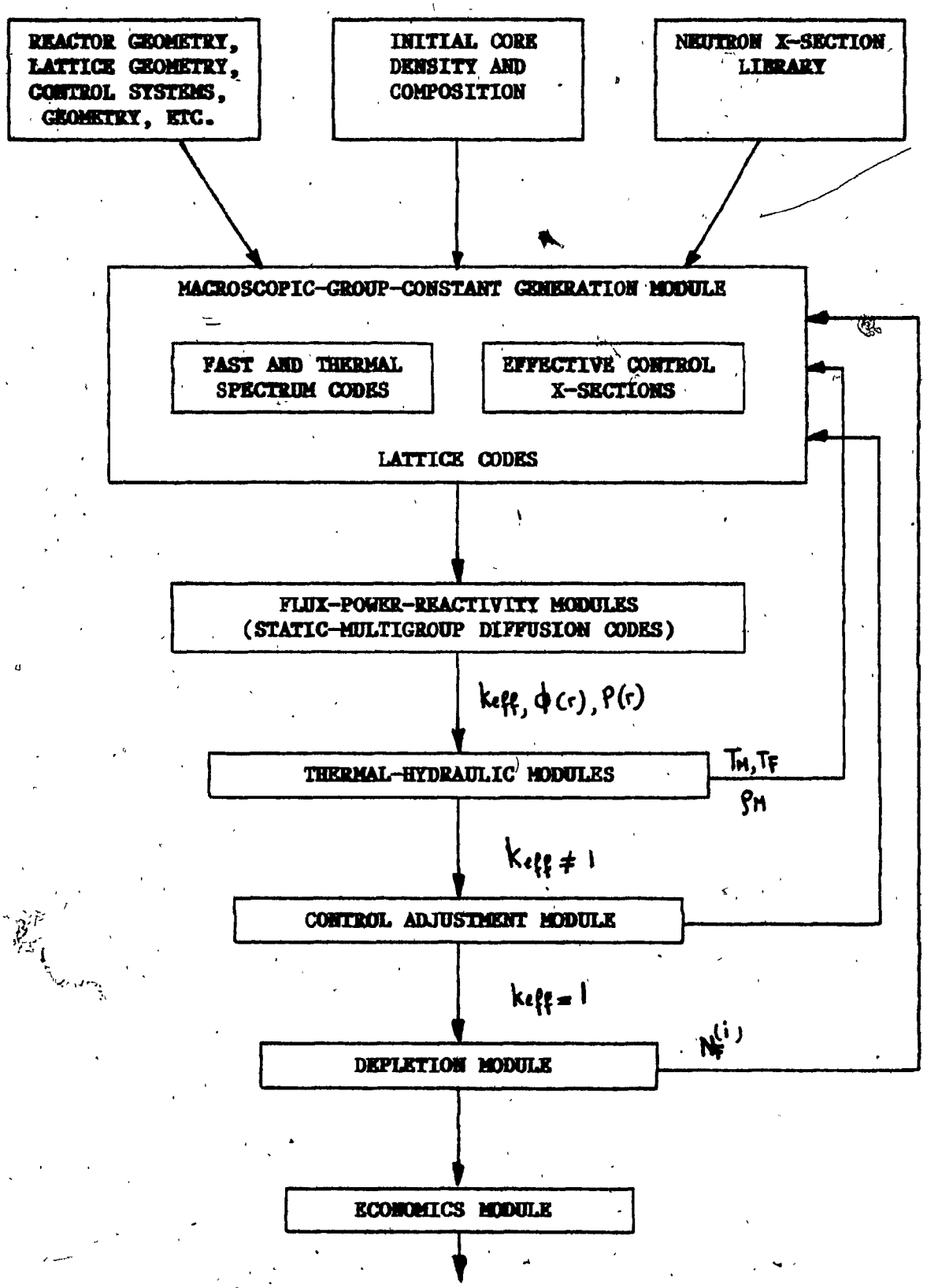

FIGURE 6.1: Reactor Core Physics Codes Management

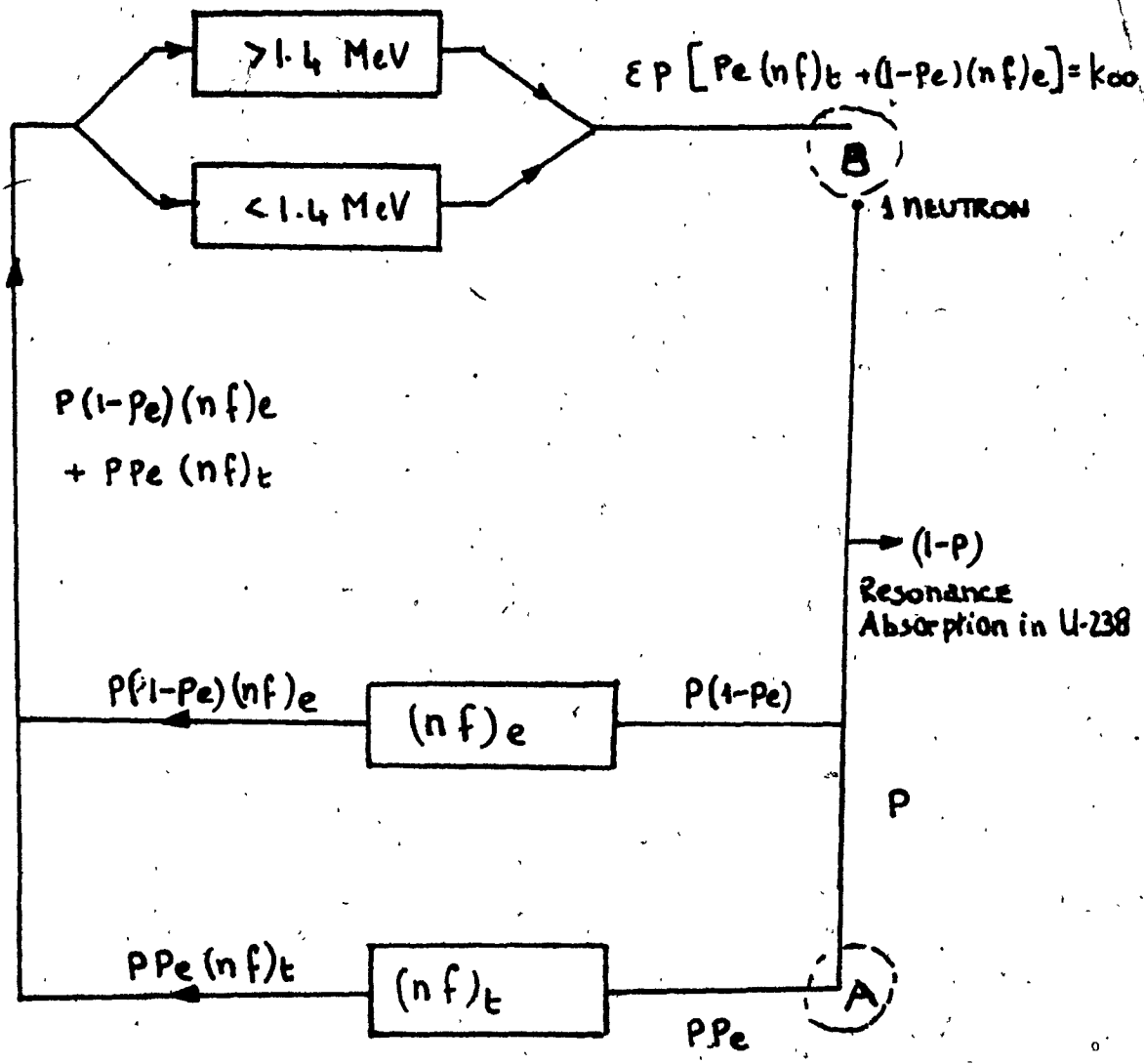

FIGURE 6.2: LATREP Neutron Cycle

the isotopic composition. To overcome this iterative process, we instead assume a representative mean flux and compute the fuel isotopic composition as a function of irradiation using this constant value.

The value usually used is the "flux-squared-weighted-mean flux", which is given by the integral over the core of

$$\frac{\int \phi \phi^2 dV}{\int \phi^2 dV} \qquad \text{Eq. 6.6}$$

where ϕ is the flux, and the integral is over the core (Ref. 8).

Lattice cell cross-sections are then calculated as a function of irradiation using lattice cells such as shown in Figure 6.3.

The cross-sections are computed in this thesis using the LATREP neutron physics code. The core configuration was chosen to be the natural uranium and four degrees of uranium enrichment:

NAT-URANIUM -; LEU - 0.9%; LEU - 1.0%; LEU - 1.1%; LEU - 1.2%

The cross-sections for the natural and for LEU cases as above are provided in this thesis in the form of curves, and they are functions of the irradiation of the fuel which is the integral of the flux seen by the fuel in its travel along the channel (Figures 6.4, 6.5, 6.6, 6.7, 6.8 and 6.9).

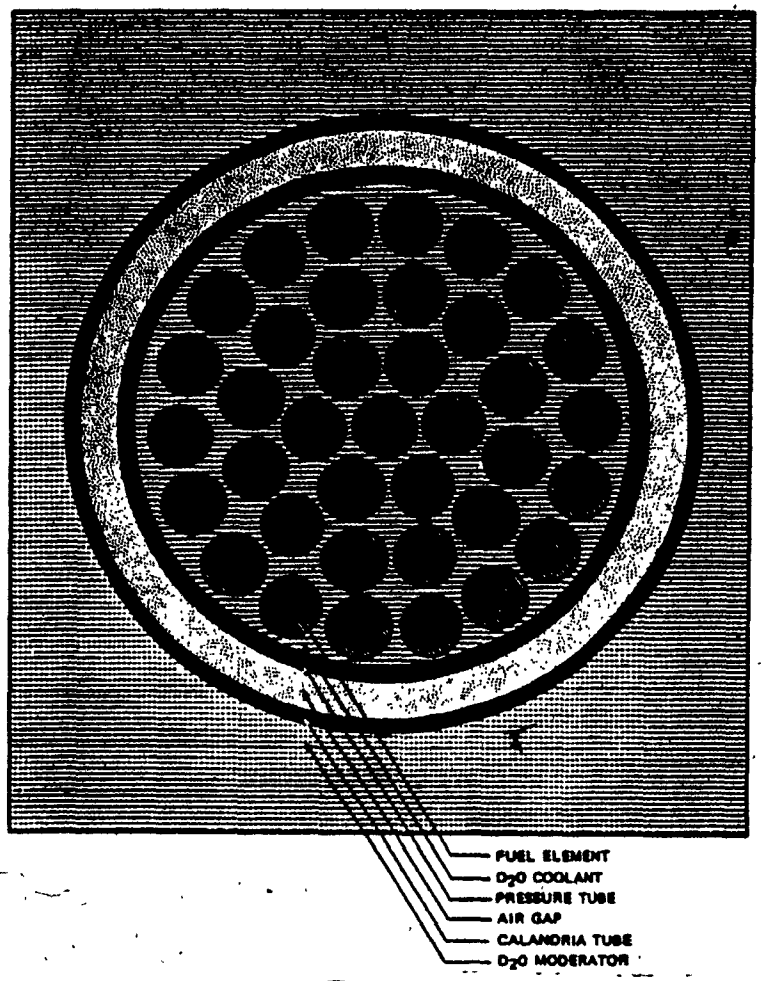

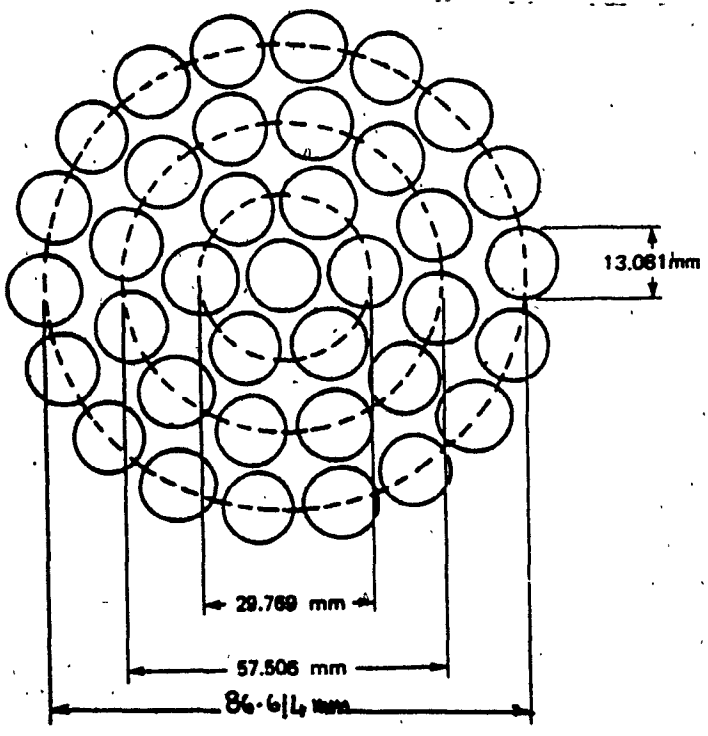

FIGURE 6.3: 37-Element Fuel Unit Cell

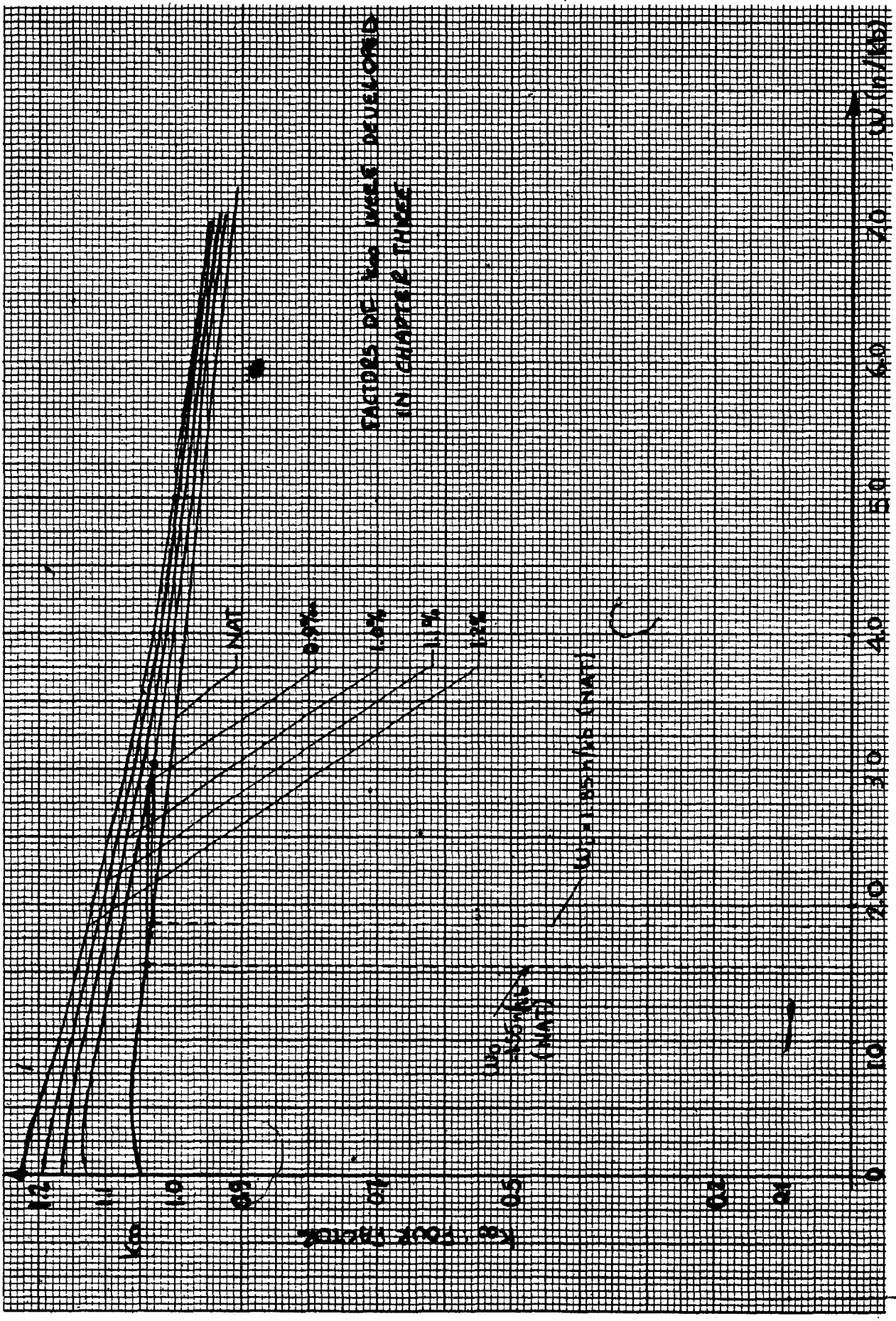

FIGURE 6.4: LATREP Based Four Factor kω vs Irradiation U

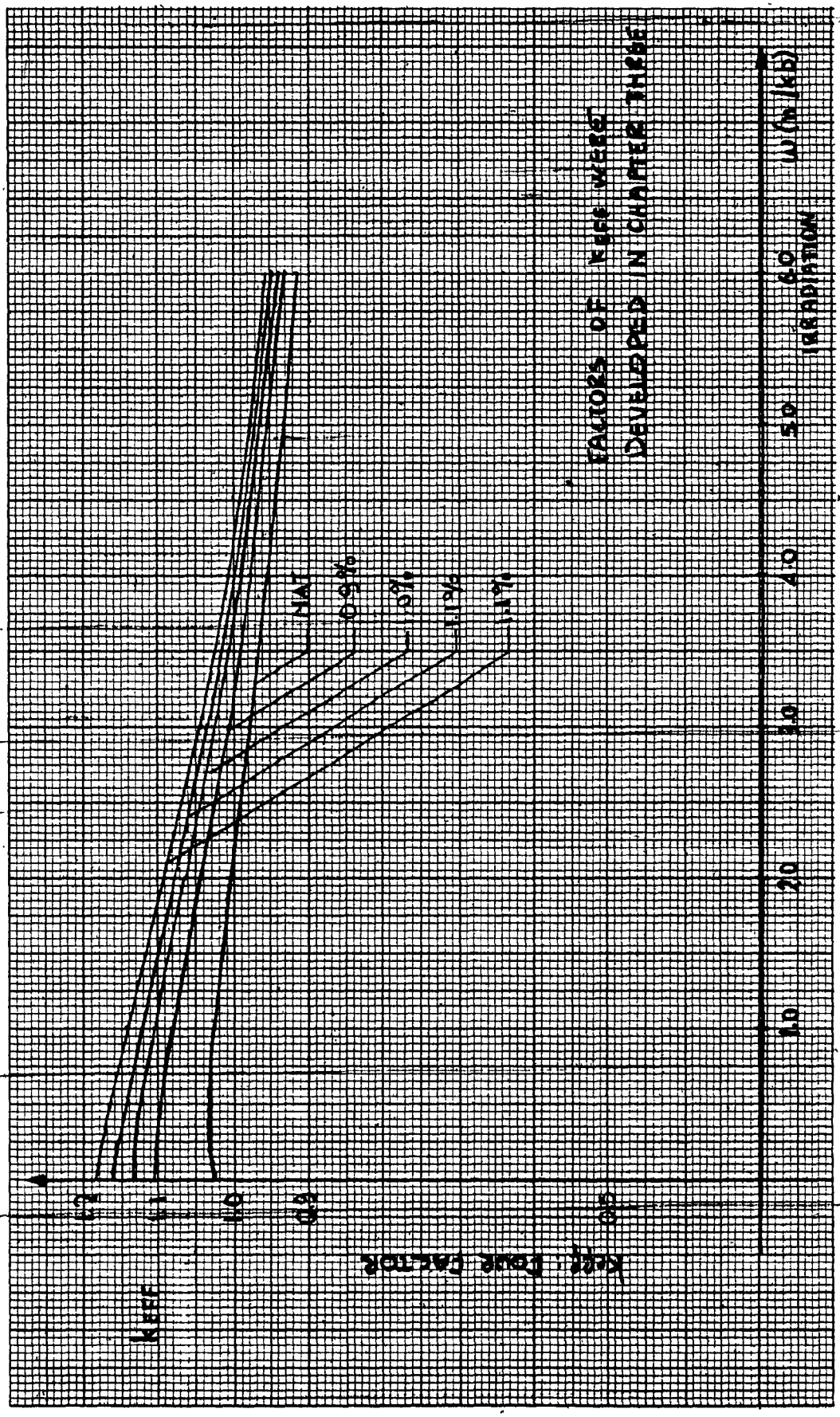

FIGURE 6.5: LATREP Based Four Factor keff

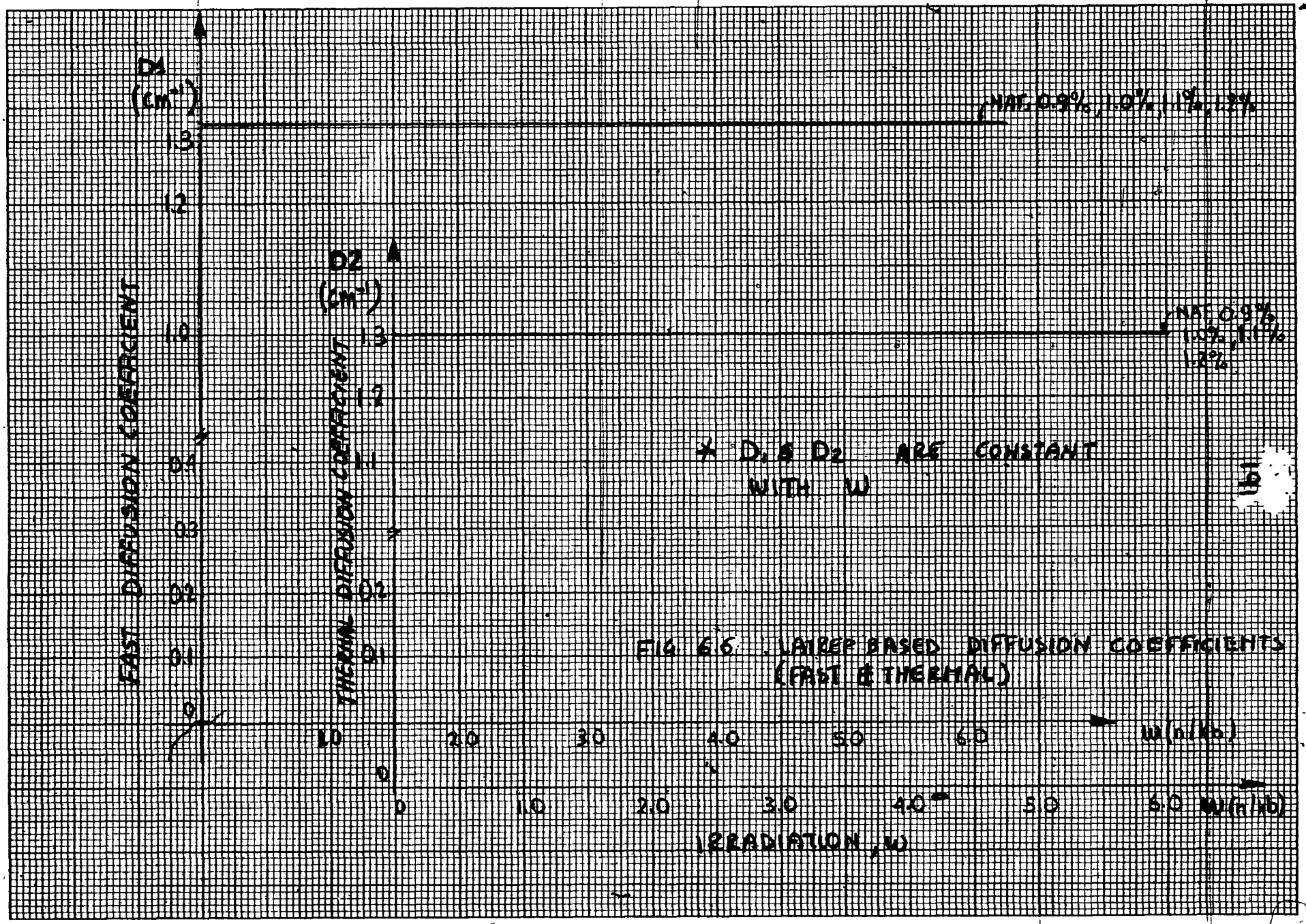

FIG 6.6 LATTICE BASED DIFFUSION COEFFICIENTS (FAST & THERMAL)

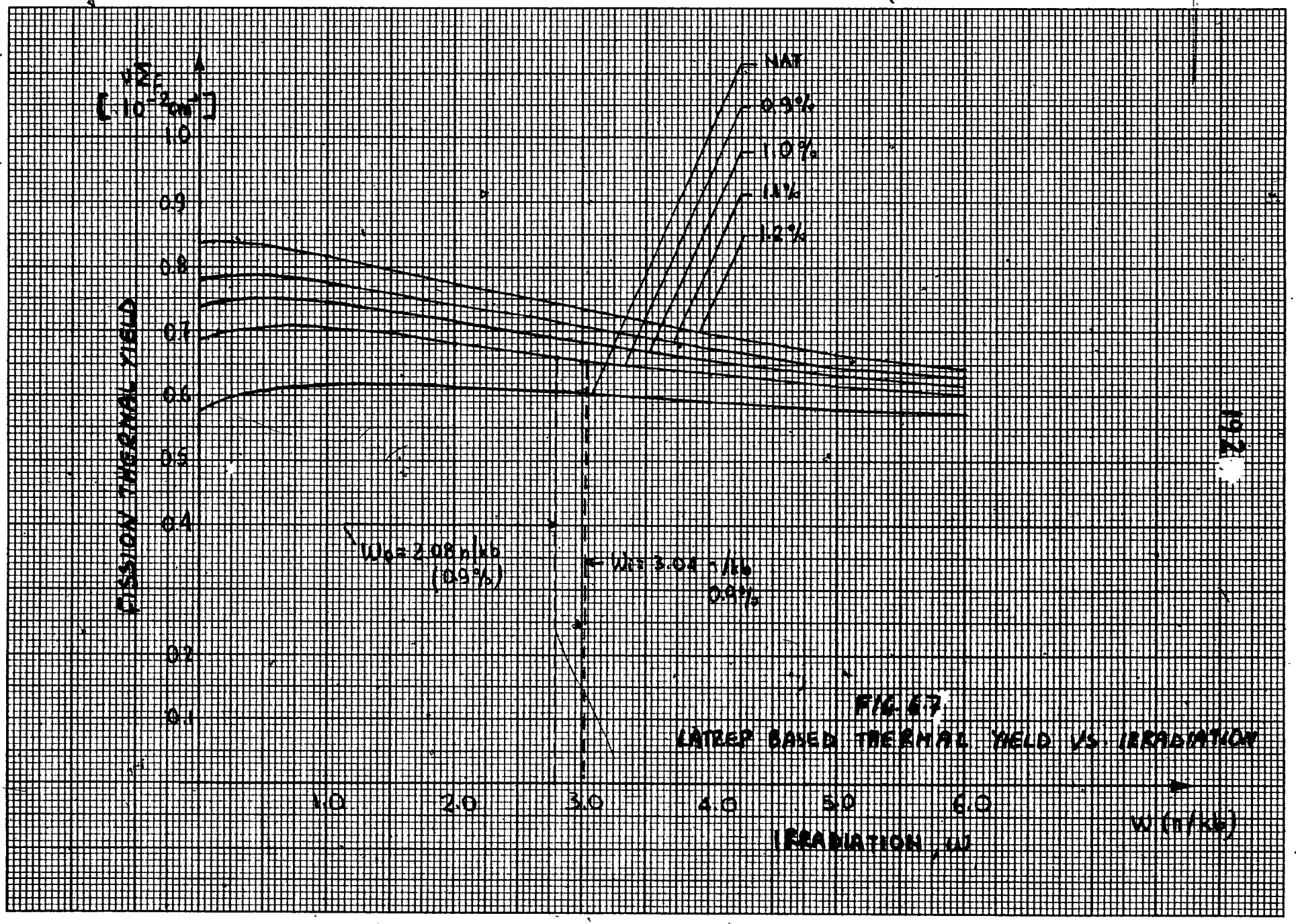

FIG 6.7
LATTICE BASED THERMAL YIELD VS IRRADIATION

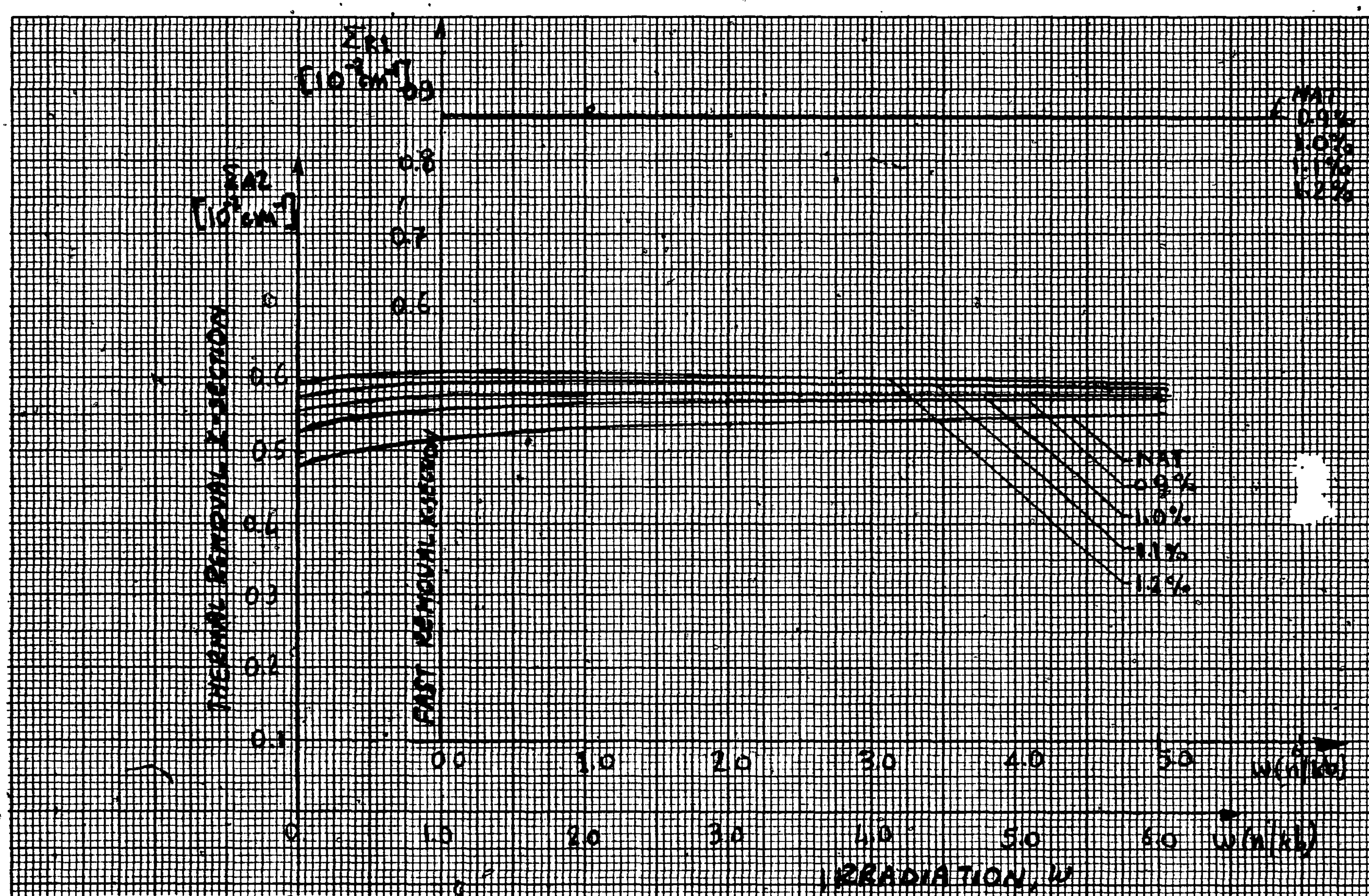

FIGURE 6.8: LATREP Based Thermal and Fast Removal X-Sections

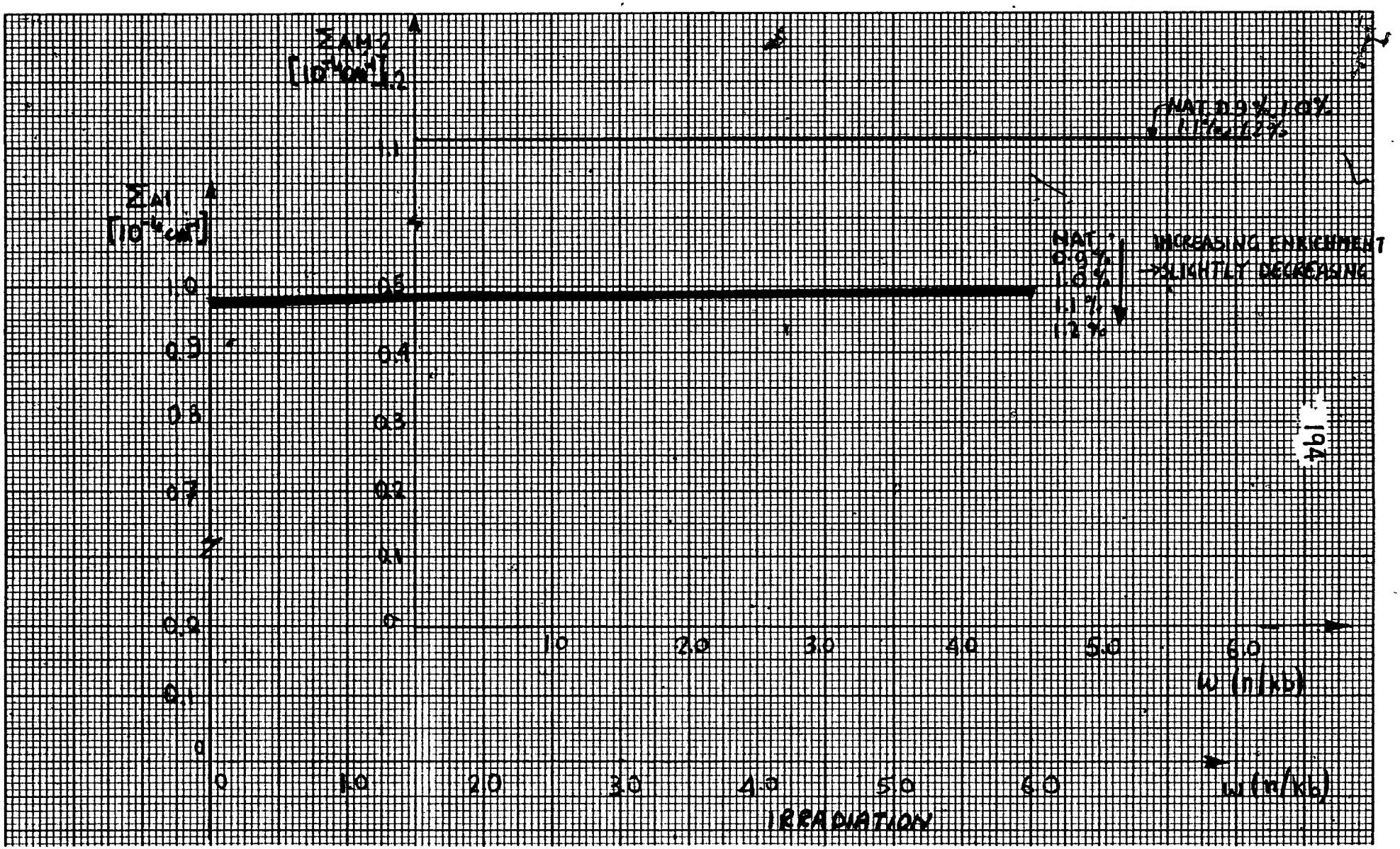

FIGURE 6.9: LATREP Based Fast Removal X-Sections

The irradiation at position Z in the channel is given by:

$$W_1(z) = \int_0^Z \frac{\Phi(z)}{R}\, dz \qquad \text{Eq. 6.7}$$

where R is the fuel displacement rate from one end to the other for a channel fuelled from Z = 0 end, and is

$$W_2(z) = \int_Z^L \frac{\Phi(z)}{R}\, dz \qquad \text{Eq. 6.8}$$

for a channel fuelled from Z = L end.

The average irradiation at point Z is thus:

$$\bar{W}(z) = \frac{1}{2}\left[W_1(z) + W_2(z)\right]$$

$$= \frac{1}{2}\int_0^L \frac{\Phi(z)}{R}\, dz$$

$$= \frac{1}{2} W(L) = \text{CONSTANT} \qquad \text{Eq. 6.9}$$

The average irradiation along the channel is therefore constant, so that average reactivity and cross-sections will also be approximately constant.

The average cross-sections to be used in the core calculations can be obtained from

$$\bar{\Sigma} = \frac{1}{W_{EXIT}} \int_0^{W_{EXIT}} \Sigma(\omega)\, d\omega \qquad \text{Eq. 6.10}$$

The two-group cross-sections based on this approximation are obtained directly a from lattice cell program that calculates isotopic compositions and cross-sections as a function of irradiation. The cross-sections are then used in a diffusion code to generate the power distribution. This is referred to as the "homogeneous model", since the cross-sections are constant along the channel, that is, axially homogeneous.

CANDU reactors are designed such that the core is divided into two concentric irradiation regions. The irradiation in the inner region is adjusted to give a flat flux distribution, that is, no radial leakage. The outer region has a lower irradiation which is selected so as to make the reactor critical. The flux in the inner region is constant (or nearly) at the maximum value. The size of the inner region determines the form factor, that is, the ratio of the average to maximum flux in the core.

6.3.5 Nuclear Cross-Sections: Time-Averaged Approximation

The homogeneous approximation cannot determine the variations in power and flux which occur because a finite number of bundles are replaced at every channel visit. The homogeneous model neglects the axial fuel management. To determine the effect of the flux axial fuelling scheme, the Time Averaged (TA) approximation is used.

In the TA model we assume that the power distribution which is calculated from cross-sections averaged over the residence time of the fuel is the time averaged power. That is, we use cross-sections which are obtained from:

$$\bar{\Sigma} = \frac{1}{\Delta W} \int_{W_1}^{W_2} \Sigma(W)\, dW \qquad \text{Eq. 6.11}$$

where W_1 and W_2 are the irradiations at the beginning and at the end of the residence time, and

$$\Delta W = W_2 - W_1 \qquad \text{Eq. 6.12}$$

The Σ's will, in general, vary with axial position in the channel since $\Delta\Sigma$ varies with the flux at each position and

$$\Delta W = \phi\, \Delta T \qquad \text{Eq. 6.12}$$

To obtain the initial and final irradiation for each axial position, we assume an axial flux distribution, then

$$\Delta W = \phi\, T \qquad \text{Eq. 6.13}$$

where T is the residence time.

Now, when the fuel is pushed to a new position, the irradiation at the start of the new cycle is equal to the end of the cycle

irradiation at the previous position. Therefore, starting from the fresh bundles, and knowing the axial fuel management scheme, we can determine W_1 and W_2 for all positions in the channel.

Generally, the residence time is not known, but the average discharge irradiation is known (for instance, from a previous homogeneous calculation). That is:

$$W_{OUT} = \frac{1}{N} \sum_{i=1}^{N} W_i \qquad \text{Eq. 6.14}$$

where the summation is over all the bundles discharged. But:

$$W_i = \sum_j \Delta W_j \qquad \text{Eq. 6.15}$$

where the summation is over all the positions occupied by the bundle during its core residence period. Thus:

$$W_{OUT} = \frac{1}{N} \sum_i \sum_j \Delta W_j \qquad \text{Eq. 6.16}$$

The double summation includes all positions in the channel. This can be observed from Figure 6.10. As a consequence:

$$W_{OUT} = \frac{1}{N} \sum_k \Delta W_k$$
$$= \frac{1}{N} \sum_k \Phi_k$$

Eq. 6.16

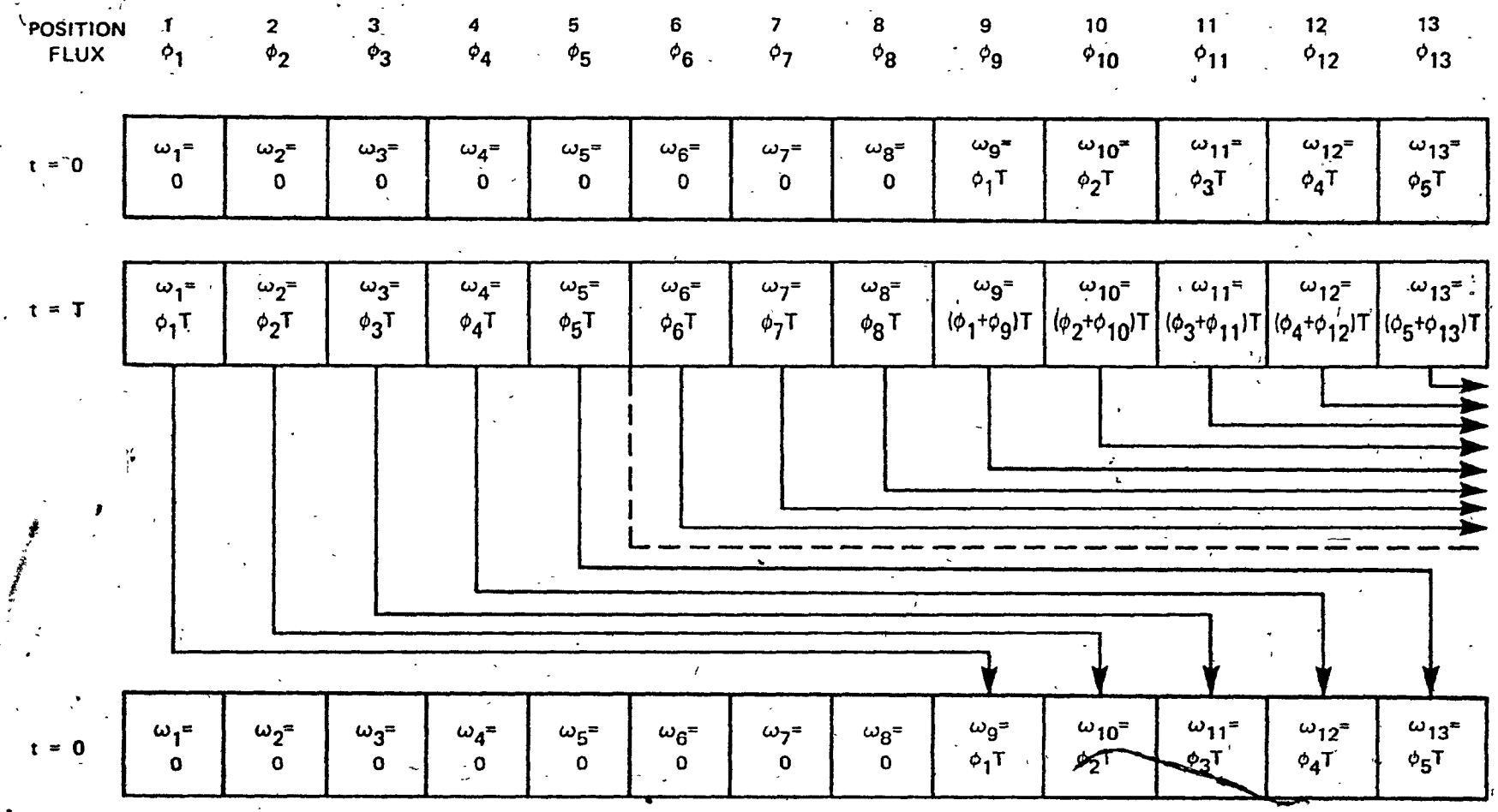

AVERAGE DISCHARGE IRRADIATION

$$= \frac{1}{8} \left\{ \phi_6T + \phi_7T + \phi_8T + (\phi_1 + \phi_9)T + (\phi_2 + \phi_{10})T + (\phi_3 + \phi_{11})T + (\phi_4 + \phi_{12})T + (\phi_5 + \phi_{13})T \right\}$$

$$= \frac{T}{8} \left\{ \phi_1 + \phi_2 + \phi_3 + \phi_4 + \phi_5 + \phi_6 + \phi_7 + \phi_8 + \phi_9 + \phi_{10} + \phi_{11} + \phi_{12} + \phi_{13} \right\}$$

FIGURE 6.10: Time-Averaged 8-Bundle Shift

Now, if we know the axial flux shape ϕ_K, we can derive the residence time

$$T = \frac{N W_{OUT}}{\sum_K \phi_K} \qquad \text{Eq. 6.17}$$

and substitute to get

$$\Delta W_K = \frac{N \bar{W}_{OUT} \phi_K}{\sum_K \phi_K} \qquad \text{Eq. 6.18}$$

The fluxes we want to use in this equation are the time averaged fluxes that we wish to calculate. We are, therefore, in an iterative situation where the output of one calculation must be used to provide the fluxes for calculating the input to the next step in the cycle until the process has converged.

The steps that are usually followed are the following:

1. An initial estimate is made of the exit irradiation, the size and the shape of the inner region. This can be obtained from previous homogeneous calculations. An initial guess of the axial flux shape is assumed.

2. The initial and discharge irradiations for each bundle are computed from the exit irradiation, the axial flux shape and the fuelling scheme.

3. For each position (bundle) in the channel, average cross-sections are calculated by integrating from initial to final irradiation as illustrated in Figure 6.11.

4. With this cross-section, a core calculation is performed to derive the flux distribution, the eigenvalue and the power distribution.

5. Steps 2 through 4 are repeated until the flux shape has converged.

6. The irradiation of the inner region is adjusted to get a flat channel power distribution. The outer region irradiation is adjusted to produce the required excess of reactivity. The relative size of the inner and outer regions is adjusted to get the desired form factor. All these factors are not necessarily adjusted at every iteration.

7. Steps 2 through 6 are repeated until the desired form factor and excess reactivity are obtained.

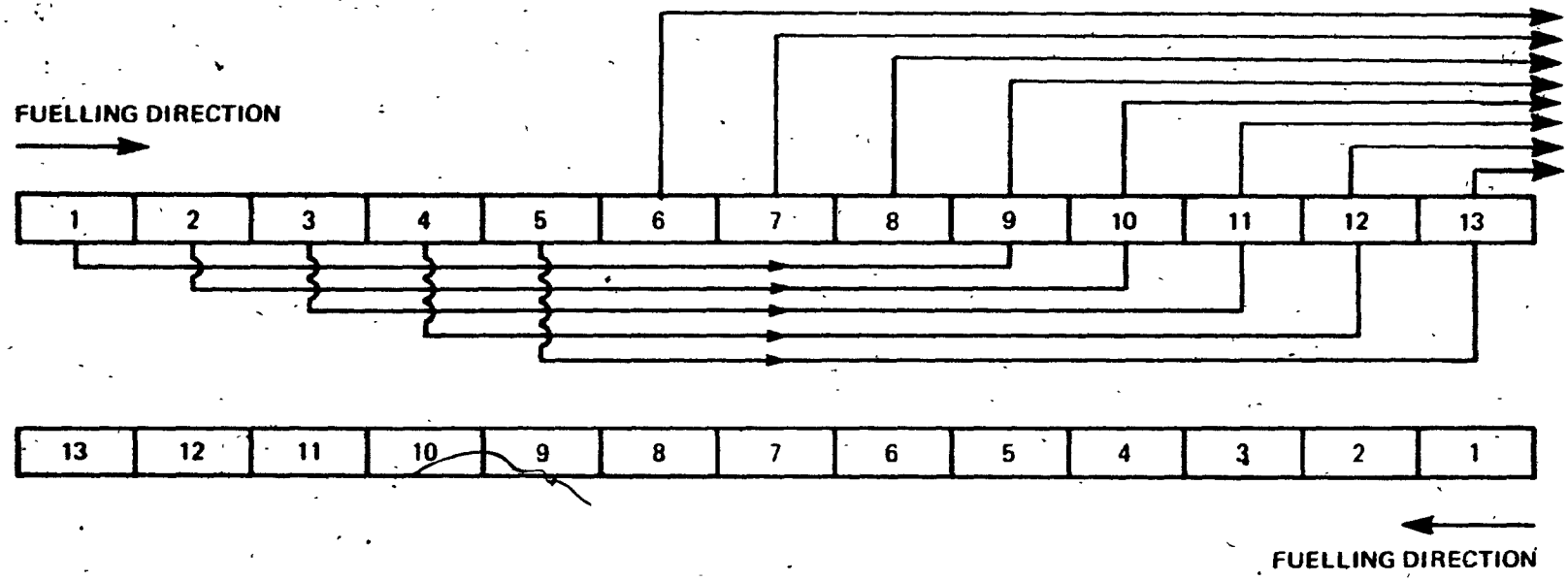

EACH CHANNEL IS

1. REFUELLED
2. IRRADIATED UNDISTURBED FOR DWELL TIME T
3. REFUELLED AGAIN
4. BUNDLES ARE SHIFTED ALONG CHANNEL N POSITIONS

IRRADIATION AT END OF T IS:

$$\omega(k) = \omega(k - N) + \int_0^T \phi(k)dt$$

$$\bar{\Sigma}(k) = \frac{1}{\omega(k)} \int_{\omega_1}^{\omega_2} \Sigma(\omega)d\omega$$

FIGURE 6.11: Time-Averaged Model

6.3.6 Calculation of Critical Channel Power (CCP)

The critical channel power (CCP or Pcr) can be calculated from Critical Heat Flux (CHF or ϕcr) correlations.

A brief discussion of the CCP calculation is given below for information purposes only.

A CHF correlation establishes a relationship between local parameters (quality x, mass velocity G, pressure P) and the particular value of the heat flux for which coolant "crisis" occurs. For safety analysis purposes, lower bound correlations are used such that all the pertinent experimental CHF values lie on or above the correlation curve.

Two correlations have been used in this study, both referring to the bundle cross-sectional average of the heat flux, and both of the form:

$$\phi_{cr} = A e^{-Bx}; \quad 0.1 \leq x \leq 0.8 \qquad \text{Eq. 6.19}$$

a) "U-1" lower-bound correlation (Ref. 31)

A = 1.595 MW/m^2

B = 3.2819

b) Interim correlation, not lower bound type

$$A = 63.9 \times 10^{-9} \left(\frac{H_{fg}}{H^*}\right)^{2.4} \text{ MW/m}^2$$

$$B = 3.44 \; ; \quad H^* = 1 \text{ kJ/kg}$$

H_{fg} = latent heat of vaporization at the exit pressure in KJ/kg

The CCP is calculated by combining the critical heat flux correlation, the heat balance along the channel and the flow power characteristics with the axial power shape assumed from the fuel management calculations. The CCP resulting from this calculation is a function of the power shape and can be particularly sensitive to the direction of the flow being with or against the refuelling direction (which governs the orientation of the power distribution); inlet-peaked shapes gives higher calculated CCP than exit-peaked ones. Further research would be needed to firm up this behaviour of CCP in relation to the LEU fuel cycle.

6.3.7 LEU Uncertainty Factors and Reactor Operating Margins

In the technical assessment of LEU fuel cycle, the following definitions were adopted:

$\hat{P} \overset{\Delta}{=}$ peak channel power in TA distribution;

$P_M \overset{\Delta}{=}$ all-time maximum channel power;

$P_{TRIP} \triangleq$ channel power at trip;

$P_{cr} \triangleq$ critical channel power;

$F \triangleq$ Channel Power Peaking Factor (CPPF) from fuel management calculations; the CPPF is defined as the maximum value, over the high-power channels, of the individual channels' ratios between maximum (in time) and TA powers.

$U \triangleq$ uncertainty in the calculation of P_{cr} such that

$$P_{trip} < P'_{trip} = \frac{P_{cr}}{1 + U} \qquad \text{Eq. 6.19}$$

Note: To take care of distorted flux shapes, the protective system may be so designed as to trip for a maximum channel power:

$$P_{trip} = \frac{P_{cr}}{1 + U + D}$$

where D = distortion factor that for modern large CANDU-PHW reactor is set equal zero.

$M \triangleq$ operating margins such that

$$P_{trip} = P_M(1+M) \qquad \text{Eq. 6.20}$$

To ensure maximum conservatism, one normally assumes:

$$P_M = \hat{FP} \qquad \text{Eq. 6.21}$$

so that

$$P_{trip} = \hat{FP}\ (1+M) \qquad \text{Eq. 6.22}$$

Equation 6.22 can be used to calculate the maximum permissible reactor power W_{max} corresponding to a given margin M_R, if the $\hat{P}$-value is known to be $\hat{P}_o$ at a given reactor power W_o. One has:

$$\hat{FP}\ (1+M_R) = P_{trip} \qquad \text{Eq. 6.23}$$

$$\frac{W_{max}}{W_o} = \frac{\hat{P}_{max}}{\hat{P}_o} \qquad \text{Eq. 6.24}$$

which, solved, gives the solution

$$\frac{W_{max}}{W_o} = \frac{P_{trip}}{F(1+M_R)\hat{P}_o} \qquad \text{Eq. 6.25}$$

Note: The operating margin is meant to absorb power peaking over the predicted F value (e.g., due to xenon transients, less-than-ideal refuelling) and instrument reading uncertainties.

6.4 ASSESSMENT OF UNCERTAINTIES AND MARGINS

6.4.1 Uncertainties

A standard uncertainty figure is presently used in CANDU-PHW reactor core studies (Ref. 31).

$$U = U_1 + U_2 \qquad \text{Eq. 6.26}$$

where $U_1 \triangleq$ systematic and random errors = 0.11

$U_2 \triangleq$ extra allowance = 0.04

6.4.2 Operating Margins

Based on fuel management data calculations and using Equation 6.24, we have:

W_o = 92% FP

$\hat{P}_o$ = 6.049 MW

P'_{trip} = P_{trip} = 8.3 MW/1.15 = 7.217 MW

F = 1.055

W_{max} = 98% FP

The margin for the LEU-CANDU-PHW reactor is calculated to be:

$$1 + M = \frac{P_{trip}}{FP_o}\frac{W_o}{W_{max}} = 1.0615 \qquad \text{Eq. 6.27}$$

6.5 LEU-CANDU-PHW REACTOR FUEL MANAGEMENT CALCULATIONS - EQUILIBRIUM CYCLE

All studies for the LEU assessment have been based on an 850 MW(e) CANDU-PHW reactor (e.g., Darlington, also defined from hereon as the reference reactor) operating at 92% FP(th), in which only the fuel is changed with respect to the natural core.

The reference reactor has been divided into two burnup zones, with the inner zone consisting of 208 channels at a higher exit burnup than the others. This interzone burnup differential is designed to preserve, as far as practicable, the same time-averaged (TA) power distribution as in the natural core.

The low enriched uranium core average burnups are normalized to that of the natural core as follows. A time-averaged calculation for the natural core is run with LATREP fuel tables and with the reference reactor burnups as calculated from PPV cross-sections; the resulting core reactivity (about 4 mk) constitutes the reference "equilibrium cycle" reactivity to be matched by all other LATREP-based time-averaged calculations.

The fuel management calculations confirmed that the bundle power distribution along a given channel (axial power distribution) is sensitive to the bundle-shifting and to enrichment.

The results are summarized in Table 6.1.

TABLE 6.1: Fuel Management Calculations (Reference Reactor Core)

ENRICHMENT AND LATTICE CODE	BUNDLE SHIFT		EXIT BURNUP (MWh/kgU)		AVG	MAX. INSTANT. POWER				CPPF	
						%CHANN. (MW)		BUNDLE (KW)			
	INNER 256 CHLS	OUTER 224 CHLS	INNER 208 CHLS	OUTER 272 CHLS		INN 256	OUT 224	INN 256	OUT 224	INN 256	OUT 224
0.711 (PPV)	4	8	179	156	166						
0.711 (LATREP)	4	8	179	156	166	6.38	6.19	784	782	1.055	1.089
0.711 (LATREP)	8	8	178	155	165	6.63		825		1.102	
0.75 (PPV)	4	8	213	192	202	6.65	6.49	809	826	1.091	1.149
0.8 (PPV)	4	8	251	231	241	6.89	6.80	837	867	1.128	1.209
0.9 (LATREP)	4	8	334	316	325	7.29	7.53	888	974	1.201	1.333
0.9 (LATREP)	4	4	336	312	323	7.08		837		1.170	
0.9 (LATREP)	2	4	336	313	324	6.58	6.46	777	772	1.089	1.137
1.0 (LATREP)	2	4	406	377	391	6.82	6.72	807	815	1.110	1.171
1.2 (LATREP)	2	4	516	487	501	7.02	6.95	913	972	1.146	1.214
1.2 (LATREP)	2	2	517	489	502	6.97		927		1.142	

6.5.1 Critical Heat Flux (CHF) Calculations vs Refuelling Direction

Local critical heat flux was calculated at the end-of-bundle for a constant header-to-header pressure drop (using a given power flow rate characteristic, and using the correlations mentioned in Section 6.3.6. The results are summarized in Table 6.2.

TABLE 6.2: Effects of Axial Power Distribution on Critical Power

APPROXIMATE CCP(MW) FOR THE INNER CORE					
ENRICHMENT	BS	FUEL → * ← FLOW		FUEL → ** FLOW	
		U-1	INTERIM	U-1	INTERIM
NAT	4/8	8.231	8.576	8.175	8.253
NAT	8/8	8.260	8.604	8.133	8.483
0.8	4/8	8.092	8.451	8.250	8.592
0.9	4/8	7.963	8.341	8.290	8.631
0.9	4/4	7.953	8.337	8.348	8.687
0.9	2/4	7.972	8.349	8.294	8.634
1.0	2/4	7.781	8.143	8.404	8.741
1.2	2/4	7.376	7.779	8.407	8.715

* against
** with

6.5.2 Technical Feasibility of Various Fuelling Schemes

- Fuelling with the flow increases the maximum allowable power by substantial amounts (3% to 9%), the differential increasing with enrichment.

- All enriched schemes lead to permissible power lower than with natural UO_2.

- The maximum permissible power occurs for 0.9 w/o enrichment with mixed 2/4 bundle shift and three fuelling machine trolleys.

- The reference core power is not optimized. Optimization of the power distribution may lead to some marginal improvements.

Results are summarized in Table 6.3.

TABLE 6.3: Technical Assessment of LEU-Core

ENRICHMENT (W/O) B-S FUELLING WITH/ AGAINST FLOW	NAT 4/8	0.8 4/8	0.9 4/4	0.9 2/4	1.0 2/4	1.2 2/4	0.9 4/4	0.9 2/4	1.0 2/4	1.2 2/4
	AGAINST	AGAINST					WITH			
P_{cr}	8.3	8.17	8.02	8.04	7.84	7.44	8.3	8.3	8.3	8.3
$P_{trip} = \frac{P_{cr}}{1.15}$ [MW]	7.217	7.102	6.974	6.991	6.817	6.470	7.217	7.217	7.217	7.217
P_{ref} = 92% [FP(P)] (MW)	6.049	6.110	6.053	6.044	6.144	6.116	6.053	6.044	6.144	6.116
Calculated CPPF = F	1.055	1.128	1.170	1.089	1.110	1.146	1.170	1.089	1.110	1.146
Operating Margin $M = \frac{P_{trip}}{FP_{ref}} - 1$	.131	0.030	-0.015	0.062	-0.0004	-.077	0.19	0.096	0.058	0.030
Expected Reference Reactor Margins M_R	0.0615	0.0615	0.0615	0.0615	0.0615	0.0615	0.0615	0.0615	0.0615	0.0615
Permissible Power ZFP $= 92\% \frac{1 + M}{1 + M_R}$	98.0	89.3	85.4	92	86.7	80.0	88.3	95.1	91.7	89.3

6.6 PPV AND LATREP BASED REACTIVITY DEVICES WORTH

The use of low enriched uranium fuel for CANDU-PHW reactors in which only the fuel is changed with respect to the natural core does not only alter power distribution and reactor operating margins with respect to fuelling schemes and enrichment, but modifies the nuclear behaviour of reactivity devices spread throughout the reactor core. The entire LEU technical assessment (within the scope of this thesis) program has been performed on LATREP-based reactivity devices worth and incremental cross-sections.

Due to different thermal cut-offs (Westcott's $\sqrt{\pi}$ kT in PPV, 0.625 eV in LATREP) and to entirely different models, the lattice Σ's of LATREP and PPV have little in common. The determination of reactor core power distribution and reactivity devices worth was performed as described in the following subsections.

6.6.1 PPV-Based Reactivity Devices Worth and Power Distribution

The following steps were performed to determine the reactor core power distribution and calculation of reactivity devices worth:

Step 1: Calculation of two-group parameters for core without reactivity devices: reflector, inner core and outer core corresponding to the design burnups:

- diffusion coefficients D_1, D_2;
- group absorption cross-sections Σ_{a1}, Σ_{a2};
- thermal yield $\nu\Sigma_f$;
- removal cross-section Σ_R;
- flux to power conversion factor H.

These parameters are reported here in the same format as they are input to core static analysis calculations (CHEBY).

The above diffusion group parameters are obtained from Darlington reactor core design manuals.

Step 2: Calculation of two-group parameters for the reference core reactivity devices: these parameters are in the form of increments with respect to those of Step 1. Incremental parameters as they are input to core static analysis codes (CHEBY):

- Group 1 and 2 Diffusion Coefficients: D_1, D_2;
- Group 1 and 2 Absorp. : Σ_{a1}, Σ_{a2};
- Fast Production : $\nu\Sigma_f$;
- Fast Remov. : Σ_R.

By device type and location.

Note: Due to the fact that the reference core has a symmetrical arrangement, only half core is considered (Figures 6.12 and 6.13).

Step 3: Prepare the reference core burnup map from Figures 6.12 and 6.13, showing:

- core burnup regions;
- location of reactivity devices.

Two examples of burnup region in Plane 8 and location of reactivity devices in Plane 8 are illustrated by Figures 6.12 and 6.13 respectively, where:

1 Reflector

2 Outer Zone Channels

3 Inner Zone Channels

Step 4: Calculation of reactivity devices' worth (liquid zone controller 50% voided, adjuster rods).

Calculation of static reactivity devices worth is performed in this thesis by means of the core design code "CHEBY". The principles adopted consisted of the following considerations:

1. When the reference core is at equilibrium, critical, and its reactivity devices (liquid zone controllers and

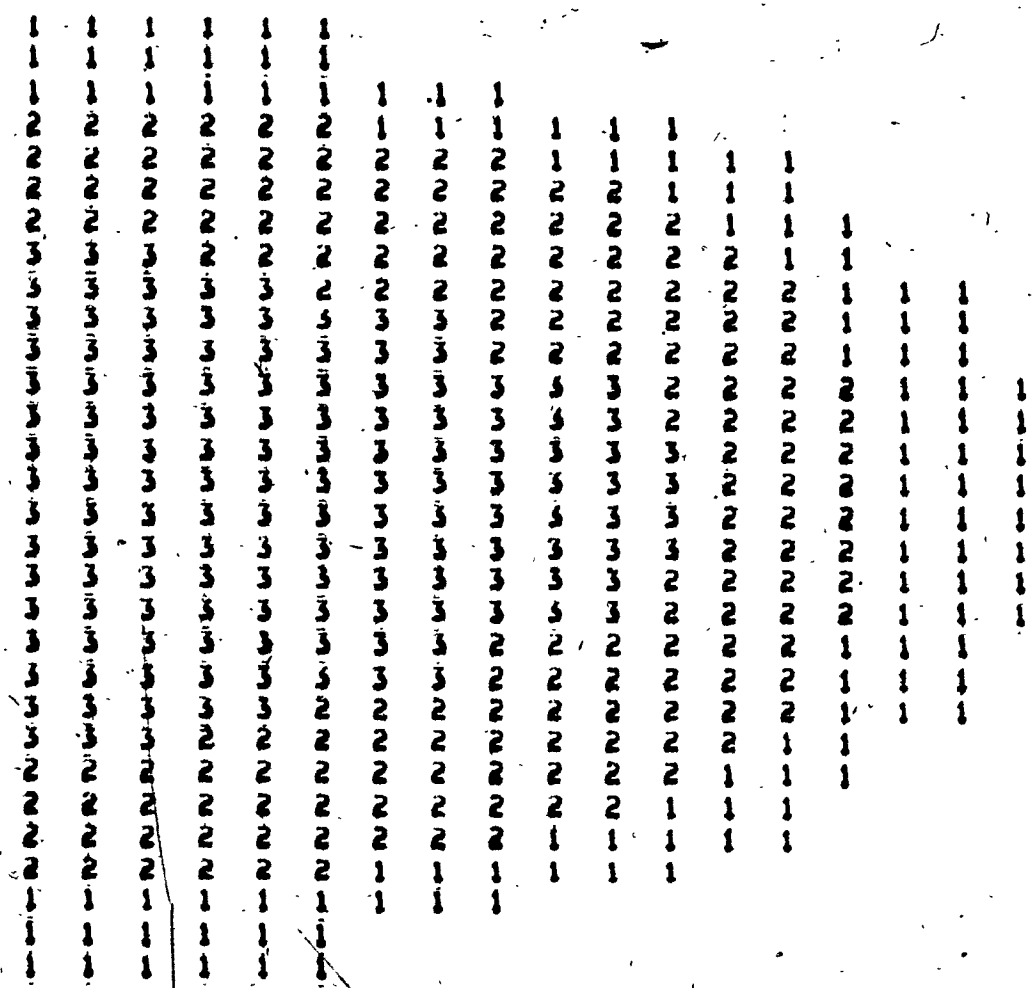

FIGURE 6.12: Reflector - Outer Core - Inner Core Map

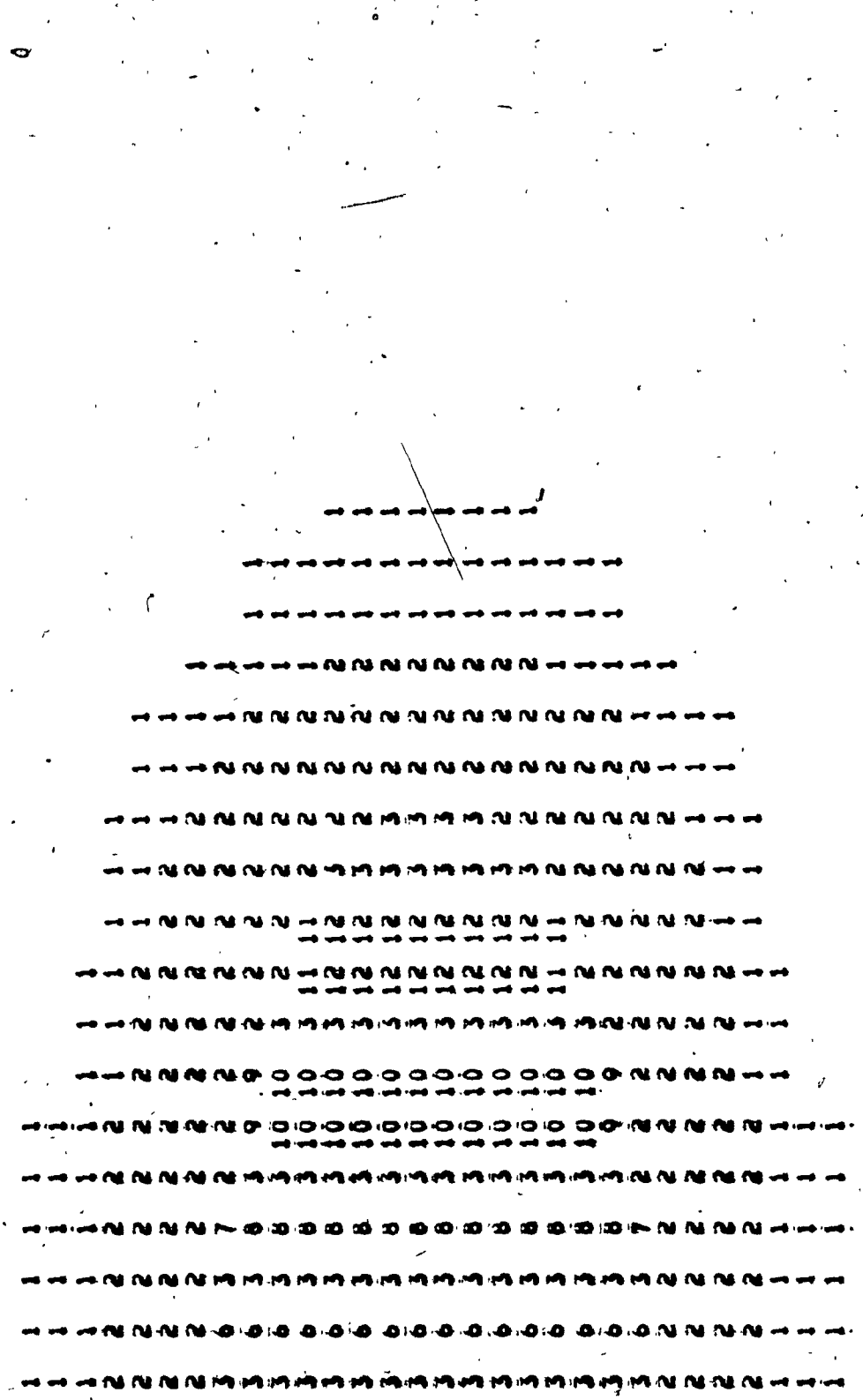

FIGURE 6.13: Core and Reactivity Devices Map

adjusters) are in the reference position (liquid zone compartment 50% voided, adjuster rods in "full-in" position), the core reactivity is such that its keff is near 1.0.

CHEBY calculation gave for this configuration:

$$keff = 0.998966$$

2. By draining the liquid zone controller compartments and by letting adjuster rods occupy the "full-in" position, CHEBY calculation gave a new core reactivity:

$$keff' = 1.00275$$

3. By moving adjuster rods to "full-out" position and by letting liquid zone controller level unchanged, the following keff was found:

$$keff'' = 1.01704$$

The reactivity worth of liquid zone controller and adjuster rods is then readily calculated.

RW (ADJ) k Adjuster reactivity worth

$$= \left[\frac{1}{keff} - \frac{1}{keff}\right] \times 10^3 = 17.789 \text{ mk}$$

TABLE 6.4: PPV-Based Core Parameters

PARAMETERS / CORE REGIONS	GRP1 TRNS XN	GRP2 TRNS XN	GRP1 ABS XN	GRP2 ABS XN	FAST PROD. XN	FAST REMOV. XN	H
Reflector	1.32282	8.85535E-01	1.00000E-10	8.22530E-05	0.0	1.00801E-02	0.0
Outer Core w = 1.55 n/kb	1.27895	9.49198E-01	7.63646E-04	3.99594E-03	4.64384E-03	7.36032E-03	2.40309E-01
Inner Core w = 1.85 n/kb	1.27895	9.49171E-01	7.63243E-04	4.02027E-03	4.62367E-03	7.36073E-03	2.37863-01

TABLE 6.5: PPV-Based Reactivity Devices' Incremental Cross-Sections

REACTIVITY DEVICES	GRP1 TRNS XN	GRP2 TRNS XN	GRP1 ABS XN	GRP2 ABS XN	FAST PROD. XN	FAST REMOV. XN	H
Liquid Zone Controller	.171562E-01	.139276E-00	.000572E-01	0.011115E-01	-.132E-04	.17534E-02	0.0
Adjuster Rod A		-1.0500E-04	0.2700E-04	0.6600E-03	0.4850E-4	0.0	0.0
Adjuster Rod B		-1.2500E-04	0.3013E-04	0.7200E-03	0.5800E-04	0.0	0.0
Adjuster Rod C		-0.7900E-04	0.2237E-04	[illegible]60E-03	0.3800E-04	0.0	0.0
Adjuster Rod D		-0.6800E-04	0.2063E-04	[illegible]20E-03	0.3300E-04	0.0	0.0

RW (LZC) $\triangleq$ Liquid zone controller reactivity worth

$$= \left[\frac{1}{keff} - \frac{1}{keff} \right] \times 10^3 = 3.7775 \text{ mk}$$

6.6.2 LATREP-Based Reactivity Devices Worth and Power Distribution

In the following steps, adjustment of reactivity devices' incremental cross-section is such that when LATREP-based core properties are used, approximately equal power distribution and reactivity devices' worth are obtained.

On completion of Steps 1 through 4 of Section 6.6.1 for the determination of LATREP-based power distribution and respective calculation of reactivity device worth for the natural UO_2 fuel and for two degrees of enrichment, namely 0.9% and 1.2%, the following steps were followed:

Step 5: Six LATREP lattice cell core runs with natural and five different degrees of enrichment were made to compute reactor core diffusion parameters versus different levels of discharge burnup.

The LATREP-based cell diffusion parameters for natural and slightly enriched cores are reported in Chapter Three for information and, of course, for verification.

Step 6: Determination of reference core natural uranium, LATREP-based diffusion parameters.

We desire to have the reference reactor core with fuel diffusion parameters that are LATREP-based and discharge burnups for the LATREP-based core equal to those of the PPV-based core. Thus, for the LATREP-based core, we still have:

$$W_{\text{inner core}} = 1.85 \text{ n/kb}$$

$$W_{\text{outer core}} = 1.55 \text{ n/kb}$$

where W irradiation in neutrons per kilobarns.

With these two irradiation values, we are able to search from Figures 6.4, 6.9 and Table 6.6.

Step 7: LATREP-based reactivity devices' (liquid zone controllers and adjuster rods) incremental cross-sections.

All core calculations for natural UO_2 use PPV lattice cross-sections plus specially smeared "incremental cross-sections" $\Delta\Sigma$ to describe the effect of reactivity devices (liquid zone controllers, adjusters, shut-off rods, mechanical control absorbers, etc.).

Due to different thermal cut-offs (Westcott's μ kT in PPV, 0.625 eV in LATREP), and due to entirely different models

(Section 6.3.3), the lattice Σ's of PPV and LATREP have little in common; in particular, one finds in the thermal group (subscript 2)(*):

$$\frac{\Sigma_{a2}^{L}}{\Sigma_{a2}^{P}} \simeq \frac{\Sigma_{f2}^{L}}{\Sigma_{f2}^{P}} \simeq \frac{D_2}{D_1} \simeq 1.3 \qquad \text{Eq. 6.28}$$

(L for LATREP, P for PPV), whereas the epithermal cross-sections are somewhat closer in the two sets.

One would then expect to have to use, for every reactivity device i, thermal $\Delta\Sigma$'s roughly given by:

$$\Delta\Sigma_i^{L} = 1.3\,\Delta\Sigma^{P} \qquad \text{Eq. 6.29}$$

in order to reproduce the same reactivity and power distribution effects.

The actual $\Delta\Sigma$ values were obtained by finding device-dependent multipliers α_i that:

$$\Delta\Sigma_i^{L} = \alpha_i\,\Delta\Sigma_i^{P} \qquad \text{Eq. 6.30}$$

(*) Most of the difference is due to the different definition of thermal cross-sections: LATREP thermal Σ's are approximately $\sqrt{4/\pi\,\vartheta/T_0}$ times the PPV $\Delta\Sigma$'s, where ϑ_m is the absolute neutron temperature in the moderator, and T_0 is 293.58°K. For ϑ_m = 100°C = 373.14°K, one finds $\sqrt{4/\pi\,\vartheta_m/T_0} = 1.272$

in conjunction with Σ^L would reproduce exactly the PPV device reactivity worth in a natural core. It was checked a posteriori that power distributions thus obtained would match the PPV results.

It was found for adjusters and liquid zone controllers that:

$$\alpha_i^{LZC} = 1.353$$

$$\alpha_i^{ADJ} = 1.342 \quad .$$

Step 8: Prepare LATREP-Based reactivity devices' incremental cross-sections.

Using the multipliers found in Step 7 and Table 6.5, we can immediately prepare Table 6.7.

TABLE 6.6: LATREP-Based Core Parameters

PARAMETERS / CORE REGIONS	GRP1 TRNS XN	GRP 2 TRNS XN	GRP1 ABS XN	GRP2 ABS XN	FAST PROD. XN	FAST REMOV. XN	H FACTOR
Reflector	1.32758	1.20851	1.00000E-10	.111492E-03	0.0	.1106681E-01	0.0
Outer Core w = 1.55 n/kb	1.32448	1.30456	1.00275E-03	5.28531E-03	6.18952E-02	8.64528E-02	2.49830E-01
Inner Core w = 1.85 n/kb	1.324513	1.304020	1.00313E-03	5.32251E-03	6.16995E-03	8.64596E-03	2.47812E-01

TABLE 6.7: LATREP-Based Reactivity Devices' Incremental Cross-Sections

REACTIVITY DEVICES	GRP1 TRNS XN	GRP2 TRNS XN	GRP1 ABS XN	GRP2 ABS XN	FAST PROD. XN	FAST REMOV. XN	H FACTOR
Liquid Zone Controller	0.232294E-01	.188578E-00	0.000773E-01	0.015049E-01	-0.178E-04	0.23741E-02	0.0
Adjuster Bank A		-1.4086E-04	0.3622E-04	0.8854E-03	0.6507E-04	0.0	0.0
Adjuster Bank B		-1.6770E-04	0.4042E-04	0.9659E-03	0.7781E-04	0.0	0.0
Adjuster Bank C		-1.0598E-04	0.3001E-04	0.7727E-03	0.5098E-04	0.0	0.0
Adjuster Bank D		- .9122E-04	0.2767E-04	0.7271E-03	0.4427E-04	0.0	0.0

6.7 NATURAL AND LEU 850 MW(e) CANDU-PHW REACTOR NUCLEAR PARAMETERS

The reactor core nuclear parameters given below are usually considered an important data basis for reactor core static and space-time studies.

The data consists of:

- Xenon, iodine yields and decay constants;
- Xenon, iodine normalized yields/fission neutrons;
- Discharge irradiation;
- Subcritical reactivities;
- Xenon integrals;
- Total flux squared weighted thermal yield;
- Total flux squared weighted thermal yield ratios;
- Inner core, outer core, reflector group diffusion parameters.

6.7.1 Xenon/Iodine Constants

The xenon and iodine decay constants used are the following:

$$\lambda^{I} = 2.92 \text{ E-05 } [\text{sec}^{-1}]$$
$$\lambda^{Xe} = 2.1 \text{ E-04 } [\text{sec}^{-1}]$$

6.7.2 Xenon and Iodine Yields/Fission

The xenon and iodine yields/fission contributed from the mixture of fissile material (U-235, Pu-239, Pu-241] used are the following:

	U-235	Pu-239	Pu-241
γ_I	6.386E-02	6.1E-02	7.694E-02
γ_{Xe}	2.28E-03	1.07E-03	2.55E-3

6.7.3 Discharge Irradiation

From Figures 6.4 through 6.9, it is possible to build up the following irradiation table:

TABLE 6.8:- Irradiation Table for Natural and Low Enriched Uranium Cores

	DISCHARGE			ROUNDED-OFF CORE AVERAGE
ENRICHMENT	INNER ZONE W_i n/kb	OUTER ZONE W_o n/kb	AVERAGE $\overline{W}$ n/kb	W SAMPLE n/kb
Natural	1.85	1.55	1.712	0.85
0.9% (w/o)	3.04	2.81	2.939	1.47
1.2% (w/o)	4.11	3.81	3.979	2.0

6.7.4 Yields/Fission Neutrons

In the space-modal-kinetics for CANDU-PHW reactor core studies, the ratios of iodine and xenon yields with the average number of neutrons per fission are used.

Due to the fact that a mixture of fissile materials are available in the CANDU-PHW reactor cores, the following averaging method is used to calculate the desired quantities:

$$\frac{\gamma_x}{\nu} = \frac{\sum_i \gamma_x^{(i)} N^{(i)} \sigma_f^{(i)}}{\sum_i \nu_i N^{(i)} \sigma_f^{(i)}} = \frac{\sum_i \gamma_x^{(i)} [\text{FISSION EDIT}]}{\sum_i [\text{YIELD EDIT}]} \qquad \text{Eq. 6.31}$$

$N^{(i)} \sigma_f^{(i)}$ can be replaced by the corresponding figure in FISSION EDIT [PPV or LATREP], and $\nu_i N^{(i)} \sigma_f^{(i)}$ can be replaced by the corresponding YIELD EDIT figure [PPV or LATREP] to generate the following Table 6.9.

6.7.5 Neutron Mean Life Time

The neutron mean life time is calculated in this section for natural and for two selected enrichment levels (0.9% and 1.2%). This nuclear parameter was analyzed in detail in Chapter Four and was defined to be the time an average neutron survives after it appears as either a prompt neutron or one

TABLE 6.9: FISSION EDIT - YIELD EDIT - Xenon/Iodine Yields (LATREP-Based)

ENRICHMENT	DISCHARGE BURNUP AVERAGE $\bar{W}$	1/2 $\bar{W}$ (n/kb)	FISSION EDIT U-235	FISSION EDIT Pu-239	FISSION EDIT Pu-241	YIELD EDIT U-235	YIELD EDIT Pu-239	YIELD EDIT Pu-241		
Natural	1.712	0.8	.211347+15	.16818+15	.5521+13	.51429+15	.48291+15	.16393+14	.023856	.002296
		1.0	.185932+15	.189121+15	.87129+13	.45245+15	.54304+15	.25871+14	.023577	.00245
		0.85							.023786	.00245
					NORM. TO PPV				0.02446	0.002293
0.9%	2.939	1.4	.162926+15	.203524+15	.16136+14	.396477+15	.584402+15	.479119+14	.023390	.002551
		1.6	.146489+15	.219064+15	.201723+14	.356476+15	.617538+15	.598961+14	.023473	.002675
		1.47							.023418	.0025915
					NORM. TO PPV				.02408	.002545
1.2%	3.979	2.0	.13767+15	.215411+15	.281472+14	.335038+15	.618541+15	.835759+14	.023234	.002629
					NORM. TO PPV				.02389	.002582

emitted from a delayed-neutron precursor. This definition is assumed to be accurate in this thesis since we deal with reasonably slow transients. In Chapter Four, we wrote it in what we may call a purely theoretical form and in the form as is implemented in the space-modal kinetics formalism.

The neutron mean life time Λ^* for the case of natural reactor core defined as $\Lambda^*(NAT)$ was given to be.

$$\Lambda^*(NAT) = 7.8443 \times 10^{-4} \text{ sec}$$

Basically, $\Lambda^* = \frac{1}{v\nu\Sigma_f}$ (v = neutron velocity) and $\nu\Sigma$ grows with enrichment.

The total fundamental flux squared weighted thermal yields and the corresponding neutron mean life time were computed and they are summarized in the following Table 6.10.

TABLE 6.10: W-Thermal Yields and Neutron Mean Life Time

ENRICHMENT W/o	$\langle \Psi_1 \mid \nu\Sigma_f \mid \Psi_1 \rangle$	$\Lambda^*(w/o)$ sec
Natural	16.752	7.8443×10^{-4}
0.9%	17.84995	7.36179×10^{-4}
1.2%	18.8894	6.95669×10^{-4}

where: $$\Lambda^*(w/o) = \Lambda^*(NAT) \frac{\langle \Psi_1 \mid \nu\Sigma_f \mid \Psi_1 \rangle_{NAT}}{\langle \Psi_1 \mid \nu\Sigma_f \mid \Psi_1 \rangle_{w/o}}$$ Eq. 6.32

6.7.6 Subcritical Reactivities

The modal subcritical reactivities ρ_{scm} of mode m relative to the fundamental mode (denoted by subscript 1) are defined as:

$$\rho_{scm} = \frac{1}{k_1} - \frac{1}{k_m}$$

where: k_1 = effective multiplication factor for the fundamental mode;

k_m = effective multiplication factor for the m-th mode.

Values of k_1 and k_m generated by MONIC two-group diffusion code for CANDU-PHW reactors provide the following values of ρ_{scm} . Table 6.11.

TABLE 6.11: Modal Subcriticalities

MODE	DESCRIPTION	SUBCRITICALITY (k)
1	Fundamental	0.0
2	1st Azimuthal (T/D)	-0.013498
3	1st Azimuthal (S/S)	-0.012988
4	2nd Azimuthal (oblique)	-0.034651
5	2nd Azimuthal (V/H)	-0.036185
6	1st Axial	-0.021671
7	2nd Axial	-0.05153
8	1st Radial	-0.067126
9	2nd Radial	-0.075839
10	3rd Azimuthal	-0.173911

The values of δ_{scri} in Table 6.11 indicate that if higher modes are excited they will face a fast decay or, in other words, it is more difficult to excite higher modes than smaller ones (Chapter Five).

6.7.7 SMOKIN Input Data

SMOKIN code has a very large data bank that is assembled such that almost all reactor spatial kinetics studies for CANDU-PHW reactors require little change from one core study to another. Examples of SMOKIN input data for natural and Low Enriched Uranium core spatial kinetics studies are available from the author on request. They are not included in the thesis because of their large volume.

CHAPTER SEVEN

7. 850 MW(e)-LEU-CANDU-PHW REACTOR SPATIAL KINETICS

7.1 GENERAL FEATURES OF REACTOR CONTROL

The purpose of controlling any type of power reactor is to bring its power output up to a desired level, maintain it at that level, shut the reactor down in a planned or emergency situation and to keep it in a shutdown state for as long as desired. From Chapter One, it may also be necessary in the future, for economic reasons, to perform reactor output step-back or setback changes by what is commonly defined as the load following control scheme.

An important feature of a nuclear reactor that has bearing on the control system is that, in most power reactors, the fuel supply cannot be continuously replaced as it is consumed. Consequently, at the beginning of each operational period, the reactor core must contain all the fuel (fissile material) that will be required to produce a predetermined quantity of energy. Hence, when a thermal power reactor core is assembled prior to commencing operation, it contains what we may call a built-in excess of reactivity due to the extra quantity of fuel. This excess reactivity is generally a function of the fuel enrichment. An essential requirement of the control system is that it must be capable of introducing negative

reactivity to compensate for the built-in positive reactivity of initial start-up of the reactor.

This requirement is much less sensitive in CANDU-PHW reactors since they are equipped with on-power refuelling scheme.

7.2 METHODS OF CONTROL

Several methods of controlling nuclear power reactors are presently being used. Addition or removal of fuel, moderator, reflector or poison, in an individual or in combined fashion, are some examples of reactor control that have been used. Most modern thermal power reactors use the "insertion" or "withdrawal" of control rods as reactor power control and shaping devices. The control rods are made of absorbing material such as boron or cadmium having a large cross-section for the absorption of neutrons. In CANDU-PHW reactors, the reactor power shaping function is taken care of by the "adjuster rods" or by the burnup distribution or both, depending on the station design, and the power regulation is performed by means of fourteen liquid zone controller compartments (Chapter Five).

The absorbers and the fissile materials may be regarded as competitors for neutrons; the larger the absorption cross-section of power control and regulation devices, the smaller the fraction of neutrons available for fission, and vice versa. When a reactor core is being assembled, the neutron-absorbing devices are in their full absorbing position, adjuster, mechanical control absorber and shut-off rods fully inserted and liquid zone controller compartment at zero void position. The neutron density is thus maintained at such a low level that the effective multiplication factor is significantly less than unity (e.g. subcritical). A total of approximately

-100 mk is usually available from CANDU solid absorbing materials and liquid zone controllers.

During start-up and shutdown, the solid absorbing materials and liquid zone control reactivity devices are operated so as to allow the increase or decrease of the reactor neutron density at a safe and controlled rate.

A summary description of CANDU-PHW reactor reactivity control devices and safety systems was presented in Chapters Three and Five.

7.3 EFFECTIVENESS OF REACTIVITY CONTROL DEVICES

When a reactivity control device is placed in a neutron flux (thermal, in our case), it absorbs neutrons in its vicinity and thereby produces distortion of the neutron flux distribution. The effect of the neutron absorber can be explained by considering a reactor in which the average neutron flux is maintained constant, with or without reactivity control device insertion. Suppose a single neutron absorber is inserted at the center of a uniform reactor core; the radial neutron flux distribution under the postulated conditions will then be as shown in Figure 7.1. It is seen that the neutron flux is decreased close to the reactivity device, but, further out near the core boundary, the flux is increased over the value without the reactivity device.

According to diffusion theory (Ref. 6), the neutron leakage from the core is determined by the gradient of the neutron flux near the boundary. The rod insertion results in an increase in this gradient, so that the neutron leakage is increased. Thus, an absorber rod can affect the average neutron flux by both absorption and leakage. The relative importance of these two factors on the core reactivity is dependent on various circumstances.

Since a single reactivity device (absorber) decreases the neutron flux in its vicinity, but increases it at a greater

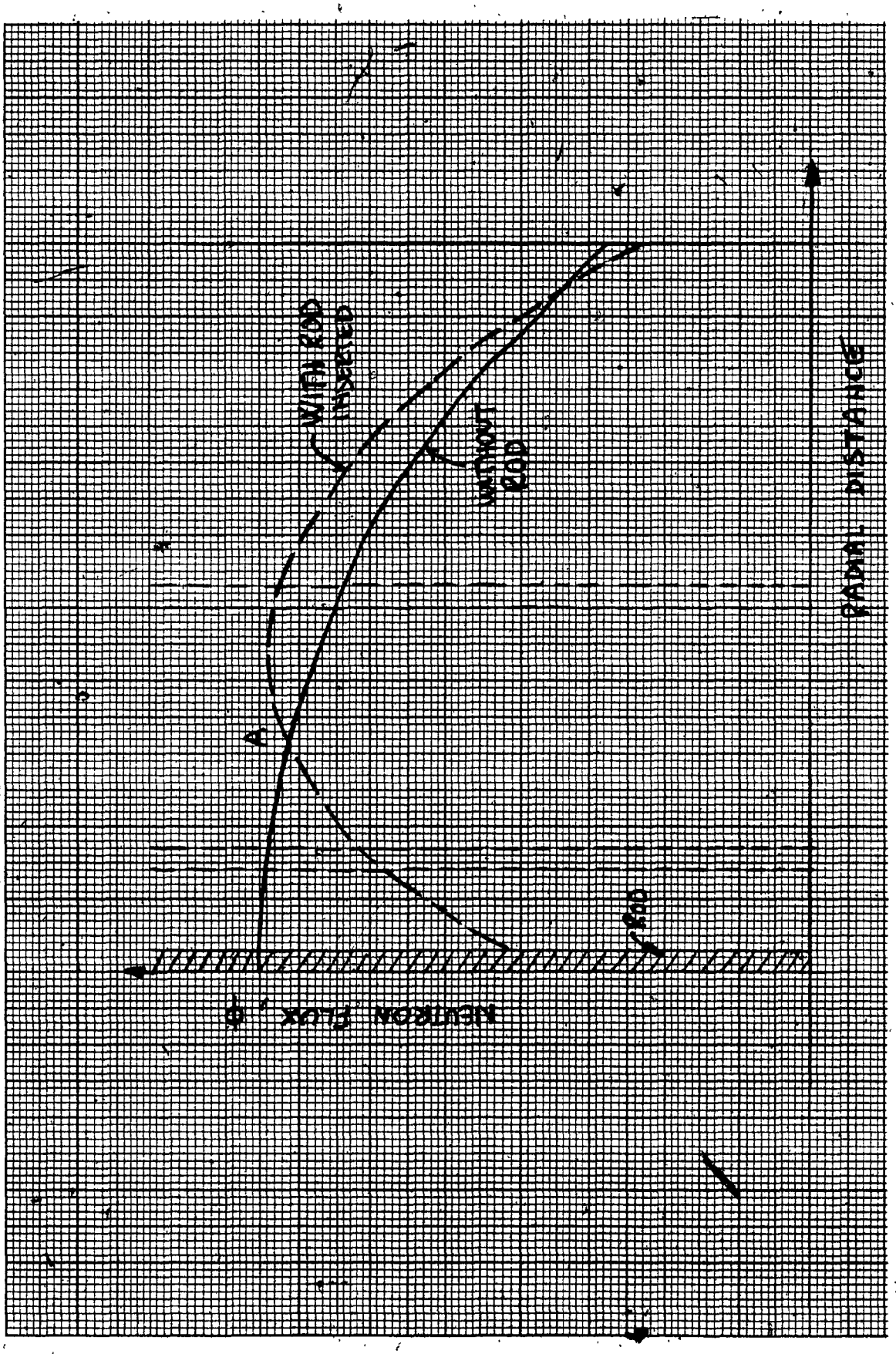

FIGURE 7.1: Effect of Control Rods on Radial Flux Distribution

radial distance, the effectiveness of reactivity "worth" of a second reactivity device, i.e., the change in reactivity it can produce, will depend on its location. The worth of an absorber (booster if reactor uses boosters) rod at a given location is roughly proportional to the square of the neutron flux at that location before the rod insertion. It therefore follows from Figure 7.1 that, at constant reactor power, a second rod will have a larger worth if it is inserted at a greater radial distance than A, where the two curves in Figure 7.1 cross, than if inserted closer in.

In a figurative language that has become commonplace in reactor physics, one would say that there is a "shadowing" effect between the two rods, the effect being positive if the second rod is closer to the control one than at point A, the shadowing being negative if they are farther apart.

7.4 REACTIVITY DEVICES SHADOWING

Reactor operation, as well as reactor power efficiency of CANDU-PHW reactors, requires the use of several (60 solid material absorber rods and, in general, fourteen liquid zone controllers appropriately distributed on a top view surface of approximately 20-25 m^2 (Figure 5.2). From this figure, we observe that on the average there are four to five reactivity control devices per square metre. It was illustrated in Chapter Five that not all reactivity control devices are inserted in the reactor during a given mode of operation. While the reactor is at full power, we know that only liquid zone controllers and adjuster rods are effective in the reactor core. The total number of these devices in the core from top view is 30, distributed over approximately 20 m^2, resulting in an average of more than one reactivity device per square metre. The average distance between these devices is of the order of one to two metres.

A term commonly used in reactor core physics is the "shadowing" to describe the effect of one control rod on the worth of another. If the worth of two reactivity control devices is less than the sum of the separate worths at the given locations, the shadowing is said to be positive. This is the case when two rods are close together and the reactor power is

maintained constant. On the other hand, if the rods are some distance apart, the shadowing is negative; the worth of the two rods is then greater than the sum of the separate rod worths at the particular position.

The location of a control rod, both absolutely and relative to the other rods, determines the rod worth. Apart from the shadowing effect, a control rod will have greater worth near the core axis, where the neutron flux is relatively high, than nearer the boundary where the flux is lower. Furthermore, the position of the rod has an important effect on the radial flux distribution.

For example, a second rod inserted close to the rod in Figure 7.1 would tend to increase the flux distortion by causing a further decrease near the center of the core and an increase nearer the boundary. If the second rod were inserted farther away, however, the result would be to produce a more uniform radial flux distribution. Because of such considerations, the power shaping rods (adjusters) in a CANDU-PHW reactor are inserted or withdrawn in a prescribed pattern to avoid severe distortion of the neutron flux (and thermal power) distribution and to promote uniform burnup of the fuel.

The radius of the region over which a control rod can produce a significant change in the neutron flux of a thermal reactor is roughly equal to the diffusion length of slow neutrons. In a heavy water-moderated reactor, the mean free path (mfp) is about 20 cm. In order to minimize local distortion of the flux, the control rods must, consequently, be fairly close together. This explains the large number of reactivity devices in large thermal power reactors (CANDU).

7.5 REACTOR CONTROL STUDIES

The reactor control system has two major operational functions; they are generally described as regulation and shutdown. The regulation system devices also provide a certain amount of shim control, i.e., the control of long-term changes in reactivity resulting from fuel depletion (or burnup) and the accumulation of fission-product poisons.

The regulation system function involves many short-term adjustments of the reactor power to the desired operating level and maintenance at (or close to) that level despite transient changes in reactivity; these changes may be caused by internal or external factors, e.g. reactor water temperature variations, system pressure changes, changes in steam demand, refuelling, and so on. The reactor control system must also have the capability to decrease the reactor power level either gradually during normal operation or very rapidly in an emergency situation or demanded reactor protection system.

A subsidiary function of the reactivity control devices is to "shape" the neutron flux, that is to say, to bring about local changes in the flux in order to achieve the optimum heat generation rate (or power) distribution in the core. Insertion of reactivity control devices (adjusters) at appropriate locations will help to minimize flux distortions, as seen earlier.

A uniform power distribution is desirable because it maximizes the overall power output of the reactor for a given maximum bundle or channel power, or, conversely, because it minimizes peak power for a given overall output. However, a strictly uniform power distribution is made impossible by neutron leakage unless very steep and extremely expensive enrichment gradients are used near the core periphery.

7.6 PHYSICS DIFFERENCES OF REACTIVITY CONTROL DEVICES

The essential properties of reactivity devices that are commonly used as neutron absorbers for reactivity control purposes are summarized in Table 7.1. The macroscopic thermal cross-sections (Ref. 6) are for the natural isotopic compositions of the various elements. With the exception of boron-10, in which the neutrons are absorbed in (n,) reactions, radiative capture (n,) is responsible for the absorption of thermal and resonance neutrons.

For most power reactors in which the ratio of moderator to fuel ratio gives a well-thermalized (approximately Maxwellian) neutron spectrum (Ref. 32, 33, 34) and which do not operate at high temperatures, cadmium has been a useful control material. In water-moderated (and cooled) power reactors, however, a significant proportion of the neutrons is in the epithermal with energies above 1 eV. Although the cadmium might be a suitable control material for such reactors from the neutronic standpoint, its low melting point of 321°C, which is below the outlet water temperature (330°C), makes it impracticable. The control material commonly used in pressurized-water reactors is an alloy of 80 (weight) percent silver, 15 percent indium, 5 percent cadmium. It is enclosed in a stainless steel tube to protect the neutron absorbing material from corrosion by the high temperature water. As seen in Table 7.1, both silver and indium have significant resonances in the epithemal neutron

regions. Although indium melts at an even lower temperature than cadmium, the melting point of silver-indium-cadmium alloy is substantially higher than that of cadmium.

Boron is a useful control material for thermal reactors because the absorption cross-section is large over a considerable range of neutron energies. Gadolinium is practically an excellent shutdown reactivity device due to its extremely high thermal neutron absorption cross-section.

TABLE 7.1: Physics Differences of Reactivity Control Devices (Ref. 35)

MATERIAL	0.0253 eV (barns)	0.0253 eV (10^2 cm^{-1})	MAJOR RESONANCES	
			ENERGY (eV)	(barns)
Boron	759	107		
Boron-10	3,838		None	
Silver	63	3.64		
Silver-107	37		16.6	630
Silver-109	92		5.1	12,500
Cadmium	2450	113		
Cadmium-113	19,800		0.18	7,200
Indium	195	7.3		
Indium-113	58			
Indium-115	202		1.46	30,000
Gadolinium	46,000	1,400		
Gadolinium-155	61,000		2.6	1,400
Gadolinium-157	255,000		17	1,000

7.7 REACTOR SPATIAL CONTROL STUDIES

CANDU-PHW reactors, from the Pickering Nuclear Power Generating Station to the largest N.G.S. in the family (Darlington), have fourteen liquid zone controller (LZC) compartments which have the main function of regulating the power and the axial distribution of the power throughout the reactor core. The neutron absorbing element used in this reactivity control scheme is H_2O. The LZC's are located on two planes along the reactor axis. Figures 5.2, 5.5.

The number of compartments corresponds to those shown in Figures 7.2 and 7.3 for the east reactor face and west face respectively. The compartments are arranged such that each controller will influence the flux in a region of the core termed the control zone. Figures 5.3 and 5.4 or 7.2 and 7.3. The present generation of CANDU-PHW reactors is divided into two axial halves with each half subdivided in the radial plane into seven control zone regions.

Each zone is equipped with two dual-redundant, in-core, self-powered platinum detectors (Chapter Five or Appendix RC) and, additionally, each axial pair of control zones contains three of four fully-instrumented (flow and temperature) channels which are used to calibrate the control detector flux readings to thermal power.

24 23 22 21 20 19 18 17 16 15 14 13 12 11 10 9 8 7 6 5 4 3 2 1

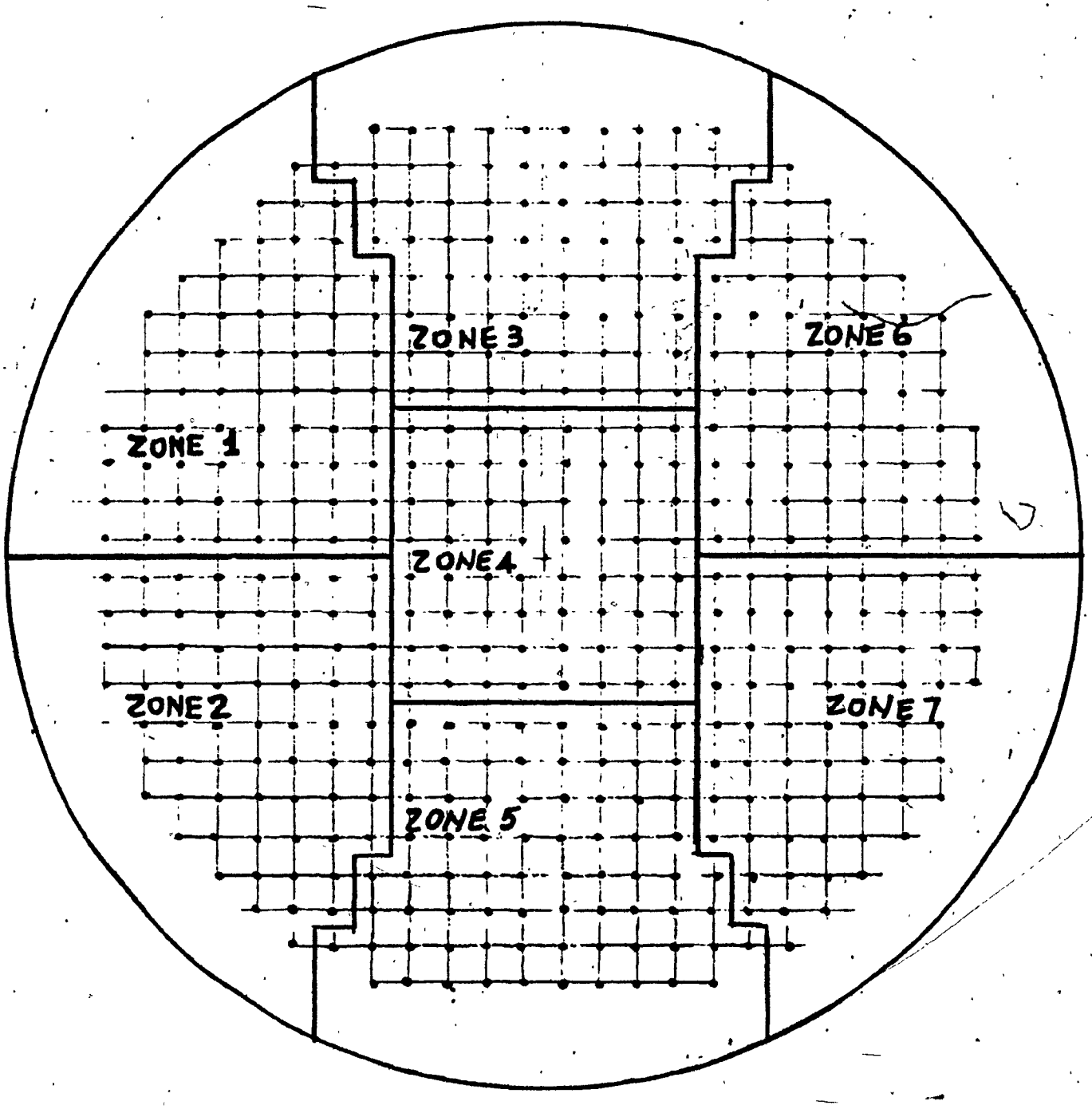

FIGURE 7.2: Darlington NGSA (Face: East)

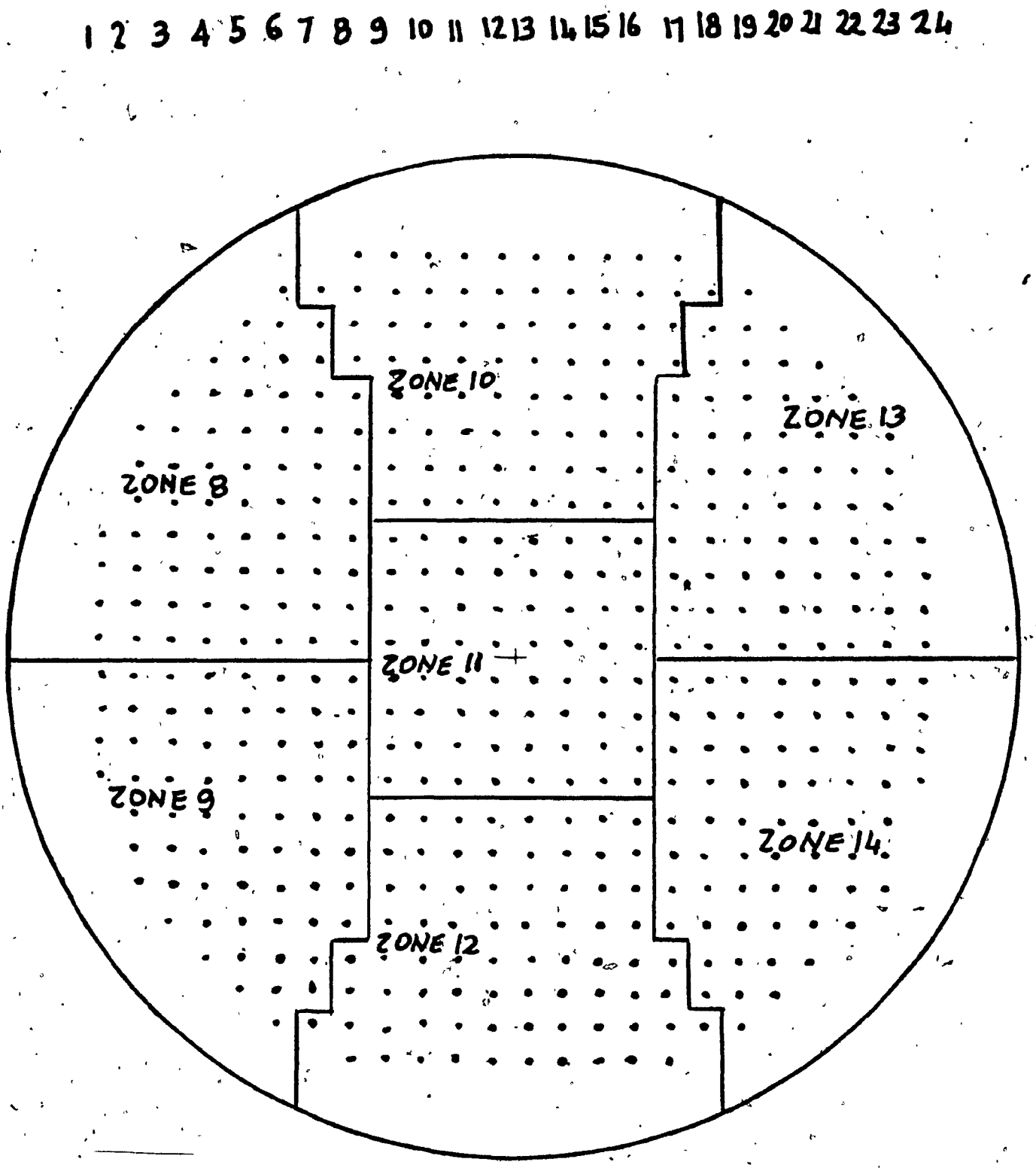

FIGURE 7.3: Darlington NGSA (Face: West)

Most of the present generation CANDU-PHW reactor control is based on a zonal-type control algorithm. The algorithm controls the volume of the H_2O in each compartment in unison to regulate the power level and differentially to regulate the distribution of power in the individual control zone regions. The differential change of light water volume in an individual zone controller is governed by the signals obtained from the in-core flux detectors and thermal power measurements (instrumented channels) in the associated zone. The volume of the LZC in a zone is adjusted by controlling the inflow of H_2O to a zone, with the outflow maintained constant.

A typical spatial control transient involves the refuelling of a channel in the reactor. This is also the most common spatial perturbation in the reactor since two or more channels are refuelled each full-power day of operation. Single- and two-channel refuelling transients have been performed in this thesis to study the behaviour of the liquid zone controllers when natural and low enriched uranium fuel was introduced into the refuelled channels. A refuelling simulation check was also performed to confirm the agreement of LATREP- or PPV-generated incremental cross-sections for adjusters and liquid zone controllers.

7.8 SMOKIN STUDIES OF REFUELLING TRANSIENTS FOR DARLINGTON N.G.S.A. WITH NATURAL OR SLIGHTLY ENRICHED FUEL

Several one-channel and two-channel refuelling operations have been simulated using the SMOKIN code in order to assess the following points:

- Comparison of PPV vs LATREP lattice constants on a natural core: LATREP data must be used for enriched fuel, and this comparison is made to ensure that the two sets of constants give consistent results.

- Assessment of the Liquid Zone Controllers (LZC) system for Low Enrichment Uranium (LEU) fuel.

From considerations described in Chapter Two, in the case of a LEU core, operating transients are more severe on the spatial control system that at the moment is used in the operating N.G.S. and in those which are being designed.

The refuelling transients in the LEU core inject approximately two to three times the perturbation amplitude when equivalent transients are simulated in a natural core [e.g. between (.1-0.2) mk and (0.3-0.6) mk for natural and LEU core respectively].

It is shown that the spatial control system responds nicely to perturbations and the response is at all times contained within the limits of linearity in the case of natural core, while most of the liquid zone controllers next to LEU refuelled channels are phased out in the case of an LEU core if the LZC system is not strengthened. The liquid zone compartmental controllers are physical cylinders of approximately 15 cm in diameter located vertically between the reactor pressure tubes. They cross the middle of the reactor zones from top to bottom. Due to design constraints and, most importantly, to the flux distribution in the reactor, the liquid zone controllers do not have a linear effectiveness when their level changes from 0% to 100%. The 20% and 80% are assumed to be the bottom and top limits between which the effectiveness is linear. Outside these limits, we say that the liquid zone controllers are phased out; or, in other words, the water level incremental changes do not have any more the same worth as if level changes took place in the 20%-80% range.

It is found that, if the LZC-induced incremental cross-sections are increased by 20% and the liquid zone controller reference levels are reduced by 20%, then single-channel and two-channel LEU refuelling transients show that the spatial control system operates within the limits of linearity.

The level of the liquid zone controllers does not exceed more than 70% in the case of single-channel refuelling, and only for some two-channel refuelling transients the does level of some liquid zone controllers reach the range of 80%.

7.8.1 SMOKIN Studies of Refuelling Transients for Darlington N.G.S.A. with Natural or Low Enriched Uranium Fuel

A systematic comparison was made of the spatial control system responses in a natural uranium core as obtained with the use of PPV lattice properties and LATREP lattice properties.(*)

The following channels were refuelled for the natural reactor (Figure 7.4):

- Single channels with PPV fuel properties (Figure 7.4):

  U13; N20; Q20.

- Single channels with LATREP fuel properties (Figure 7.5):

  U13; N20; Q20; J5; M12.

- Two channels with LATREP fuel properties (Figure 7.6):

  Q20-J5; U13-F13; U13-M13.

(*) Reactivity device incremental cross-sections (originally derived for PPV lattice constants) were also modified for use with LATREP lattice constants.

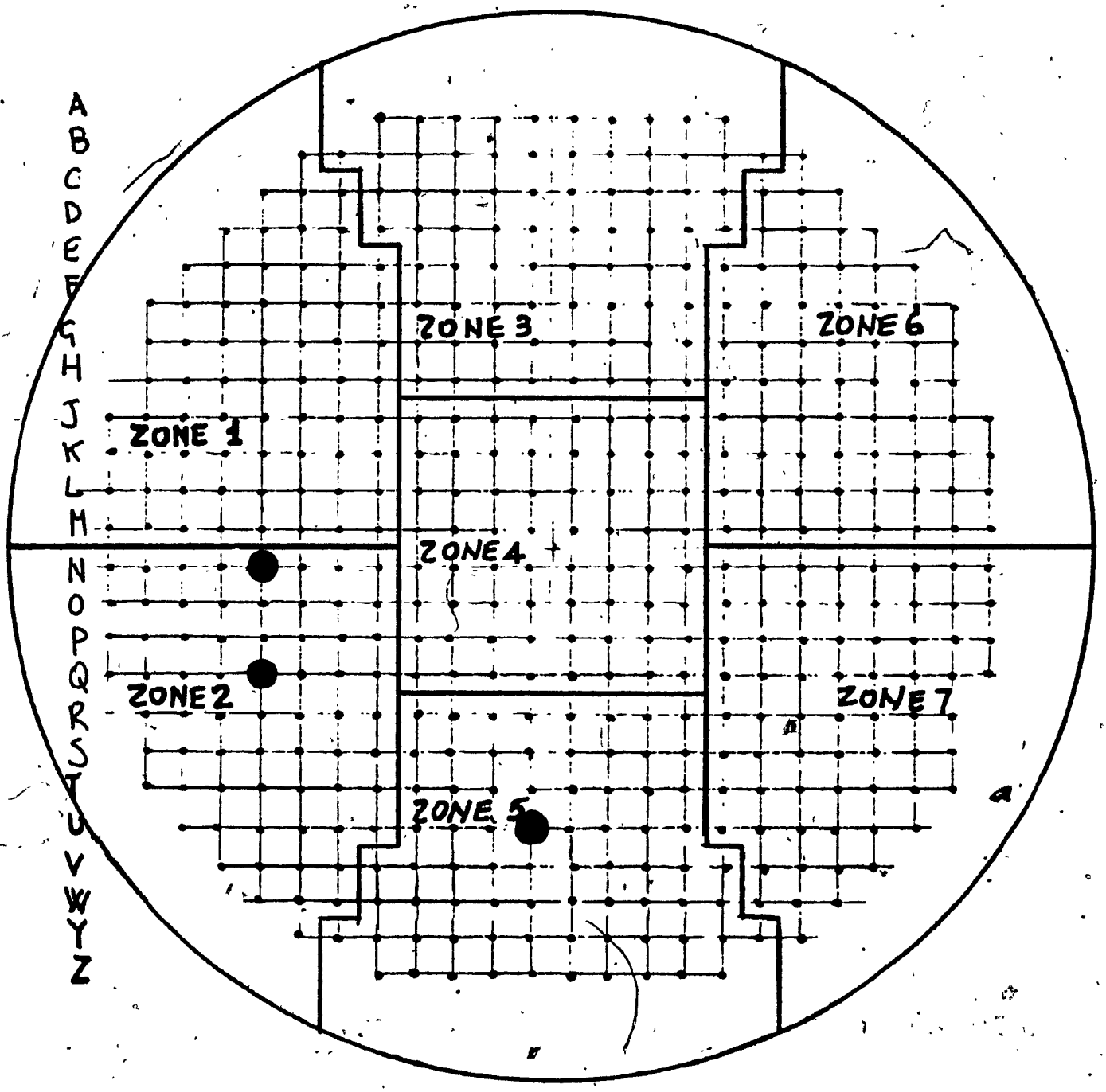

FIGURE 7.4: Darlington NGSA (Face: East)

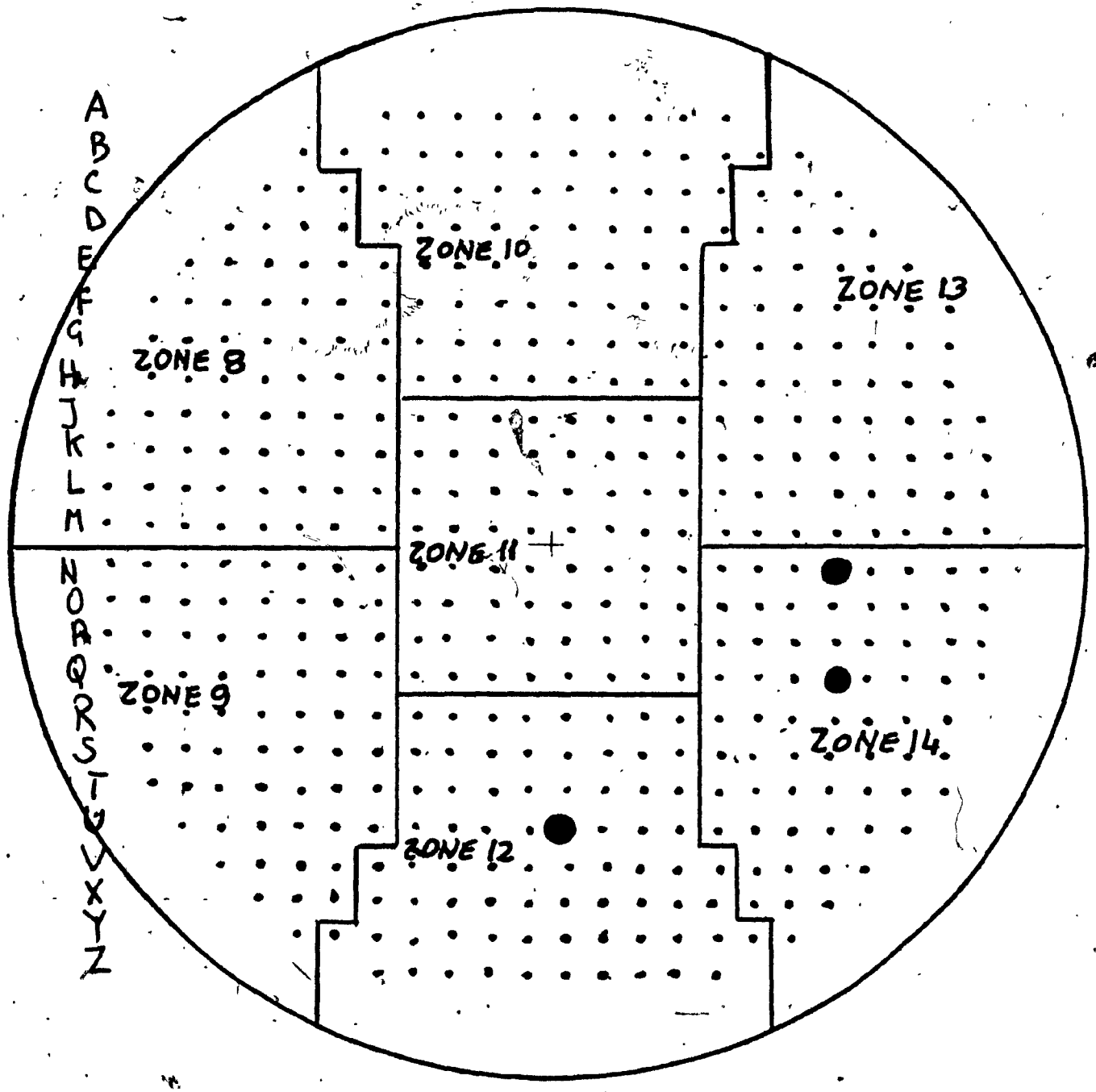

FIGURE 7.5: Darlington NGSA (Face: West)

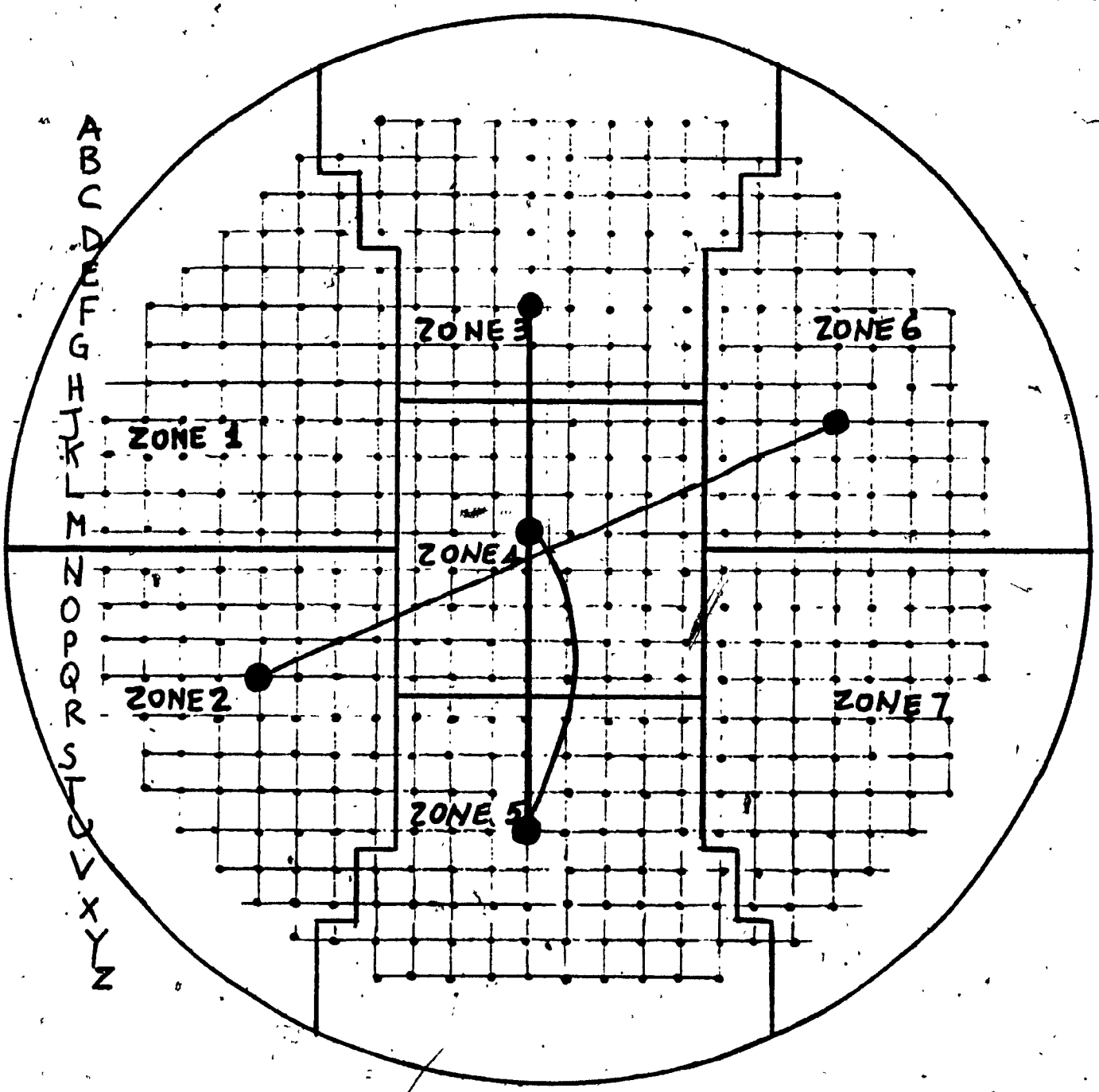

FIGURE 7.6: Darlington NGSA (Face: East) (Two-Channel Refuelling)

The detailed results of some of the simulated transients can be found in Table 7.2.

Two main conclusions on the natural core study can be drawn:

a) A very reassuring result is that the spatial control system response in the case of natural core is, for all practical purposes, independent of the lattice code used. The few cases which were run for comparison showed a very tight consistency (within 0.6% in the liquid zone controller level).

b) In all cases considered, the spatial control system was "strong" enough that no liquid zone controllers were phased out of spatial control (phasing-out starts at 80% level).

7.8.2 Spatial Controllability Assessment of Darlington N.G.S.A. with LEU Core

The assessment of the LZC system for Darlington N.G.S.-A was based on the use of (0.9% and 1.2%) enriched fuel (4- and 2-bundle shift fuel management respectively). Several one-channel refuelling transients were simulated to investigate whether or not and by how much to change the LZC H_2O reference level in order to not phase out any controllers during refuelling.

TABLE 7.2: Natural Reactors 4-B-Shift Refuelling
Single Channel Refuelling

SPATIAL CONTROL IN; ORIGINAL $\Delta\Sigma$'s; REFERENCE ZONE LEVEL = 50%						
% ZONE LEVEL AT t = 20 min						
ZONE #	Transient #1 CH: Q20		Transient #2 CH: U13		Transient #3 CH: N20	
	PPV	LTR	PPV	LTR	PPV	LTR
1	48.4	48.5	49.9	49.8	54.3	54.1
2	59.6	59.5	48.9	48.9	59.1	58.8
3	53.8	53.9	54.5	54.4	50.4	50.5
4	46.3	46.6	45.5	45.6	49.3	49.2
5	53.6	53.7	71.6	70.9	52.5	52.5
6	49.0	49.1	50.1	50.0	50.7	50.6
7	49.0	49.2	47.7	47.7	50.4	50.4
8	49.5	49.5	49.5	49.5	50.1	50.1
9	49.9	49.9	46.7	46.9	49.4	49.6
10	54.6	54.5	53.5	53.6	49.5	49.8
11	47.8	47.8	43.9	44.3	47.6	47.9
12	54.9	54.8	70.2	69.8	51.0	51.3
13	48.9	48.9	49.3	49.4	53.0	53.6
14	60.6	60.2	47.9	48.1	58.1	58.0

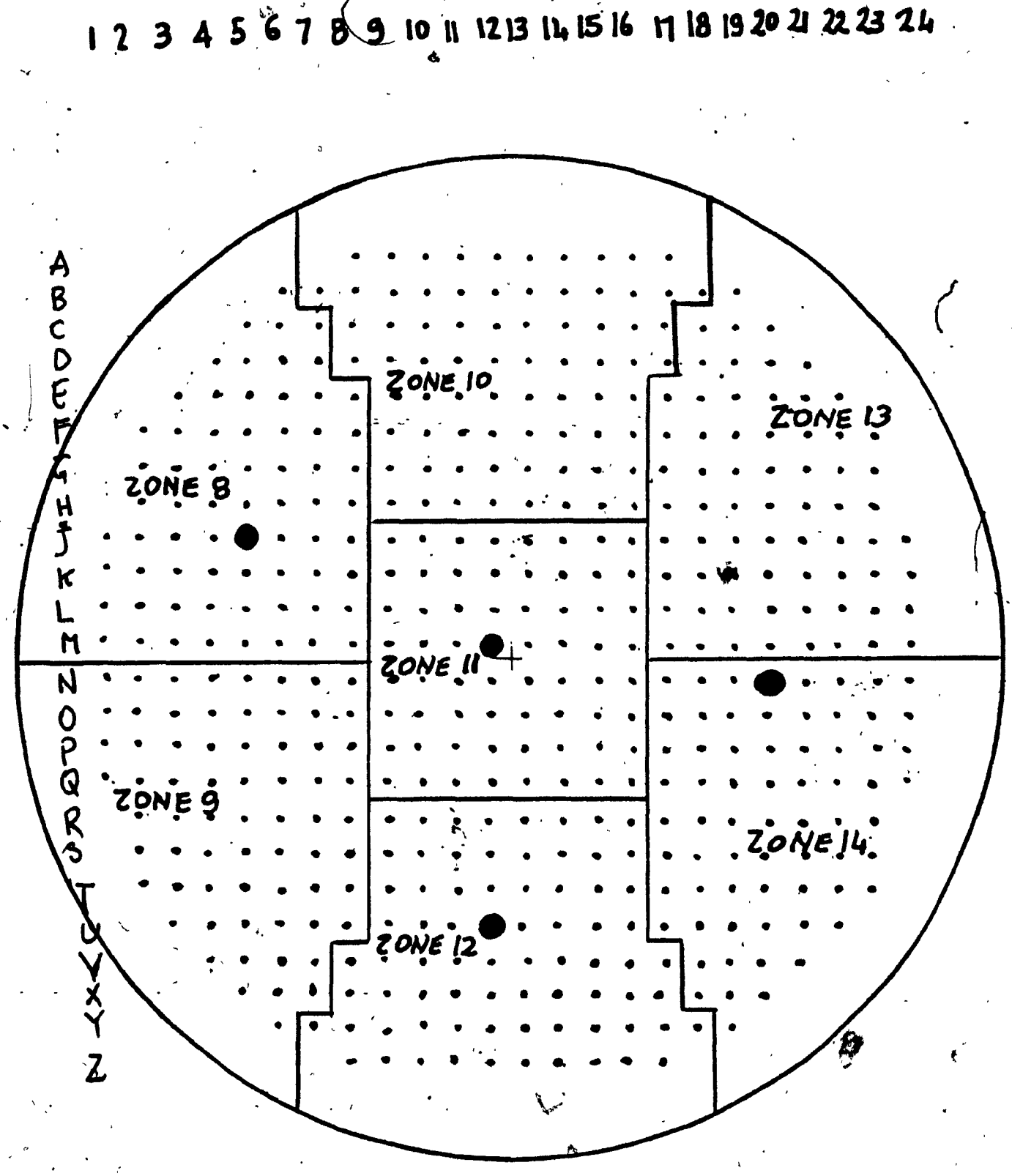

FIGURE 7.7: Darlington NGSA (Face: West) (Single-Channel Refuelling)

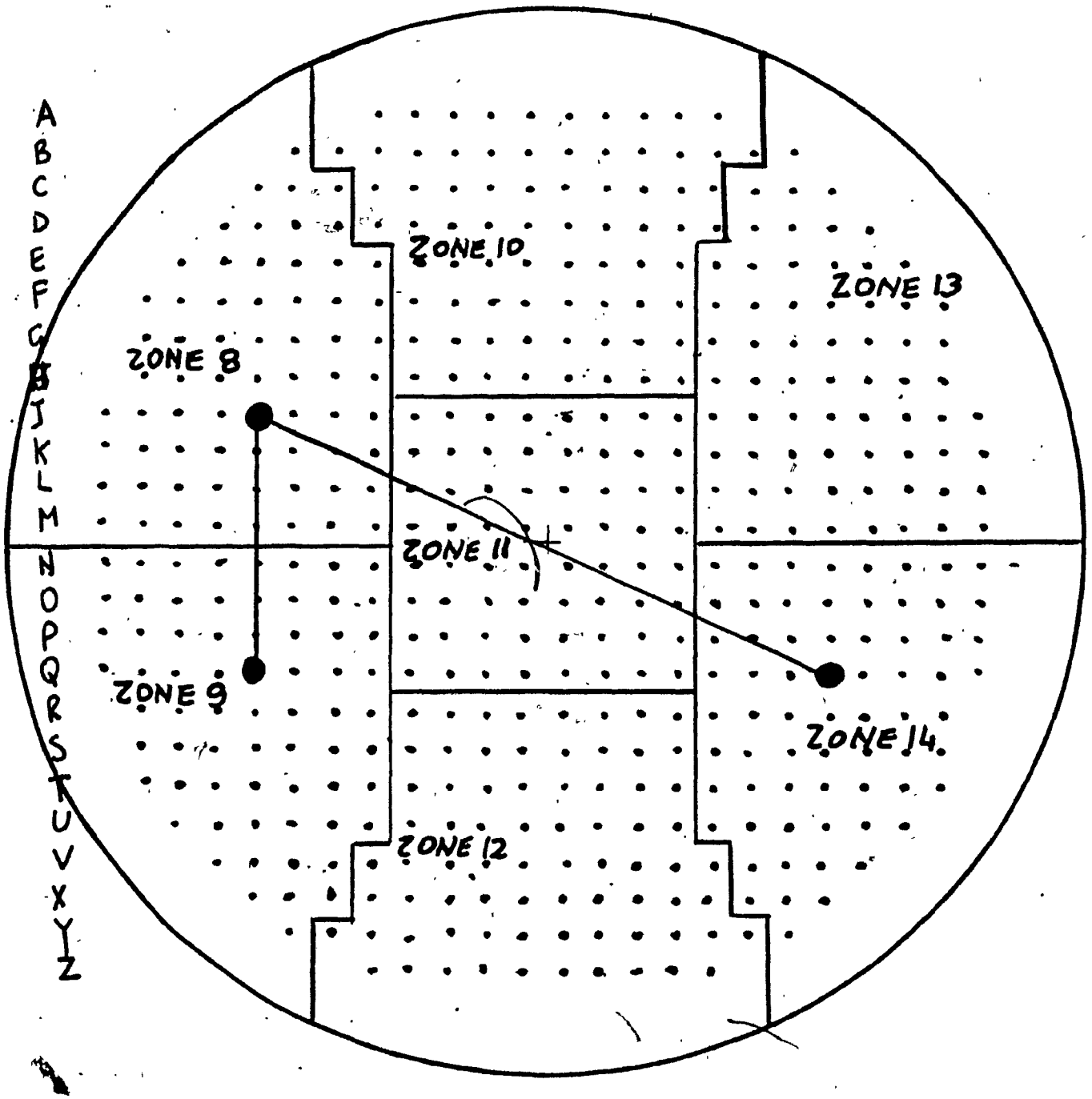

FIGURE 7.8: Darlington NGSA (Face: West) (Two-Channel Refuelling)

7.8.2.1 Assessment of LZC System in a LEU Core with All LZC H_2O Reference Levels Uniformly at 50%

With all LZC reference levels at 50%, the following channels were refuelled to assess the severity of LEU refuelling transients on the spatial control system.

- Single channel refuelled with LATREP fuel properties: (Figure 7.7)

  U-13; N-20; J-5; M-13.

- Two-channel refuelling with LATREP fuel properties: (Figure 7.8)

  J5-Q5; Q20-J5.

It was observed that with the LEU core with 0.9% and 1.2% enrichment:

- The H_2O water level in each liquid zone controller follows the same pattern as in the case of the natural core.

- If refuelling is attempted at a site near a 50% full LZC:

  a) This nearest LZC is partially phased out:

     - Always with 0.9% enrichment and 4-bundle shift (refuelling reactivity ~0.3 mk);

- Sometimes with 1.2% enrichment/2-bundle shift (~0.2 mk);

- Never with natural fuel/4-bundle shift (~0.1 mk).

b) The residual power mismatch is at most:

- 2.4% for 0.9%/4-bundle shift;
- 0.8% for 1.2%/2-bundle shift;
- 0.5% for natural/4-bundle shift.

However, the 0.9% simulations do not correspond to the bundle shift selected for that enrichment, which is 2-bundle shift in the higher power region; this fuel management scheme would, in fact, give very much the same results as in the natural fuel/4-bundle shift case, simply because the CPPF's are much closer in these two cases.

- Due to the stronger perturbation introduced by enriched fuel, an increase in the level is sometimes also induced in neighbouring zones. The level rose in the LZC "next nearest" to the perturbed channel (not the nearest to it) as a function of the perturbation intensity.

7.8.2.2 Assessment of LZC System in a LEU Core with Some LZC Reference Reference Levels Set at 30% and 50%

When the refuelled channel is adjacent to a LZC, the H_2O reference level in this LZC was reduced to 30% and in all remaining LZC the H_2O reference level was left uniformly distributed at 50%.

Refuelling transients of 1.2% core were performed.

These studies led to the main conclusions that:

- The reduction of LZC H_2O reference level next to refuelled channels (say from 50% down to 20% or 30%) prevents phasing out of the LZC.

- It is evident from this study and the one performed previously (with level reduction and LZC modified 's) that higher perturbations can be handled in an LEU core with 1.2% enrichment without phasing out any liquid zone controllers.

- It is evident from this study that refuelling transients of an LEU core with 1.2% enrichment can be handled with the existing spatial control system provided that not more than two channels are refuelled, and also provided that the 2-bundle shift management is employed.

Results of refuelling transient studies with 1.2% fuel are reported in Tables 7.3, 7.4, 7.5 and 7.6.

Examples of Liquid Zone Control behaviour during refuelling transients are reported on Figures 7.12, 7.13, 7.14, 7.15, 7.16, 7.17 and 7.18 (end of this chapter).

Typical profiles of Liquid Zone Control fundamental reactivity versus water level are shown on Figure 7.19 (end of this chapter).

The fundamental reactivity for Liquid Zone Controllers and adjusters embedded in natural, 0.9%-U235 and 1.2%-U235 reactor core are shown on Tables 7.7, 7.8 and 7.9 respectively.

TABLE 7.3: Channel: M13 t(min)

LZC #	t = 0.0 min		t = 25.0 min		t = 0.0 min		t = 25.0 min	
	% LZC Level	Det. Flux	% LZC Level	Det. Flux	% LZC Level	Det. Flux	% LZC Level	Det. Flux
1	50	0.9994	48.0	1.002	50	0.9994	48.9	1.001
2	50	0.9994	47.2	1.002	50	0.9994	46.6	1.001
3	50	0.9994	50.6	.9956	50	0.9994	51.8	.9952
4	50	0.9994	69.4	1.001	30	0.9994	52.8	1.002
5	50	0.9994	52.6	.9963	50	0.9994	50.6	.9966
6	50	0.9994	46.9	1.001	50	0.9994	47.7	1.001
7	50	0.9994	46.0	1.002	50	0.9994	45.28	1.002
8	50	0.9994	48.3	1.002	50	0.9994	49.2	1.001
9	50	0.9994	48.5	1.002	50	0.9994	47.7	1.001
10	50	0.9994	52.8	.9957	50	0.9994	54.0	.995
11	50	0.9994	73.3	1.002	30	0.9994	56.7	1.002
12	50	0.9994	56.0	.996	50	0.9994	54.1	.9965
13	50	0.9994	49.3	1.002	50	0.9994	50.3	1.001
14	50	0.9994	49.6	1.002	50	0.9994	49.1	1.001

Starting level is constant at 50% — Starting level is variable

TABLE 7.4: Channel: J5 t(min)

LZC #	t = 0.0 min		t = 25.0 min		t = 0.0 min		t = 25.0 min	
	% LZC Level	Det. Flux	% LZC Level	Det. Flux	% LZC Level	Det. Flux	% LZC Level	Det. Flux
1	50	0.9994	56.0	1.000	50	0.9994	51.5	1.004
2	50	0.9994	50.1	.999	50	0.9994	49.6	1.003
3	50	0.9994	37.7	.993	50	0.9994	48.3	.995
4	50	0.9994	50.9	1.001	50	0.9994	48.9	.9999
5	50	0.9994	52.7	.9939	50	0.9994	55.4	.995
6	50	0.9994	75.8	.9998	30	0.9994	49.7	1.002
7	50	0.9994	58.5	.998	50	0.9994	54.2	1.001
8	50	0.9994	74.9	1.000	30	0.9994	48.9	1.002
9	50	0.9994	57.0	.998	50	0.9994	52.8	1.001
10	50	0.9994	36.3	.994	50	0.9994	47.0	.995
11	50	0.9994	48.5	1.001	50	0.9994	46.6	.9999
12	50	0.9994	50.6	.994	50	0.9994	53.4	.995
13	50	0.9994	55.1	1.000	50	0.9994	50.7	1.004
14	50	0.9994	48.5	.9994	50	0.9994	48.2	1.003

Starting level is constant at 50% — Starting level is variable

TABLE 7.5: Channel: U13 t(min)

LZC #	t = 0.0 min		t = 25.0 min		t = 0.0 min		t = 25.0 min	
	% LZC Level	Det. Flux	% LZC Level	Det. Flux	% LZC Level	Det. Flux	% LZC Level	Det. Flux
1	50	0.9994	48.9	1.000	50	0.9994	48.1	1.001
2	50	0.9994	50.6	1.000	50	0.9994	46.7	1.003
3	50	0.9994	53.8	.9917	50	0.9994	52.3	.9945
4	50	0.9994	38.8	.9987	50	0.9994	41.7	1.002
5	50	0.9994	81.3	1.008	30	0.9994	63.7	.9977
6	50	0.9994	49.5	1.001	50	0.9994	48.6	1.001
7	50	0.9994	48.1	1.001	50	0.9994	44.1	1.003
8	50	0.9994	50.7	1.002	50	0.9994	49.7	1.001
9	50	0.9994	50.3	1.002	50	0.9994	45.9	1.002
10	50	0.9994	55.7	.9918	50	0.9994	53.9	.9944
11	50	0.9994	42.2	.9987	50	0.9994	44.5	1.002
12	50	0.9994	81.0	1.008	30	0.9994	66.2	.997
13	50	0.9994	50.1	1.001	50	0.9994	49.2	1.001
14	50	0.9994	52.8	1.001	50	0.9994	48.5	1.003

Starting level is constant at 50% — Starting level is variable

TABLE 7.6: Channel: Q20 t(min)

LZC #	t = 0.0 min		t = 25.0 min		t = 0.0 min		t = 25.0 min	
	% LZC Level	Det. Flux	% LZC Level	Det. Flux	% LZC Level	Det. Flux	% LZC Level	Det. Flux
1	50	0.9994	47.6	1.004	50	0.9994	51.7	1.003
2	50	0.9994	73.3	1.003	30	0.9994	57.5	1.002
3	50	0.9994	56.3	.9958	50	0.9994	53.3	.995
4	50	0.9994	46.2	.9992	50	0.9994	49.0	1.000
5	50	0.9994	55.4	.9959	50	0.9994	49.4	.995
6	50	0.9994	49.6	1.005	50	0.9994	49.8	1.003
7	50	0.9994	50.7	1.004	50	0.9994	52.0	1.002
8	50	0.9994	48.7	1.005	50	0.9994	48.8	1.003
9	50	0.9994	49.1	1.004	50	0.9994	50.4	1.002
10	50	0.9994	54.9	.996	50	0.9994	51.9	.995
11	50	0.9994	43.8	.999	50	0.9994	46.4	1.000
12	50	0.9994	53.2	.996	50	0.9994	47.1	.995
13	50	0.9994	46.7	1.004	50	0.9994	50.7	1.003
14	50	0.9994	71.7	1.003	30	0.9994	55.9	1.003

Starting level is constant at 50% — Starting level is variable

TABLE 7.7.1: Liquid Zone Controller Fundamental Reactivity (in k) (LEU Core: 0.9%)

LZC #	LEVEL %					
	0.0 %	20%	50%	70%	80%	100%
1	0.0	-.11142-3	-.27890-3	-.37691-3	-.40267-3	-.42344-3
2	0.0	-.06913-3	-.20454-3	-.32838-3	-.39131-3	-.49713-3
3	0.0	-.10080-3	-.25810-3	-.33720-3	-.36501-3	-.38177-3
4	0.0	-.07956-3	-.20521-3	-.30625-3	-.35669-3	-.45231-3
5	0.0	-.05857-3	-.17151-3	-.26991-3	-.32124-3	-.42142-3
6	0.0	-.11142-3	-.27889-3	-.37689-3	-.40265-3	-.42342-3
7	0.0	-.06913-3	-.20454-3	-.32838-3	-.39131-3	-.49712-3
8	0.0	-.11142-3	-.27889-3	-.37689-3	-.40265-3	-.42342-3
9	0.0	-.06913-3	-.20454-3	-.32838-3	-.39131-3	-.49712-3
10	0.0	-.10880-3	-.25810-3	-.33720-3	-.36510-3	-.38177-3
11	0.0	-.07956-3	-.20521-3	-.30625-3	-.35669-3	-.45231-3
12	0.0	-.05857-3	-.17155-3	-.26991-3	-.32124-3	-.42142-3
13	0.0	-.11142-3	-.27889-3	-.37689-3	-.40265-3	-.40521-3
14	0.0	-.06913-3	-.20454-3	-.32838-3	-.39131-3	-.47913-3

TABLE 7.7.2: Adjuster Rod Fundamental Reactivity (in k) (LEU Core: 0.9%)

ADJ #	WITHDRAWAL PERCENTAGE						
	0.0 %	20%	30%	50%	80%	90%	100%
1	.20896-2	.19443-2	.17168-2	.11265-2	.13212-3	.12047-4	0.0
2	.19817-2	.18120-2	.15884-2	.10327-2	.94848-4	.21119-4	0.0
3	.12032-2	.11487-2	.10203-2	.64649-3	.78149-4	.59567-5	0.0
4	.16973-2	.15825-2	.13675-2	.83100-3	.91989-4	.13714-4	0.0
5	.16973-2	.15825-2	.13675-2	.83100-3	.91986-4	.13714-4	0.0
6	.13685-2	.12232-2	.10042-2	.61901-3	.69589-4	.12680-4	0.0
7	.14324-2	.12684-2	.10255-2	.61190-3	.55957-4	.19419-4	0.0
8	.13187-2	.11264-2	.88453-3	.50342-3	.86714-5	.33087-4	0.0

TABLE 7.8.1: Liquid Zone Controller Fundamental Reactivity (in k) (LEU Core: 1.2%)

LZC #	LEVEL %					
	0.0 %	20%	50%	70%	80%	100%
1	0.0	-.10663-3	-.26690-3	-.36068	-.38534-3	-.40521-3
2	0.0	-.06615-3	-.19574-3	-.31425-3	-.37443-3	-.47573-3
3	0.0	-.10412-3	-.24699-3	-.32269-3	-.34929-3	-.36533-3
4	0.0	-.07613-3	-.19637-3	-.29306-3	-.34139-3	-.43283-3
5	0.0	-.05605-3	-.16416-3	-.25829-3	-.30741-3	-.40327-3
6	0.0	-.10663-3	-.26690-3	-.36068-3	-.38534-3	-.40521-3
7	0.0	-.06615-3	-.19574-3	-.31425-3	-.37443-3	-.47573-3
8	0.0	-.10663-3	-.26690-3	-.36060-3	-.38534-3	-.40521-3
9	0.0	-.06217-3	-.16315-3	-.22900-3	-.26098-3	-.31107-3
10	0.0	-.10412-3	-.24699-3	-.32269-3	-.34929-3	-.36533-3
11	0.0	-.07613-3	-.19637-3	-.29306-3	-.34134-3	-.43283-3
12	0.0	-.05605-3	-.16416-3	-.25829-3	-.30741-3	-.40327-3
13	0.0	-.10663-3	-.26690-3	-.36068-3	-.38534-3	-.40521-3
14	0.0	-.06615-3	-.19574-3	-.31425-3	-.37443-3	-.47573-3

TABLE 7.8.2: Adjuster Rod Fundamental Reactivity (in k) (LEU Core: 1.2%)

ADJ #	WITHDRAWAL PERCENTAGE						
	0.0 %	20%	30%	50%	80%	90%	100%
1	.19637-2	.18272-2	.16135-2	.10588-2	.12419-3	.11314-4	0.0
2	.18585-2	.16996-2	.14903-2	.09691-2	.89078-4	.19770-4	0.0
3	.17221-2	.16735-2	.15252-2	.97853-3	.11020-3	.82366-5	0.0
4	.15986-2	.14908-2	.12886-2	.78311-3	.86798-4	.12867-4	0.0
5	.15986-2	.14908-2	.12886-2	.78311-3	.86798-4	.12867-4	0.0
6	.12854-2	.11489-2	.09432-2	.58140-3	.65362-4	.11910-4	0.0
7	.13454-2	.11914-2	.09631-2	.57473-2	.52558-4	.18240-4	0.0
8	.12346-2	.10546-2	.82794-3	.47133-3	.81186-5	.30969-4	0.0

TABLE 7.9.1: Liquid Zone Controller Fundamental Reactivity (in k) (Natural Core)

LZC #	LEVEL Z					
	0.0 Z	20Z	50Z	70Z	80Z	100Z
1	0.0	-.11718-3	-.29331-3	-.39638-3	-.42348-3	-.44532.3
2	0.0	-.07270-3	-.21511-3	-.34535-3	-.41153-3	-.52282-3
3	0.0	-.11443-3	-.27143-3	-.35463-3	-.38387-3	-.40149-3
4	0.0	-.08366-3	-.21581-3	-.33207-3	-.37512-3	-.47568-3
5	0.0	-.06160-3	-.18041-3	-.28385-3	-.33783-3	-.44319-3
6	0.0	-.11718-3	-.29331-3	-.39638-3	-.42348-3	-.44532-3
7	0.0	-.07270-3	-.21511-3	-.34535-3	-.41153-3	-.52282-3
8	0.0	-.11718-3	-.29331-3	-.39638-3	-.42348-3	-.44532-3
9	0.0	-.06833-3	-.17929-3	-.25167-3	-.28681-3	-.34186-3
10	0.0	-.11443-3	-.27143-3	-.35463-3	-.38387-3	-.40149-3
11	0.0	-.08366-3	-.21581-3	-.32207-3	-.37512-3	-.47568-3
12	0.0	-.06160-3	-.18041-3	-.28385-3	-.33783-3	-.44319-3
13	0.0	-.11718-3	-.29331-3	-.39639-3	-.42348-3	-.44532-3
14	0.0	-.07270-3	-.21511-3	-.34535-3	-.41153-3	-.52282-3

TABLE 7.9.2: Adjuster Rod Fundamental Reactivity (in k) (Natural Core)

ADJ #	WITHDRAWAL PERCENTAGE						
	0.0 Z	20Z	30Z	50Z	80Z	90Z	100Z
1	.22479-2	.20915-2	.18466-2	.12117-2	.14211-3	.12967-4	0.0
2	.21259-2	.19441-2	.17045-2	.11083-3	.10184-3	.22613-+	0.0
3	.19623-2	.19035-2	.17382-2	.11153-2	.12556-3	.93841-5	0.0
4	.18222-2	.16990-2	.14683-2	.89228-3	.98805-4	.14707-+	0.0
5	.18222-3	.16990-2	.14683-2	.89228-3	.98805-4	.14707-4	0.0
6	.14729-2	.13165-2	.10809-2	.66623-3	.74898-4	.13647-4	0.0
7	.15417-2	.13652-2	.11037-2	.65859-3	.60227-4	.20901-4	0.0
8	.14132-2	.12071-2	.94771-3	.53951-3	.92930-5	.35449-4	0.0

7.9 SHIM TRANSIENT STUDIES FOR NATURAL AND SLIGHTLY ENRICHED CORE DARLINGTON G.S. A MODEL

It this section are described the shim transient studies that have been performed and the detailed analysis of the Darlington G.S. A Vertical Liquid Zone Control System (LZC) response to withdrawal of the first three adjuster banks for reactivity shim purposes.

The study covers the response of the LZC for the cases of natural core and two slightly enriched level cores (enrichment of 0.9% and 1.2%).

Withdrawal of the first five adjuster rod banks in reactivity shim mode with no prior derating of reactor power is performed two minutes after a negative reactivity is ramped-in uniformly to all modes. The time at which negative reactivity is ramped in and adjuster banks are withdrawn can be seen from Figures 7.20, 7.21 and 7.22. Typical grouping of adjusters is shown on Figure 7.23, which also provides group fundamental reactivity.

The negative reactivity ramps force the average zone levels to drop to an average level of 20%. At the levels, signals are generated to trigger automatic withdrawal of an adjuster bank. Withdrawal of the three banks was performed over a short time span (30 minutes) to determine the basic response of the LZC system.

Power calculations were done at 8, 18 and 28 minutes into the transient to estimate approximately the reactor power derating requirements to avoid exceeding channel power limits. Typical power distortions caused by the withdrawal of adjuster rods at different channel rows of the reactor are reported on Figure 7.24, 7.25 and 7.26. The type of reactor core considered is shown on the figures.

The results indicate that there are no appreciable differences on the response of the LZC system when natural or slightly enriched cores are considered.

The effect of the transient tilting during adjuster withdrawal on ROP detector response is not taken into consideration during the study.

The results of average liquid zone levels vs time and power reactor derating calculation are given in Tables 7.10, 7.11, 7.12, 7.13, 7.14 and 7.15 respectively.

The plots of average zone level vs time during withdrawal of the first three banks are shown on Figures 7.23, 7.28 and 7.29 for natural and two slightly enriched level cores (0.9% and 1.2% enrichment respectively).

TABLE 7.10: % Average Zone Level vs Time (Natural Core)

t(min)	% ZONE LEVEL
0	50.0
1.15	16.7
2.4	16.1
3.2	23.5
3.4	33.5
3.6	43.9
3.8	51.3
7.02	50.18
9.07	50.88
10.07	50.29
11.07	48.87
12.97	18.77
13.22	26.77
13.6	37.46
14.8	53.05
17.02	52.34
19.02	51.79
20.02	50.97
21.02	23.56
22.97	22.58
23.22	29.28
23.5	45.69
23.8	54.88
26.99	54.65
28.55	54.71
30.02	54.25

TABLE 7.11: % Average Zone Level vs Time (LEU 0.9%)

t(min)	% ZONE LEVEL
0.0	50.0
1.18	18.36
2.38	18.48
3.2	23.48
3.4	33.51
3.8	50.77
4.9	50.65
7.0	50.33
9.0	50.16
10.0	50.07
11.0	20.28
12.0	19.12
13.2	25.73
13.6	44.43
13.8	50.8
16.0	52.13
18.52	51.57
20.0	52.27
21.0	24.66
22.95	23.63
23.2	28.52
23.5	45.09
23.8	53.75
25.0	52.26
28.0	53.48
29.0	52.69
30.0	53.31

TABLE 7.12: % Average Zone Level vs Time (LEU 1.2%)

t(min)	% ZONE LEVEL
0.0	50.0
1.19	18.2
2.3	18.36
3.2	23.46
3.4	33.41
3.6	42.75
3.8	50.81
7.0	50.39
9.00	50.08
10.00	50.03
11.0	20.36
12.95	20.03
13.2	25.52
14.86	51.82
17.0	51.82
19.00	51.05
20.00	52.22
21.00	26.33
22.95	23.30
23.4	38.97
23.8	54.01
25.2	52.81
26.9	53.17
30.0	54.02

TABLE 7.13: Power Derating Calculation (Natural Fuel)

TIME (min)	MAX. CHANNEL POWER MW(th)	DERATING %
0.0	6.66	0
8.5524	6.89	3.5
18.5524	7.10	6.6
23.506	7.40	11.1*
25.0232	7.22	8.4
28.55	7.21	8.3

TABLE 7.14: Power Derating Calculation (1.2% Enriched Fuel)

TIME (min)	MAX. CHANNEL POWER MW(th)	DERATING %
0.0	6.65	0
8.8592	6.88	3.5
18.5292	7.03	5.6
23.5	7.33	10.1*
25.00	7.20	8.1
28.5292	7.16	7.5

TABLE 7.15: Power Derating Calculation (0.9% Enriched Fuel)

TIME (min)	MAX. CHANNEL POWER MW(th)	DERATING %
0.0	6.66	0
8.5292	6.88	3.5
18.5292	7.07	6.2
23.5	7.35	10.4*
25.0	7.20	8.1
28.3513	7.19	8.0

$$\text{Derating} = \left(\frac{P_{ch,max(t>0)}}{P_{ch,max(t=0)}} - 1 \right) \times 100$$

* This value refers to derating during bank withdrawal.

7.10 START-UP SIMULATION OF DARLINGTON NUCLEAR POWER GENERATING STATION

7.10.1 General Considerations

The reactor shutdown-start-up simulation was considered the most significant to assess the following:

- Determination of start-up behaviour of a Low Enriched Uranium (LEU) core compared with a Natural fuel core;

- Determination of response of average zone levels during start-up at points where adjuster banks were inserted into the core;

- Determination of xenon reactivity feedback behaviour during shutdown and start-up.

The reactor core properties in the case of each start-up simulation were consistently LATREP-based parameters.

Precursors and delayed-neutron kinetics parameters were calculated separately for the case of natural core, core enriched at 0.9% and core enriched at 1.2%, as reported in Chapter Six.

No channel overrating was allowed in this simulation. The channel overrating is the increase in maximum channel power at time (t) over the maximum channel power at steady state full power and bundle overrating was limited to 10%.

The constraint on maximum bundle overpower was removed. Bundle overpower is the increase in bundle power at the same location at steady state full power.

Withdrawal of adjuster rod banks in sequence is automatically initiated when the Average Zone controller Level (AZL) reaches 20% full and insertion is initiated when AZL is 70% full. The speed of adjuster movement depends on the power error and varies between a normalized speed of 0.4 to 1.0 if the absolute value of the power error is between 4 and 5%. Below 4% power error, the speed is held constant at the minimum value of 0.4. The time to withdraw a bank of rods at full speed (normalized speed = 1.0) is 1 minute.

Spatial control action of the zone controllers is fully phased out at power levels below 15% Full Power (FP). Between 15% and 25% FP spatial control is phased in. Individual zone controllers begin to be phased out of spatial control when their levels are lower than 10% or greater than 80% fill, with phasing out occurring over a 10% level range.

7.10.2 Transient Description

Reactor shutdown was initiated by ramping in the shut-off rods (SOR's) during the first 2 seconds of the simulation. The power setpoint was reduced to 1% FP at time zero. After 20 minutes of decision and action time, SOR's were withdrawn

over an approximate 6-minute interval. The reactor trip was cleared when the SOR's were fully withdrawn and adjuster bank withdrawal was performed automatically by the reactor regulating system. When all banks were out, power was initially raised at a rate of 4% of present power/sec up to 25% FP and then at the specified rate of 1% FP/sec. Reinsertion of adjuster banks was performed automatically by the regulating system. A constant power level within the interval between insertions of adjuster banks was set by the power optimization scheme in the SMOKIN program. When the "optimized", or constant, power setpoint was obtained, the demand power was manoeuvred to the setpoint at the specified manoeuvring rate and bulk power regulation caused reactor power to track demand power. When all adjusters were reinserted, power calculation was performed at 0.1-hour intervals to determine the allowable power setpoint until full power was attained.

Results of Darlington N.G.S.A. power transient simulations for natural and low enriched cores are provided analytically by Tables 7.16, 7.17 and 7.18 for natural, 0.9% and 1.2% enriched cores respectively. Graphical results are shown on Figures 7.30, 7.31 and 7.32, 7.33 and 7.34. From these figures, it can be concluded that the power behaviour during the start-up of the reactor when Low Enriched fuel is used follows very closely the power behaviour during the start-up of the reactor when Natural fuel is used, and that during the process of the reactor shutdown, the following was observed:

a) Power raising from 0.% to 100% full power takes approximately 4 hours;

b) Xe reactivity build-up rate upon shutdown is practically independent of enrichment and equals -0.48 mk/min;

c) Consequently, due to the lower reactivity worth of adjusters in enriched cores, a smaller Decision and Action Time (DAT) is obtained for a higher enrichment:

- Enrichment - natural DAT = 23.7 min;
- Enrichment - .9% DAT = 21.7 min;
- Enrichment - 1.2% DAT = 19.4 min.

TABLE 7.16: Darlington Start-Up Simulation with Enrichment Level = Natural

TIME (hours)	POWER SETPOINT (% FP)	REACTOR POWER (% FP)	XENON REACTIVITY FEEDBACK (mk)	# ADJUSTER BANKS INSERTED	AVERAGE ZONE LEVEL
0 (+)	100 0	100	-	8	50.0
0.656	69.93	1.0	-18.71	0	42.08
0.8604	69.93	69.93	-17.3	0	70.42
0.911	73.04	69.93	-16.83	1	34.98
1.1071	73.04	73.04	-14.96	1	70.18
1.157	75.66	73.04	-14.54	2	37.39
1.374	75.66	75.66	-12.69	2	70.87
1.425	75.78	75.66	-12.32	3	43.47
1.63	75.78	75.78	-10.89	3	70.03
1.69	79.02	75.78	-10.58	4	36.58
2.04	79.02	79.02	- 8.39	4	70.16
2.1	83.38	79.02	- 8.13	5	38.63
2.502	83.38	83.38	- 5.907	5	70.30
2.557	89.58	83.38	- 5.673	6	38.51
3.033	89.58	89.58	- 3.293	6	70.41
3.084	95.03	89.58	- 3.111	7	39.24
3.60	95.03	95.03	- 1.0	7	70.47
3.70	99.6	95.03	- 0.707	8	39.42
4.0	99.6	99.6	+ 0.2367	8	52.83

TABLE 7.17: Darlington Start-Up Simulation with Enrichment Level = 0.9%

TIME (hours)	POWER SETPOINT (% FP)	REACTOR POWER (% FP)	XENON REACTIVITY FEEDBACK (mk)	# ADJUSTER BANKS INSERTED	AVERAGE ZONE LEVEL
0 (+)	100 .1.0	100.0	0.0	8	50.0
0.616	71.72	1.0	-17.37	0	39.01
0.8799	71.72	71.72	-15.71	0	70.24
0.9337	74.65	71.72	-15.24	1	41.59
1.11	74.65	74.65	-13.67	1	70.14
1.16	77.64	74.65	-13.27	2	40.08
1.365	77.64	77.64	-11.61	2	70.18
1.416	77.78	77.64	-11.23	3	44.83
1.625	77.78	77.78	- 9.87	3	70.12
1.676	79.67	77.78	- 9.59	4	37.92
2.0466	79.67	79.67	- 7.57	4	70.13
2.097	85.71	79.67	- 7.35	5	39.06
2.462	85.71	87.71	- 5.31	5	70.97
2.5125	90.76	85.71	- 5.09	6	40.06
2.912	90.76	90.76	- 2.914	6	70.28
3.029	95.63	90.76	- 2.74	7	41.76
3.609	95.63	95.63	- 0.653	7	70.26
3.661	99.79	95.63	- 0.539	8	41.57
4.01	99.79	99.79	+ 0.453	8	55.81

TABLE 7.18: Darlington Start-Up Simulation with Enrichment Level = 1.2%

TIME (hours)	POWER SETPOINT (% FP)	REACTOR POWER (% FP)	XENON REACTIVITY FEEDBACK (mk)	# ADJUSTER BANKS INSERTED	AVERAGE ZONE LEVEL
0 (+)	100 0	100.0	0.0	8	50.0
0.580	73.09	1.0	-16.31	0	36.47
0.854	73.09	73.09	-14.66	0	70.01
0.906	75.67	73.09	-14.23	1	41.29
1.09	75.64	75.64	-12.69	1	70.51
1.14	78.16	75.64	-12.333	2	41.15
1.3473	78.16	78.16	-10.784	2	70.20
1.4	78.26	78.16	-10.43	3	48.88
1.602	78.26	78.26	- 9.234	3	70.15
1.6550	81.58	78.26	- 8.96	4	39.73
1.995	81.58	81.58	- 7.073	4	70.22
2.046	85.69	81.58	- 6.85	5	39.37
2.41	85.69	85.69	- 5.008	5	70.30
2.46	90.57	85.69	- 4.797	6	40.33
2.94	90.57	90.57	- 2.754	6	70.37
2.99	95.9	90.57	- 2.602	7	41.46
3.554	95.9	95.9	- 0.643	7	70.70
3.604	99.5	95.9	- 0.532	8	41.27
4.0	99.5	99.5	+ 0.482	8	55.60

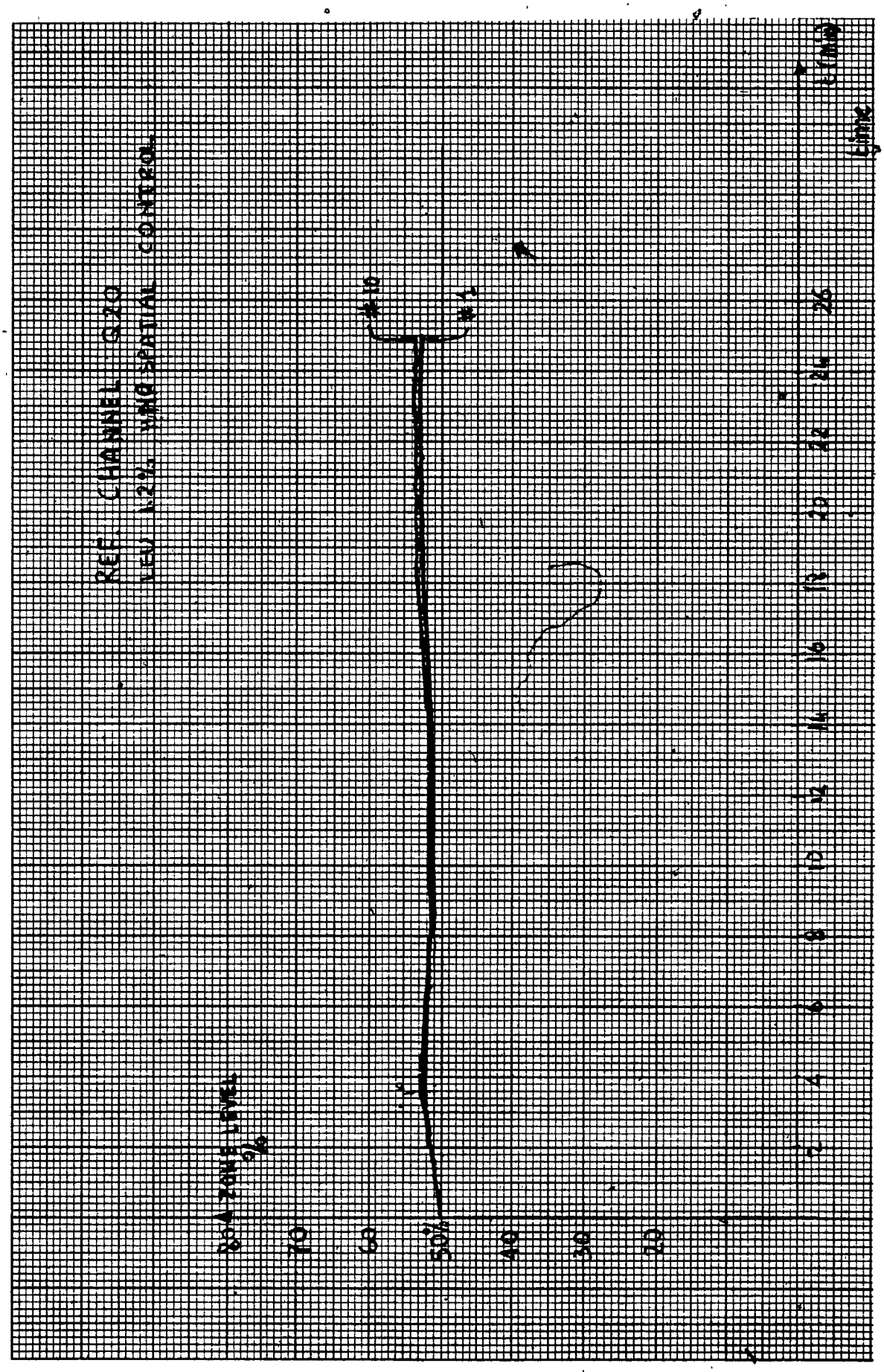

FIGURE 7.9: Zones 1, 10 Level Behaviour During One-Channel Refuelling

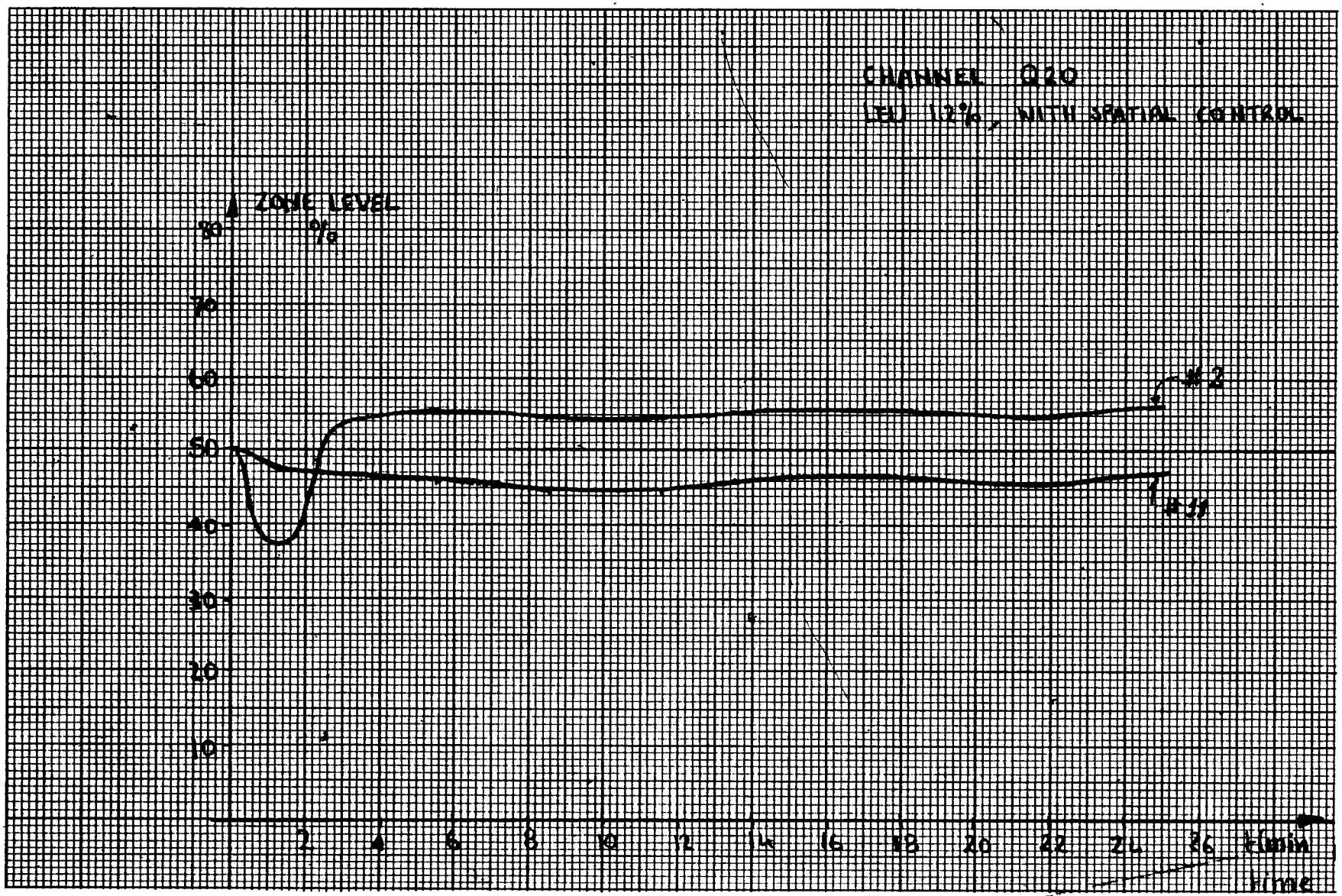

FIGURE 7.10: Zones 2 and 11 Level Behaviour with Spatial Control

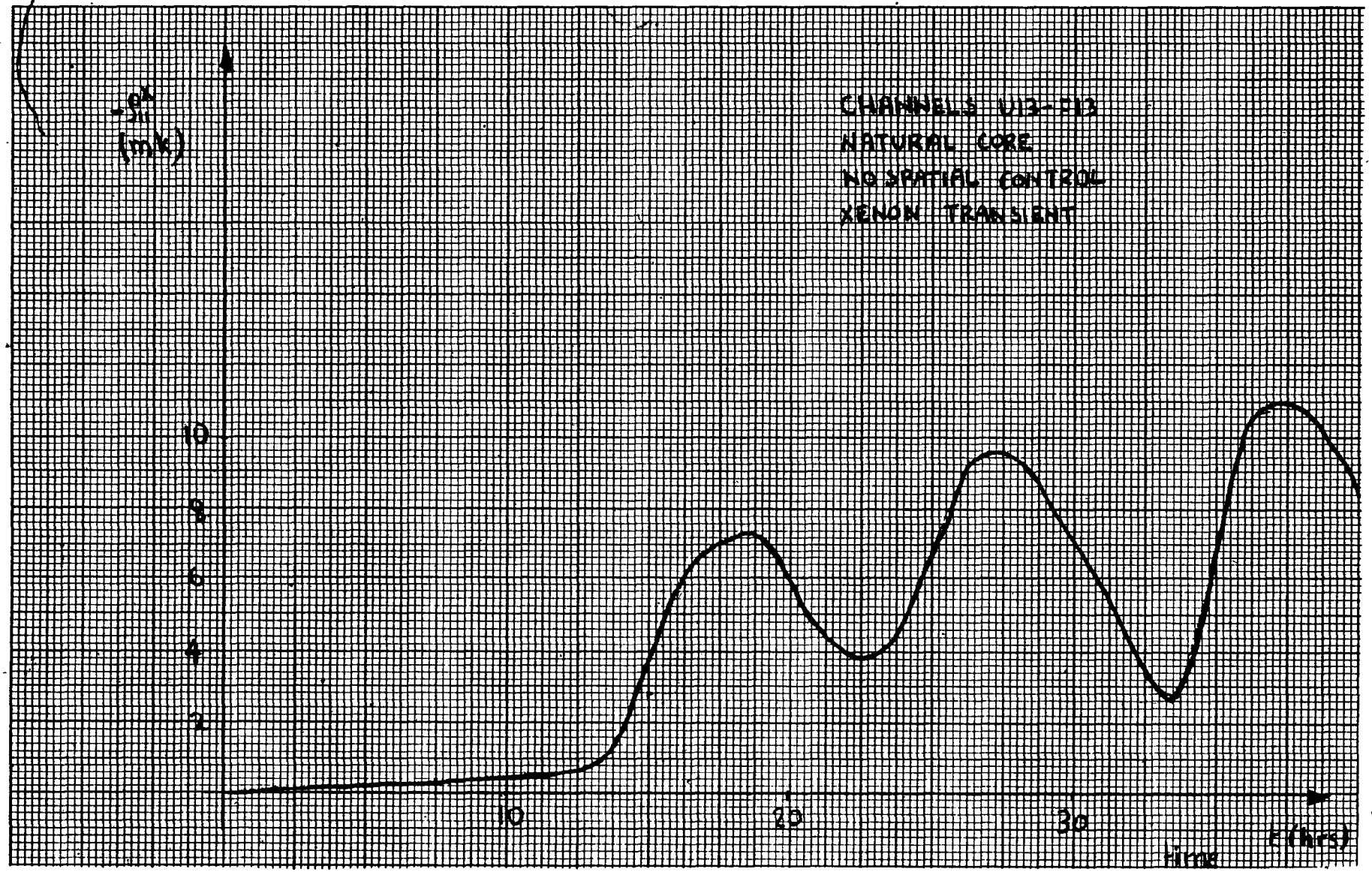

FIGURE 7.11: Xenon Load Behaviour During Refuelling without Spatial Control

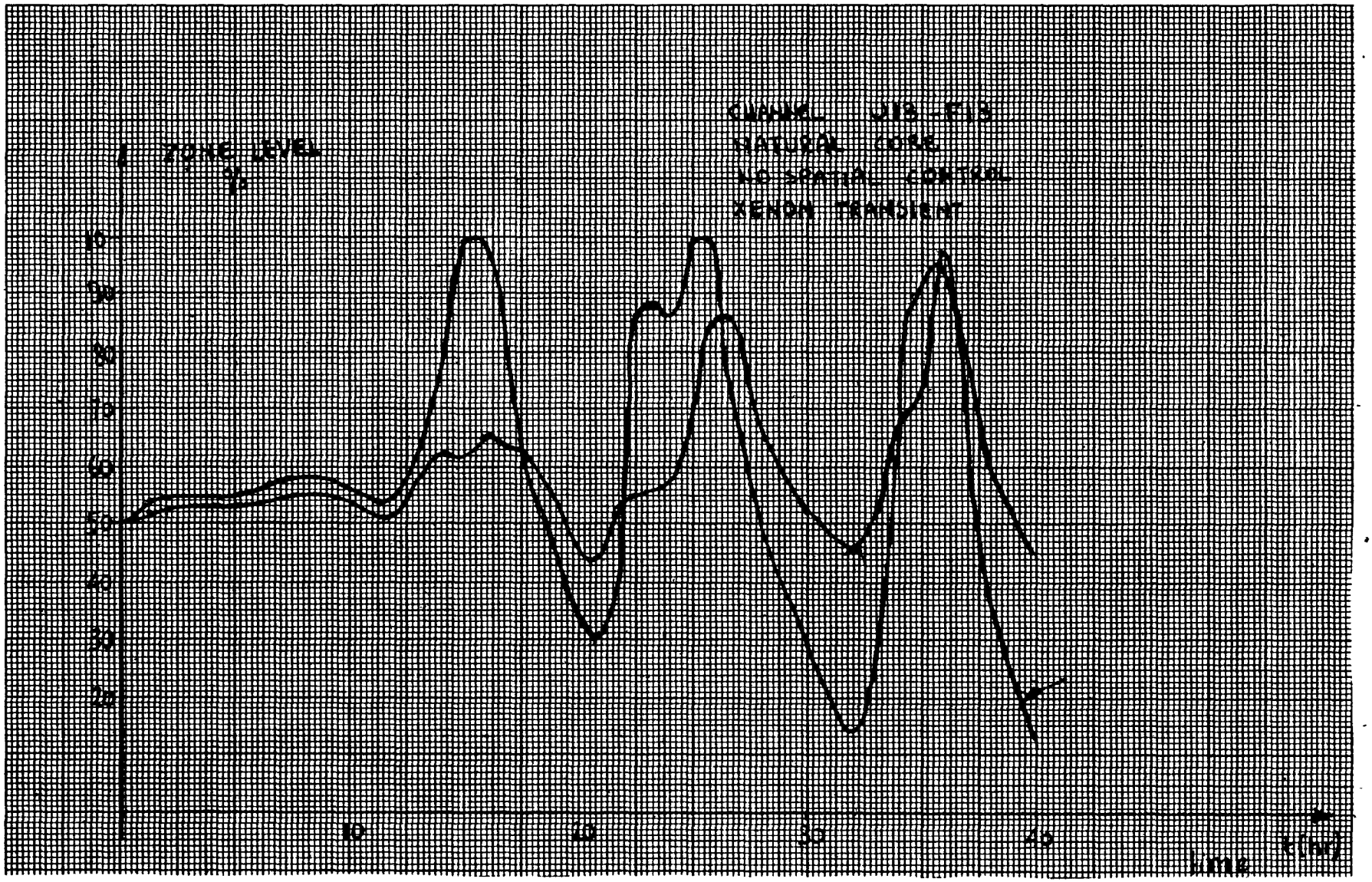

FIGURE 7.12: Zones 3 and 10, 4, 11 Level Behaviour with Two-Channel Refuelling and No Spatial Control

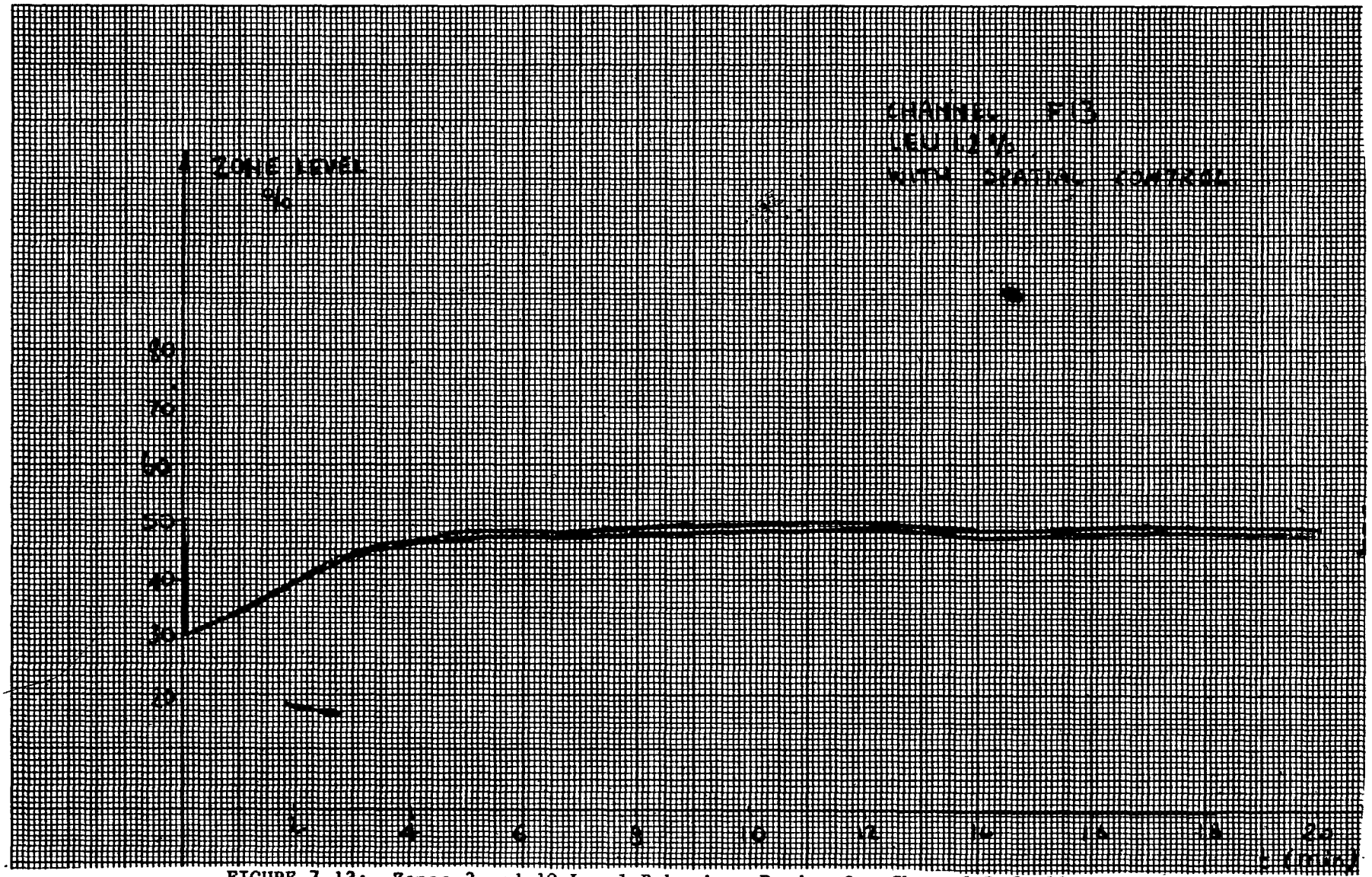

FIGURE 7.13: Zones 3 and 10 Level Behaviour During One-Channel Refuelling

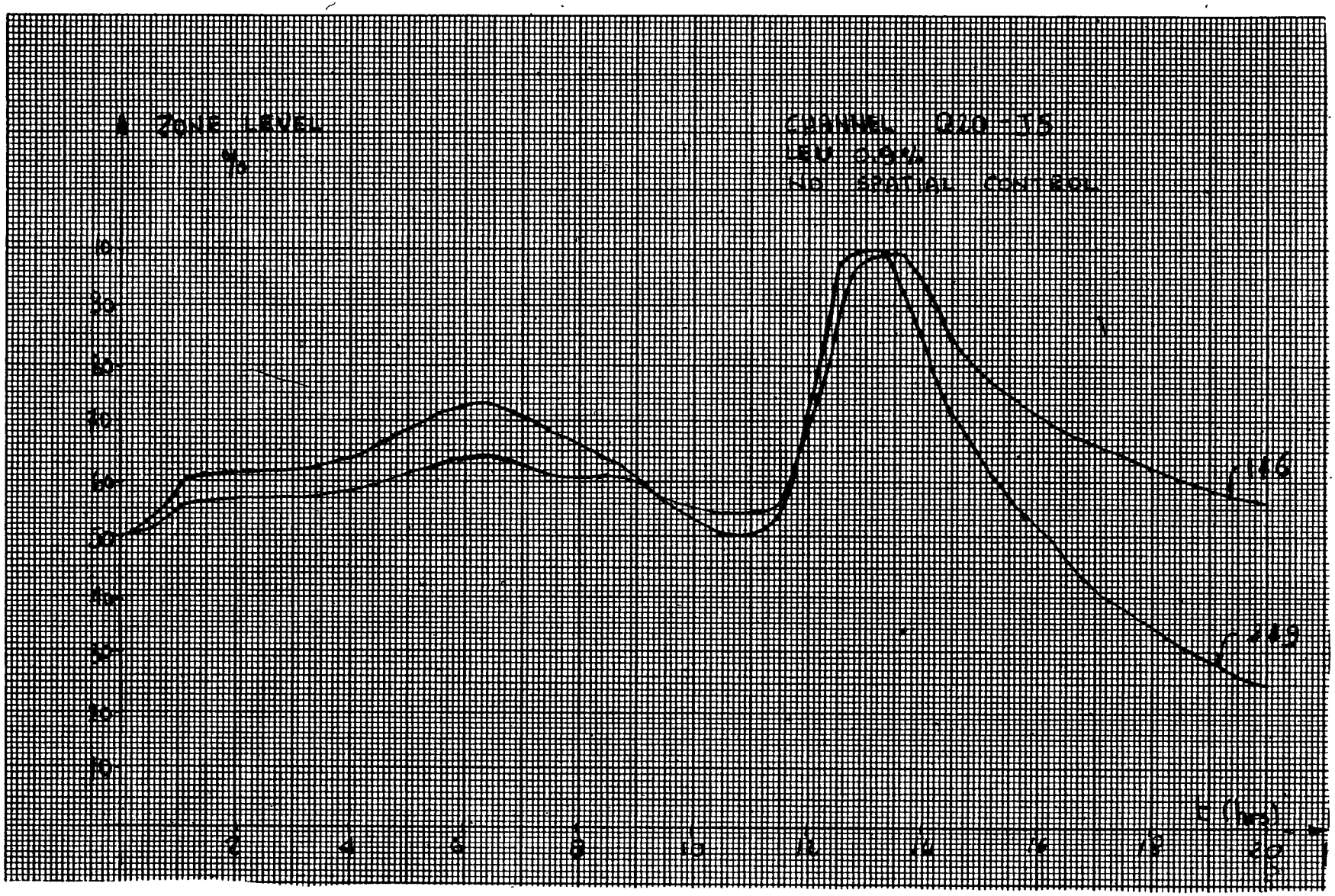

FIGURE 7.14: Zones 1 and 6, 2 and 9 Level Behaviour During Two-Channel Refuelling with No Spatial Control

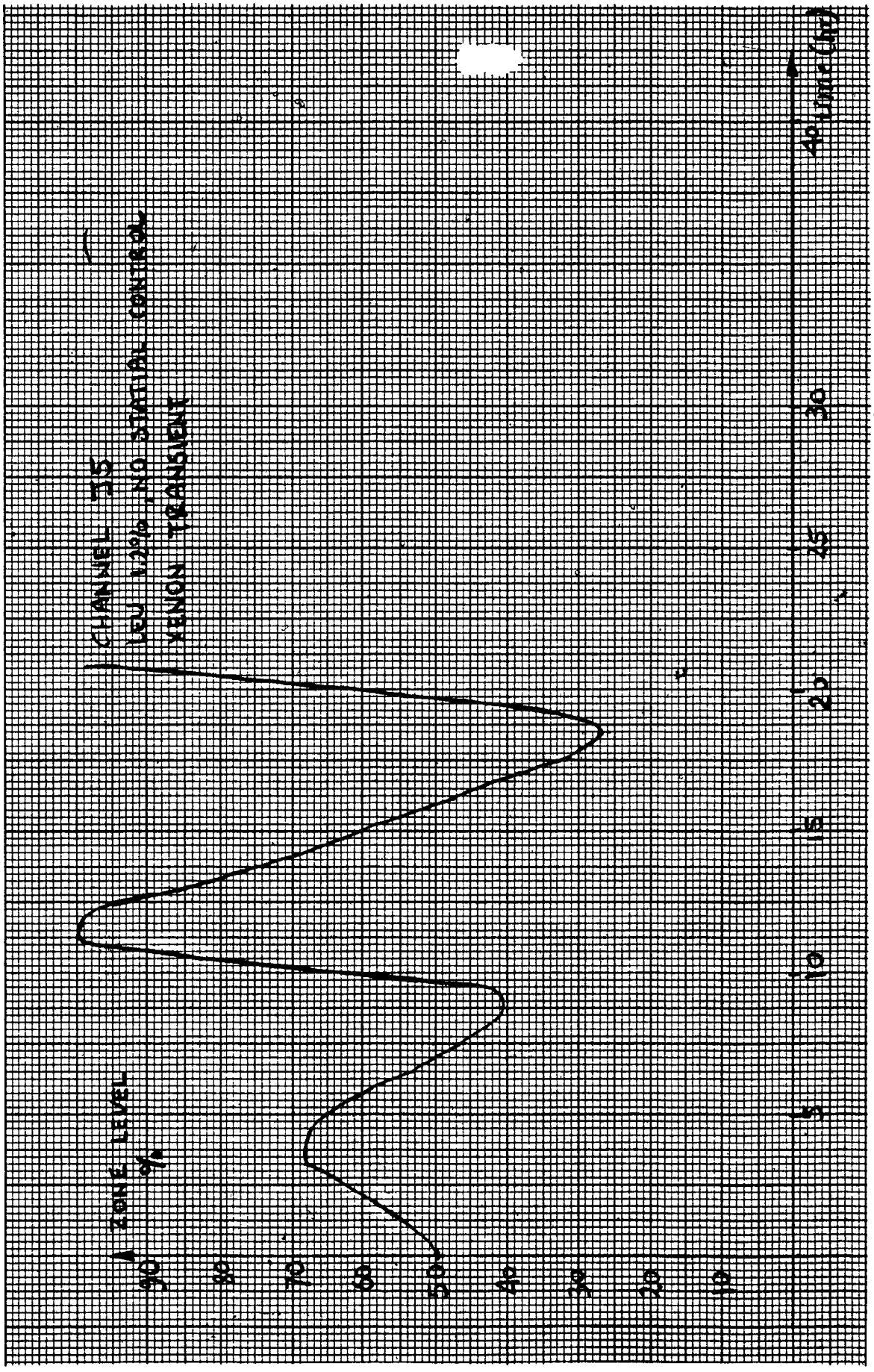

FIGURE 7.15: Zones 2 and 14 Level Behaviour During One-Channel Refuelling with No Spatial Control

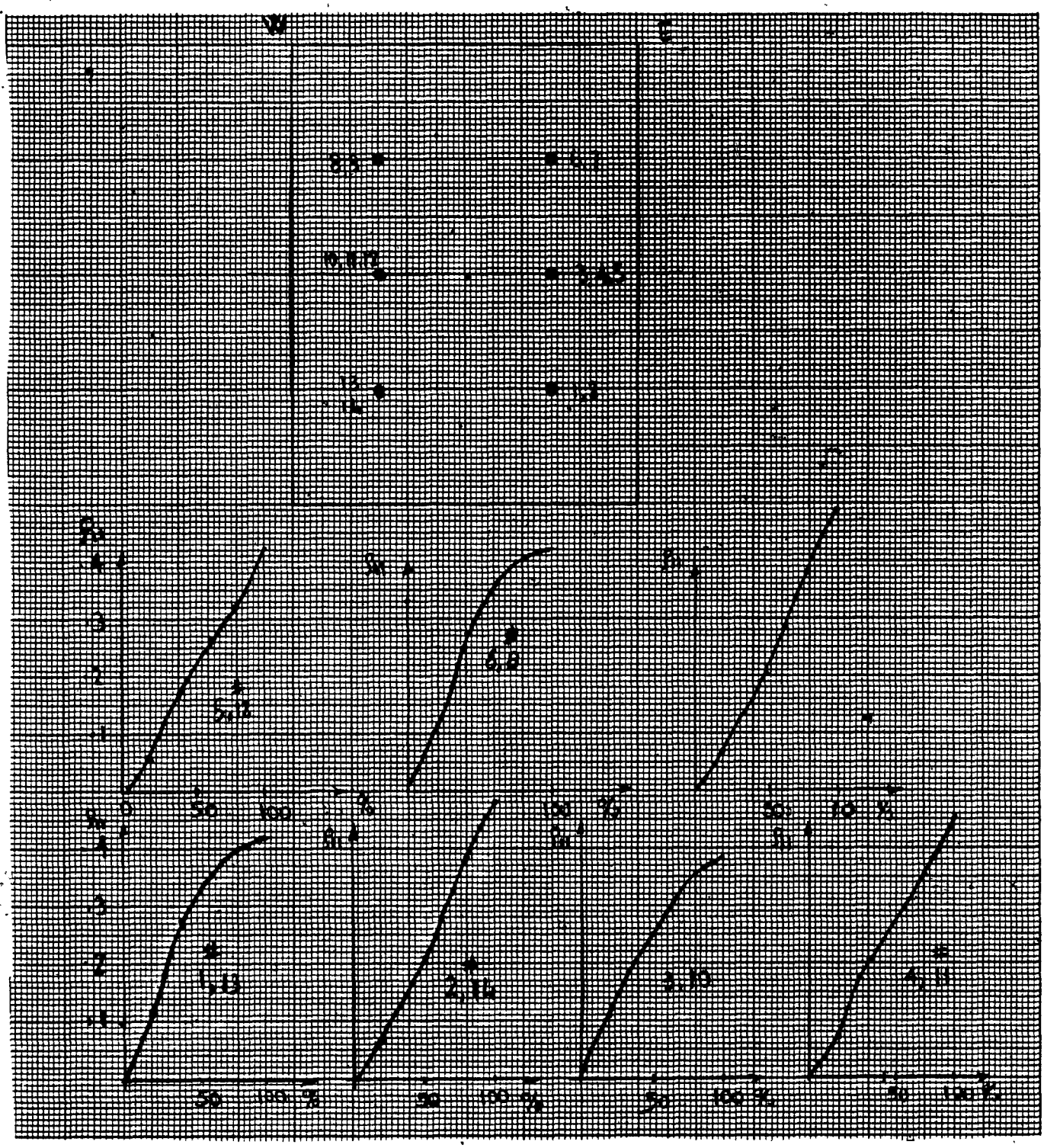

FIGURE 7.16: Zone Fundamental Reactivity vs Full Level (%)
(0.9% LEU-Core)

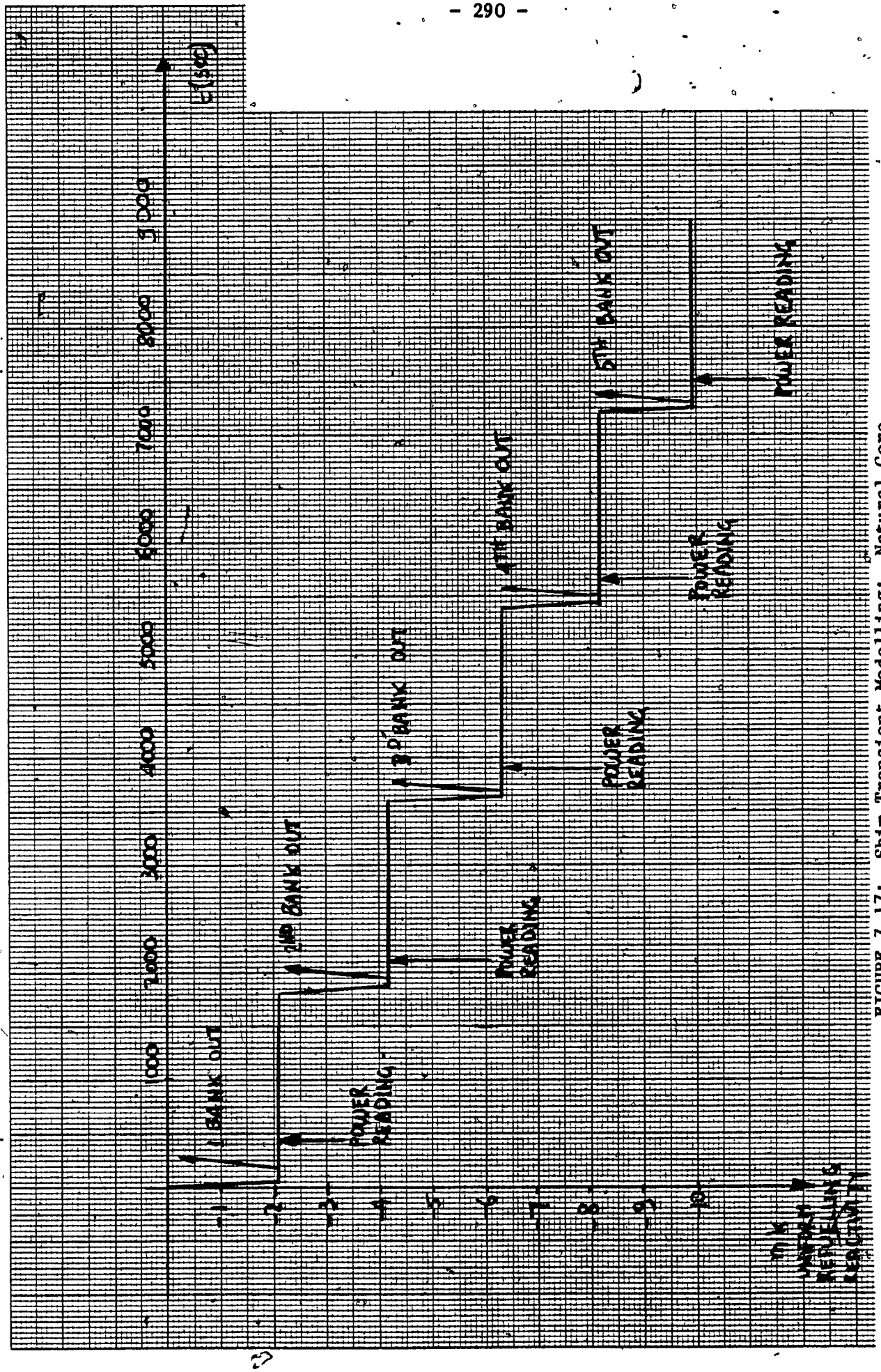

FIGURE 7.17: Shim Transient Modelling: Natural Core

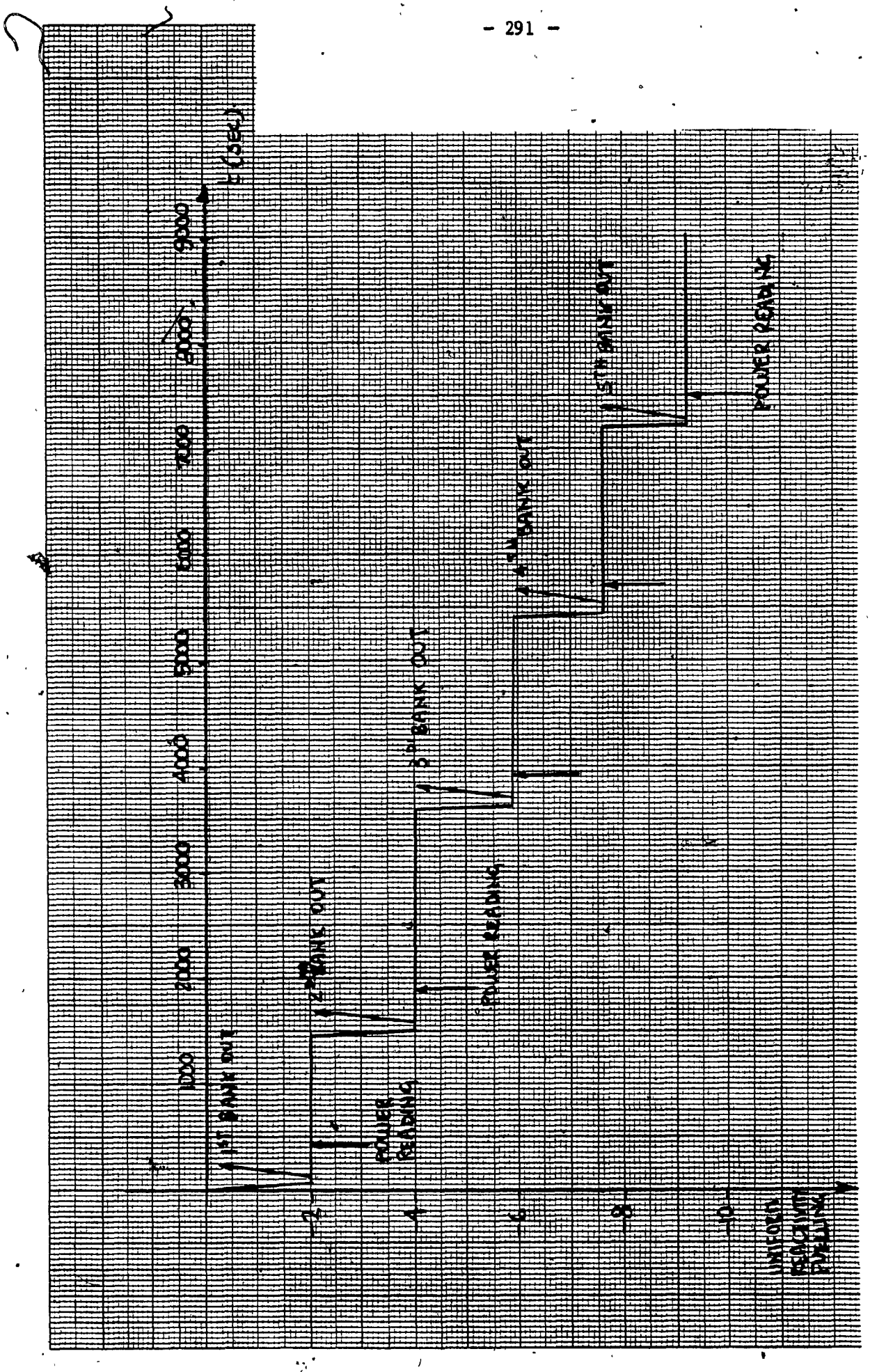

FIGURE 7.18: Shim Transient Modelling: LEU-0.9% Core

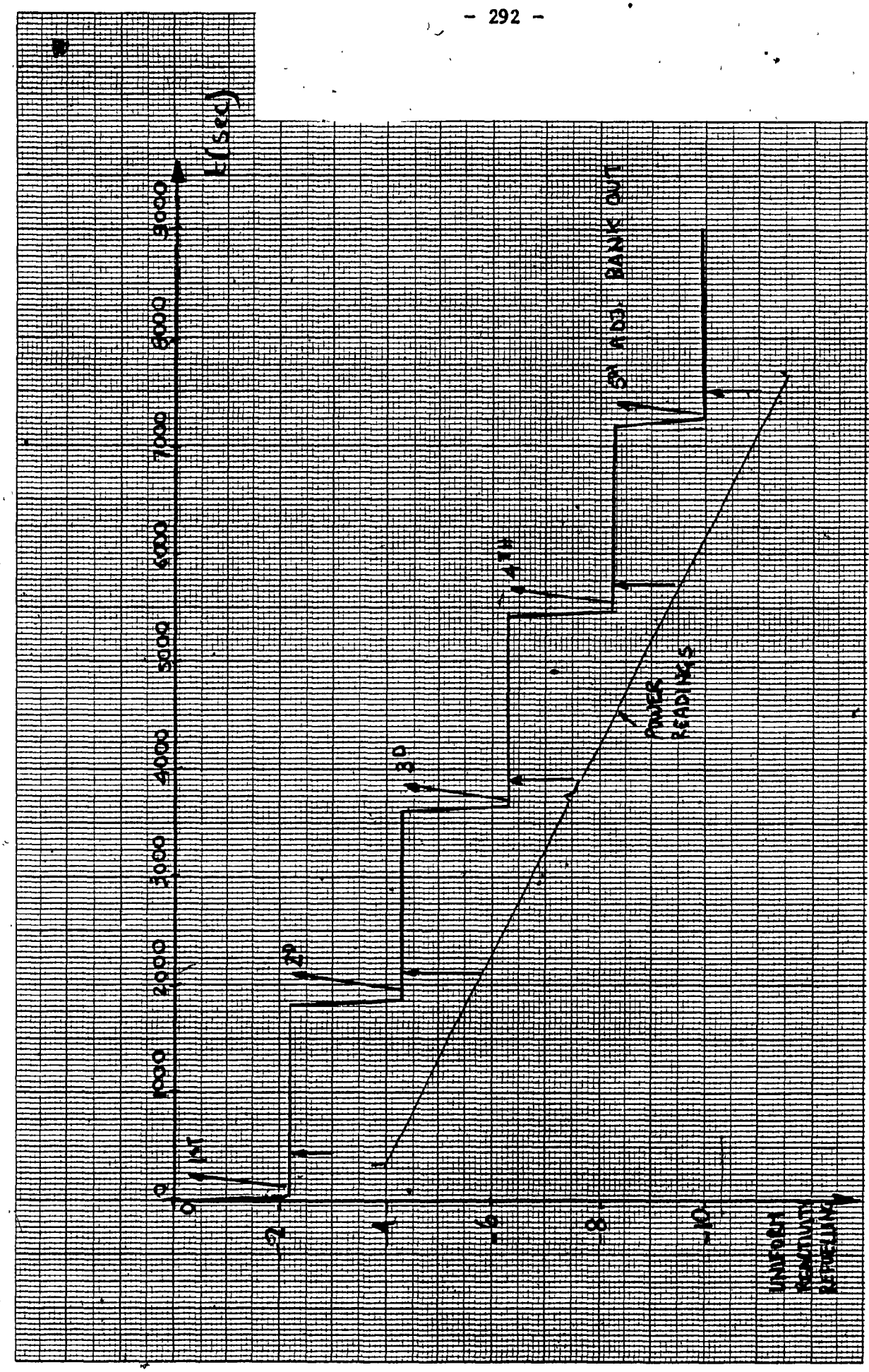

FIGURE 7.19: Shim Transient Modelling: LEU-1.2%-U235 Core

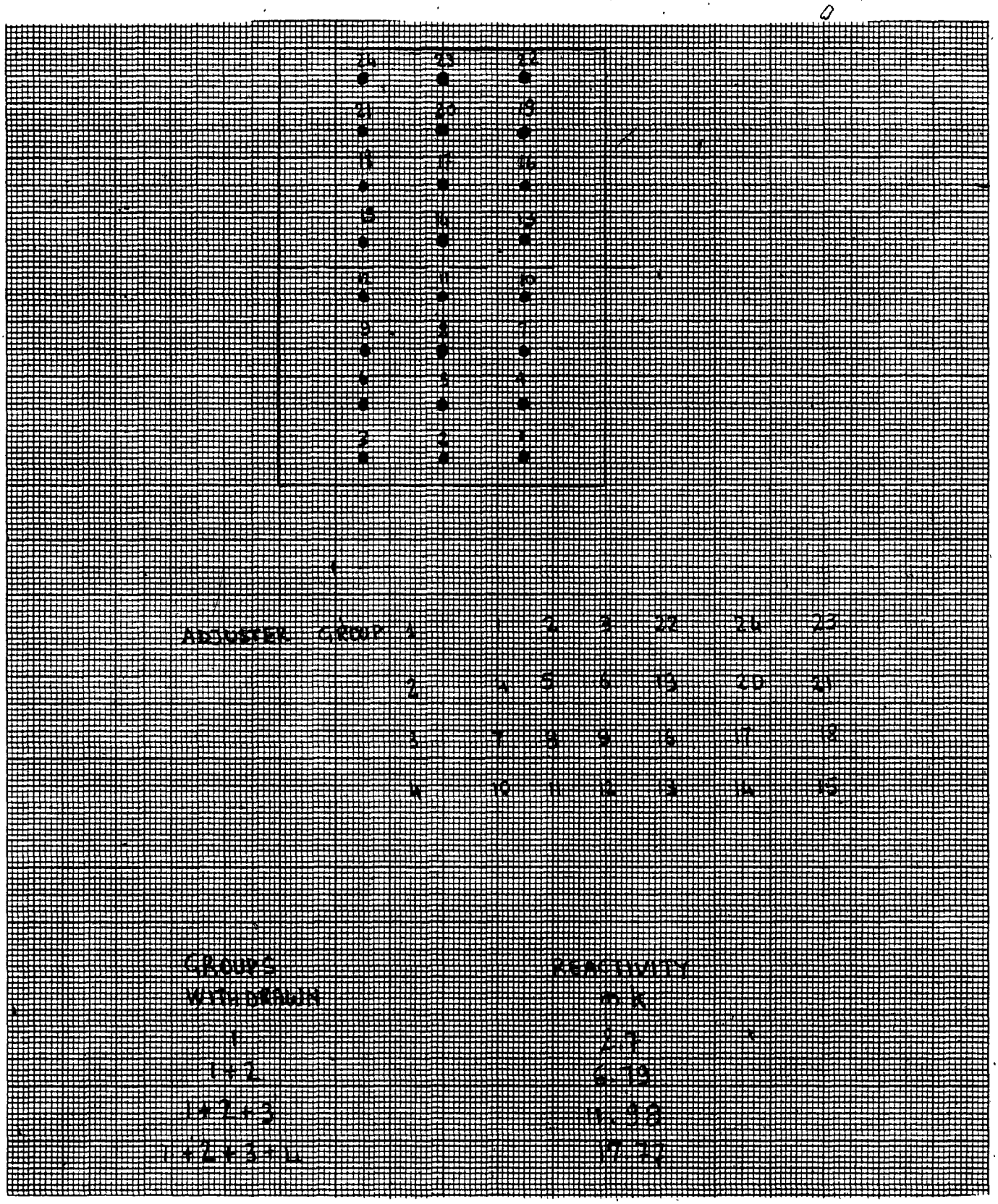

FIGURE 7.20: Adjuster Groups Reactivity

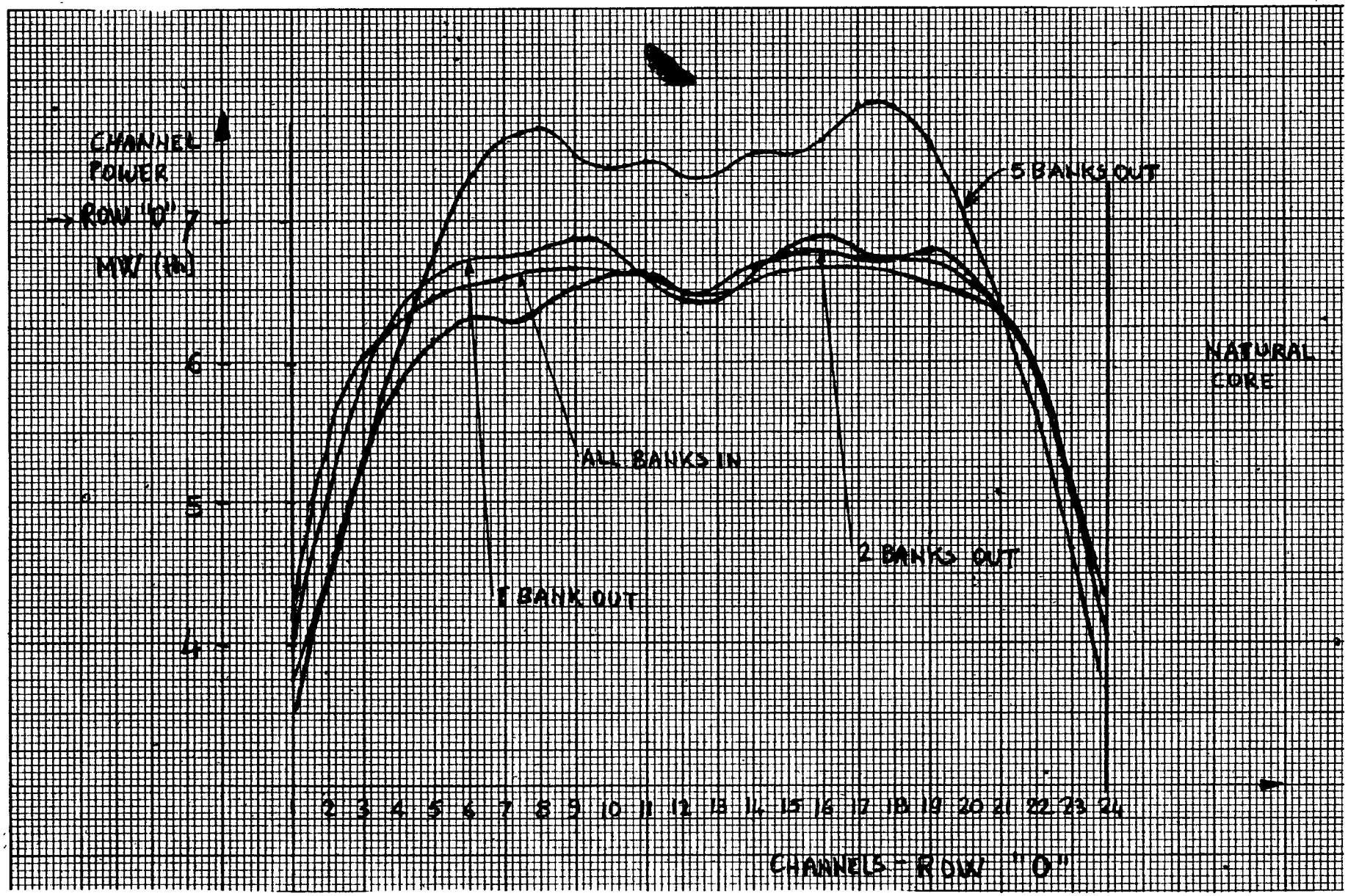

FIGURE 7.21: Power Distribution Along Channel Row "O"
Shim Transients O-I-2-5 Adjuster Banks Out

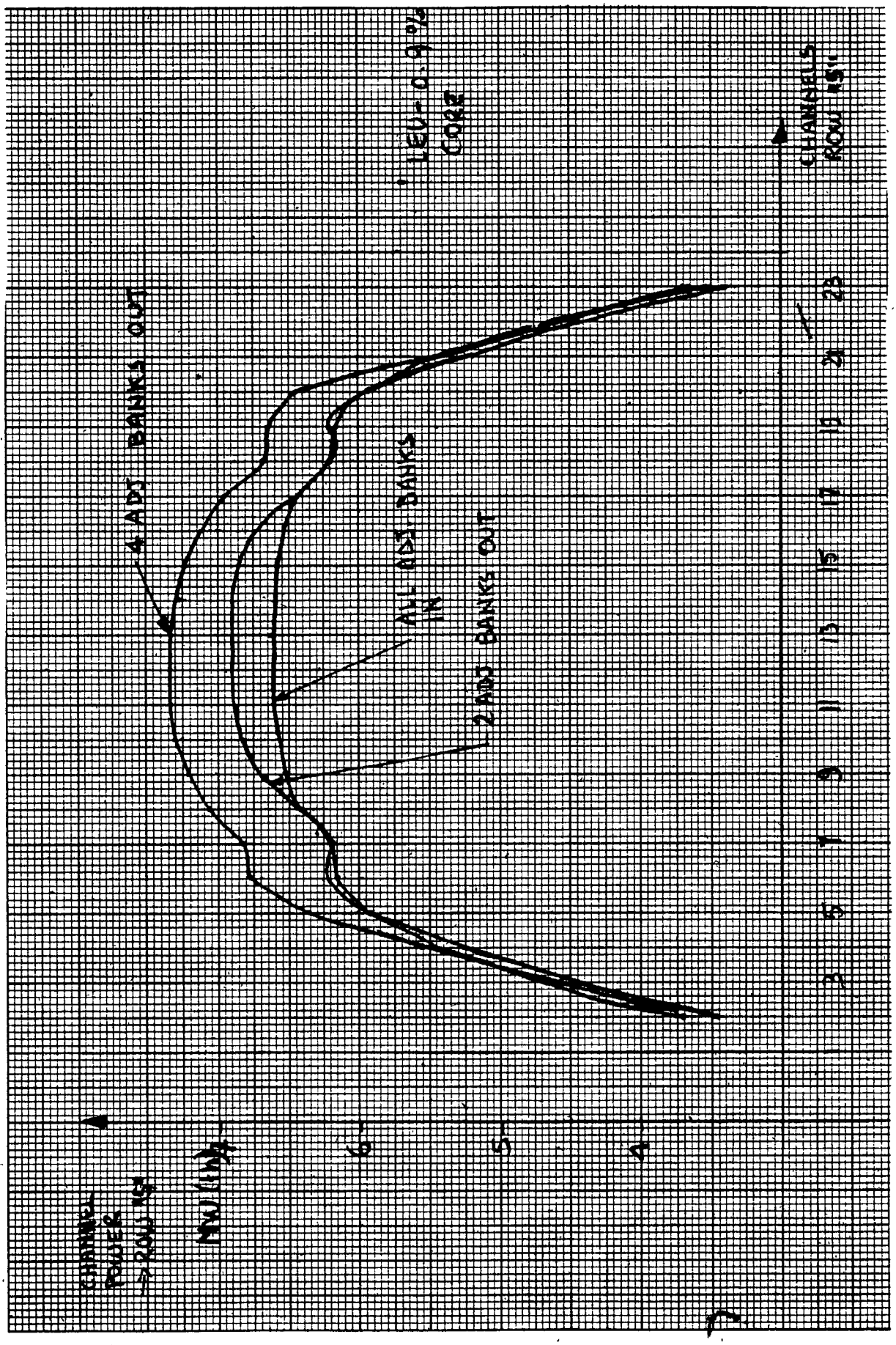

FIGURE 7.22: Power Distribution Along Channel Row "S"
Shim Transients 0-2-4 Adjuster Banks Out

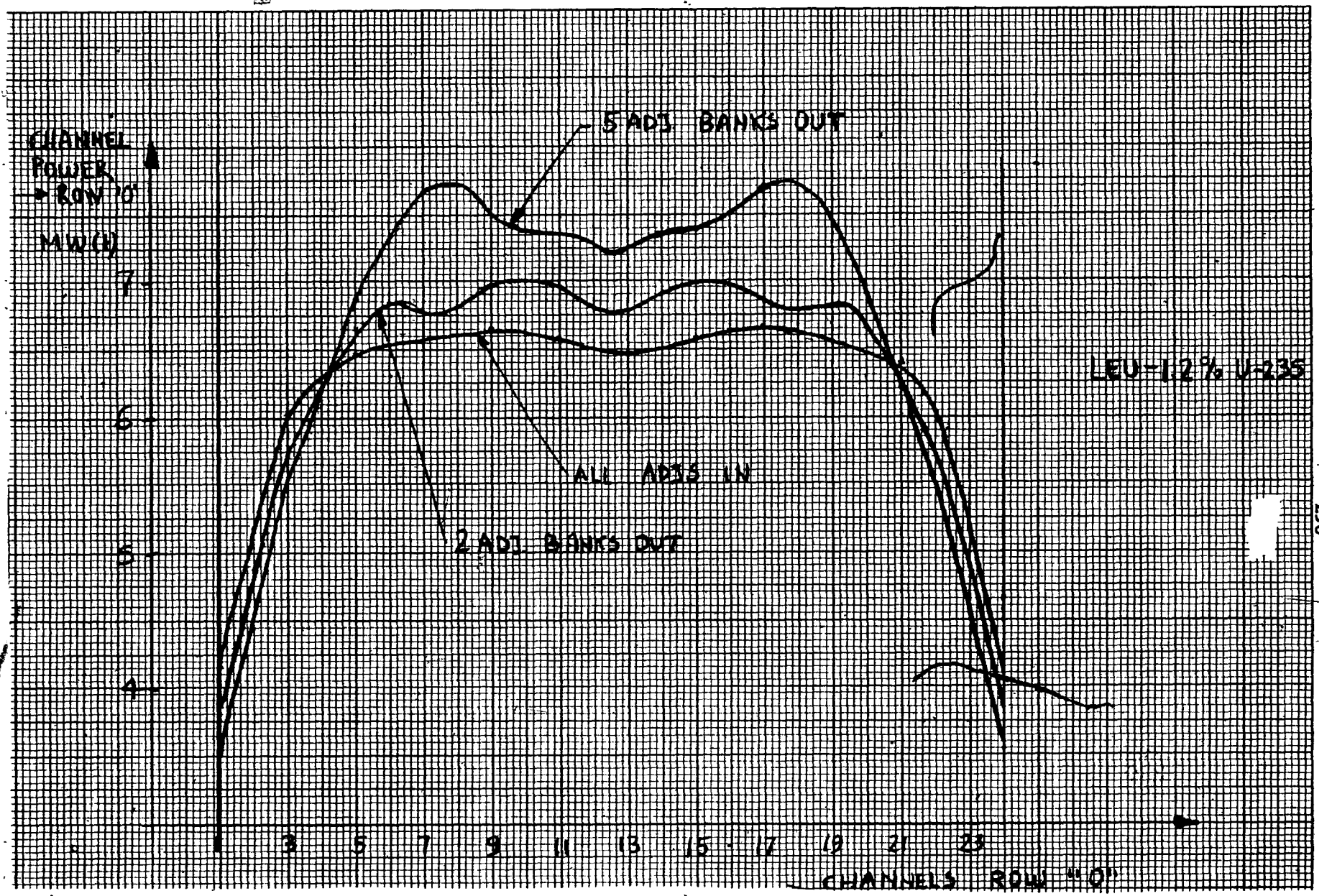

FIGURE 7.23: Shim Transient 0-2-5 Adjuster Banks Out
(Power Distribution Along Channel Row "0"

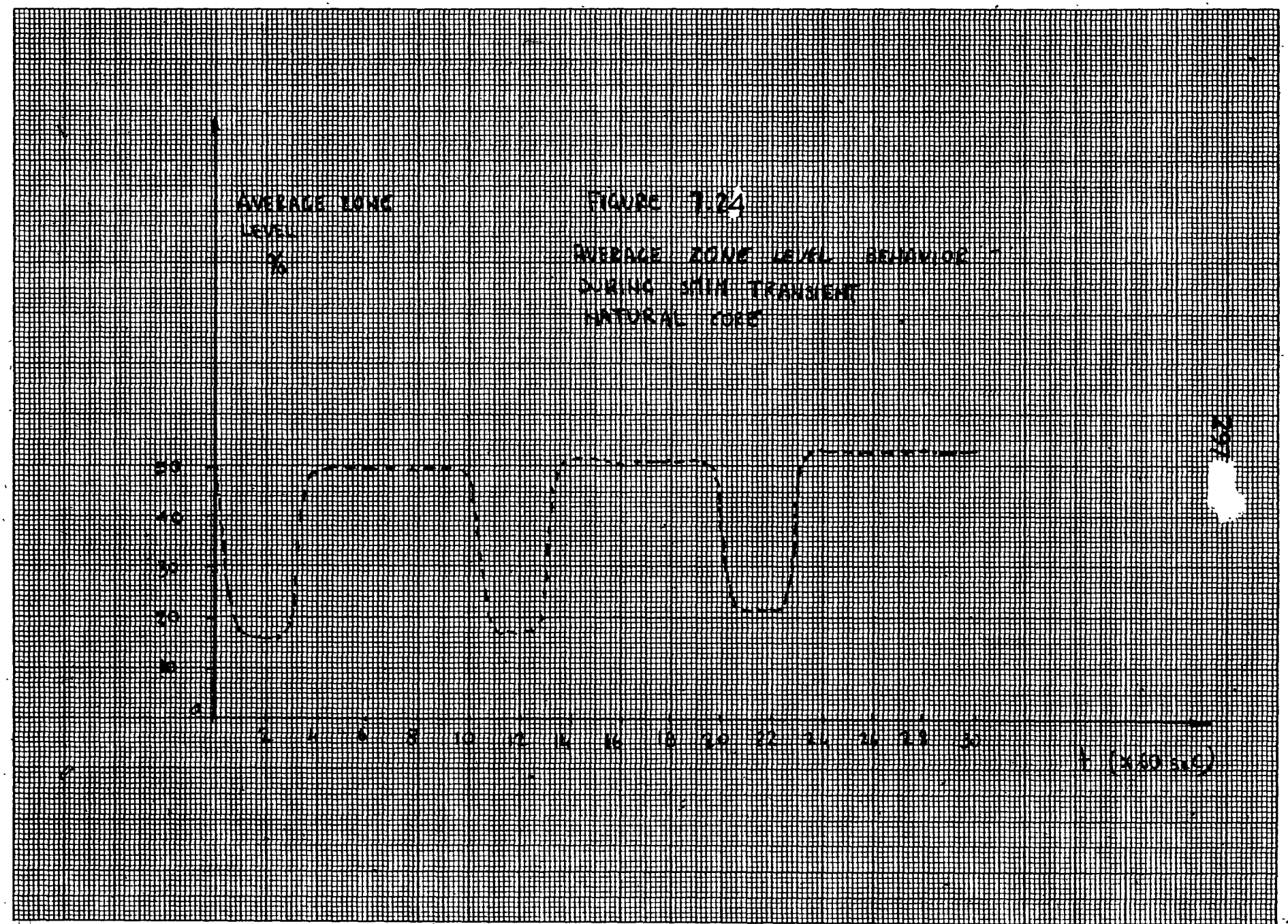

FIGURE 7.24
AVERAGE ZONE LEVEL BEHAVIOR DURING SKIN TRANSIENT NATURAL CORE

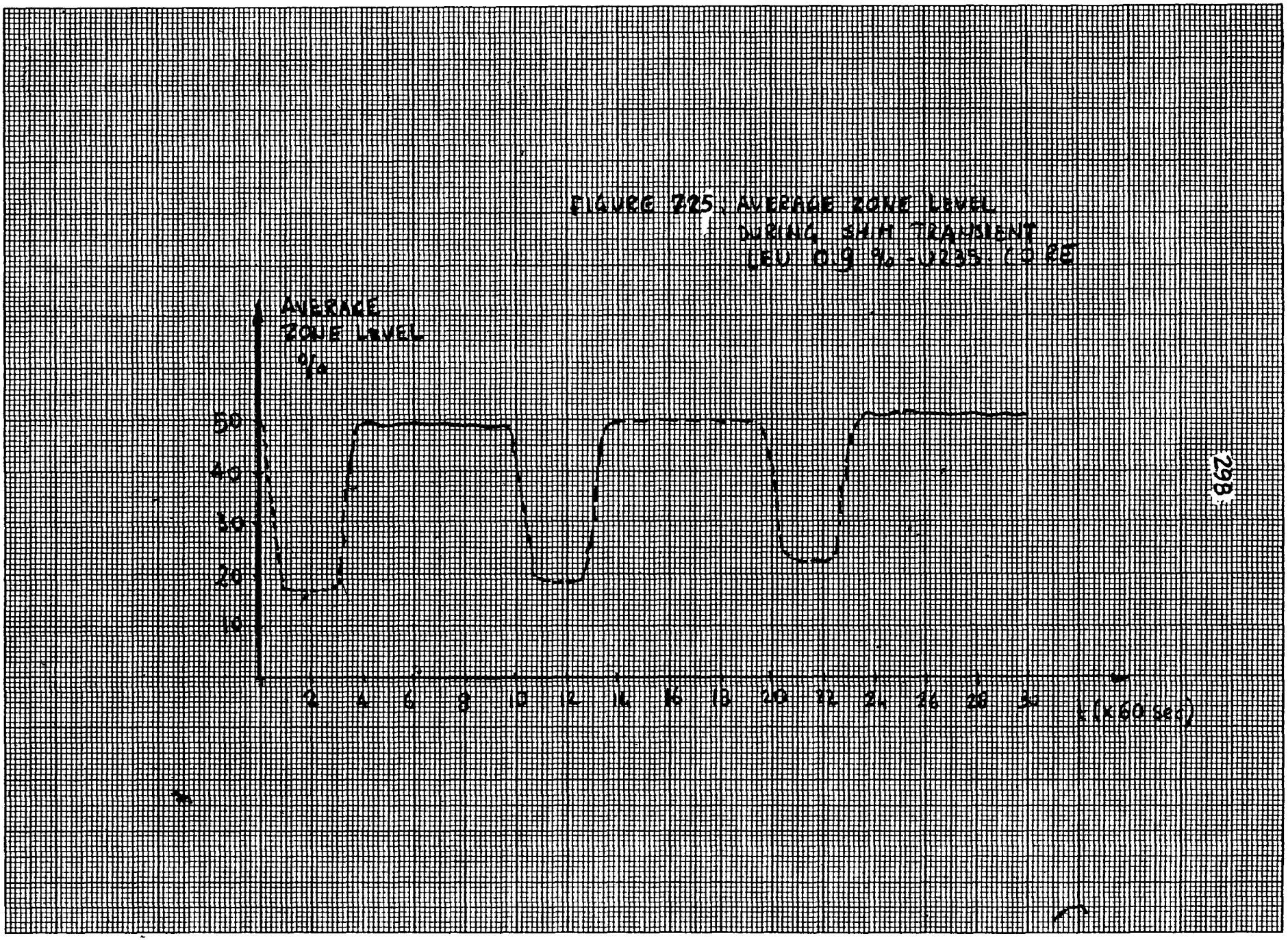

FIGURE 225. AVERAGE ZONE LEVEL DURING SHIM TRANSIENT UEU 0.9 %-U235, 0 EG

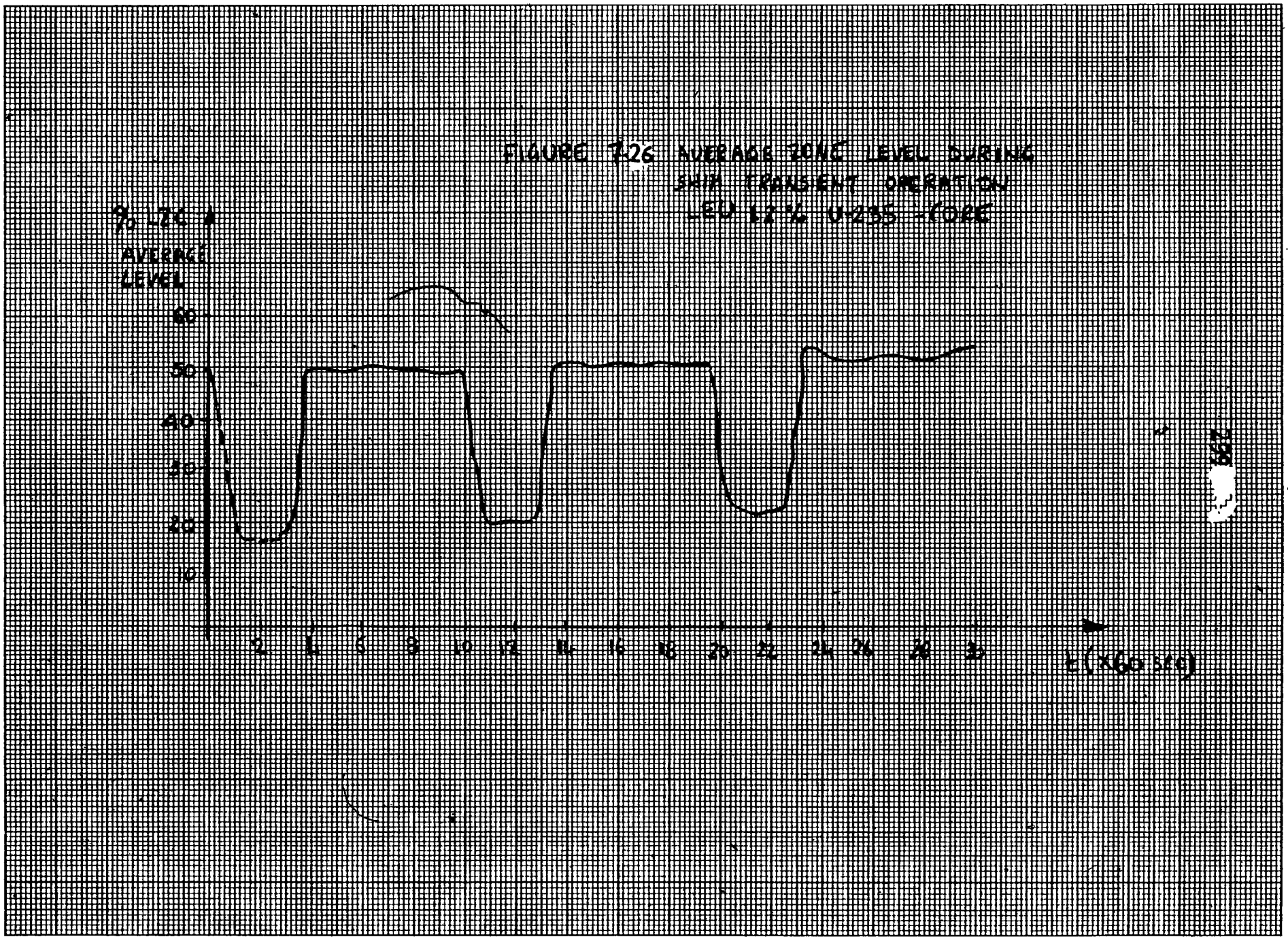

FIGURE 7.26 AVERAGE ZONE LEVEL DURING SHIM TRANSIENT OPERATION LEU 2.7% U-235 CORE

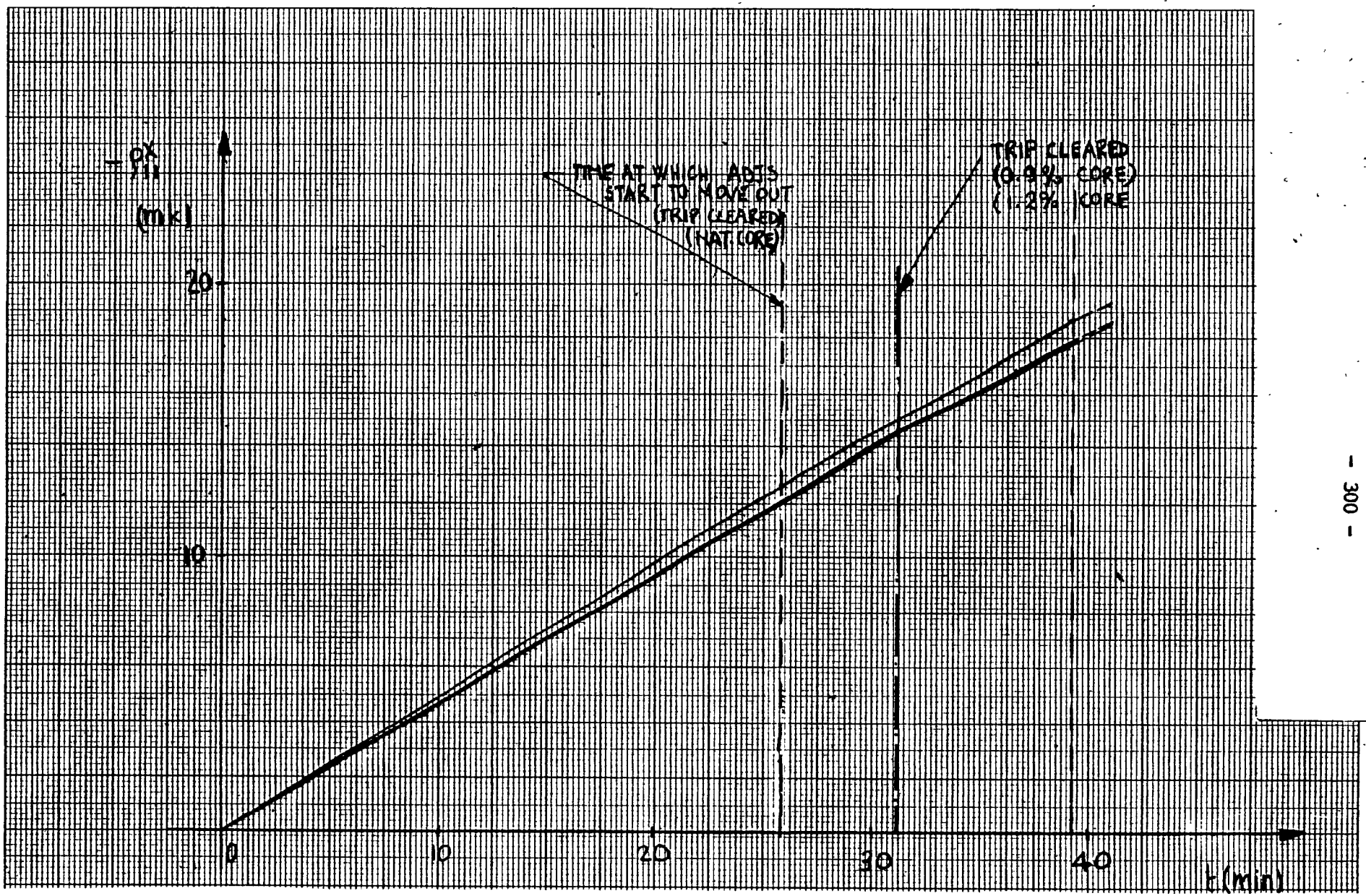

FIGURE 7.27: Trip Clearing Time After Shutdown and Corresponding Xenon Load

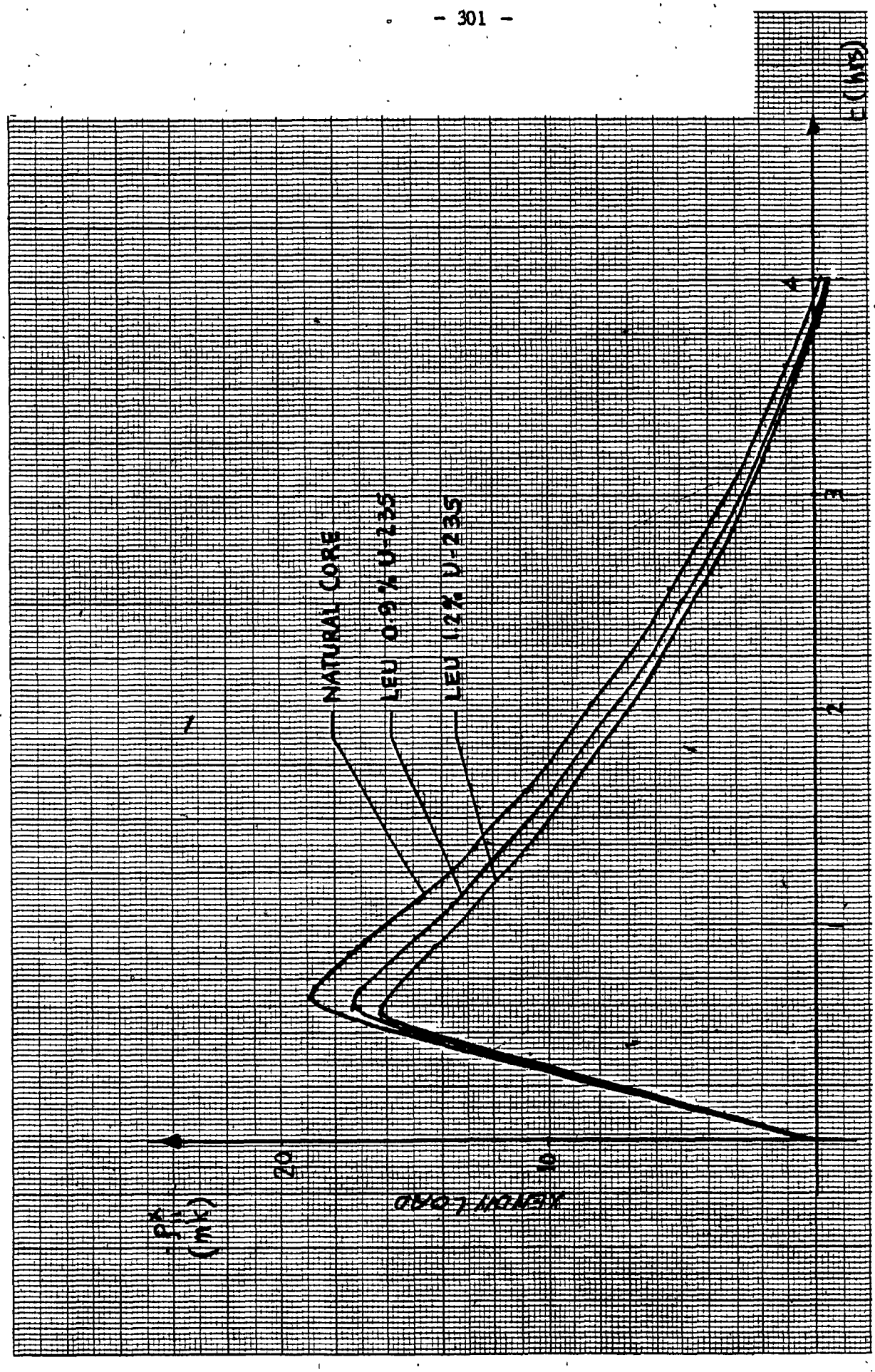

FIGURE 7.28: Xenon Fundamental Load During Shutdown-Start-up

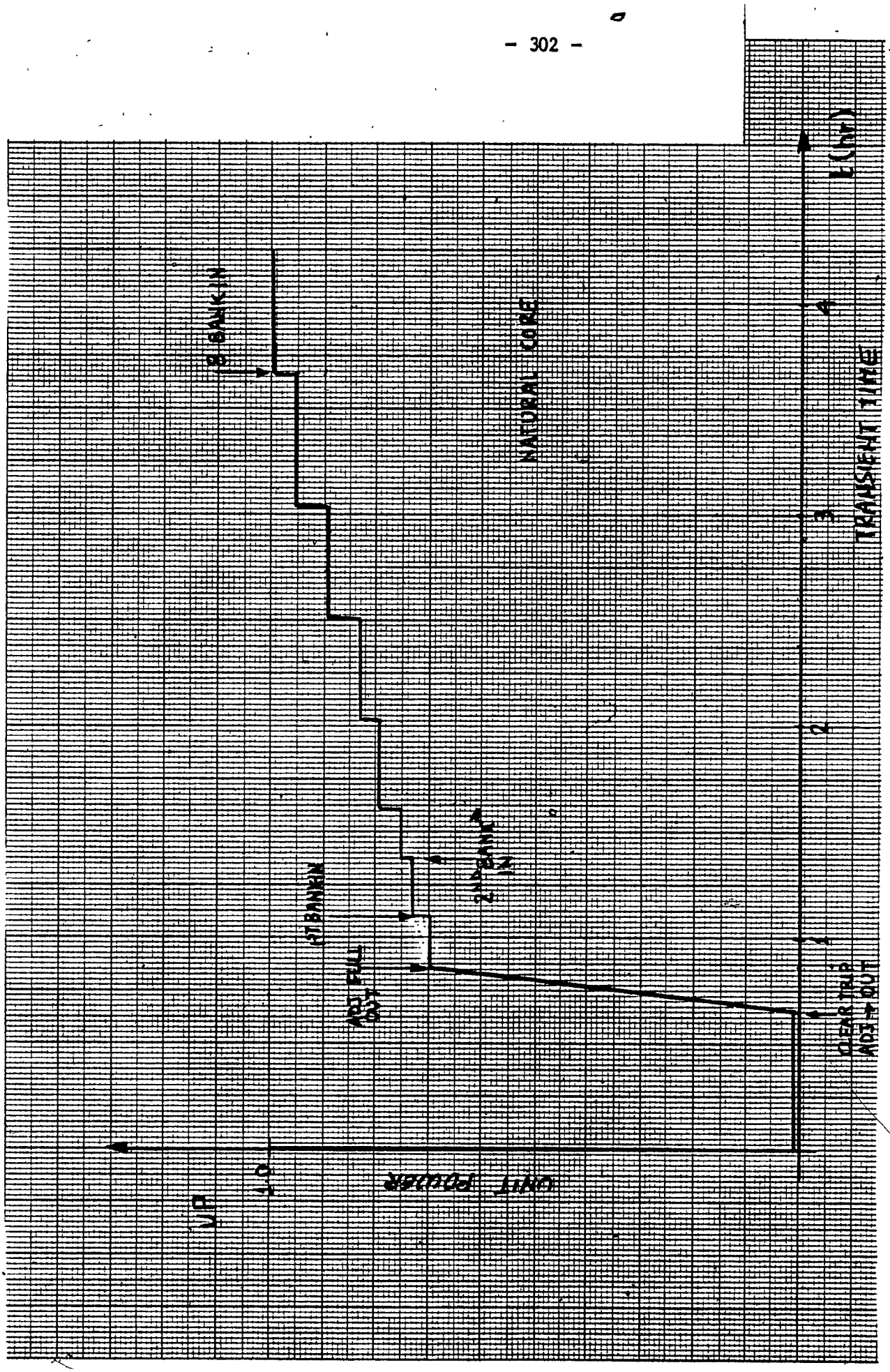

FIGURE 7.29: Power Transient Profile (Shutdown-Start-up) (Natural Core)

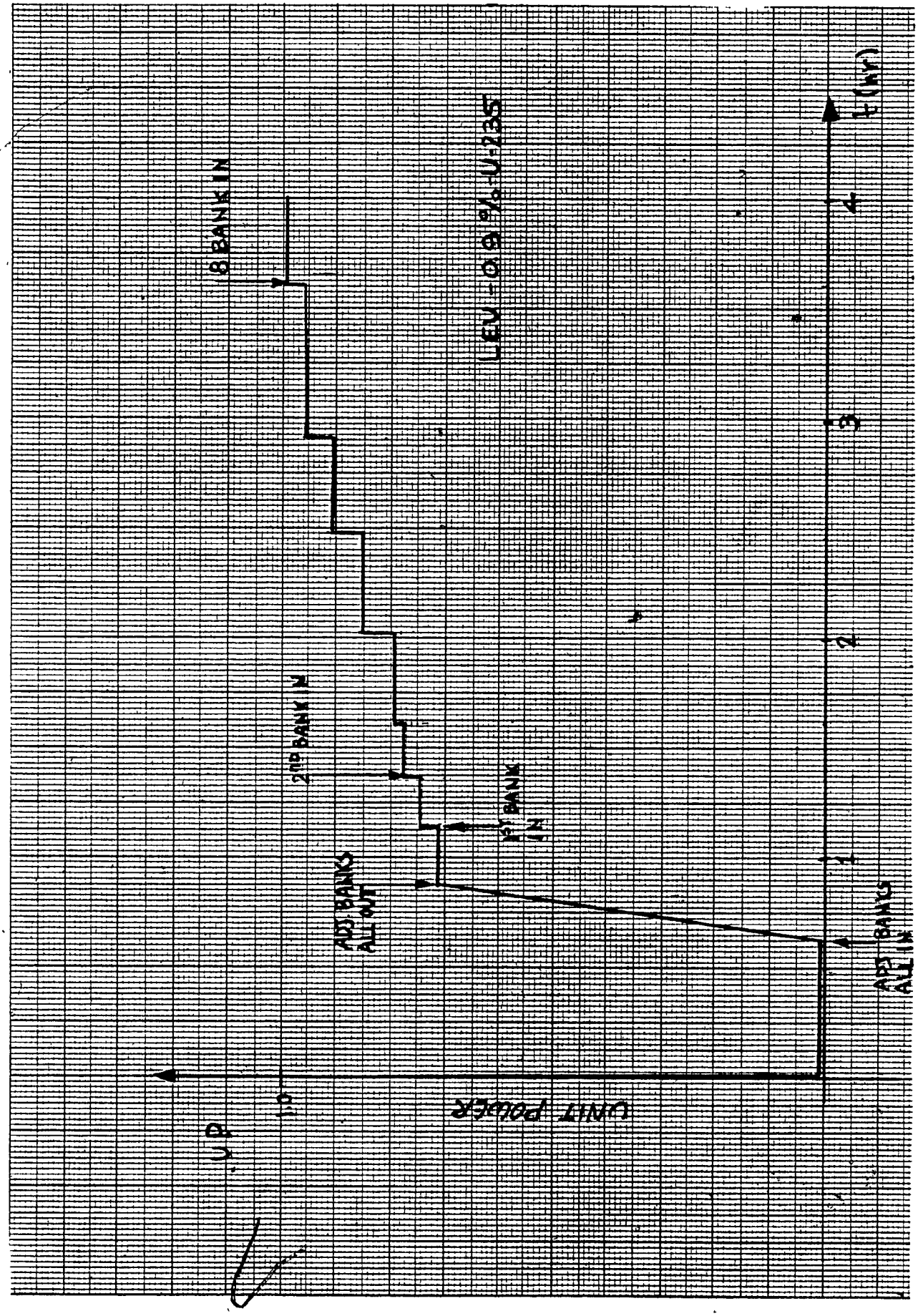

FIGURE 7.30: Power Transient Profile (Shutdown-Start-up) (LEU-0.9%-U235 Core)

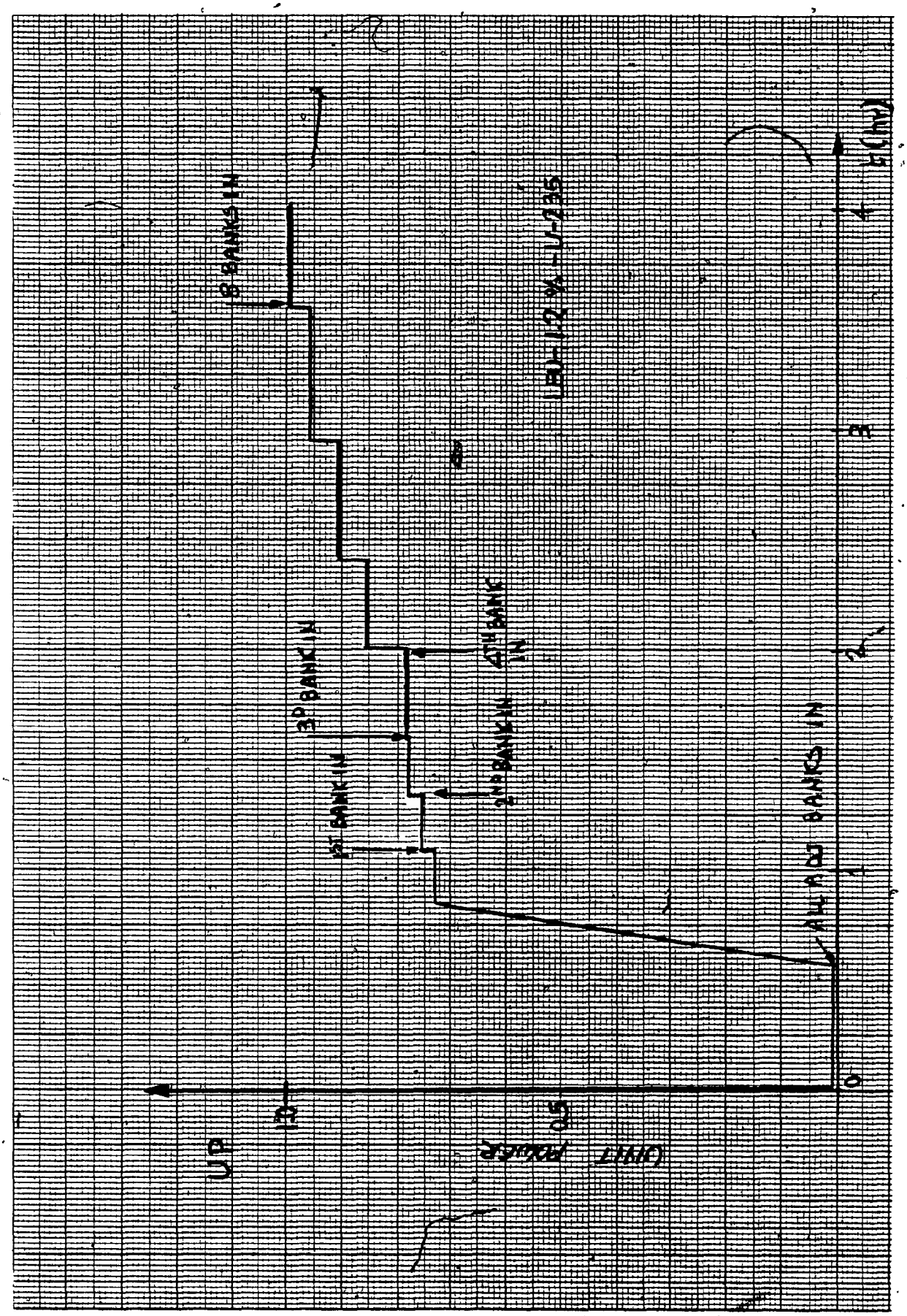

FIGURE 7.31: Power Transient Profile (Shutdown-Start-up) (LEU-1.2%-U235 Core)

CHAPTER EIGHT

8. CONCLUSIONS

8.1 THE IMPORTANCE OF ADVANCED FUEL CYCLES

It was illustrated in Chapters One and Two, and supported by Appendix EN, that nuclear energy will play a very important role in the world energy demand at the turn of this century.

Some energy projections indicate that the world will have in the order of 1,000 nuclear power plants to meet its energy demand at the turn of this century, and projections for the year 2020 range in the order of 5,000. These projections are, however, in this day, the object of national and international disagreement. Nevertheless, we all recognize that energy demand will increase and so will the number of nuclear power plants.

Adequacy in uranium supply should be given proper international attention if power supply, stability, less economic impact and common peaceful nuclear energy objectives are desired.

The natural uranium supply may meet the growth rate of nuclear power demand from now until the end of this century. However, it is not possible to confidently estimate the availability or price of uranium after the turn of the century.

The uncertainty of an assured long-term supply of low cost uranium has led to consideration of uranium conserving alternate fuel cycles for use in thermal power reactors.

Six fuel cycles have been discussed and major physics differences between thorium and uranium cycles have been elaborated on in detail.

The possible fuel cycles considered for the Canadian nuclear system (that is, the CANDU-PHW reactor) are reported here:

a) Once-Through Uranium Cycles (including both natural uranium and enriched uranium). Uranium is fabricated in either a natural or enriched form, used in a reactor, and the spent fuel stored.

b) Uranium Cycle with Plutonium Recycle. In the self-sufficient version, natural uranium is mixed with recycled Pu, fabricated into fuel, and irradiated in a reactor. The spent fuel is reprocessed and the separated Pu is added to more natural uranium, fabricated into fuel and the cycle repeated. Variations include a Pu-burning version in which additional Pu from an external source is added to the fuel in each cycle, and a Pu-producing version in which some of the recycled Pu is available for sale.

c) Once-Through (Th + U^{235}) Cycle. Highly enriched uranium (93%) is added to thorium. The mixture is fabricated into fuel and fed into a reactor. The spent fuel is stored.

d) The Thorium Cycle with U Recycle and Net U^{235} Feed. Highly enriched uranium (93%) is added to thorium along with recycled uranium. After fabrication, the fuel is used in a reactor. The spent fuel is reprocessed and the separated uranium is added to more thorium, plus highly enriched uranium, and the cycle is repeated.

e) The Thorium Cycle with U Recycle and Net Pu Feed. An external source of Pu takes the place of the U-235 in the previous cycles.

Advanced fuel cycles possess the potential to sharply reduce uranium consumption, thereby reducing the depletion of low-cost reserves. A suitable strategy for making a fuel cycle efficient for fuel consumption reduction would be the following:

a) Assume the continued use of natural uranium fuel cycle up to the mid-1990's.

b) At that time, the low enriched uranium (LEU) cycle is gradually introduced into the existing power generation grid.

c) In the mid-2020's, one of the four advanced fuel cycles is introduced.

The use of the LEU fuel cycle as a stepping stone to an advanced fuel cycle is shown to have numerous advantages over proceeding directly from a natural uranium cycle to an advanced cycle. Technical expertise necessary for the introduction of any of the advanced cycles would be gained by first introducing the LEU cycle. Furthermore, omitting the LEU cycle as an intermediate cycle would require more rapidly fluctuating throughput rates for the secondary industries, as well as higher annual and cumulative uranium requirements. Thus, in addition to reducing refuelling costs, the introduction of the LEU cycle would facilitate the later commercialization of an advanced fuel cycle.

8.2 LEU-CANDU-PHW REACTOR RESULTS

8.2.1 Economic Analysis

Figure 2.9 of Chapter Two provides a summary of the variation of equilibrium system economic efficiencies for "close-to-optimum" cases as a function of yellowcake costs.

The fuel cycles listed in the previous section have burnup levels as follows:

a) Once-through natural uranium cycle: 7,500 MWd/te;

b) 1.2%-U235 enriched uranium once-through cycle with an average burnup of: 20,800 MWd/te;

c) Uranium cycle with self-sustaining Pu recycle and average burnup of: 18,000 MWd/te;

d) A thorium cycle with fissile Pu topping and uranium recycle (average burnup in Pu burner = 30,000 MWd/te) with fissile Pu supplied from a natural uranium PHW (average burnup: 7,500 MWd/te);

e) A (Th + U-235) cycle with U recycle and an average burnup of 30,000 MWd/te;

f) A (Th + U-235) once-through cycle with an average burnup of 52,000 MWd/te.

The main points that can be drawn from Figure 2.9 are the following:

a) While the natural uranium cycle does reign supreme of the very low yellowcake price, other cycles start to become attractive at current yellowcake costs.

b) If reprocessing costs are low, the first cycle to compete favourably with natural uranium is the uranium cycle with Pu recycle, followed closely by the thorium system using Pu topping made in a natural PHW reactor. It can be seen qualitatively why the Pu/U recycle competes first. The advantages are lower fabrication penalty, lower inventory charges, fewer natural PHW reactors to supply plutonium and, at this yellowcake cost, lower fissile material supply cost (i.e., the U-235 in natural uranium is cheaper than Pu). The only advantage which the thorium cycle has is the better physics.

c) At high reprocessing costs, the first cycle to compete with natural uranium cycle as yellowcake costs increase is the enriched uranium once-through cycle.

d) The once-through (Th + U-235) cycle does not seem attractive under any foreseeable circumstances.

e) The rate of decrease of economic efficiency with increasing yellowcake cost goes in the following order (highest to lowest):

- natural uranium once-through;
- enriched uranium once-through;
- U cycle with Pu recycle;
- Th cycles with U recycle.

f) If yellowcake prices continue to increase indefinitely, the thorium cycles with U recycle would eventually become the most attractive.

g) One further point is worth commenting on. If fissile Pu were available in unlimited amounts at the price assumed here (i.e., reprocessing cost), the curves for the thorium + Pu topping case would be horizontal lines at the positions shown by the bars at the left of the curves. This case, if reprocessing costs were low, would be an obvious choice at all yellowcake costs above about $35/kg U.

8.2.2 Technical Feasibility

8.2.2.1 Reactor Power Margins

With respect to power peaking, any fuel management scheme can, in principle, be used provided that the power peak limits are accommodated by adjusting the maximum permissible reactor power. This limit is a function of the required operational margin to trip.

The margin considered is based on an expected permissible power of 98% FP for the natural fuel Bruce NGS-B cores. For sensitivity purposes, another set of calculations was made with a "conservative" margin corresponding to 96% FP permissible power for the natural core.

Table 6.3 shows the maximum permissible powers for the expected margin in a number of fuel management cases: the refuelling direction appears to be important, and Fuelling With the coolant Flow (FWF) is preferable in most cases.

8.2.2.2 Reactor Spatial Control

8.2.2.2.1 Reactivity Worth

Some concern was expressed before any attempt on the study of CANDU-PHW reactor spatial control when LEU fuel is introduced into an equilibrium core. It was illustrated in Chapter Two that higher than natural enrichment in the fuel translates into

higher reactivity of the fuel, and this forces us to consider that the reactor is somewhat less easy than in the natural core during refuelling and shutdown-start-up transients. At every refuelling, more concentrated reactivity is injected into the visited channel. It had been thought that the resulting local power peaking might lead to undersirably high control-detector readings and false tilt control.

A large number (approximately one hundred) of reactor core studies and operation transients was performed, and they were described in detail in Chapters Six and Seven.

Major reactor core studies consisted of generating diffusion theory coefficients and core parameters for the case of natural and Low Enriched Uranium cores.

Channel reactivity for natural and LEU cases was calculated as a function of bundle shift and, within the perimeter bundle shift scheme, it was found that 0.1 mk, 0.2 mk and 0.3 mk of reactivity are introduced into the core for natural (0.711%-U235), LEU-0.9%-U235 and LEU-1.2%-U235 respectively. Reactivity worth of reactor regulating systems (liquid zone controllers, adjuster rods, mechanical control absorbers, shut-off rods) was calculated and tabulated in the format ready for use in the SMOKIN code. All SMOKIN input data banks for each reactor configuration case and operational transients are

available from the author of this thesis (they are not included due to their large size: approximately 2,000 lines of data per operational transient).

8.2.2.2.2 Reactor Operational Transients

Shim, shutdown-start-up and one-, two-channel refuelling transients were thoroughly performed to assess the controllability of CANDU-PHW reactors fuelled with natural and Low Enriched Uranium (LEU) fuel. Reactor methods of control were discussed in Chapter Seven and physics differences between control devices were also analyzed. The reactor operational transients are summarized below:

Refuelling Transients:

Several one-channel and two-channel refuelling operations have been simulated using the SMOKIN code to assess the independence of the lattice physics code used to generate diffusion theory coefficients and the behaviour of Liquid Zone Controllers (LZC) with respect to core configuration (natural or LEU fuel).

It is shown that the spatial control system responds nicely to perturbations and the response is at all times contained within the limits of linearity in the case of natural core, while most of the liquid zone controllers next to LEU refuelled channels are phased out in the case of an LEU core if the LZC system is not strenghtened.

It is found that, if the LZC-induced incremental cross-sections are increased by 20% and the liquid zone controller reference levels are reduced by 20%, then single-channel and two-channel LEU refuelling transients show that the spatial control system operates within the limits of linearity.

The level of the liquid zone controllers does not exceed more than 70% in the case of single-channel refuelling, and only for some two-channel refuelling transients does the level of some liquid zone controllers reach the range of 80%.

A very reassuring result is that the spatial control system response in the case of the natural core is, for all practical purposes, independent of the lattice code used. The few cases which were run for comparison showed a very tight consistency (within 0.6% in the liquid zone controller level).

In all cases considered, the spatial control system was "strong" enough that no liquid zone controllers were phased out of spatial control (phasing-out starts at 80% level).

Shim Transients:

Withdrawal of the first five adjuster rod banks in reactivity shim mode with no prior derating of reactor power is performed two minutes after a negative reactivity is ramped-in uniformly to all modes.

The negative reactivity ramps force the average zone levels to go to 20% region to trigger automatic withdrawal of an adjuster bank. Withdrawal of the three banks was performed over a short time span (30 minutes) to determine the basic response of the LZC system.

Power calculations were done at 8, 18 and 28 minutes into the transient to estimate approximately the reactor power derating requirements in order to not exceed channel power limits. The power distortions caused by the withdrawal of adjuster rods at a midpoint of the reactor axis are reported in Chapter Seven. The plots of average zone level versus time are also shown.

The results indicate that there are no applicable differences on the response of the LZC system when natural or slightly enriched cores are considered.

The effect of the transient tilting during adjuster withdrawal on ROP detector response is not taken into consideration during the study.

Shutdown-Start-up Transients:

Reactor shutdown-start-up operational transients were simulated to assess the following:

- Determination of start-up behaviour of a Low Enriched Uranium (LEU) core to a natural fuel core;

- Determination of response of average zone levels during start-up at points where adjuster banks were inserted into the core;

- Determination of xenon reactivity feedback behaviour during shutdown and start-up.

Detailed descriptions of this simulation are provided in Chapter Seven. Analytical and graphical results are provided in table and curve format (Figures 7.30 to 7.34).

From the figures and table, it can be concluded that the power behaviour during the start-up of the reactor when Low Enriched fuel is used follows very closely the power behaviour during the start-up of the reactor when natural fuel is used, and that during the process of the reactor shutdown, the following was observed:

a) Power raising from 0% to 100% full power takes 4 hours;

b) Xe reactivity build-up rate upon shutdown is practically independent of enrichment and equals 0.48 mk/min;

c) Consequently, due to the lower reactivity worth of adjusters in enriched cores, a lower Decision and Action Time (DAT) is obtained for a higher enrichment:

Enrichment	DAT
nat	= 23.7 min
.9%	21.7 min
1.2%	19.4 min

8.3 GENERAL CONCLUSIONS

The main conclusions are as follows:

- It is feasible to operate CANDU-PHW reactors with Low Enriched Uranium fuel. Increased power peaking due to enrichment can be accommodated by proper fuel management at equilibrium. The reactor controllability and response to accident situations are not different than with natural fuel.

- Capitalized lifetime savings with respect to natural uranium can be as high as several tens of millions of dollars per CANDU-PHW reactor of an 850 MW(e) power output type, depending on operating margins to trip the target power.

- Low Enriched Uranium once-through fuel cycle will attenuate transition technical problems from current generation of CANDU-PHW reactor systems to CANDU's with advanced fuel cycles.

8.4 RECOMMENDATIONS

In view of the beneficial effects on the economics of the LEU fuel cycle, it is recommended that Canadian utilities commit themselves to more detailed studies on alternative fuel management schemes for CANDU-PHW reactors based on Low Enriched Uranium fuel.

These studies should be concentrated on optimizing the fuel management scheme by taking into account fuel machine operation, fuelling with flow practice, critical heat flux correlations, transition from start-up core into equilibrium cycle, effects of higher burnup on safety assessment.

The behaviour of the reactor regulating systems has been shown to be satisfactory but, in order to further improve the nuclear power plant economic performance, additional studies would be recommended in the areas of developing an optimal modal control algorithm for future LEU-CANDU-PHW load following operation schemes.

REFERENCES

1. Ontario Hydro, Nuclear Studies and Safety Department, ESTIMATE OF CANADIAN FUEL FABRICATION COSTS FOR USE IN STRATEGY ANALYSIS, Report No. 79260, August 1979.

2. Ontario Hydro, Nuclear Studies and Safety Department, ALTERNATE FUEL CYCLES: WHICH OPTIONS TO DEVELOP, Report No. 79050, May 1979.

3. A.J. Mooradian, CANDU FUEL CYCLES: PRESENT AND FUTURE, Atomic Energy of Canada Limited, Report No. AECL 5516.

4. J.S. Foster, THE CANADIAN NUCLEAR PROGRAM, Canadian Electrical Engineering Journal, Vol. 1, No. 1, pages 3-14.

5. Ontario Hydro, Nuclear Studies and Safety Department, THE LOW ENRICHED URANIUM FUEL CYCLE IN ONTARIO: A RESOURCE UTILIZATION STUDY, Report No. 79011, February 1979.

6. M. Barbone, THE TRANSPORT THEORY FOUNDATION OF ONE-POINT REACTOR POISONING, Master thesis, Concordia University, Montréal, 1978.

7. S.R. Hatcher et al, THORIUM CYCLE IN HEAVY WATER MODERATED PRESSURE TUBE (CANDU) REACTORS, invited paper, ANS 1975, Winter Meeting, San Francisco, 16-21, 1975.

8. R.A. Bonalumi, Ontario Hydro, Nuclear Studies and Safety Department, private communication.

9. M.F. Duret, G.J. Phillips, J.I. Weeder, W.A. Wolfe, Atomic Energy of Canada Limited, and R.M. Williams, Energy, Mines & Resources Canada, REPORT ON NUCLEAR RESOURCES (1985 TO 2020), World Energy Conference, Conservation Commission, August 1977.

10. W.B. Lewis, WHY MAXIMUM CANDU POTENTIAL LIES WITH ORGANIC COOLANT AND A THORIUM FUEL CYCLE, DM-138, January 1973.

11. R.A. James, W.J. Peen, ADVANCED NUCLEAR FUEL CYCLES: WHAT IS THEIR ECONOMIC POTENTIAL?, presented at CNA Conference, June 1978.

12. J.H.K. Lau et al, THE INFLUENCE OF URANIUM AVAILABILITY ON NUCLEAR STRATEGY FOR ONTARIO, presented at CNA Conference, June 14, 1978.

13. R.A. Bonalumi, Ontario Hydro, Nuclear Studies and Safety Department, private communication.

14. K.O. Otto, D.A. Meneley, ACCURACY OF THE QUASISTATIC TREATMENT OF SPATIAL REACTOR KINETICS, Nuclear Science Engineering, 36, 402-411, 1969.

15. G. Kugler, A.R. Duster, ACCURACY OF THE I.Q.S. SPACE-TIME METHOD CHECKED WITH EXPERIMENTS, Trans., ANS 23, 592, 1976.

16. G.S. Keepin, PHYSICS OF NUCLEAR KINETICS, Addison-Wesley Publishing Co. Inc., 1965.

17. F.N. McDonnell, R.E. Green, SPATIAL POWER CONTROL IN LARGE CANDU REACTORS, AECL Report No. 6912.

18. W.M. Stacey, Jr., SPACE-TIME NUCLEAR REACTOR KINETICS, Academic, New York, 1969, Sections 1, 4.

19. A.Z. Akcasu, G.S. Lellouche, L.M. Smotkin, MATHEMATICAL METHODS IN NUCLEAR REACTOR DYNAMICS, Academic, New York, 1971.

20. J.B. Yasinsky, A.F. Henry, Nuclear Science Engineering, 22, 171, 1965.

21. J.C. Luxat, THE POTENTIAL OF A GENERALIZED MODAL ANALYSIS METHOD IN THE DESIGN AND ANALYSIS OF CANDU-PHW REACTOR CONTROL AND SAFETY SYSTEMS, Ontario Hydro, Nuclear Studies and Safety Department, 1978.

22. J.C. Luxat, A MODAL KINETICS APPROACH TO REACTOR SPATIAL CONTROL STUDIES, Ontario Hydro, Nuclear Studies and Safety Department, 1975.

23. ADVANCED NUCLEAR REACTOR ANALYSIS, lecture notes, University of Toronto, 1979.

24. J.C. Luxat, R.A. Bonalumi, Ontario Hydro, Nuclear Studies and Safety Department, private communications, 1979-1980.

25. Atomic Energy of Canada Limited proprietary, MONIC, A PROGRAM FOR NUMERICAL CALCULATION OF FLUX HARMONICS.

26. J.C. Luxat, G.M. Frescura, Ontario Hydro, Nuclear Studies and Safety Department, SPACE-TIME NEUTRONIC ANALYSIS OF POSTULATED LOSS OF COOLANT ACCIDENTS IN CANDU REACTORS, Nuclear Technology, Vol. 46, ANS 1979.

27. J.C. Luxat, Ontario Hydro, Nuclear Studies and Safety Department, draft of SMOKIN ENGINEERING MANUAL.

28. M.J. Roth, WIMS, AEEW R414.

29. I.H. Gibson, THE PHYSICS OF LATREP, AECL Report No. 2548, March 1966.

30. P.C. Loken, THE PHYSICS OF POWDERPUFS-V, TDAI-31, Part 1 of 3, April 1979.

31. R.A. Bonalumi, Ontario Hydro, Nuclear Studies and Safety Department, PRELIMINARY ASSESSMENT OF THE LOW-ENRICHED URANIUM CYCLE IN BRUCE NGS B, Volumes 1, 2, November 1979.

32. J.J. Duderstat, L.J. Hamilton, NUCLEAR REACTOR ANALYSIS, John Wiley & Sons Inc., 1976.

33. J.D. Stewart, THE THEORY OF THERMAL NEUTRON DIFFUSION IN A REACTOR LATTICE, AECL Report No. 1637, 1962.

34. A.M. Weinberg, E.P. Wigner, THE PHYSICAL THEORY OF NEUTRON CHAIN REACTORS, University of Chicago Press, 1958.

35. Samuel Glasstone, Alexander Sesonske, NUCLEAR REACTOR ENGINEERING, Van Nostrand Reinhold Company, 1981.

36. David Crabbe, R. McBride, THE WORLD ENERGY BOOK, Nichols Publishing Co., New York, 1978.

37. IEA International Agency, WORKSHOPS ON ENERGY SUPPLY AND DEMAND, Organization for Economic Cooperation and Development, 1978.

38. Science and Public Policy Program, A COMPARATIVE ANALYSIS, Energy Alternatives, University of Oklahoma, Norman, Oklahoma, May 1975.

39. R. Siever, Harvard University, ENERGY AND ENVIRONMENT, American Scientific, W.H. Freeman and Company, San Francisco, California, 1980.

40. Dr. Ralph E. Lapp, AMERICA'S ENERGY, Reddy Communications Inc., Greenwich, Connecticut, 1976.

41. D.C. Ion, AVAILABILITY OF WORLD ENERGY RESOURCES, Graham and Trotman Ltd., United Kingdom, 1975.

42. United States National Committee, SURVEY OF ENERGY RESOURCES, World Energy Conference (WEC), 1974.

43. M. Granger Morgan, Editor, TECHNICAL AND SOCIAL ASPECTS OF ENERGY, Energy and Man, IEEE Press Inc., New York, 1975.

44. Geoffrey Greenhalgh, THE NECESSITY OF NUCLEAR POWER, Graham & Trotman Ltd..

45. BGR Federal Institute for Geosciences and Natural Resources, Hanover, Federal Republic of Germany, SURVEY OF WORLD ENERGY RESOURCES, prepared for 11th WEC, Munich, September 1980.

APPENDIX MG

THE MULTI-GROUP AND TWO-GROUP GENERALIZED DIFFUSION EQUATIONS

MG.1 INTRODUCTION

The one-speed diffusion theory model that is frequently used in reactor physics suffices to illustrate the most important aspects of modern reactor design and analysis. However, for specific problems in reactor design and analysis, this simplistic model is simply not adequate. Neutrons in a power reactor are characterized by energies spanning from 15 MeV down to approximately 0.01 eV and it is not surprising that practical reactor calculations require a more realistic treatment of neutron energy dependence.

To derive energy-group theory in a general way, we first partition the reactor into a number of spatial regions (quantities associated with the k-th spatial region being labelled with superscript k) and position the energy range into a number of energy groups,

$$\Delta E_1 = E_0 - E_1 \; ; \; \Delta E_2 = E_1 - E_2 \; ; \; \ldots \; \Delta E_g = E_{g-1} - E_g \qquad \text{Eq. MG.1}$$

$$\ldots\ldots \; \Delta E_G = E_{G-1} - E_G$$

This expression is graphically depicted in Figure MG1,

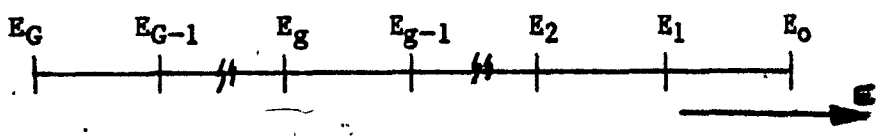

FIGURE MG.1: Multigroup Representation

where E_0 is the highest energy of interest to reactor problems (E_0 15 MeV) and $E_G = 0$. The backward indexing scheme is used to more physically represent the fact that the neutrons usually lose energy during their lifetime.

The essential approximation is that the flux per unit energy $\phi(r,E)$ for r in region K and E in energy group ΔE_g may be written

$$\phi(\bar{r},E) = \phi_g(\bar{r})\, \psi^k(E) \qquad \text{Eq. MG.2}$$

where $\psi^k(E)$ is a "spectrum function for each energy group g in region k", normalized so that

$$\int_{E_g}^{E_{g-1}} \psi^k(E)\, dE = 1 ; \quad g = 1, 2, 3 \cdots G \qquad \text{Eq. MG.3}$$

and $\phi_g(\bar{r})$ is the "scalar flux for energy group g" described hereinafter.

$$\phi_g(\bar{r}) \approx \int_{E_g}^{E_{g-1}} \phi(\bar{r},E)\, dE \qquad \text{Eq. MG.4}$$

Note the following:

$\phi_g(\bar{r})$ = group g flux = [neutrons/cm^2.sec]

$\phi(\bar{r},E)$ = flux per unit energy in group g
= [neutrons/cm^2.sec.eV]

Assuming for the moment that $\psi_g^k(E)$ are known, we find coupled partial differential equations for $\phi_g(\bar{r})$ by simply substituting

$$-\nabla \cdot D(\bar{r},E)\nabla\phi(\bar{r},E) + \Sigma_t(\bar{r},E)\,\phi(\bar{r},E) =$$

$$= \int_0^\infty \left[\sum_j \chi^j(E)\,\nu^j \Sigma_f^j(\bar{r},E') + \Sigma_s(\bar{r},E'\to E)\right]\phi(\bar{r},E')dE' \qquad \text{Eq. MG.5}$$

into the transport equation (actually, the transport equation would be written for the vector flux, which is also a function of the neutron direction). A widely-used approximation consists of replacing the transport equation with a continuous energy diffusion equation (Ref. 6).

$$-\nabla \cdot D(\bar{r},E)\,\nabla\phi(\bar{r},E) + \Sigma_t(\bar{r},E)\,\phi(r,E)$$

$$= \int_0^\infty \left[\sum_j \chi_j(E)\,\nu^j\,\Sigma_f^j(\bar{r},E') + \Sigma_s(\bar{r},E'\to E)\right]\phi(r,E)dE' \qquad \text{Eq. MG.6}$$

The substitution for r in region k and E in ΔE yields:

$$-\nabla D(\bar{r},E)\,\nabla\left[\psi_g^k(E)\,\phi_g(\bar{r})\right] + \Sigma_t(\bar{r},E)\left[\psi_g^k(E)\,\phi_g(\bar{r})\right]$$

$$= \sum_{g'=1}^{G} \int_{E_g}^{E_{g-1}'} \left[\frac{1}{\lambda}\sum_j \chi_j(E)\,\nu^j \Sigma_f^j(\bar{r},E') + \Sigma_s(\bar{r},E')\,\psi_{g'}^k(E')\,\phi_{g'}(r)\,dE' \qquad \text{Eq. MG.7}$$

Since $\psi^k(E)\phi(\bar{r})$ is the only approximation to $\phi(r,E)$, the RHS and LHS of this equation cannot be exactly equal for all E in r. The RHS and LHS are equal in "an integral sense", that is, for each energy group, we require that $\phi_g(\bar{r})$ be such that the integral of the LHS of the equation over that group be exactly equal to the integral of the RHS, e.g.:

$$-\nabla\left[\int_{\Delta E_g} D(\bar{r},E)\,\psi_g^k(E)\,dE\right]\nabla\phi_g(\bar{r})$$

$$+\left[\int_{\Delta E_g}\Sigma_t(\bar{r},E)\,\psi_g^k(E)\,dE\right]\Delta\phi_g(\bar{r}) =$$

$$=\sum_{g'=1}^{G}\left\{\frac{1}{\lambda}\sum_j\int_{\Delta E_g}\chi^j(E)dE\left[\int_{\Delta E_{g'}}\nu^j\Sigma_f^j(r,E')\,\psi_{g'}^k(E')dE'\right]\phi_{g'}(\bar{r})\right.$$

$$\left.+\left[\int_{\Delta E_g}dE\int_{\Delta E_{g'}}dE'\,\Sigma_s(\bar{r},E'\to E)\,\psi_{g'}^k(E')\right]\phi_{g'}(\bar{r})\right. \qquad \text{Eq. MG.8}$$

$$g=1,2\ldots G$$

We now define the "group parameters"

$$D_g^k(\bar{r}) = \int_{\Delta E_g} D(\bar{r},E)\,\psi_g^k(E)\,dE \qquad \text{Eq. MG.9}$$

$$\Sigma_{tg}^k(\bar{r}) = \int_{\Delta E_g}\Sigma_t(\bar{r},E)\,\psi_g^k(E)\,dE \qquad \text{Eq. MG.10}$$

$$\chi_g^j = \int_{\Delta E_g}\chi^j(E)\,dE \qquad \text{Eq. MG.11}$$

$$\nu^j\Sigma_{fg}^{jk}(r) = \int_{\Delta E_g}\nu^j\Sigma_f^j(\bar{r},E)\,\psi_g^k(E)\,dE \qquad \text{Eq. MG.12}$$

$$\Sigma_{gg'}^k(\bar{r}) = \int_{\Delta E_{g'}}dE\int_{\Delta E_g}dE'\,\Sigma_s(\bar{r},E'\to E)\,\psi_g^k(E') \qquad \text{Eq. MG.13}$$

Since it is assumed that we know the $\psi^k(E)$ and that D(r,E), Σ_t(r,E), etc., are known(*) from the nuclear data and the isotopic concentration of materials throughout the reactor, all these group parameters are known.

Substitution of the "group parameters" into the integral equation (Eq. MG.8) yields the general form of the energy-group diffusion equation (Eq. MG-14).

$$-\left[D_g^k(\vec{r}) \nabla \phi_g(\vec{r}) \right] + \Sigma_{tg}^k(\vec{r}) \phi_g(\vec{r}) =$$

$$\sum_{g'=1}^{G} \left\{ \frac{1}{\lambda} \sum_j \chi_j^k \nu^j \Sigma_{fg'}^{jk}(\vec{r}) + \Sigma_{gg'}^k(\vec{r}) \right\} \phi_{g'}(\vec{r}) \qquad \text{Eq. MG.14}$$

The continuity conditions on the $\phi_g(\vec{r})$ are obtained from those imposed on $\phi(\vec{r},E)$ in the classical and conventional way.

This is generally <u>not</u> true. In a true multigroup calculation, D(E) is generated <u>after</u> the slowing down spectrum has been calculated using transport theory (Ref. 8).

MG.2 MULTI-GROUP THEORY AND ITS LIMITATION

The multi-group theory is one in which:

- For a given energy group g, the $\phi_g(E)$ is used throughout the reactor (i.e., superscript k is dropped).

- The "energy shape" for each $\psi_g(E)$ (i.e., a plot of $\psi_g(E)$ versus E in the region ΔE_g) is taken to be the same for reactors to which the energy-group diffusion equation is applied.

Once the shapes of $\psi_g(E)$ are chosen, it is possible to compute and tabulate microscopic multigroup cross-sections σ_{dg}^{j} for reaction d of isotope J in energy group g. The corresponding macroscopic multi-group cross-sections can then be written as a sum of microscopic cross-sections multiplied by local number densities. We have, for example:

$$\Sigma_{tg}(\bar{r}) = \sum_j \eta^j(\bar{r})\sigma_{tg}^{j} \qquad \text{Eq. MG.15}$$

Thus, all the multi-group parameters $D_g(r)$, $\Sigma_{tg}(r)$, etc. in the energy-group diffusion equation can be obtained from a knowledge of the local concentrations of isotopes $\eta^j(\bar{r})$, the microscopic cross-sections for the various processes in each energy group being permanently tabulated as a "cross-section library".

The multi-group diffusion theory is capable of predicting neutron behaviour throughout the reactor with an accuracy limited only by the validity of the diffusion theory approximation and by the quality of the basic nuclear data. In practice, it is also limited by the expense of solving the multi-group diffusion equations. In practice, the only method for solving the spatial part of the equations for a multi-dimensional, multi-compositional reactor is to convert the differential Eq. MG.14 into the same form of difference equation. The ultimate set of equations is thus algebraic. However, the number of unknown is roughly equal to the number of spatial mesh points multiplied by the number of energy groups; moreover, the equations containing these unknowns are coupled together. It is not today realistic to attempt a solution for a problem involving, say, a hundred thousand spatial mesh points and two thousand energy groups in three dimensions.

MG.3 TWO-GROUP THEORY

The basic principle of the two-group diffusion theory is based on the fact that two energy groups are chosen to characterize the energy dependence in a reactor. One is chosen to characterize fast neutrons and the other for thermal neutrons. The cut-off energy for the thermal group is chosen sufficiently high such that upscattering out of the thermal group can be ignored. This corresponds to an energy of about 1 eV in water-moderated reactors, but it may range as high as 3 eV in high-temperature gas-cooled reactors (HTGCR). Mathematically, the assumptions of two-group diffusion theory may be summarized as follows:

The scalar flux function may be written at point r in the system as

$$\phi_1(\bar{r}) = \int_{E_c}^{\infty} dE\, \phi(\bar{r},E) \equiv \text{fast flux} \qquad \text{Eq. MG.16}$$

$$\phi_2(\bar{r}) = \int_{0}^{E_c} dE\, \phi(\bar{r},E) \equiv \text{thermal flux} \qquad \text{Eq. MG.17}$$

Physically, $\phi_1(\bar{r})$ is the two-group approximation to the number of neutrons per cc having energies in the range E_c to , $[\int_{E_c}^{\infty} dE\, n(\bar{r},E)]$, multiplied by the average "fast" speed

$$v_1 = \frac{\int_{E_g}^{\infty} v(E)\, n(\bar{r},E)\, dE}{\int_{E_c}^{\infty} n(\bar{r},E)\, dE} \qquad \text{Eq. MG.18}$$

and $\phi_2(\bar{r})$ is the two-group approximation to the number of neutrons in the range 0 to E_c multiplied by the average thermal speed

$$v_2 = \frac{\int_0^{E_c} v(E)\, n(\bar{r}, E)\, dE}{\int_0^{E_c} n(\bar{r}, E)\, dE} \qquad \text{Eq. MG.19}$$

From the previous section, it is possible to write the following set of equations that are at the base of most activities in thermal reactor design:

$$-D^k(E)\,\psi_1^k(E)\,\nabla^2\phi_1(\bar{r}) + \Sigma_t^k(E)\,\psi_1^k(E)\,\phi_1(\bar{r})$$
$$= \int_{E_c}^{\infty}\left[\frac{1}{\lambda}\chi^k(E)\,\nu\Sigma_f^k(E') + \Sigma_s^k(E'\to E)\,\psi_1^k(E')\right]dE'\phi_1(r)$$
$$+ \int_{E_c}^{\infty}\left[\frac{1}{\lambda}\chi^k(E)\,\nu\Sigma_f^k(E')\,\psi_2(E')\right]dE'\phi_2(r) \qquad \text{Eq. MG.20}$$

for $E > E_c$

and

$$-D^k(E)\,\psi_2^k(E)\,\nabla^2\phi_2(\bar{r}) + \Sigma_t^k(E)\,\psi_2^k(E)\,\phi_2(\bar{r})$$
$$= \int_0^{E_c}\left[\frac{1}{\lambda}\chi^k(E)\,\nu\Sigma_f^k(E')\,\psi_1^k(E') + \Sigma_s^k(E'\to E)\,\psi_1^k(E')\right]dE'\phi_1^k(\bar{r})$$
$$+ \int_0^{E_c}\left[\frac{1}{\lambda}\chi^k(E)\,\nu\Sigma_f^k(E')\,\psi_2^k(E) + \Sigma_s^k(E'\to E)\,\psi_2^k(E')\right]dE'\phi_2^k(\bar{r})$$

for $E < E_c$. Eq. MG.21

For thermal reactors, the cutpoint is always such that $\chi^k(E)$ is zero for $E<E_c$; hence, no fission terms will appear in Eq. MG.21. The fission terms are now retained for generality in case of possible application to fast reactors.

Defining as was done for multi-group diffusion theory, the "two-group constants" we will get are:

$$D_1^k \equiv \int_{E_c}^{\infty} D(E)\,\psi_1^k(E)\,dE$$

$$D_2^k \equiv \int_{0}^{E_c} D(E)\,\psi_2^k(E)\,dE$$

$$\Sigma_{t1}^k \equiv \int_{E_c}^{\infty} \Sigma_t^k(E)\,\psi_1^k(E)\,dE$$

$$\Sigma_{t2}^k \equiv \int_{0}^{E_c} \Sigma_t^k(E)\,\psi_2^k(E)\,dE$$

$$\chi_1^k \equiv \int_{E_c}^{\infty} \chi^k(E)\,dE$$

$$\chi_2^k \equiv \int_{0}^{E_c} \chi^k(E)\,dE$$

Eq. MG.22
to MG.27

$$\nu\Sigma_{f1}^{k} \equiv \int_{Ec}^{\infty} \nu\Sigma_{f}^{k}(E)\,\psi^{k}(E)\,dE$$

$$\nu\Sigma_{f2}^{k} \equiv \int_{0}^{Ec} \nu\Sigma_{f}^{k}(E)\,\psi_{2}(E)\,dE$$

$$\Sigma_{11}^{k} \equiv \int_{Ec}^{\infty} dE \int_{Ec}^{\infty} dE'\,\Sigma_{s}^{k}(E'\rightarrow E)\,\psi_{1}^{k}(E)$$

$$\Sigma_{22}^{k} \equiv \int_{0}^{Ec} dE \int_{0}^{Ec} dE'\,\Sigma_{s}^{k}(E'\rightarrow E)\,\psi_{2}^{k}(E')$$

$$\Sigma_{21}^{k} \equiv \int_{0}^{Ec} dE \int_{0}^{Ec} dE'\,\Sigma_{s}^{k}(E'\rightarrow E)\,\psi_{1}^{k}(E)$$

$$\Sigma_{1}^{k} \equiv \Sigma_{t1}^{k} - \Sigma_{11}^{k}$$

$$\Sigma_{2}^{k} \equiv \Sigma_{t2}^{k} - \Sigma_{22}^{k}$$

Eq. MG.28 to MG.34

Using these definitions, and performing the appropriate integration of Eq. MG-20 and Eq. MG.21, we will get:

$$-D_{1}^{k}\nabla^{2}\phi_{1}(\vec{r}) + \Sigma_{1}^{k}\phi_{1}(\vec{r}) = \frac{1}{\lambda}\chi_{1}^{k}\left[\nu\Sigma_{f1}^{k}(r)\phi_{1} + \nu\Sigma_{f2}^{k}\phi_{2}(\vec{r})\right]$$ Eq. MG.35

$$-D_{2}^{k}\nabla^{2}\phi_{2}(\vec{r}) + \Sigma_{2}^{k}\phi_{2}(\vec{r}) = \frac{1}{\lambda}\chi_{2}^{k}\left[\nu\Sigma_{f1}^{k}\phi_{1}(\vec{r}) + \nu\Sigma_{f2}\phi_{2}(\vec{r})\right] + \Sigma_{21}^{k}\phi_{1}(\vec{r})$$

Eq. MG.36

These two generalized two-group diffusion equations have the following boundary conditions:

- $\phi_1(\vec{r})$, $\phi_2(\vec{r})$ are continuous everywhere;

- $n \cdot D \nabla \phi_1(\vec{r})$ and $n \cdot D_2 \nabla \phi_2(\vec{r})$ must be continuous across interfaces separating different material compositions.

- $\phi_1(\vec{r}) = \phi_2(\vec{r}) = 0$ on the outer boundary of the reactor.

The solution of the two-group diffusion equation is usually performed by converting them into a set of algebraic equations by finite-difference methods and then solving these by using a digital computer. The computer code that is used to solve the two-group diffusion equations for CANDU-PHW reactors is called CHEBY. A speedier version calculating also higher than fundamental modes is called MONIC (Ref. G. Kugler, #25)

APPENDIX G

GLOSSARY

ADJUSTER RODS — Control rods normally fully inserted into the core; they can be withdrawn for the purpose of providing positive reactivity for xenon override or reactivity shim.

BIDIRECTIONAL FUELLING — Adjacent channels are refuelled in opposite directions.

BOOSTER RODS — Rods of highly enriched uranium which provide positive reactivity when inserted into the core for xenon override or reactivity shim. CANDU reactors have either booster rods or adjuster rods, but not both.

BUNDLE POWER ENVELOPE — A fictitious bundle power history which gives a power for every burnup which is greater than or equal to the power produced by any bundle in the core at any time which has that burnup.

BUNDLE SHIFTING SCHEME — The number of new bundles charged to a channel at one fuelling. For example, in an "eight-bundle shift", eight bundles are inserted into one end of the channel; the bundles in the channel are shifted along by eight positions and eight irradiated bundles are discharged.

BURNUP — The integrated thermal energy produced by the fuel per unit mass of heavy elements initially in the fuel. It is usually expressed in MWh/kg or MWd/kg.

CALANDRIA — Cylindrical vessel which holds the moderator. It is also called the reactor vessel.

CALANDRIA TUBES — Zirconium alloy tube which surrounds the pressure tube. It separates the cold moderator from the pressure tube containing the hot coolant.

CHANNEL AGE — The fraction of dwell time for a channel since its last refuelling.

CHANNEL POWER PEAKING FACTOR (CPPF) — The ratio of the channel power at a particular time to the reference channel power for that channel. The CPPF for a region, or the whole core, is taken as the maximum CPPF of all channels in the region.

CONTINUOUS BIDIRECTIONAL FUELLING — An approximation used in calculations which assumes the fuel moves continuously through the channels, in opposite directions in adjacent channels.

CORE CODE	A computer program which computes flux distribution and reactivity from lattice cell cross-sections, using discrete diffusion theory.
DEPLETED FUEL BUNDLES	Fuel bundles having U-235 concentration lower than natural uranium, used for flux flattening or for fuel defects replacement.
DISCHARGE BURNUP	The burnup corresponding to the discharge irradiation.
DISCHARGE IRRADIATION	Average irradiation of fuel bundles discharged from a channel. As an approximation in calculations, the average discharge irradiation in a region is fixed at constant value. It is often referred to as "exit irradiation".
DWELL TIME	The length of time between fuellings for a channel in full power days.
FLUX DISTRIBUTION	The set of neutron flux values at various points in the reactor core.

FLUX-SQUARED-WEIGHTED-MEAN — The integral of the flux over the core, weighted by the flux squared.

FRESH CORE — Core consisting entirely of unirradiated (fresh) fuel.

FRESH FUEL — Unirradiated fuel

FUEL — The fissionable material, uranium or plutonium, which generates the heat and the neutrons to sustain the chain reaction, in the form of a metal or oxide.

FUEL BUNDLE — Assembly of fuel elements into a single structural unit. There are 28 or 37 fuel elements in commercial CANDU fuel bundles. The bundles are about 0.5 m long and 0.1 m in diameter.

FUEL CHANNEL — Assembly of pressure tube containing the fuel bundles, associated fittings, feeders, closures and other hardware. Also used loosely to mean the pressure tube containing the fuel.

FUEL DEFECT — Any hole, crack or leak in the fuel sheath which allows the escape of fission products. Also called fuel failure.

FUEL ELEMENT — Rod of zirconium alloy (sheath) and the cylindrical pellets of fuel material, usually UO_2, contained therein.

FUEL HANDLING SYSTEM — All the mechanisms which take part in charging the fuel to the reactor, and removing irradiated fuel. It includes new and irradiated fuel bays, transfer mechanism, trolleys, fuelling machines, fuelling machine carriages, and associated cooling, hydraulic and electrical systems and control computers.

FUEL SCHEDULING — The selection of channels for fuelling during the operation of a reactor.

FUELLING — The act of charging fresh fuel to the reactor and removing spent fuel. It is done on-power in CANDU reactors. The term "refuelling" is sometimes used interchangeably with "fuelling". The act of putting fuel into the fresh core is referred to as "fuel loading" rather than "fuelling", and is usually done manually.

FUELLING MACHINE — Mechanical device for charging new fuel to a fuel channel and removing irradiated fuel. Fuelling machines usually work in pairs, one at each end of the channel.

FUELLING RATE — Number of channels or bundles which must be fuelled per unit time to keep the reactor critical.

FUELLING SCHEME — A more general term than "bundle shifting scheme". It refers to the replacement pattern of fuel in the channel and applies to systems where schemes more elaborate than simple push-through fuelling are allowed.

FUELLING STRATEGY — The selection of channels for fuelling, or the set of rules by which channels are selected for fuelling.

FULL-POWER DAY (FPD) — The energy generated in 24 hours of normal full-power operation.

INITIAL CORE — Core which has not been refuelled. The "initial core" extends from the fresh core to onset of fuelling.

INITIAL FUEL LOADING — Pattern of depleted and natural fuel bundles in the initial core.

INSTANTANEOUS POWER DISTRIBUTION — The power distribution at a particular time in a real reactor, or a power distribution calculated with a varying irradiation distribution.

IRRADIATION — The integrated flux to which the real fuel has been exposed. It is usually expressed in units of neutrons/kilobarn (n/Kb). Since burnup and irradiation are almost directly proportional, they are frequently used in qualitative discussions.

LATTICE CELL — See **UNIT CELL.**

LATTICE CELL CODE — A computer program which computes neutron balance and flux distribution for a unit cell in an infinite repeating array of unit cells. These codes are used to calculate cross-sections as functions of irradiations.

LIQUID ZONE CONTROLLERS — Tubes in the core having compartments partially filled with light water. Reactivity is controlled by emptying or filling the compartments.

NOMINAL POWER DISTRIBUTION	The time-averaged or reference power distribution used in the CPPF and other calculations. The ROP design and fuelling strategy are based on this distribution.
ONSET OF FUELLING	Time at which the core is first fuelled. It must occur before the excess reactivity has dropped below zero.
OVERPOWER	Fuel bundle or channel power in excess of specified safety related limits.
POWER DISTRIBUTION	The variation of the relative value of bundle (or channel) power from point to point in the core.
POWDERPUFS	A computer code used for lattice cell calculations for CANDU reactors.
PRESSURE TUBES	Zirconium alloy tube which runs horizontally through the core. It contains fuel bundles and coolant.
REGIONAL OVERPOWER SYSTEM (ROP)	The system which detects an overpower condition somewhere in the core and causes a rapid shutdown (trip).

RESIDENCE TIME — Length of time a bundle has resided in the core in full-power days.

SHEATH — The rod which contains fuel pellets, usually made of zirconium alloy. It provides structural support for the fuel and prevents escape of fission products. It is sometimes called "clad" or "cladding".

SMOKIN — A computer code which simulates reactor transients by expanding the flux distribution in a series of modes based on the higher harmonics of the diffusion equation.

SPENT FUEL — Fuel which has been irradiated in the core and discharged. Fuel is usually discharged because of low reactivity (high burnup) or because of a defect detected in the channel. Fuel bundles are not recycled in current CANDU reactors, so all discharged fuel bundles are "spent fuel".

SUPERCELL — A special unit cell which contains a reactivity device in addition to the fuel channel. Since the reactivity devices are perpendicular to the fuel channels, the supercell is inherently three-dimensional and requires special computer programs for calculations of the cross-section.

TILT — An imbalance in the power between one location in the core and the symmetrically opposite location.

TIME AVERAGED POWER DISTRIBUTION — The power distribution of channels or bundles, averaged over a sufficiently long time. For an equilibrium core, the time averaged power distribution is a constant.

TRIP — A rapid shutdown of the reactor in response to the detection of certain abnormal and potentially dangerous conditions.

UNIT CELL — A fuel bundle, pressure tube and calandria tube and associated coolant and moderator, used in the calculation of cross-sections by lattice cell code. It is also called "lattice cell".

APPENDIX EN

WORLD ENERGY AND ITS NUCLEAR CONTRIBUTION

EN.1 INTRODUCTION

As late as 1810, about three quarters of all energy used by society was still coming from fuel wood, but the transition to coal was under way and coal soon became the dominant source. What was of primary significance in this transition was not that coal could be substituted for wood in existing energy use, but rather that this was a change from a fuel resource severely limited in supply to another in apparently endless amounts. The use of coal thus opened the way for the large-scale, unimpeded growth of iron and steel production.

Ample supplies of iron and steel, in turn, made it possible to build and operate a railroad network that blanketed the country and to produce the machines required for the expansion of manufacturing. Once the fuel constraint was broken, one development led to another - a dynamic sequence that laid the foundation for modern industrial society.

In a similar way, with the expansion of liquid fuels and electricity, other constraints to economic growth were overcome. Electricity and the electric motor made possible productivity increase in manufacturing by replacing power drives by shafts and belting from the in-house prime mover. With the liquid hydrocarbons, the tractors and synthetic fertilizers enabled agricultural production increase beyond the limits set by the natural fertilizers, animal draft power and hard manual

labour. Geographical constraints were removed by the railways, motor vehicles and aircraft which have enabled raw materials, finished goods and people to move freely, and, with air conditioning, previously hostile environments with extremes of heat or cold can now be more readily settled and developed.

The energy demand has steadily increased and the following four statements illustrate the demand growth rate over a generation or so (Ref. 36, 37, 38, 39, 40):

- For the grandparents ... who found 110 kWh/capita/day was more than adequate.

- For the parents ... who thought 150 kWh/capita/day was about right.

- For the brothers and sisters ... who have been doing well on 250 kWh/capita/day.

- For the children ... who will probably feel like they are having to skimp at 350 kWh/capita/day.

Demand, dependent as it is upon the nature of society, technical development, economic cycles and major events of the time, is not easy to foretell. Nevertheless, certain trends and influences seem clear: economic development is still vital, and people everywhere want the improvements it can bring. The

poor want the products and services which make life less precarious, less arduous, and more interesting; the more affluent want increased personal services, additional cultural activity and improved care of the environment in order to enjoy a fuller life in an unspoiled world. All want greater justice and harmony, which no economic progress can ensure, but which economic progress can make possible. But the quest for these goals on a universal scale will require increasing amounts of energy for a long time to come.

This increasing demand for energy is, unfortunately, preparing society for some limitations in the conventional primary energy resources, as historical production peaks are already established.

The peak of world production of crude oil is expected to occur at about year 2000 and that for coal production at about year 2150 or 2200. The conventional oil, which accounts for 40% of primary energy, will decline by the year 2020 to about 10%. Natural gas may provide 20% of prime energy by the year 2020. Based on these marginal considerations, we may conclude that two thirds of the energy supply will have to be provided from alternate energy sources (Ref. 41, 42, 43).

Coal, nuclear and solar energy are the most suitable candidates for providing the above world energy needs by the year 2020. The production of coal will be required to increase by more

than three times. Experts in the field of coal see the required increase in production as allowable, but only if major efforts are made in the development of mines and supply infrastructures. Coal should provide about one quarter of the world's energy supply by the year 2020. Solar energy in all its forms and geothermal energy will provide as much energy as the primary energy equivalent of all the electric energy used today, or, in oil equivalent, equal to two thirds of the world's annual oil production today. It is predicted that around 30% of primary energy supply will be provided by nuclear energy from fission.

EN.2 WORLD ENERGY PROFILE

The basic forces pushing up energy demand are population and increase in economic growth. From an assessment of these, it is possible to estimate future energy requirements.

One indication of future growth of demand by IIASA (International Institute of Advance System Analysis) is based upon a population increase rising from four billion in 1975 to six billion in 2000, and eventually levelling off at something over ten billion by the year 2070 as indicated by Figure EN.1 (Ref. 44, 45).

Gross World Product (GWP) growth rate (high and low) scenarios are reported to be 4.1% and 3.0% respectively over the period 1975–2020 (Cavendish Model). The complete GWP growth rates in the Cavendish Report are reported here for convenience by Table EN.1 (Ref. 44, 45).

TABLE EN.1: GWP Growth Rates, (%), Cavendish Report

	OECD	CENTRALLY PLANNED ECONOMY NATIONS	DEVELOPING NATIONS	WORLD
High Growth Rate	3.7	4.5	5.3	4.1
Low Growth Rate	2.8	3.2	3.8	3.0

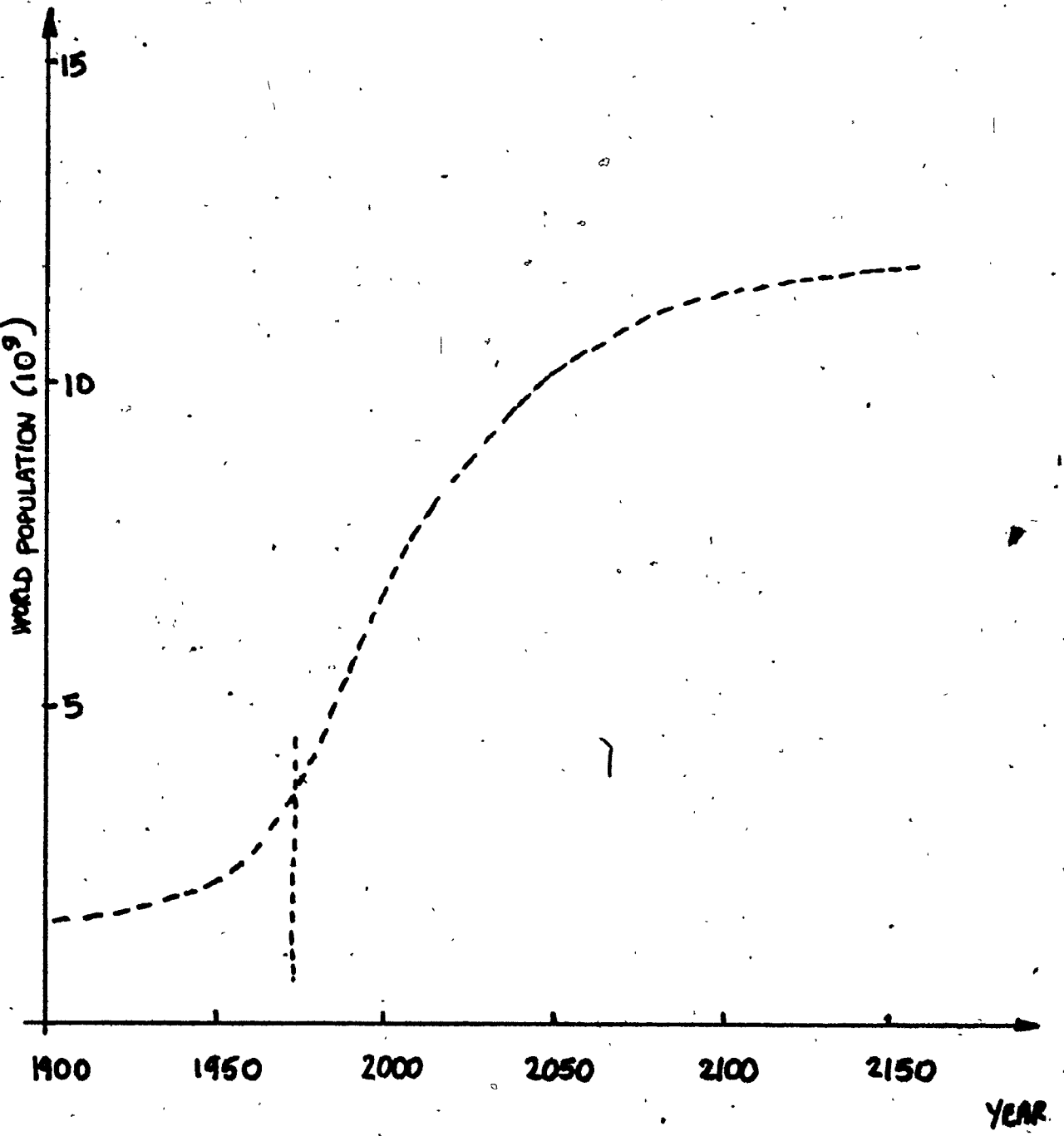

FIGURE EN.1: World Population Growth

The Conservation Commission of the World Energy Conference (WEC) considered that the Cavendish projections, not taking sufficient account of a changing relationship between economic growth and energy input, may overestimate the energy demand for the industrialized countries and underestimate the energy demand of the developing nations. Taking rather high economic growth rates of 4.2% per year for OECD, 3.3% per year for centrally-planned economy nations, and 5.7% for the developing countries, the following scenario demand projection resulted (Table EN.2):

TABLE EN.2: Scenario Demand Projection

YEAR	PRIMARY ENERGY DEMAND (EXAJOULES)			
	OECD	CENTRALLY PLANNED ECONOMY NATIONS	DEVELOPING NATIONS	WORLD
1972	150	66	27	243
1980	178	86	46	310
1990	212	120	86	418
2000	242	167	152	561
2010	262	233	253	748
2020	278	325	397	1000

1 EXAJOULE = 10^{18}J

Table EN.3 (Ref. 36) illustrates the world primary energy production and consumption over the period 1972-2020.

TABLE EN.3

WORLD PRIMARY ENERGY PRODUCTION (EJ)				
YEAR / RESOURCE	1972	1985	2000	2020
Coal	66	115	170	259
Oil	115	216	195	106
Gas	46	77	143	125
Nuclear	2	23	88	314
Hydraulic	14	24	34	56
Unconventional Oil-Gas	0	0	4	40
Renewable (Solar, Geothermal)	26	33	56	100
TOTAL	269	488	690	1000

Table EN.4 (Ref. 36) illustrates the world primary energy production over the period 1972-2020.

TABLE EN.4: (Canadian Forum on Energy)

WORLD PRIMARY ENERGY PRODUCTION (EJ)				
YEAR / RESOURCE	1972	1985	2000	2020
Coal	66	115	170	259
Oil	115	146	146	125
Gas	46	77	143	125
Unconventional Oil-Gas	0	0	7	44
Nuclear	2	23	44	157
Hydraulic	14	24	34	56
Renewable (Solar, (Geoth., Biomass)	26	33	56	100
TOTAL	269	418	600	866

Table EN.5 is provided to illustrate the energy sources as a percentage of total in the year 2000 and increase over 1972 (from Table EN.4).

TABLE EN.5

RESOURCE	% SHARE IN 2000	INCREASE OVER 1972
Coal	24.6	x 2.6
Oil	28.3	x 1.7
Gas	20.7	x 3.1
Nuclear	12.8	x 44
Hydro and Other	13.6	x 4.4

EN.3 PERSPECTIVES OF NUCLEAR POWER

It is well recognized that nuclear power will certainly make a significant contribution to the world energy demand around the turn XXth and during the XXIst Centuries. The technology of nuclear energy has developed to the point where nuclear power reactors operating on a once-through fuel cycle and using uranium as primary fuel are a commercial reality.

By the beginning of 1979, there were over 220 power reactors (Ref. 44) in operation in 22 countries, with a total capacity of just over 120 GW(e).

When the nuclear power plants now under construction or on order are included, the nuclear power capacity increases nearly fourfold to 420 GW(e) from 549 stations in 31 countries (Ref. 44).

Nuclear power is already making a substantial contribution towards electricity supply. In some countries, such as Belgium, Sweden, Switzerland, U.S.A. and Canada, nuclear electricity already accounts for over 1000 kWh per capita, that is, 20% of the total electricity. The reasons for the rapid growth of nuclear power are primarily of an economic nature. Nuclear power generates electricity at a lower cost than other fuels and also reduces dependence on fuel imports. The first point

is of prime importance to the individual utility companies; the second is often seen as a matter of national economic policy.

The cost structure of nuclear power differs from conventional power in that the nuclear power stations have a high initial capital cost but low fuel cost, whereas a conventional fossil-fired station has lower capital cost but much higher fuel costs.

Countries with national electricity boards are less affected by movements in interest rates since the nuclear ordering programme is treated as a matter of national policy for which government provides the funds directly or backs commercial loans.

With the higher interest and inflation rates now being experienced in many countries, the additional costs of financing will be even higher for those countries without national electricity boards. It is under this consideration that strong emphasis is needed to reduce delays in the licensing and regulatory procedures once construction has started.

There are nuclear power plants that have been built in four to five years - Japan and Switzerland. In the United States, delays in construction are remarkably high - twelve to fourteen years are now required for completion to commercial operation.

First, technical factors arising from the rapid increase in plant size and a continuing lack of standardization of plant design; second, the increasing number and stringency of safety and environmental regulations, the linkage of power plant licensing to the resolution of the nuclear waste disposal issue, and the continuing fluidity and uncertainty surrounding the content and application of regulations.

Of particular importance is the effect of regulatory changes during construction and design with the "ratchetting" and "backfitting" that this entails. This 12-14 year construction time, combined with high interest rates, has temporarily halted the nuclear ordering in many countries. Minimization of construction time, design standardization, the high costs of fossil fuels, the environmental effects of fossil power plants, the reduced inflation associated with nuclear fuel, the importance of nuclear power from a national point of view in that it can reduce the dependence on imported fuel, are but a few promising factors to encourage the development of nuclear energy.

In some countries, the dependence on fuel imports is very high. As of 1975, the majority of European countries had not more than 30% self-sufficiency in energy. The United States hardly exceeded 85% self-sufficiency.

A very attractive characteristic of nuclear fuel, besides the fact of being a strong contributor to leading the world nations to self-sufficiency, is that it is widespread and that there is a number of competing suppliers offering fuel cycle services. It would, in any case (with the much smaller quantities involved), be relatively easy for an importing country to store several years of supply of nuclear fuel.

By the year 2000, the Korean electrical demand growth rate will not decline to less than 12%. Brazil is another rapidly developing country which, over the past ten years, has experienced electrical growth rates averaging over 10% per year.

The World Energy Conference (WEC) adopts more modest growth rates for their forecast of world electrical demand.

Table EN.6 provides the estimates adopted by WEC.

TABLE EN.6: Estimated Potential World Electrical Demand
(Exajoules Electrical Output)

WORLD REGIONS	1972	2000	2020	AVERAGE GROWTH RATE 1972-2020
OECD Countries	14.1	40	77	3.6
Centrally-Planned Economies	4.7	28	64	5.6
Developing Nations	1.7	9	32	6.3
TOTAL	20.5	77	173	4.5

(Ref. World Energy to 2090 WEC).

By the year 2000, the assumed 77 EJ for the world electrical demand would correspond to some 220 EJ.

EN.4 HOW MUCH NUCLEAR POWER IN THE YEAR 2000? A QUANTITATIVE ANALYSIS

The number of nuclear power plants that will be required in the year 2000 depends on world power requirements, the degree of energy self-sufficiency that nations will reach, the number that can be built, etc. Until the end of this century, nuclear energy will be used mainly for generation of electricity. Electricity demand growth rates throughout the world are very different. Up to 1975, there were countries that experienced electrical energy demand growth rates as high as 18% (Korea), and it is expected that of primary energy, about 40% of primary energy demand. In our days (1980's), the percentage of primary energy transferred into electricity is about 30% for OECD.

Nuclear power now provides about 4% of the world's electrical requirements, mostly in the industrially advanced countries. An estimation of how rapidly nuclear technology could replace conventional technology for the production of electricity is provided by the Fisher model.

The fraction of electricity produced by nuclear means and the total installed nuclear power [GW(e)] are indicated by Tables EN.7 and EN.8 respectively.

TABLE EN.7: Fraction of Electricity Produced by Nuclear Means

WORLD REGION	1975	1985	2000	2020
1. North America	0.08	0.26	0.48	0.50
2. Western Europe	0.07	0.16	0.36	0.48
3. Japan, Australia, New Zealand	0.05	0.21	0.46	0.50
4. U.S.S.R. & Eastern Europe	0.01	0.07	0.37	0.50
5. China & Communist Asia	-	-	0.04	0.08
6. OPEC	-	0.12	0.37	0.50
7. Latin America	-	0.15	0.37	0.47
8. Middle East & North Africa	-	0.07	0.27	0.40
9. Africa South of Sahara	-	0.13	0.31	0.49
10. East Asia	-	0.12	0.35	0.49
11. South Asia	-	0.14	0.37	0.46

TABLE EN.8: Installed Nuclear Power [GW(e)]

WORLD REGIONS		2000	2020
OECD	68	800	3225
Centrally-Planned Economy	7	560	1850
Developing Nations	1	180	925
TOTAL	76	1540	5000

The World Energy Conference believes that by the year 2000 the fraction of electrical energy supplied by nuclear power will lean towards 45%. If this percentage is pushed up to the region of 50%, an installed nuclear capacity of between 1450-2100 GW(e) results. Other studies in the field, however, indicate that installed capacity of between 900-2000 are also possible.

Regardless of which projection we select, an important question always to be asked is associated with the time factor, which, for many countries, is a major constraint. A time range of the order of 8-10 years seems to be required for almost any new energy project.

This means that, even with a lead time of ten years, new nuclear programmes even started today can hardly begin to make a contribution to world energy supplies by the early 1990's. It must then be assumed that it is only the plants being planned and ordered by 1990 that will come into operation in the next ten-year period, 1990-2000.

On this time scale, it is unlikely that there will be any major advance in nuclear technology.

There could, with large programmes, be a greater incentive towards standardization of design, in particular for the specification and manufacture of key components and systems.

APPENDIX F

U-238 AND Th-232 FUEL CYCLE DIFFERENCES

F.1 PHYSICS DIFFERENCES BETWEEN U-238 AND Th-232 IN THERMAL REACTORS

In order to understand some of the questions involved, an understanding of the major differences between U-238 and Th-232 is useful. These include the following (it should be noted that we are referring only to thermal reactors. The situation in fast reactors, where U-238 is clearly the preferred fertile material, is quite different):

a) U-238 occurs in conjunction with a fissile isotope U-235, in natural uranium, but natural thorium consists entirely of the fertile isotope with no fissile component. As already pointed out, this gives U-238 an enormous advantage for use in early reactor units.

b) The physics properties of the two fertile isotopes differ in several respects. Some of these are:

   i) The effective absorption cross-section of Th-232 in typical CANDU spectra is some three times that of U-238, and is less sensitive to hardness of the spectrum. This tends to be an advantage in keeping parasitic absorption low and permits somewhat greater design freedom. However, the amount of enrichment required is correspondingly larger than in natural uranium.

ii) The fast fission effect, whereby some fissions are caused in the fertile material by fast neutrons, is smaller in thorium than uranium. This is, in general, a disadvantage for thorium, although under certain circumstances, e.g. in terms of void effects, it can be an advantage. It is a relatively unimportant effect.

iii) Both U-238 and Th-232 go through intermediate products after absorbing a neutron before the fissile isotope forms. These intermediate products are Pa-233 in the case of Th-232, and Np-239 in the case of U-238. These intermediate products have quite different half-lives - 27.4 d for Pa-233 and 2.35 d for Np-239. This means that there is a significant hold-up of Pa-233 in a reactor using thorium. This Pa-233 inventory reduces the efficiency of the fissile material production, and can lead to large, slow reactivity and flux distortions associated with power changes, shutdowns, fuel management, etc. The analogous effect in a reactor using U-238, associated with Np-239, is less important.

Figures F.1 and F.2 illustrate the thorium and uranium fuel cycles (Ref. 6).

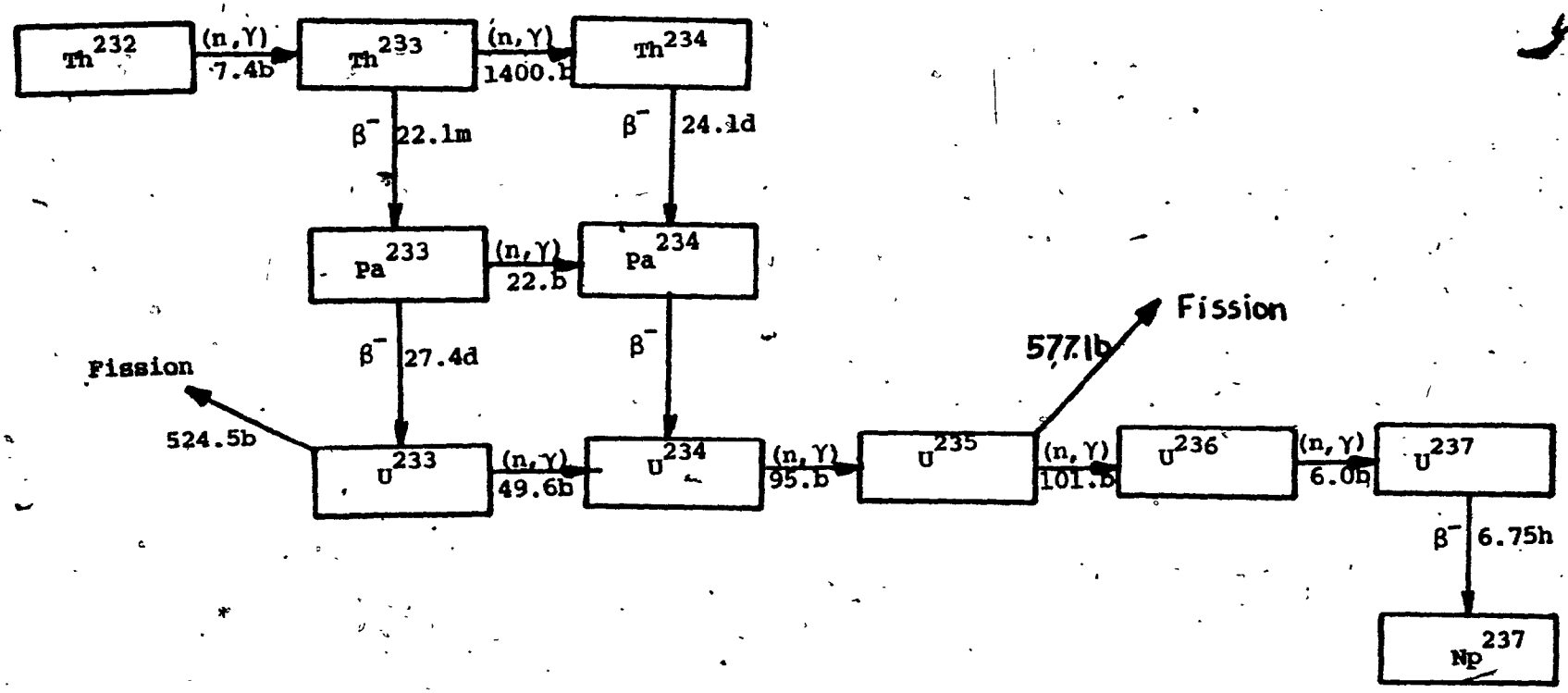

FIGURE F.1: The Chain of Isotopes Created by Neutron Irradiation of Th^{232}

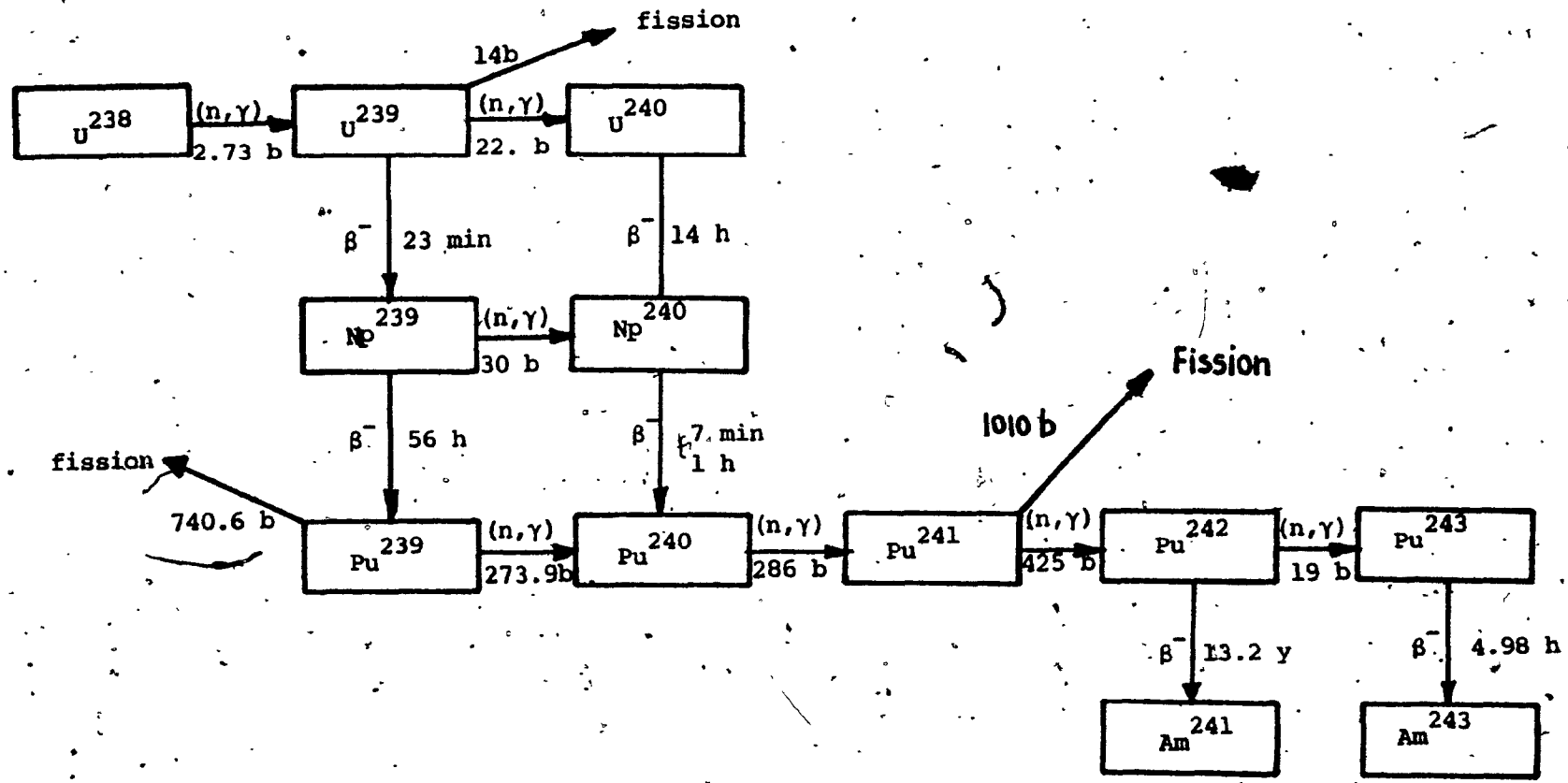

FIGURE F.2: The Chain of Isotopes Created by Neutron Irradiation of U^{238}

c) The fissile isotopes produced from the two fertile materials are different. U-238 yields plutonium (Pu-239 and Pu-241), whereas Th-232 yields U-233. These fissile products have quite different properties and these differences must also be considered when choosing between the fertile isotopes.

i) The neutron yield per neutron absorbed is higher for U-233 than for plutonium. This means that a higher conversion efficiency can be obtained with U-233 than plutonium. This is a very important advantage of U-233 over plutonium and, hence, of thorium over U-238 (once again, this is true in thermal reactors only).

ii) Plutonium has a higher cross-section - both absorption and fission - than U-233. This is not an important point and has both advantages and disadvantages.

iii) The chain of plutonium isotopes following Pu-239 (i.e., Pu-240, Pu-241, Pu-242) plays a larger role with respect to reactor characteristics than that of uranium isotopes following U-233 (i.e., U-234, U-235, U-236).

Figure F.3 illustrates the neutron yields (Ref. 6),

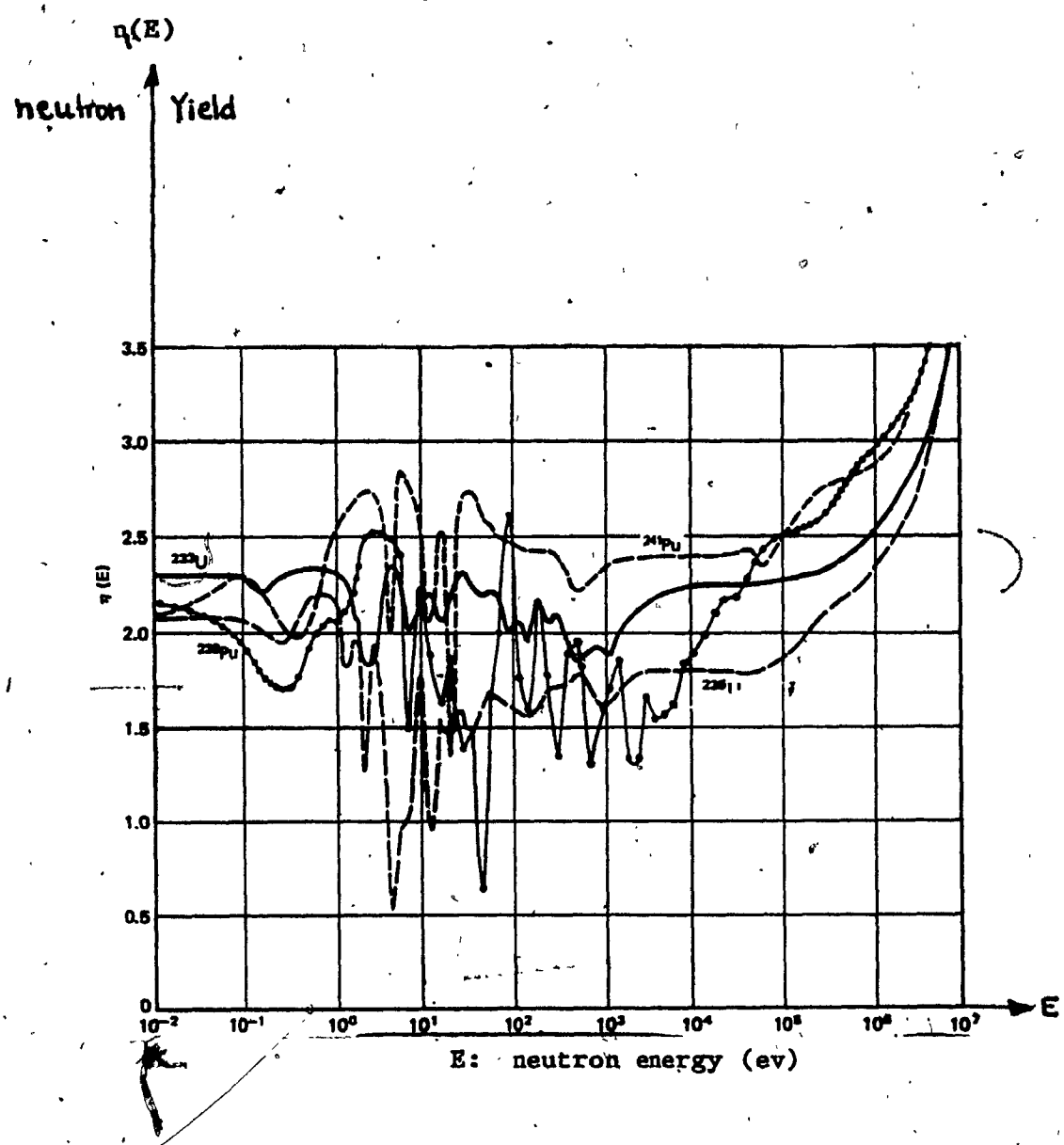

FIGURE F.3: Variation of n with Neutron Energy

d) Other irradiation products from the two materials are similar from the point of view of effects, although they differ in detail (e.g. fission product poisoning).

The most important difference arises from the effects of daughters of U-232 (which is always present at some level in irradiated thorium) on fabrication techniques for U-233-bearing fuel.

The γ-rays from these daughters make shielding mandatory in the fabrication facility and probably dictate completely automated fabrication. Since U-233 and plutonium both have a toxicity problem which dictates glove box fabrication, this added complication for U-233 introduces a further penality which makes U-233 more difficult to fabricate than plutonium.

e) Thorium and uranium occur in roughly analogous forms (e.g. metal, oxides, carbide, etc.), and there are no obvious striking advantages of one set of compounds compared to other with respect to behaviour under irradiation.

The above considerations clearly indicate that the thorium fuel cycle in CANDU reactors has certain fundamental advantages, the most important, by far, being the better physics of U-233 in thermal reactors, which means that nuclear fuel resources could extend by at least an order of magnitude through using the thorium cycle.

F.2 DIFFERENCES IN THE PHYSICS OF THORIUM AND URANIUM CYCLES

The basic efficiencies of once-through uranium and thorium cycles are compared as a function of U-235 concentration in the heavy element (HE) feed for a CANDU-PHW reactor. These efficiencies are shown qualitatively in Figure F.4. The uranium cycle curves are reprinted from Figures 2.1 and 2.1 of Chapter Two. The thorium curves have been added.

Inspection of Figure F.4 indicates that a much higher U-235 content is required in thorium than in uranium to get into a region of comparable basic efficiency. In fact, for U-235 contents corresponding to natural uranium, thorium is not usable at all as reactor fuel. The reason is that the effective thermal neutron cross-section of Th-232 is almost a factor of three higher than that of U-238. Therefore, the use of thorium in a once-through cycle requires U-235 contents some three times higher than natural uranium. The implication with respect to inventory changes can be seen from Figure 2.1.

Secondly, the efficiencies for the thorium cycle eventually become higher than those for the uranium cycle at a given initial U-235 content. This is due to a higher neutron yield per thermal neutron absorbed in U-233 as compared to fissile Pu.

Both of these physics differences have a significant effect on economics.

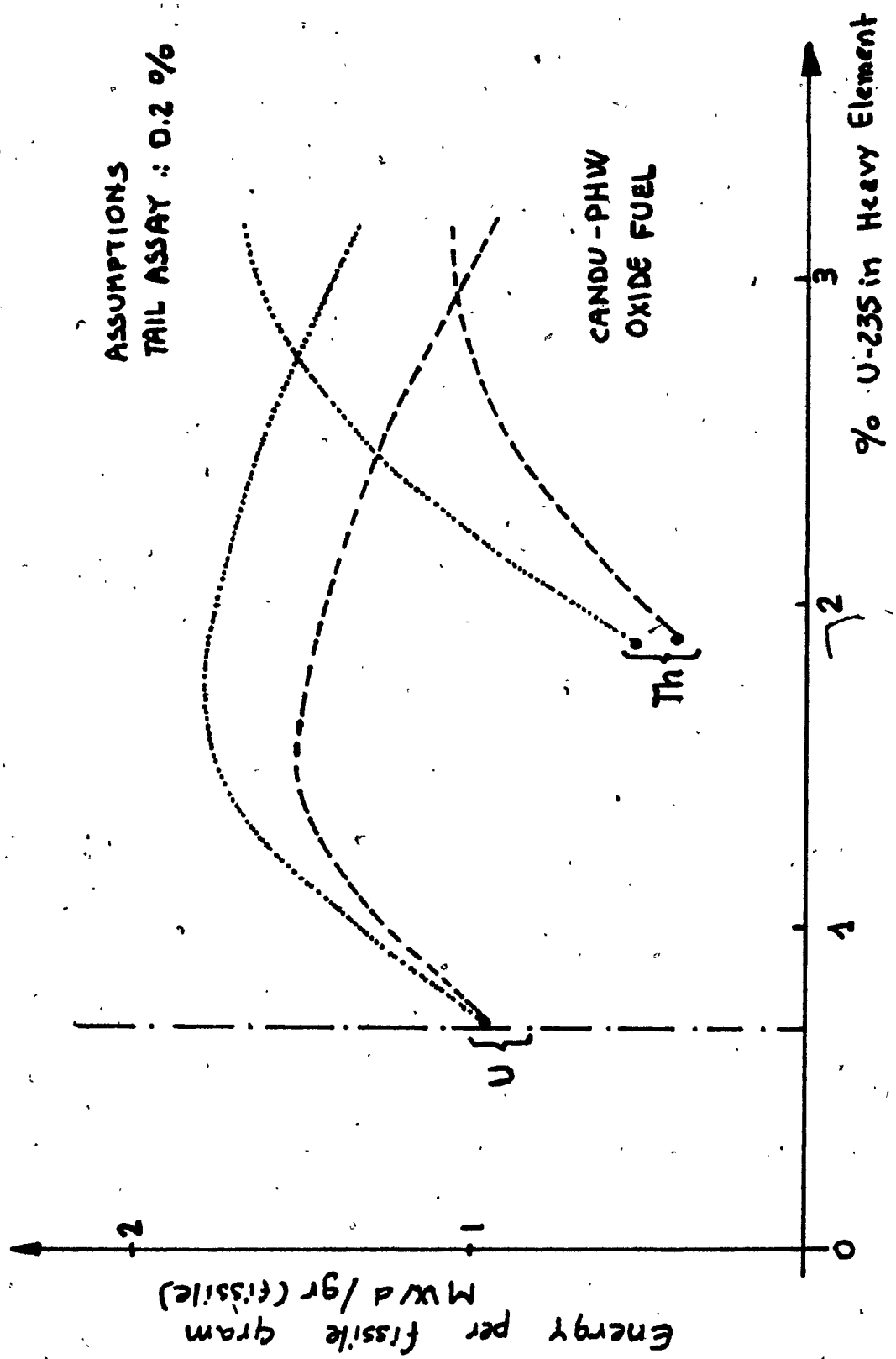

FIGURE F.4: Comparison of Fundamental Efficiency
Once-Through U and Th Cycle

Note that the burnup of the fuel at any particular point on the curves of Figure F.4 can be obtained by multiplying the U-235 content in the fuel in grams per kilogram (HE) by the energy produced per initial fissile gram.

Thus, for example, the burnup for a point in the thorium cycle at 2.5% - U-235 in heavy element is 25 x 1.71 = 42.75 MWd/kg, or 42,750 MWd/te/HE. Burnups of this order would have to be achieved to get close to optimum performance for the once-through thorium cycle.

F.3 OTHER DIFFERENCES BETWEEN THORIUM AND URANIUM CYCLES

F.3.1 Fuel

Generally speaking, there are two major differences between thorium and uranium reactor fuels:

a) We have a good deal of experience with UO_2 fuel, but relatively little with ThO_2. In order to commit a reactor with ThO_2 fuel, more information and experience would have to be amassed. The same is also true of other forms of thorium fuel, but information and experience is also lacking in their uranium counterparts, and so the difference is less striking.

b) Burnups at least three times the burnup of our current systems must be achieved in a viable Th system, at least in the near future. To a large extent, this high burnup requirement is a property of enriched recycle systems rather than a difference between thorium and uranium per se. If economic conditions change in the expected direction, the competition for thorium fuelling will not be natural uranium fuelling, but enriched uranium fuelling or Pu recycle, also implying higher burnups. Nevertheless, the tendency is to require still higher burnup from thorium. High burnups probably necessitate changes in fuel design which must be subjected to large scale tests.

Thus, a considerable development program on any chosen thorium fuel is indicated.

F.3.2 Control and Safety

Average delayed neutron fractions and mean neutron lifetimes are, in general, smaller for thorium systems than uranium systems. In itself, this would have a detrimental effect in the areas of both control and safety (Ref. Master thesis).

However, there are also differences in other relevant parameters, including:

- reactivity coefficients;
- xenon parameters;
- thermal conductivity.

The net effect is that, in general, both fast and slow control in thorium fuelled reactors is expected to be similar to natural uranium reactors of equivalent size, and no major feasibility questions in safety are anticipated which are related to differences between thorium and uranium. An exception to this general statement is the added problem associated with Pa-233 in thorium systems. This effect has the potential for causing reactivity perturbations and spatial flux distortions which necessitate added bulk (and possibly spatial) control during and following protracted shutdowns.

During a protracted shutdown in a thorium fuelled reactor, Pa-233 decays to U-233. This causes an increase in reactivity (of the order of 100 mk) and can cause severe distortions in flux and power distributions on start-up. This introduces a new control problem (Ref. 7, 8).

APPENDIX FC

REPRESENTATION OF FUEL CYCLES

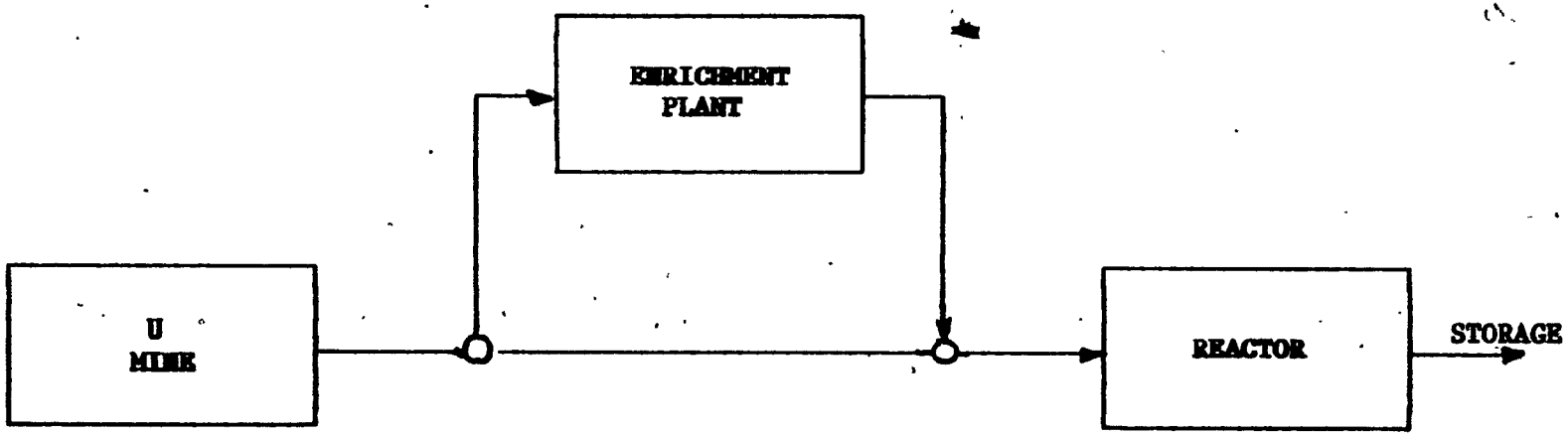

FC-2

FIGURE FC.1: Once-Through U Cycle

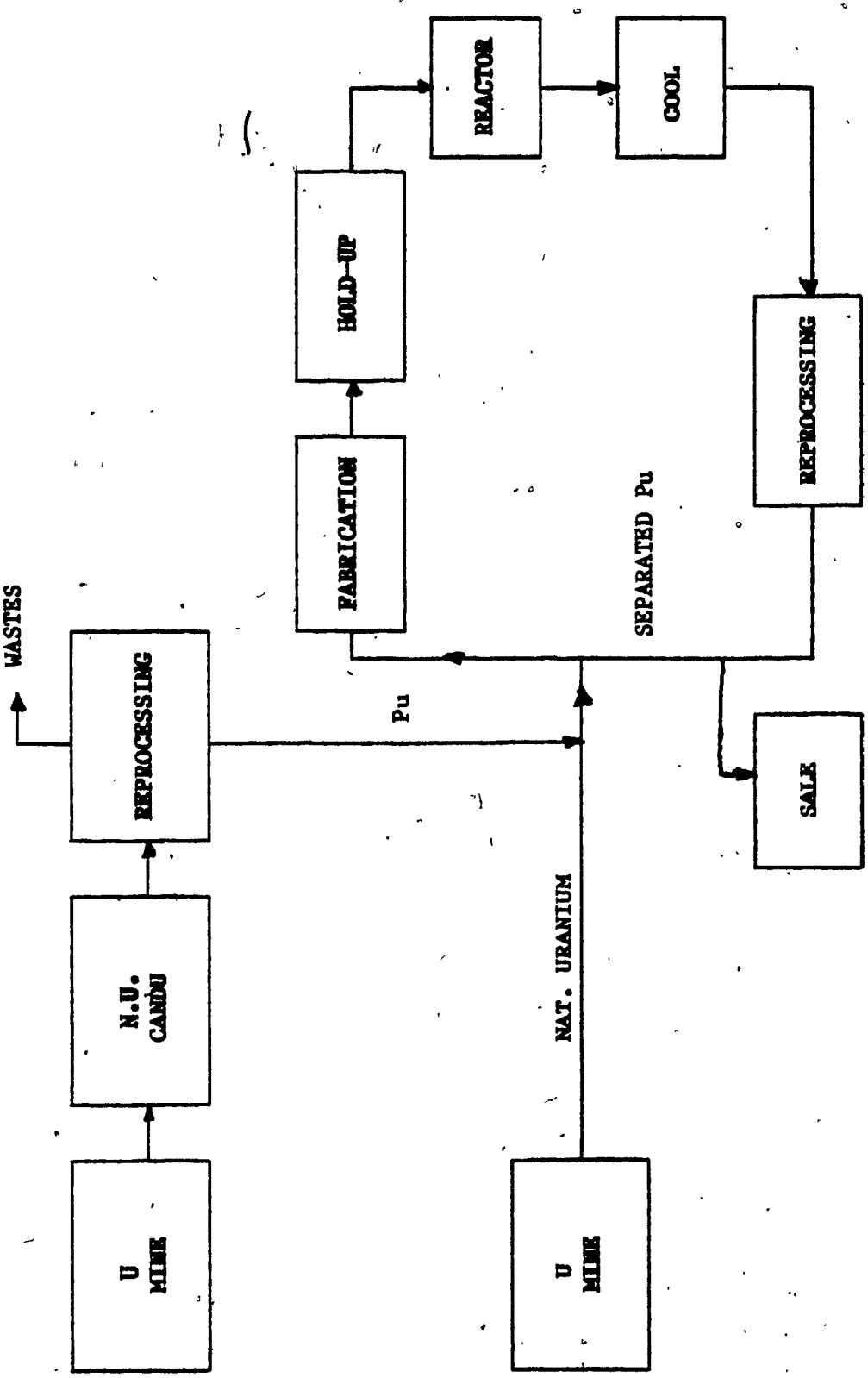

FIGURE FC.2: U with Pu Recycle and Net Nat. U ± Pu Feed

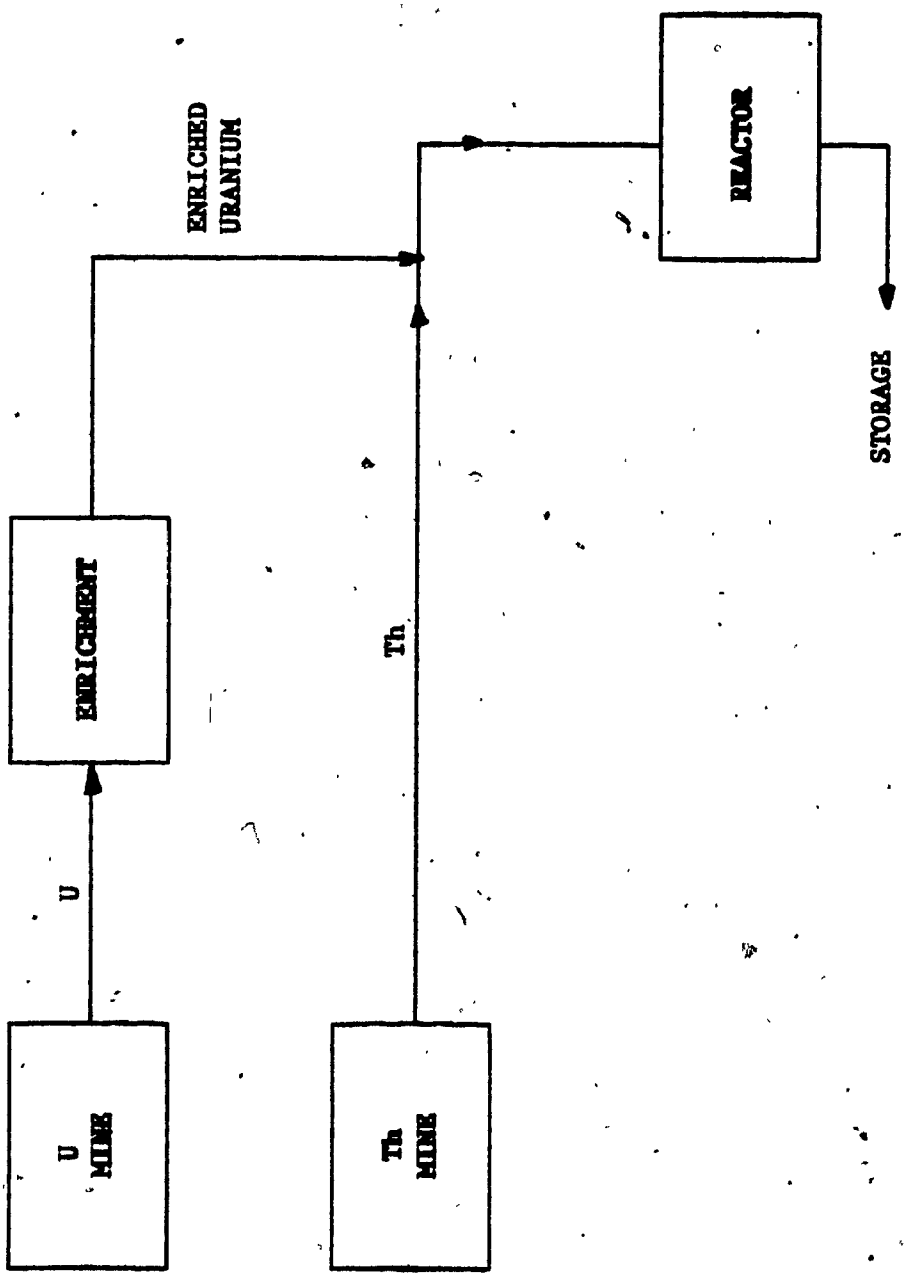

FIGURE FC.3: Once-Through Th + U235 Cycle

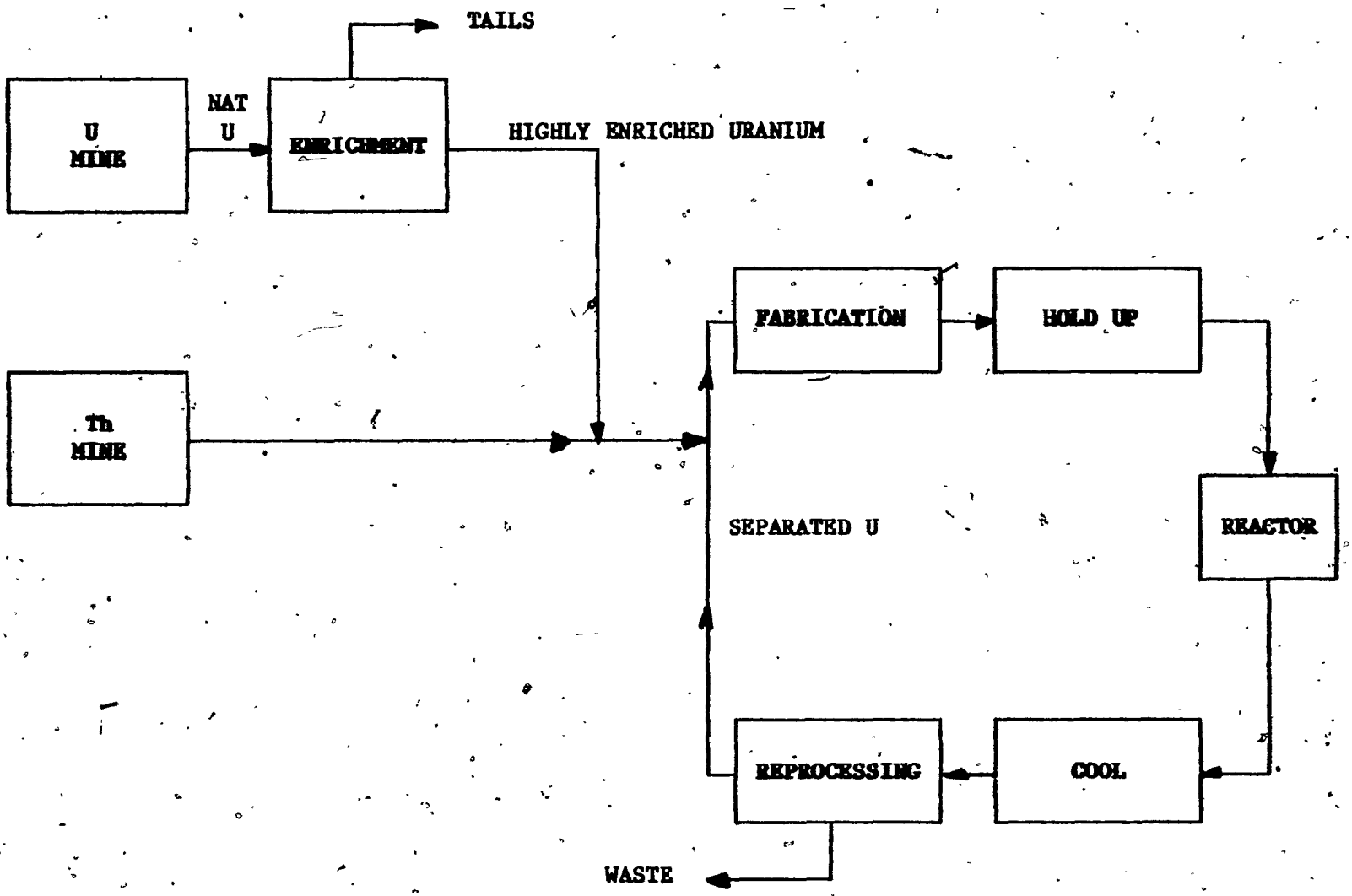

FIGURE FC.4: Th with U Recycle and Net U-235 Feed

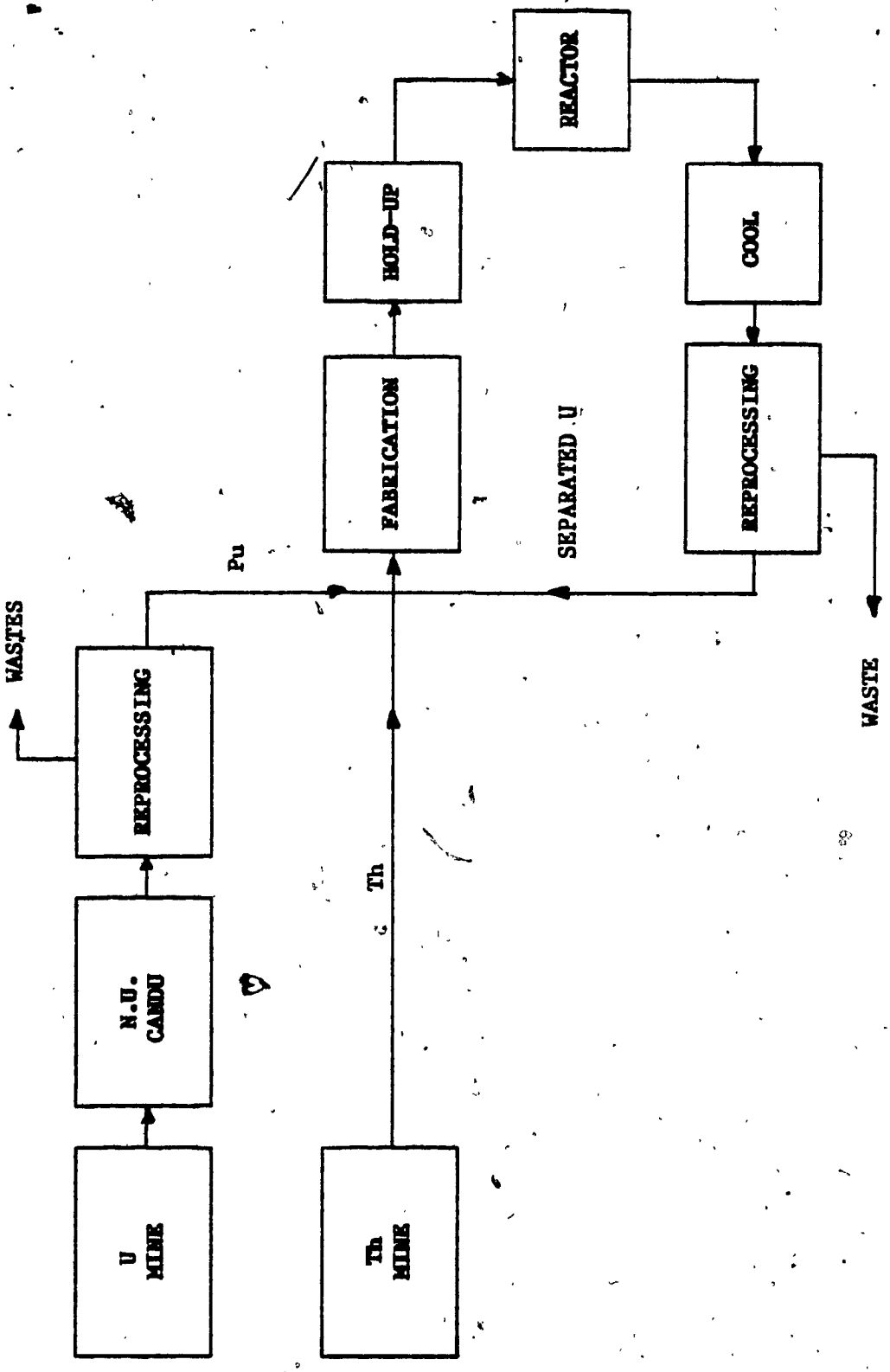

FIGURE FC.5: Th with U Recycle and Net Pu Feed